STUDIES IN

PHOTOPRODUCTION OF PIONS FROM NUCLEI

THESIS

SUBMITTED TO

THE UNIVERSITY OF MADRAS

FOR

THE DEGREE OF DOCTOR OF PHILOSOPHY

BY

K. SRINIVASA RAO, M.Sc.,

'MATSCIENCE', THE INSTITUTE OF MATHEMATICAL SCIENCES, MADRAS-20, INDIA

JULY 1970

ACKNOWLEDGEMENTS

This thesis is based upon the work done during the years 1965-1970, on photoproduction of pions from certain nuclei, under the guidance of Professor Alladi Ramakrishnan, Director, The Institute of Mathematical Sciences, Madras.

It is a pleasure to record gratefully the benefit derived from useful discussions and collaboration with co-research workers, and due acknowledgement has been made at the appropriate places. The Computations have been done on the IBM 1620 Computer at the Fundamental Engineering Research Establishment, Madras, the IBM 1130 Computer at the Advanced Centre for Bio-Physics, University of Madras, Madras, and the CDC 3600 Computer at the Tata Institute of Fundamental Research, Bombay. I am thankful to the concerned authorities for making available the Computer facilities.

I am deeply indebted to Professor Alladi Ramakrishnan for his constant encouragement and guidance throughout the preparation of this work. I am also thankful to the Council of Scientific and Industrial Research, Government of India, for the award of a Junior Research Fellowship from January 1965 to September 1967 and to the Institute of Mathematical Sciences, for providing excellent facilities for research as well as for the award of a Senior Research Fellowship from October 1967 onwards.

K. Srinivasa Rao

(K.Srinivasa Rao)

C O N T E N T S

		Page No.
INTRODUCTION		(i)
PART I:	PHOTOPRODUCTION OF PIONS FROM NUCLEONS AND DEUTERONS.	
CHAPTER 1:	THE CGLN AMPLITUDES AND PHOTOPRODUCTION OF PIONS FROM NUCLEONS	1
CHAPTER 2:	PHOTOPRODUCTION OF NEUTRAL PIONS AND CHARGED PIONS FROM DEUTERONS....	17
PART II:	PHOTOPRODUCTION OF CHARGED PIONS FROM CERTAIN CLOSED-SHELL NUCLEI.	
CHAPTER 3:	PHOTOPRODUCTION OF POSITIVE PIONS FROM ^{16}O: (i)CONFIGURATION MIXING AND THE PRODUCTION MECHANISM	57
CHAPTER 4:	PHOTOPRODUCTION OF POSITIVE PIONS FROM ^{16}O: (ii) EFFECT OF GROUND STATE CORRELATIONS	105
CHAPTER 5:	PHOTOPRODUCTION OF POSITIVE PIONS FROM ^{16}O: (iii) EFFECT OF SHORT-RANGE CORRELATIONS	129
CHAPTER 6:	PHOTOPRODUCTION OF POSITIVE PIONS FROM ^{16}O: (iv) ANALOGS OF GIANT RESONANCES	149
CHAPTER 7:	PHOTOPRODUCTION OF CHARGED PIONS FROM CARBON	164
PART III:	PHOTOPRODUCTION OF CHARGED PIONS FROM CERTAIN NON-CLOSED-SHELL NUCLEI.	
CHAPTER 8:	PHOTOPRODUCTION OF CHARGED PIONS FROM BORON	180
CHAPTER 9:	PHOTOPRODUCTION OF CHARGED PIONS FROM ^{27}Al, ^{51}V and ^{60}Ni	198
APPENDIX A	....	214
APPENDIX B	....	217
APPENDIX C	....	221

INTRODUCTION

The main aim of this thesis is to make a quantitative analysis of photoproduction of charged pions from nuclei and use it as a probe for studying the production mechanism, as well as the structure of nuclei.

Hitherto, charged pion photoproduction has been studied only in the framework of the independent particle model[1,2]. We present here a detailed study of charged pion photoproduction from nuclei based on a model of direct interaction between the incident photon and the individual nucleons, coupled with the impulse approximation. The nuclear transition operator is expressed in terms of the free single nucleon photoproduction amplitudes. We realize that the π^+ photoproduction process is similar to the muon capture process since the same initial and final nuclear states are involved in both the processes.(+) Based on this realization, for the first time, we use the configuration mixing particle-hole models besides the simple independent particle model in our studies of photoproduction of charged pions from certain closed-shell nuclei.

In order to provide a background to the work presented here, we now describe briefly some of the important experimental and theoretical studies on photoproduction of charged pions conducted so far.

---

1) E.W.Laing and R.G.Moorhouse, Proc.Phys.Soc.A70,629 (1957).
2) V.Devanathan and G.Ramachandran, Nucl.Phys.38,654 (1962); ibid. 42, 25 (1963); ibid 66, 595 (1965).

(+)Further, it is well known that nuclear structure effects play a significant role in the muon capture process.

Earlier experimental investigations[3,4] on photoproduction of charged pions from Complex nuclei have been devoted to the measurement of the total cross section, mostly accompanied by nucleon emission, based on an observation of the emitted pions rather than of the product nuclei. These experiments have shown that the sum of the π^+ and π^- cross sections exhibits very accurately an $A^{2/3}$ dependence, where A is the mass number of the target nucleus. This $A^{2/3}$ dependence has been readily explained by means of a surface production model proposed by Wilson[5] and Butler[6]. Surface production implies that the production is predominantly from the 'surface nucleons' due to a suppression of pion production from the interior of the nucleus; 'surface nucleons' being defined as those nucleons which the photon catches outside the main core of the nucleus, or, in other words, nucleons with radial coordinates greater than the nuclear radius, which are subject to weaker nuclear interaction. Calculations of Butler, based on the surface production mechanism, not only explain the correct $A^{2/3}$ dependence for the sum of the π^+ and π^- cross sections but

3) J.Steinberger and A.Bishop, Phys.Rev.78,494 (1950); R.F.Mozley,Phys.Rev.80, 493 (1950);W.R.Hogg and D.Sinclair, Phil.Mag.,series 8, 1, 466 (1956); R.M.Littauer and D.Walker,Phys.Rev.83,206(1951); ibid 86,838(1952).
4) E.H.Bellamy, Prog. in Nucl.Phys. 8, 237 (1960). References to original studies can be found in this review article.
5) R.R.Wilson, Phys.Rev. 86, 125 (1952).
6) S.T.Butler, Phys.Rev. 87, 1117 (1952).

also yield the π^- / π^+ cross section ratios which have the same trend as a function of A as the observed ratios.

From a theoretical point of view, the study of photoproduction of pions from nuclei is simplified if experimentalists distinguish the reactions in which the pion is the only particle emitted from the other reactions in which the pion is accompanied by the emission of one or more nucleons. Reactions of the former type, $A(\gamma,\pi^{\pm})B$, may readily be experimentally investigated, if the residual nucleus, B, can be identified by some characteristic activity, such as β or γ decay. The first measurement of this type has been made by Hughes and March[7] in 1958. They studied the reaction $^{11}B(\gamma,\pi^-)^{11}C$ where the final nucleus was identified by observing its positron activity. Subsequently, during the last decade, there has been a continuing program of the study of photopion production reactions, of the type $A(\gamma,\pi^{\pm})B$, especially by Hummel and his coworkers at Illinois, U.S.A. They have reported[8], so far, cross sections for the following reactions: $^{11}B(\gamma,\pi^-)^{11}C$, $^{11}B(\gamma,\pi^+)^{11}Be$, $^{16}O(\gamma,\pi^+)^{16}N$ and $^{27}Al(\gamma,\pi^+)^{27}Mg$, while Nydhal and Forkman[9] have reported the cross sections for the reactions $^{27}Al(\gamma,\pi^+)^{27}Mg$, $^{51}V(\gamma,\pi^+)^{51}Ti$ and $^{60}Ni(\gamma,\pi^-)^{60}Cu$. Since these experimentalists[8,9] measure the radioactivities of the product nuclei, they report total

7) I.S.Hughes and P.V.March, Proc.Phys.Soc. 72, 259 (1958).
8) P.Dyal and J.P.Hummel, Phys.Rev. 127, 2217 (1962); R.A.Meyer, W.B.Walters and J.P.Hummel, Phys.Rev.138, B1421 (1965); W.B.Walters and J.P.Hummel, Phys.Rev.143, 833 (1966).
9) G.Nydhal and B.Forkman, Nucl.Phys. B7, 97 (1968).

cross sections which are the sums of "partial" cross sections due to photon induced transitions to specific states of the final nucleus which are stable against nucleon emission.

Laing and Moorhouse[1] studied charged pion photoproduction on the basis of a simple independent particle model. They calculated the cross sections, for the process $^{11}B(\gamma,\pi^-)^{11}C$, for pion photoproduction occurring throughout the entire volume of the nucleus, as well as for pion production being restricted to the nuclear surface. Based on a comparison with preliminary experimental results[7] they conclude that surface production alone cannot account for the observed data. However, after making a detailed comparison between theory and experiment, Hughes and March[7] report that the cross sections for the reaction $^{11}B(\gamma,\pi^-)^{11}C$ are in good agreement with theoretical values, for surface production, predicted by Laing and Moorhouse[1]. Further, without making a detailed calculation, Meyer et.al.[8] state that their results are in qualitative agreement with those expected from the theory outlined by Laing and Moorhouse[1] in the surface production formalism, for the reactions $^{11}B(\gamma,\pi^+)^{11}Be$ and $^{16}O(\gamma,\pi^+)^{16}N$, with the added assumption that, "the transition probabilities depend more on the total number of states available than on the specific details of the states involved."

More recently, expressions for the cross sections for photoproduction of charged pions from nuclei, were derived by

Devanathan and Ramachandran[2]. They have studied the reaction $^{29}Si(\gamma,\pi^-)^{29}P$ for which experimental results are not available and they have digressed into a discussion of the dependence of the cross section on free and bound nucleon magnetic moments. Their calculation is also based on the independent particle model.

In the present study of charged pion photoproduction from nuclei, we assume the validity of the impulse approximation+ according to which the transition operator for a bound nucleon is identical to that of a free nucleon and we use the free single-nucleon photoproduction amplitudes of Chew, Goldberger, Low and Nambu[10]. The emphasis placed on the energy dependence of the total cross section is due to the nature of the available experimental results. The processes of photoproduction of neutral and charged pions from the deuteron and charged pions from ^{16}O, ^{12}C, ^{11}B, ^{27}Al, ^{51}V and ^{60}Ni are studied theoretically and the results are compared with the available experimental data. Of the above mentioned nuclei, ^{16}O and ^{12}C, being closed-shell nuclei, offer the following special features:

^{16}O:

Being a doubly closed "magic" nucleus, this is one of the few nuclei which has been extensively studied and good wave functions for its ground state and excited states are available. Photoproduction of π^+ from ^{16}O leads to the final nucleus ^{16}N which has only four experimentally observed bound states. These

---

+ See Appendix B.

10) G.F.Chew, M.L.Goldberger, F.E.Low and Y.Nambu, Phys.Rev. 106, 1345 (1957).

final nuclear states are well established to be the T=1 isobaric analogs of states in ^{16}O and this enables us to take the wave functions of ^{16}N bound states from those of ^{16}O under the valid assumption of good isobaric spin.

^{12}C:

Though this is not a "magic" nucleus, like ^{16}O, reasonably good wave functions are available for the excited states of ^{12}C. Photoproduction of π^+ from ^{12}C leads to the final nucleus ^{12}B which has only five experimentally observed bound states and four of these five states have been identified to be the T=1 isobaric analogs of states in ^{12}C. This identification enables us to take the wave functions of ^{12}B from those of ^{12}C under the assumption of good isobaric spin. But, more interesting is the case of π^- photoproduction from ^{12}C, since this leads to the final nucleus ^{12}N whose ground state alone is stable against nucleon emission and which is a positron emitter. This process $^{12}C(\gamma,\pi^-)^{12}N$ is, thus, perhaps the ideal process for an analysis of the production mechanism from an experimental point of view. Therefore, we predict the cross sections for π^-, as well as π^+ photoproduction from ^{12}C in the hope that experimental data will shortly be forthcoming.

This thesis consists of nine chapters, three of which are based on published papers and the available reprints are enclosed.(*) For the sake of convenience, it has been divided into three parts dealing with photoproduction of pions from nucleons and the deuteron, from certain closed-shell nuclei and from

(*) Please see back cover.

certain non-closed-shell nuclei. We will now present the main results of the study:

Part I consists of two chapters. In Chapter.1, we give the explicit expressions of the Chew, Goldberger, Low and Nambu[10] amplitudes, used in all our studies of photopion production from nuclei, mainly to establish certain facts, conventions and notations to be used later. We show that these amplitudes yield differential and total cross sections, for neutral as well as charged pion photoproduction, which are in reasonably good agreement with experimental results in the energy region of interest to us, viz. threshold to 400 Mev incident photon energy.

In Chapter.2, we study the sensitivity of the differential and total cross sections for neutral and charged pion photoproduction from the deuteron to the choice of the deuteron wave function which has a D-state admixture and a hard-core radius. We have used the functional forms of Hulthen and Sugawara[11] and the numerical wave functions of Reid[12] in our present study.[13] We find that the neutral pion photoproduction cross section is extremely sensitive to the choice of the deuteron wave function and the deuteron wave functions obtained by Reid[12] whose nucleon-nucleon hard-core and soft-core potentials yield the deuteron properties - viz. the binding energy, the electric quadrupole

11) L.Hulthen and M.Sugawara, Handbuch der Physik 39, 1 (1957).
12) R.V.Reid,Jr., Ann. Phys. 50, 411 (1968).
13) K.Ananthanarayanan and K.Srinivasa Rao, Nuo.Cimento 44, 31(1966); K.Srinivasa Rao, R.Parthasarathy and V.Devanathan, to be published.

moment, the D-state probability and the asymptotic D to S wave ratio - accurately, lead to a better agreement with experimental data. On the other hand, the charged pion photoproduction cross sections are shown to be not very sensitive to the choice of the deuteron wave functions.

Part II consists of five chapters. The first four chapters (Chapters 3,4,5 and 6) deal exclusively with photoproduction of positive pions from ^{16}O, which has been fairly extensively studied, while the fifth Chapter (Chapter 7) deal with photoproduction of positive and negative pions from ^{12}C. In three of the four Chapters (Chapters 3,4 and 5) on photoproduction of positive pions from ^{16}O, we are concerned only with photon induced transitions to the four low-lying bound states of ^{16}N, while in Chapter.6 we consider photon induced transitions to giant multipole resonance states in ^{16}N.

In Chapter.3, the configuration mixing particle-hole wave functions of Elliott and Flowers[14] and the Gillet-Vinh Mau[15] wave functions obtained in both the Tamm-Dancoff Approximation (TDA) and the Random Phase Approximation (RPA) are used for the low-lying bound states of ^{16}N. Of these, the RPA wave functions of Gillet and Vinh Mau include long-range correlations in the ground state of ^{16}O in an approximate way, We find that the TDA and RPA results do not differ appreciably from each other. The particle-hole wave functions yield cross sections which are smaller than those obtained with the independent particle model,

14) J.P.Elliott and B.H.Flowers, Proc.Roy.Soc.A242, 57 (1957).
15) V.Gillet and N.Vinh Mau, Nucl.Phys. 54, 321 (1964).

but they are still larger, by almost a factor of two, than the experimental results of Meyer, Walters and Hummel[7]. The phenomenological Migdal theory wave functions for ^{16}N, which were successful[16] in accounting for the experimental muon capture rates and inelastic electron scattering cross sections, also yield cross sections for $^{16}O(\gamma,\pi^+)^{16}N$ which are larger than the experimental results. We show that this discrepancy can be accounted for by invoking the phenomenological surface production mechanism[17].

In Chapter.4, we take into account, explicitly, the two-particle-two-hole (2p-2h) correlations in the ground state of ^{16}O, in the study of photoproduction of positive pions from ^{16}O. This is in contrast to our study in Chapter.3, where the ground state correlations were taken into account by the RPA. For the bound states of ^{16}N we use, in addition to the wave functions of Elliott and Flowers and Gillet and Vinh Mau, the wave functions of Kuo[18] calculated with matrix elements derived from the realistic Hamada-Johnson potential which include core-polarization ("screening") corrections. Without invoking the phenomenological surface production mechanism, we find that a better agreement between theory and experiment can be obtained when we use the Kuo wave functions with "screening" for ^{16}N states, together with the ground state wave function of ^{16}O which explicitly includes

16) M.Rho, Phys.Rev. Letts.18, 671 (1967); Phys.Rev.161,955 (1967).
17) V.Devanathan, M.Rho, K.Srinivasa Rao and S.C.K.Nair, Nucl.Phys. B2, 329 (1967).
18) Private communication of Kuo quoted by A.M.Green and M.Rho, Nucl.Phys. A130, 112 (1969).

2p-2h correlations[19].

In Chapter.5, we study the effect of nucleon-nucleon short-range correlations in the nuclear wave functions on photoproduction of positive pions from ^{16}O, with an essentially phenomenological correlation function. In the preliminary results, which we report here, we use only the independent particle model description for ^{16}N states and we find that there is no appreciable change in the character of the angular distributions due to the inclusion of short-range correlations. So, we are of the view that nucleon-nucleon short-range correlations can be ignored in the case of photoproduction of pions from nuclei near the first pion-nucleon resonance region.

In Chapter.6, we are concerned with photoproduction of positive pions from ^{16}O leading to giant multipole resonance states in ^{16}N. We find that the cross sections due to transitions to these higher excited states are considerably larger than the contributions from the low-lying bound states of ^{16}N. We also observe(*) that the total cross sections near the threshold for photopion production are dominated by the dipole resonances but that near the first pion-nucleon resonance region the quadrupole resonances are dominant, making it, thereby, possible to experimentally identify these two types of resonances. Hence, it would be of value to measure these experimentally.

In Chapter.7, we study the case of photoproduction of positive and negative pions from ^{12}C. We predict[20] the energy

19) K.Srinivasa Rao and V.Devanathan, to appear in Phys.Letts.
20) K.Srinivasa Rao, V.Devanathan and G.N.S.Prasad, submitted to Nucl.Phys.

(*) K.Srinivasa Rao, to be published.

dependence of the cross sections using the independent particle model and the configuration mixing particle-hole model wave functions of Gillet and Vinh Mau for the final nuclear states, in both the volume and surface production mechanisms. Of the two processes $^{12}C(\gamma,\pi^+)^{12}B$ and $^{12}C(\gamma,\pi^-)^{12}N$, the latter is ideally suited for an experimental study since only the ground state of ^{12}N is stable against nucleon emission.

Part III consists of two Chapters. In these chapters we are concerned with photoproduction of charged pions from ^{11}B, ^{27}Al, ^{51}V and ^{60}Ni, for which experimental results are available. Being non-closed-shell nuclei, we are constrained to study these processes in terms of single particle transitions from occupied to unoccupied shells, in the absence of detailed information about the excited state wave functions for these nuclei.

In Chapter.8, we study the reactions $^{11}B(\gamma,\pi^+)^{11}Be$ and $^{11}B(\gamma,\pi^-)^{11}C$. Of these, the former is better suited for a theoretical study since there are only two low-lying bound states of ^{11}Be which are stable against nucleon emission, while there are many possible bound states of ^{11}C which have not yet been correctly enumerated. We obtain a good agreement[21] with the experimental results[7] for $^{11}B(\gamma,\pi^+)^{11}Be$ when we assume surface production of pions. Due to the uncertainty about the number of final states, and their spin-parities, which would have contributed to the experimental cross sections, we are unable to draw any definite conclusion in the case of $^{11}B(\gamma,\pi^-)^{11}C$, except that

21) V.Devanathan, K.Srinivasa Rao and R.Sridhar, Phys.Letts. 25B, 456 (1967).

a reasonably good agreement with experiment can be obtained when we consider the cross sections in the surface production mechanism to arise from the single particle transitions: $1p_{3/2}, \longrightarrow 1p_{3/2}$, $1p_{1/2}$ and $1d_{5/2}$ only.[21)]

In Chapter.9, we study the reactions $^{27}Al(\gamma,\pi^+)^{27}Mg$, $^{51}V(\gamma,\pi^+)^{51}Ti$ and $^{60}Ni(\gamma,\pi^-)^{60}Cu$ using the independent particle model and the volume and surface production of pions. As in the case of $^{11}B(\gamma,\pi^-)^{11}C$, discussed above, we are handicapped in the study of these reactions due to lack of adequate and conclusive information about the number and nature of the final states involved. Only in the case of $^{27}Al(\gamma,\pi^+)^{27}Mg$, we obtain a reasonably good agreement[22)] with experiment[7)] when we consider the cross sections in the volume or surface production mechanism to arise from the single particle transition: $1d_{5/2} \longrightarrow 2s_{1/2}$.

We now project the salient features which we realize as a consequence of our study of photoproduction of pions from nuclei:

(a) The differential and total cross sections for neutral pion photoproduction from the deuteron are very sensitive to the choice of the deuteron wave function.

(b) The ground state correlations taken into account by the Random Phase Approximation under-estimate the actual particle-hole correlations in the ground state of ^{16}O.

(c) Realistic nucleon-nucleon potentials lead to wave functions which give rise to theoretical cross sections which are

22) V.Devanathan, G.N.S.Prasad and K.Srinivasa Rao, submitted to Nucl.Phys.

in good agreement with experiment in the case of $^{16}O(\gamma,\pi^+)^{16}N$. Hence, perhaps, there is no need to resort to wave functions obtained from purely phenomenological theories like (for example) the Migdal theory.

(d) A detailed description of the final nuclear states involved in more important than a mere knowledge of their total number. This conclusion is contrary to the expectation of Meyer et.al. that the cross sections "depend more on the total number of states available than on the specific details of the states involved".

(e) In the absence of detailed information about the initial and final state nuclear wave functions, it is possible to obtain better agreement between theory and experiment for reactions of the type $A(\gamma,\pi^{\pm})B$ by using the surface production mechanism than by using the volume production mechanism.

One feature which has not been considered in our studies of photopion production from nuclei is the effect of final state interactions (of the outgoing pion with the residual nucleus). However, in Chapter.4, we shall discuss this aspect to some extent.

PART. I

PHOTOPRODUCTION OF PIONS FROM NUCLEONS AND DEUTERONS.

CHAPTER 1

THE CGLN AMPLITUDES AND PHOTOPRODUCTION OF PIONS FROM NUCLEONS

1. Photoproduction of single pions from nucleons is one of the fundamental reactions encountered in the study of pion phenomenon and hence it is considered to be a very useful tool to investigate the properties of pion-nucleon interaction. The first measurements of the differential cross section for photoproduction of positive pions from hydrogen were those of Steinberger and Bishop[1]. Since then π^+ and π^o photoproduction reactions:

$$\gamma + p \longrightarrow n + \pi^+ \quad , \qquad (I.1.1)$$

$$\gamma + p \longrightarrow p + \pi^o \quad , \qquad (1.1.2)$$

have been extensively studied both theoretically and experimentally. At present copious results are available[2] for pion photoproduction from threshold upto an incident photon energy of 1.5 Bev. Chew, Goldberger, Low and Nambu[3] (hereinafter referred to as CGLN), were the first

---

1) J.Steinberger and A.S.Bishop, Phys.Rev. 86, 171 (1952).

2) See, for example, J.T.Beale, S.D.Ecklund and R.L.Walker, Report CTSL-42, California Institute of Technology; F.A.Berends, A.Donnachie and D.L.Weaver, Nucl.Phys. B4, 1 (1967);

3) G.F.Chew, M.L.Goldberger, F.E.Low and Y.Nambu, Phys.Rev. 106, 1345 (1957).

to treat the photoproduction reaction around the first pion-nucleon resonance by means of fixed t dispersion relations. They formulated the general dispersion relations for photopion production and evaluated the dispersion integrals in the static limit. Several attempts were made[4-10] to improve the work of CGLN. Gourdin and Salin[4] introduced additional terms by taking into account explicitly the higher resonances of the π-N channel (ρ, ω, etc.) while Ball[5] and others[6-9] took the meson resonances of the $N\bar{N}$ channel into account. But it turns out that the deviations due to these theoretical refinements are not larger than the discrepancies between the results from different laboratories. Thus, as pointed out by Höhler and Schmidt[11], the present experimental accuracy does not allow a reliable test of the additional terms included in the theoretical expressions for the production amplitude and hence the work of CGLN survives almost unchanged from a practical point of view.

---

4) M.Gourdin and Ph.Salin, Nuovo Cim. 27, 193 (1963); ibid.28, 1294 (1963).

5) J.S.Ball, Phys.Rev. 124, 2014 (1961).

6) J.McKinley, Technical Report No.38 (1962), University of Illinois.

7) M.Gourdin, D.Lurie and A.Martin, Nuovo Cim.18, 933 (1960).

8) B.De Tollis and A.Veganelakis, Nuovo Cim.22, 403 (1961).

9) C.S.Robinson, Ph.M.Baum, L.Crigee and J.McKinley, Phys.Rev.Letts. 9, 349 (1962).

10) S.L.Adler, Ann.Phys.50, 189 (1968). A detailed, unified treatment of single pion photo-,electro- and weak-production is given in this paper.

11) G.Höhler and W.Schmidt, Ann.Phys. 28, 34 (1964).

In this Chapter, we give the complete forms of the CGLN amplitudes and we also give the explicit expressions for certain combinations of these amplitudes which occur in the study of photoproduction of pions from nuclei. We show that the angular distributions as well as energy distributions of the cross sections for (1.1.1) and (1.1.2), calculated using the CGLN amplitudes, are in good qualitative agreement with the experimental results[2].

2. We now discuss the case of photoproduction of pions from a single nucleon using the Chew, Goldberger, Low and Nambu (CGLN) amplitudes for the basic photoproduction processes:

$$\gamma + p \longrightarrow p + \pi^0 ,$$
$$\gamma + n \longrightarrow n + \pi^0 ,$$
$$\gamma + p \longrightarrow n + \pi^+ ,$$
$$\gamma + n \longrightarrow p + \pi^- . \qquad (1.2.1)$$

The CGLN amplitudes can be written for these processes as:

$$t(\gamma+p \longrightarrow p+\pi^0) = f^{(+)} + f^{(o)} , \qquad (1.2.2)$$
$$t(\gamma+n \longrightarrow n+\pi^0) = f^{(+)} - f^{(o)} , \qquad (1.2.3)$$
$$t(\gamma+p \longrightarrow n+\pi^+) = \sqrt{2}(f^{(-)} + f^{(o)}) , \qquad (1.2.4)$$
$$t(\gamma+n \longrightarrow p+\pi^-) = -\sqrt{2}(f^{(-)} - f^{(o)}) \qquad (1.2.5)$$

where $f^{(+)}$, $f^{(-)}$ and $f^{(o)}$ are given(*) by:

(*) We use throughout the natural system of units, in which $\hbar = c =$ pion mass $= 1$.

$$f^{(+)} = \frac{2\pi e f}{\sqrt{\mu_o \nu_o}} \left[i\, \underline{\sigma} \cdot \underline{\mu} \times (\underline{\nu} \times \underline{\epsilon}) \lambda h^{+-} + i (\underline{\sigma} \cdot \underline{\mu}) \frac{(\underline{\mu} \cdot \underline{\epsilon})}{2M\mu_o} + \right.$$

$$\left. + \underline{\mu} \cdot (\underline{\nu} \times \underline{\epsilon}) \lambda h^{++} \right], \qquad (1.2.6)$$

$$f^{(-)} = \frac{2\pi e f}{\sqrt{\mu_o \nu_o}} \left[\frac{1}{(1 + \frac{\mu_o}{M})} \left\{ i\, \underline{\sigma} \cdot \underline{\epsilon} + \frac{2i}{k^2+1} (\underline{\sigma} \cdot \underline{k})(\underline{\mu} \cdot \underline{\epsilon}) \right\} + \right.$$

$$\left. + i\, \underline{\sigma} \cdot \underline{\mu} \times (\underline{\nu} \times \underline{\epsilon}) \lambda h^{--} - i (\underline{\sigma} \cdot \underline{\mu}) \frac{(\underline{\mu} \cdot \underline{\epsilon})}{2M\mu_o} + \underline{\mu} \cdot (\underline{\nu} \times \underline{\epsilon}) \lambda h^{+-} \right], \qquad (1.2.7)$$

and

$$f^{(o)} = \frac{2\pi e f}{\sqrt{\mu_o \nu_o}} \left[-i (\underline{\sigma} \cdot \underline{\epsilon}) \alpha \mu_o^2 - i\, \underline{\sigma} \cdot \underline{\mu} \times (\underline{\nu} \times \underline{\epsilon}) \alpha + \right.$$

$$\left. + i (\underline{\sigma} \cdot \underline{\mu}) \frac{(\underline{\mu} \cdot \underline{\epsilon})}{2M\mu_o} \right], \qquad (1.2.8)$$

where

$\underline{\sigma}$ is the Pauli spin operator for the nucleon,

M is the mass of the nucleon,

$\underline{\nu}$ and ν_o are the momentum and energy of the photon,

$\underline{\mu}$ and μ_o are the momentum and energy of the pion,

$\underline{\epsilon}$ is the photon polarization vector,

e^2 is the electromagnetic coupling constant,

f is the unrationalized, renormalized pion-nucleon coupling constant,

μ_p and μ_n are the anamolous magnetic moments of the proton and neutron,

$$h^{++} = \frac{1}{3\mu^3} \left(e^{i\delta_{11}} \sin\delta_{11} + 4 e^{i\delta_{13}} \sin\delta_{13} + 4 e^{i\delta_{31}} \sin\delta_{31} + 4 e^{i\delta_{33}} \sin\delta_{33} \right), \qquad (1.2.9)$$

$$h^{+-} = \frac{1}{3\mu^3}\left(e^{i\delta_{11}}\sin\delta_{11} + e^{i\delta_{13}}\sin\delta_{13} + e^{i\delta_{31}}\sin\delta_{31} - 2e^{i\delta_{33}}\sin\delta_{33}\right), \tag{1.2.10}$$

$$h^{--} = \frac{1}{3\mu^3}\left(e^{i\delta_{11}}\sin\delta_{11} - 2e^{i\delta_{13}}\sin\delta_{13} - 2e^{i\delta_{31}}\sin\delta_{31} + e^{i\delta_{33}}\sin\delta_{33}\right), \tag{1.2.11}$$

δ_{11}, δ_{13}, δ_{31} and δ_{33} are respectively the (1/2,1/2), (1/2, 3/2), (3/2, 1/2) and (3/2, 3/2) pion-nucleon P-wave scattering phase shifts, $\underline{k} = \underline{\nu} - \underline{\mu}$, is the momentum transfer to the nucleon,

$$\lambda = \frac{\mu_p - \mu_n}{4Mf^2}\ , \tag{1.2.12}$$

and

$$\alpha = \frac{\mu_p + \mu_n}{2M\mu_o}\ . \tag{1.2.13}$$

The single nucleon photoproduction amplitude has the general structure

$$\underline{\sigma}\cdot\underline{K} + L \tag{1.2.14}$$

where $\underline{K}$ and L are respectively the spin-dependent and spin-independent parts of the transition amplitude. Explicitly, $\underline{K}$ and L in the case of neutral pion photoproduction are given by:

$$\underline{K} = i\frac{2\pi ef}{\sqrt{\mu_o\nu_o}}\left[\lambda h^{+-}\,\underline{\mu}\times(\underline{\nu}\times\underline{\epsilon}) \mp \alpha\left\{\mu_o^2\underline{\epsilon} + \underline{\mu}\times(\underline{\nu}\times\underline{\epsilon})\right\} + \right.$$

$$\left. + \frac{(\underline{\mu}\cdot\epsilon)\underline{\mu}}{M\mu_o}\ H_p\right], \tag{1.2.15}$$

and

$$L = \frac{2\pi e f}{\sqrt{\mu_o \nu_o}} \underline{\mu} \cdot (\underline{\nu} \times \underline{\epsilon}) \lambda h^{++}, \tag{1.2.16}$$

where the upper and lower signs in Eq.(1.2.15) refer respectively to π^o photoproduction from the proton and neutron, $H_p = 1$ for π^o production from the proton and $H_p = 0$ for π^o production from the neutron. In the case of charged pion photoproduction $\underline{K}$ and L are explicitly given by:

$$\underline{K} = i \frac{2\sqrt{2}\pi e f}{\sqrt{\mu_o \nu_o}} \left[\frac{1}{(1+\frac{\mu_o}{M})} \left\{ \underline{\epsilon} + \frac{2(\underline{\mu}\cdot\underline{\epsilon})\vec{k}}{k^2+1} \right\} + \lambda h^- \underline{\mu} \times (\underline{\nu} \times \underline{\epsilon}) + \right.$$

$$\left. \mp \alpha \left\{ \mu_o^2 \underline{\epsilon} + \underline{\mu} \times (\underline{\nu} \times \underline{\epsilon}) - \frac{(\underline{\mu}\cdot\underline{\epsilon})\underline{\mu}}{M\mu_o} H_- \right] \right., \tag{1.2.17}$$

and

$$L = i \frac{2\sqrt{2}\pi e f}{\sqrt{\mu_o \nu_o}} \underline{\mu} \cdot (\underline{\nu} \times \underline{\epsilon}) \lambda h^{+-}, \tag{1.2.18}$$

where the upper and lower signs in Eq.(1.2.17) refer respectively to π^+ and π^- photoproduction, $H_- = 1$ for π^- production and $H_- = 0$ for π^+ production.

We make the justifiable assumption that the recoil nucleon receives only momentum but no appreciable energy. Under this assumption, we have for the differential cross section for photoproduction of pions from a single nucleon, after summing over final spins:

$$\frac{d\sigma}{d\Omega} = (2\pi)^{-2} \mu\mu_o \left(\underline{K} \cdot \underline{K}^* + LL^* \right), \tag{1.2.19}$$

where the quantities $\underline{K}.\underline{K}^*$ and LL^* can be easily calculated from the above given expressions for $\underline{K}$ and L. For this, we choose a frame of reference with the direction of the incident photon as z-axis and the plane in which the momentum vectors $\underline{\nu}$ and $\underline{\mu}$ lie as Y-Z plane. The angle which the pion makes with the Z-axis is represented by θ. In this frame of reference,

$$\underline{\nu} = \nu\hat{k} \quad \text{and} \quad \underline{\mu} = \mu\cos\theta\,\hat{k} + \nu\sin\theta\,\hat{j}$$

and $\hat{k}$ and $\hat{j}$ are respectively unit vectors along the Z and Y axis.

After averaging over photon polarizations, we obtain for the case of neutral pion photoproduction:

$$\begin{aligned}
\underline{K}\cdot\underline{K}^* = \frac{4\pi^2 e^2 f^2}{\mu_0 \nu_0}\Bigg\{ & \left(\frac{\nu\lambda}{3\mu^2}\right)^2 (1+\cos^2\theta)\tfrac{1}{2}\big[\sin^2\delta_{11} + 4\sin^2\delta_{13} + \sin^2\delta_{31} + \\
& + 4\sin^2\delta_{33} + 2\sin^2\delta_{11}(2\sin^2\delta_{13} + \sin^2\delta_{31} - 2\sin^2\delta_{33}) + \\
& + 4\sin^2\delta_{13}(\sin^2\delta_{31} - \sin^2\delta_{33}) - 4\sin^2\delta_{31}\sin^2\delta_{33} + \\
& + \sin 2\delta_{11}(\sin 2\delta_{13} + \tfrac{1}{2}\sin 2\delta_{31} - \sin 2\delta_{33}) + \\
& + 2\sin 2\delta_{13}(\tfrac{1}{2}\sin 2\delta_{31} - \sin 2\delta_{33}) - \sin 2\delta_{31}\sin 2\delta_{33}\big] + \\
& + \alpha^2\big[\mu_0^2(\mu_0^2 - 2\mu\nu\cos\theta) + \frac{\mu^2\nu^2}{2}(1+\cos^2\theta)\big] + \\
& \mp \alpha\,\frac{\nu\lambda}{3\mu}\Big[\frac{\nu}{\mu}(1+\cos^2\theta) - \frac{2\mu_0^2}{\mu^2}\cos\theta\Big]\tfrac{1}{2}(\sin 2\delta_{11} + 2\sin 2\delta_{13} + \\
& + \sin 2\delta_{31} - 2\sin 2\delta_{33}) + H_p\,\frac{\mu^2\sin^2\theta}{2M}\Big(\frac{\mu^2}{\mu^2\mu_0^2} - 2\alpha\mu_0\Big)\Bigg\},
\end{aligned}$$

(1.2.20)

where the upper sign is for the process $\gamma+p \longrightarrow p+\pi^0$ while the lower sign is for $\gamma+n \longrightarrow n+\pi^0$ and $H_p = 1$ for $\gamma+p \longrightarrow p+\pi^0$ while $H_p = 0$ for $\gamma+n \longrightarrow n+\pi^0$, and

$$\begin{aligned} L L^* = \frac{4\pi^2 e^2 f^2}{\mu_0 v_0} \left(\frac{v\lambda}{3\mu^2}\right)^2 \frac{1}{2} \Big[& \sin^2\delta_{11} + 16(\sin^2\delta_{13} + \sin^2\delta_{31} + \sin^2\delta_{33}) + \\ & + 2\sin 2\delta_{11}(\sin 2\delta_{13} + \sin 2\delta_{31} + \sin 2\delta_{33}) + \\ & + 8\sin 2\delta_{13}(\sin 2\delta_{31} + \sin 2\delta_{33}) + 8\sin 2\delta_{31}\sin 2\delta_{33} + \\ & + 8\sin^2\delta_{11}(\sin^2\delta_{13} + \sin^2\delta_{31} + \sin^2\delta_{33}) + \\ & + 32\sin^2\delta_{13}(\sin^2\delta_{31} + \sin^2\delta_{33}) + 32\sin^2\delta_{31}\sin^2\delta_{33}\Big] \sin^2\theta. \end{aligned} \tag{1.2.21}$$

Similarly, after averaging over photon polarizations, we obtain for the case of charged pion photoproduction:

$$\begin{aligned} \underline{K}\cdot\underline{K}^* = \frac{4\pi^2 e^2 f^2}{\mu_0 v_0} \Bigg\{ & \frac{2}{(1+\frac{\mu_0}{M})^2}\left[1 - \frac{2\mu^2\sin^2\theta}{(k^2+1)^2}\right] + \\ & + \left(\frac{v\lambda}{3\mu^2}\right)^2 \left[\sin^2\delta_{11} + 4\sin^2\delta_{13} + 4\sin^2\delta_{31} + \sin^2\delta_{33}\right] + \\ & - 2\sin^2\delta_{11}(2\sin^2\delta_{13} + 2\sin^2\delta_{31} - \sin^2\delta_{33}) - 4\sin^2\delta_{31}\sin^2\delta_{33} + \\ & - \sin 2\delta_{11}(\sin 2\delta_{13} + \sin 2\delta_{31} - \tfrac{1}{2}\sin 2\delta_{33}) + \\ & + 2\sin 2\delta_{13}(\sin 2\delta_{31} - \tfrac{1}{2}\sin 2\delta_{33}) - \sin 2\delta_{31}\sin 2\delta_{33}\Big](1+\cos^2\theta) + \\ & + \alpha^2\left[2\mu_0^2(\mu_0^2 - 2\mu v\cos\theta) + \mu^2 v^2(1+\cos^2\theta)\right] + \end{aligned}$$

(contd. on next page)

$$+\frac{4}{(1+\frac{\mu_0}{M})}\frac{\nu\lambda}{3\mu}\left[\frac{1}{2}\sin 2\delta_{11}-\sin 2\delta_{13}-\sin 2\delta_{31}+\frac{1}{2}\sin 2\delta_{33}\right]\times$$

$$\times\left(\frac{\nu\sin^2\theta}{k^2+1}-\frac{\cos\theta}{\mu}\right)+$$

$$\mp\alpha\left[\frac{1}{(1+\frac{\mu_0}{M})}\left\{\frac{4\mu^2\sin^2\theta}{k^2+1}(\nu^2-\mu_0^2)+4(\mu_0^2-\mu\nu\cos\theta)\right\}+\right.$$

$$+\frac{2}{3}\nu\lambda\left\{\frac{\nu}{\mu}(1+\cos^2\theta)-\frac{2\mu_0^2}{\mu^2}\cos\theta\right\}\left(\frac{1}{2}\sin 2\delta_{11}-\sin 2\delta_{13}-\sin 2\delta_{31}+\frac{1}{2}\sin 2\delta_{33}\right)\Big]+$$

$$+H_-\left[\frac{\mu^4\sin^2\theta}{M^2\mu_0^2}-\frac{2\mu^2\sin^2\theta}{(1+\frac{\mu_0}{M})M\mu_0}\left(1+\frac{2(\mu\nu\cos\theta-\mu^2)}{k^2+1}\right)+\right.$$

$$\left.\left.-\frac{2\alpha}{M}\mu_0\mu^2\sin^2\theta\right]\right\},$$

(1.2.22)

where the upper sign is for $\gamma+p\longrightarrow n+\pi^+$ and the lower sign is for $\gamma+n\longrightarrow p+\pi^-$, $H_-=1$ for $\gamma+p\longrightarrow p+\pi^0$ and $H_-=0$ for $\gamma+p\longrightarrow n+\pi^+$, and

$$LL^*=\frac{4\pi^2e^2f^2}{\mu_0\nu_0}\left(\frac{\nu\lambda}{3\mu^2}\right)^2\left[\sin^2\delta_{11}+\sin^2\delta_{13}+\sin^2\delta_{31}+4\sin^2\delta_{33}+\right.$$

$$+2\sin^2\delta_{11}(\sin^2\delta_{13}+\sin^2\delta_{31}-2\sin^2\delta_{33})+$$

$$+2\sin^2\delta_{13}(\sin^2\delta_{31}-\sin^2\delta_{33})-4\sin^2\delta_{31}\sin^2\delta_{33}+$$

$$+\sin 2\delta_{11}\left(\frac{1}{2}\sin 2\delta_{31}+\frac{1}{2}\sin 2\delta_{13}-\sin 2\delta_{33}\right)+$$

$$\left.+\sin 2\delta_{13}\left(\frac{1}{2}\sin 2\delta_{31}-\sin 2\delta_{33}\right)-\sin 2\delta_{31}\sin 2\delta_{33}\right]\sin^2\theta. \quad (1.2.23)$$

In the case of charged pion photoproduction from nuclei, we would require the expression for $(\underline{k}.\underline{K})\,(\underline{k}.\underline{K}^*)$

in addition to the expressions given above for $\underline{K}.\underline{K}^*$ and LL^*, which we give here:

$$(\underline{k}\cdot\underline{K})(\underline{k}\cdot\underline{K}^*) = \frac{4\pi^2 e^2 f^2}{\mu_0 v_0}\,\mu^2\sin^2\theta\left\{\left(\frac{v^2\lambda}{3\mu^3}\right)^2\left[\sin^2\delta_{11}+4\sin^2\delta_{13}+4\sin^2\delta_{31}+\sin^2\delta_{33}+\right.\right.$$

$$-2\sin^2\delta_{11}(2\sin^2\delta_{13}+2\sin^2\delta_{31}-\sin^2\delta_{33})+$$

$$+4\sin^2\delta_{13}(2\sin^2\delta_{31}-\sin^2\delta_{33})-4\sin^2\delta_{31}\sin^2\delta_{33}+$$

$$-\sin 2\delta_{11}(\sin 2\delta_{13}+\sin 2\delta_{31}-\tfrac{1}{2}\sin 2\delta_{33})+$$

$$\left.-2\sin 2\delta_{13}(\sin 2\delta_{31}-\tfrac{1}{2}\sin 2\delta_{33})-\sin 2\delta_{31}\sin 2\delta_{33}\right]+$$

$$+\left[\frac{1}{\left(1+\frac{\mu_0}{M}\right)}\left(\frac{k^2-1}{k^2+1}\right)\mp\alpha(v^2-\mu_0^2)+H_-\frac{(\mu^2-\mu v\cos\theta)}{M\mu_0}\right]\times$$

$$\times\left[\frac{1}{\left(1+\frac{\mu_0}{M}\right)}\left(\frac{k^2-1}{k^2+1}\right)\mp\alpha(v^2-\mu_0^2)+H_-\frac{(\mu^2-\mu v\cos\theta)}{M\mu_0}+\right.$$

$$\left.+\frac{2v^2\lambda}{3\mu^3}\left(\tfrac{1}{2}\sin 2\delta_{11}-\sin 2\delta_{13}-\sin 2\delta_{31}+\tfrac{1}{2}\sin 2\delta_{33}\right)\right]\Bigg\}, \qquad (1.2.24)$$

where, as in the case of Eq.(1.2.22) the upper sign is for $\gamma+p\longrightarrow n+\pi^+$ and the lower sign is for $\gamma+n\longrightarrow p+\pi^-$, $H_-=1$ for $\gamma+n\longrightarrow p+\pi^-$ and $H_-=0$ for $\gamma+p\longrightarrow n+\pi^+$.

3. Numerical calculations, in the centre of mass (c.m.) frame of reference, have been made for the differential and total cross sections for photoproduction of pions from single nucleons using the expressions (1.2.20) and (1.2.21) or, (1.2.22) and (1.2.23), in Eq.(1.2.19).

In Fig.1, the c.m. differential cross section for process (1.1.1) has been plotted as a function of the c.m. pion angle for incident photon energies of 280 Mev and 350 Mev. The experimental results are those of Lazarus et.al.[12], Tollestrup et.al.[13], Walker et.al.[14] and Schwille[15]. Fig.2 shows the energy dependence of the total cross section for $\gamma + p \longrightarrow n + \pi^+$. The experimental results shown are those of Tollestrup et.al[13], Walker et.al.[14] and Knapp et.al.[16].

In Fig.3, the c.m. differential cross sections for process (1.1.2) is plotted as a function of the c.m. pion angle for incident photon energies of 260 Mev and 320 Mev. The experimental results are those of Fischer et.al.[17], McDonald et.al.[18], Oakely et al.[19] and Miller et.al.[20].

---

12) A.J.Lazarus, W.K.H.Panofsky and F.R.Tangherlini, Phys.Rev.113, 1330 (1959).
13) A.V.Tollestrup, J.C.Keck and R.M.Worlock, Phys.Rev.99, 220 (1955).
14) R.L.Walker, J.G.Teasdale, V.Z.Peterson and J.I.Vette, Phys.Rev.99, 210 (1955).
15) W.J.Schwille, Ph.D.Thesis, University of Bonn. See D.Freytag, W.J.Schwille, and R.J.Wedemeyer, Z.Physik 186, 1 (1965).
16) E.A.Knapp, R.W.Kenney and V.Perez-Mendez, Phys.Rev. 114, 605 (1959).
17) G.Fischer, H.Fischer, G.Von Holtey, H.Kampen, G.Knop, P.Schutz, H.Wessels, W.Braunschweig, H.Genzel and R.Wedemeyer, Nucl.Phys. B16, 93 (1970).
18) W.S.McDonald, V.Z.Peterson, and D.R.Corson,Phys.Rev. 107, 577 (1957).
19) D.C.Oakely and R.L.Walker, Phys.Rev.97, 1283 (1955).
20) D.B.Miller and E.H.Bellamy, Proc.Phys.Soc.(London) 81, 343 (1963).

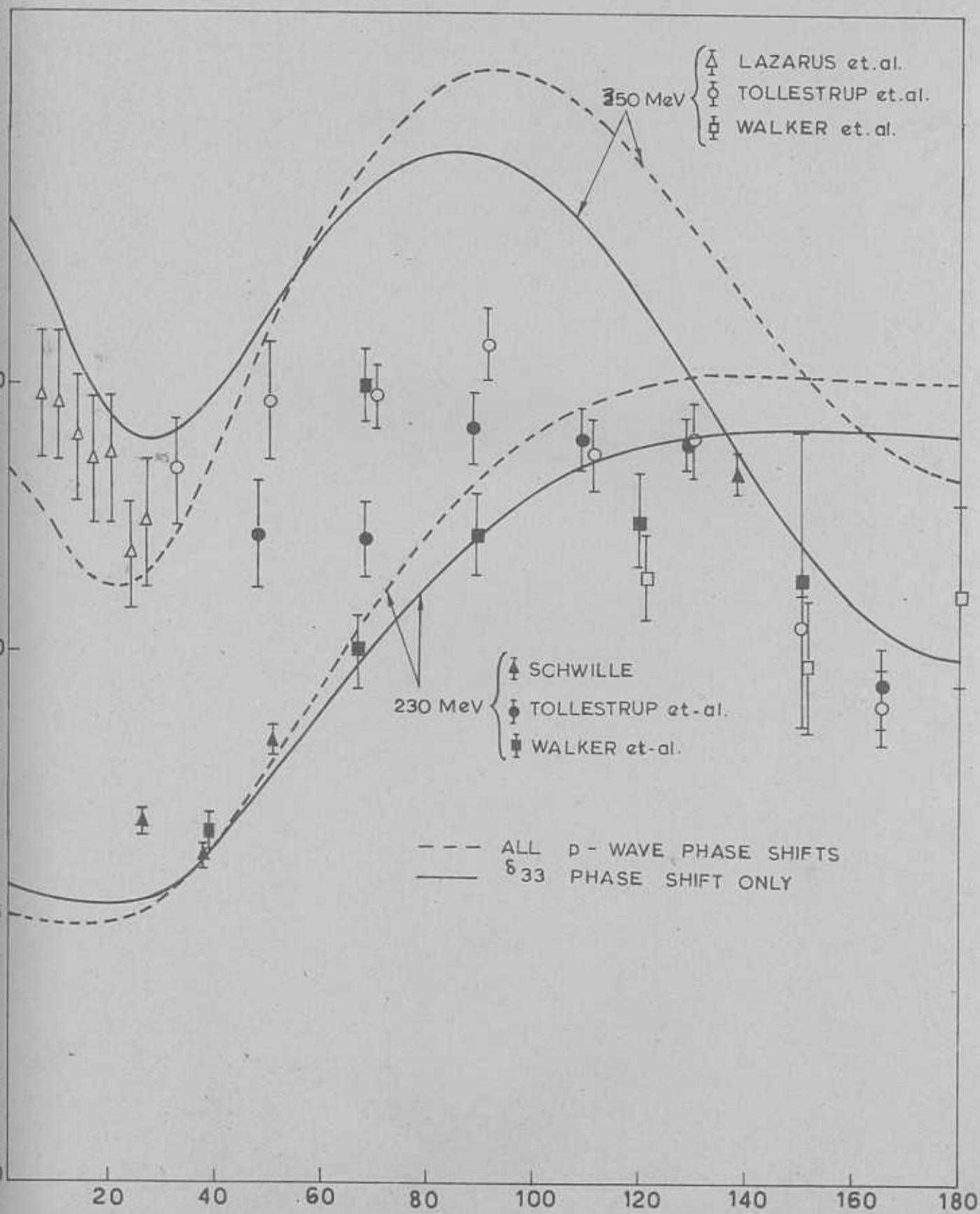

Fig.1: The center-of-mass differential cross section for $p(\gamma, \pi^+)n$.

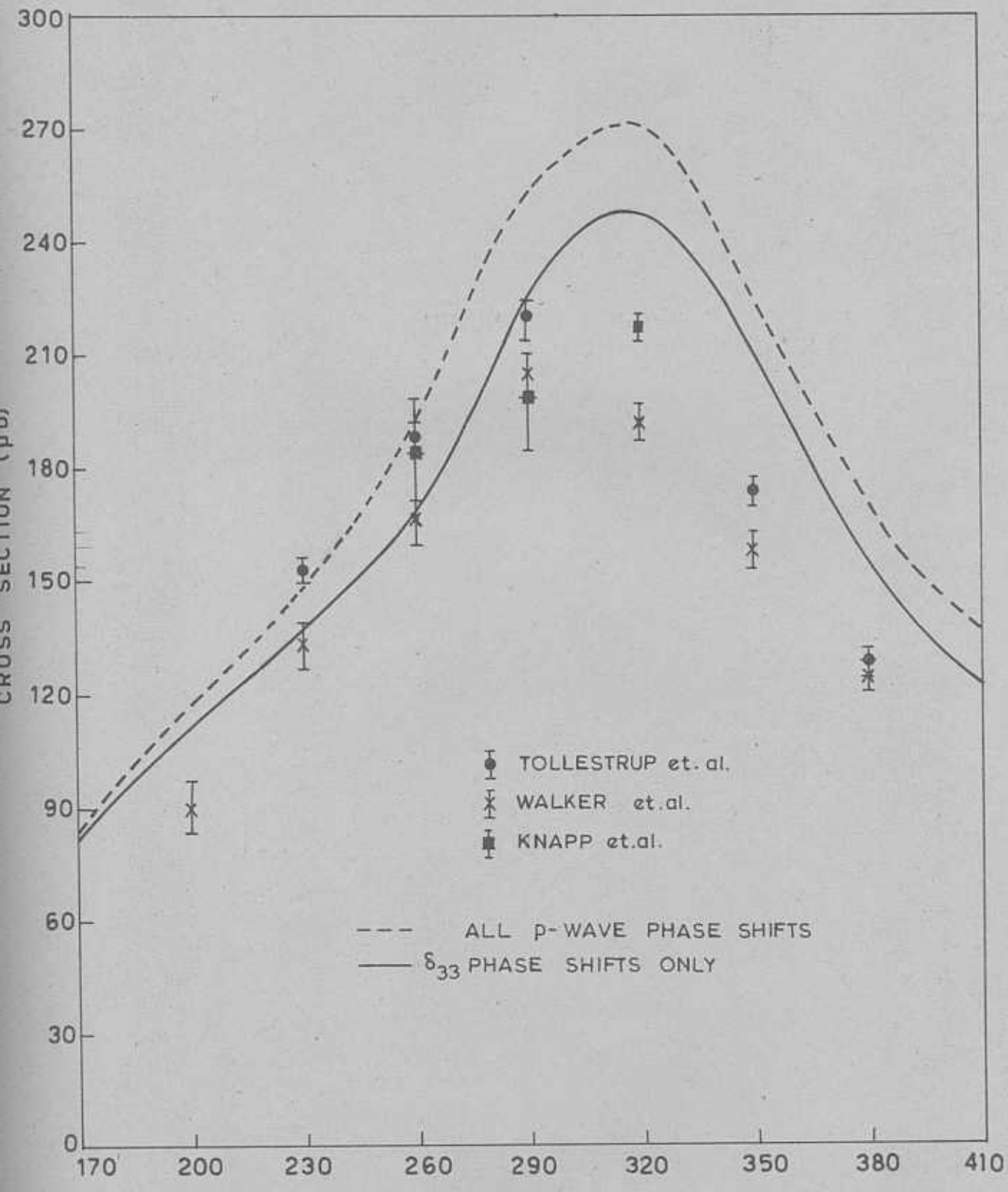

Fig.2. The energy dependence of the total cross section for $p(\gamma, \pi^+)n$.

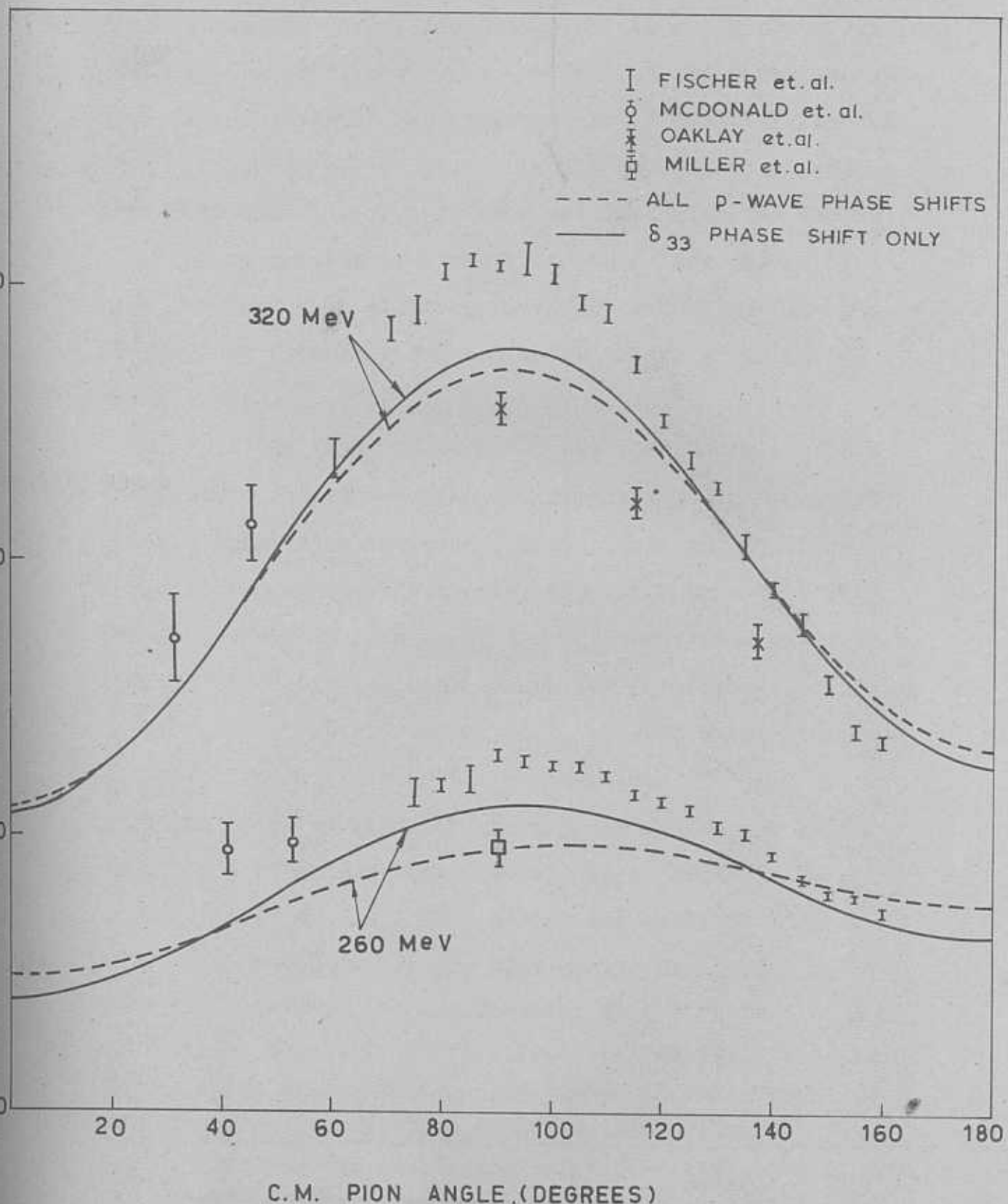

Fig.3. The center-of-mass differential cross section for $p(\gamma, \pi^0)p$.

Fig.4 shows the energy dependence of the total cross section for $\gamma+p \longrightarrow p+\pi^o$ and $\gamma+n \longrightarrow n+\pi^o$. The experimental results are those of Berkelman et.al.[21] and Vasil'kov et. al.[22] for $\gamma+p \longrightarrow p+\pi^o$. In all these four graphs, the solid line curves have been obtained with the dominant δ_{33} phase shift only while the dashed line curves have been obtained with all the p-wave phase shifts. The phase shifts used in the present calculation are given in Appendix A.

From the figures, we note that the theory of CGLN qualitatively describes the experimental photoproduction results throughout the energy region from threshold to about 400 Mev. Quantitatively, the total cross sections for $\gamma+p \longrightarrow p+\pi^o$ are in better agreement with experimental results[21,22] (Fig.4), than those for $\gamma+p \longrightarrow n+\pi^+$ (Fig.2). However, as Alvarez[23] points out, we should note that the results of most experimental measurements[13-16] of the absolute cross section for the process $\gamma+p \longrightarrow n+\pi^+$ begin to diverge and this discrepancy is known to be particularly large near 300 Mev, especially at large angles.

Having found that the CGLN amplitudes give a fairly good fit with experimental results, from threshold upto 400 Mev, we assure ourselves about the reliability of using these as the single nucleon amplitudes in our further studies of photoproduction of pions from nuclei.

---

21) K.Berkelman and J.A.Waggoner, Phys.Rev.117, 1364 (1960).
22) R.G.Vasil'kov, B.B.Govorkov and V.I.Gol'danski, JETP 10, 7 (1960).
23) R.A.Alvarez, Phys.Rev.142, 957 (1966).

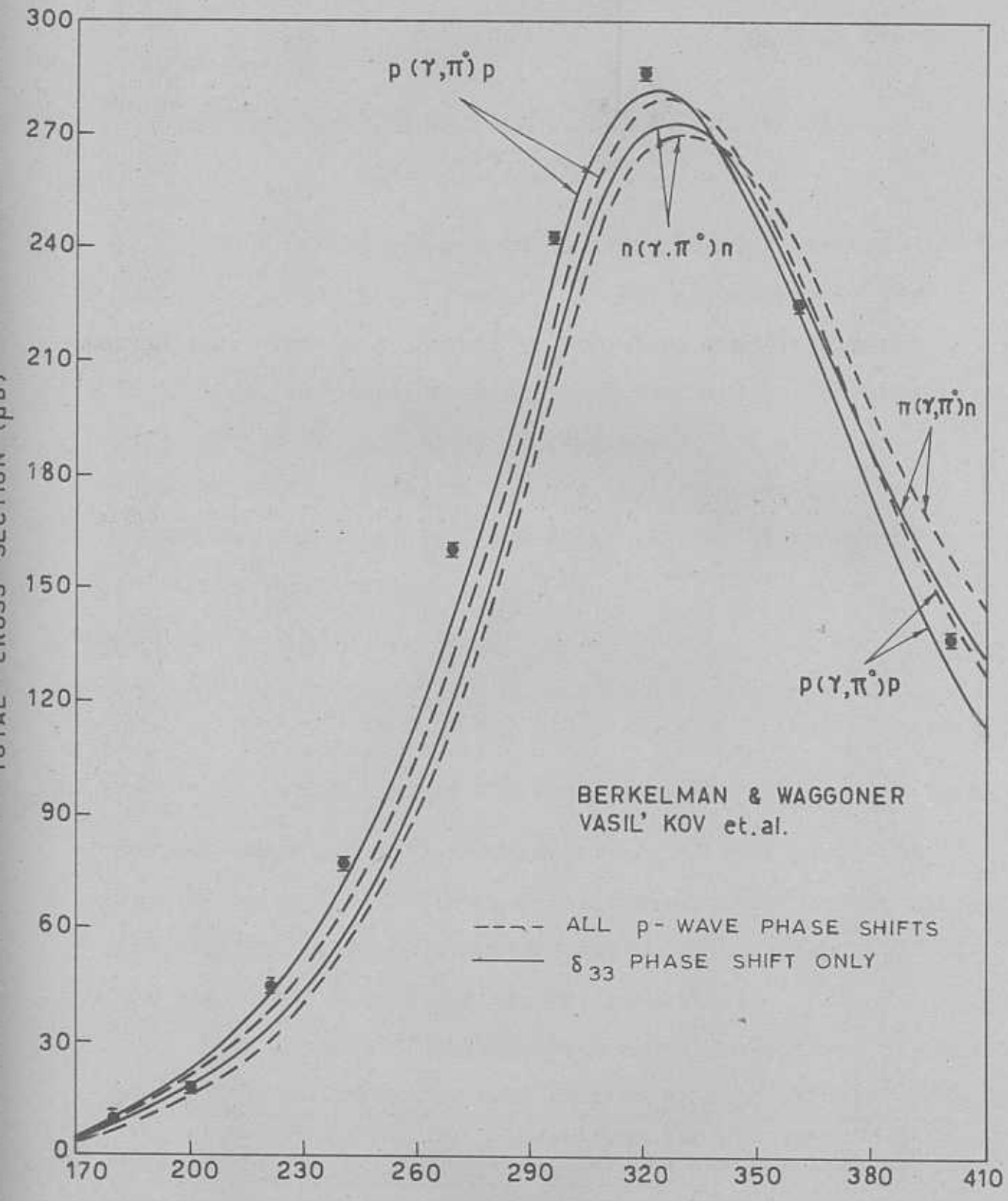

Fig.4. The energy dependence of the total cross section for $p(\gamma,\pi^0)p$ and $n(\gamma,\pi^0)n$.

CHAPTER 2

PHOTOPRODUCTION OF NEUTRAL PIONS+ AND CHARGED PIONS FROM DEUTERONS++

1. Most of the studies on phenomenological nucleon-nucleon potentials are used to fit the properties of the deuteron. For this reason, it is interesting to obtain theoretical information about the deuteron wave function from, for example, a study of photoproduction of pions from deuterons. Here, we use the deuteron wave functions of Hulthen and Sugawara[1] and Reid[2] in our study of the following reactions:

$$\gamma + D \longrightarrow D + \pi^0 , \qquad (2.1.1)$$

$$\gamma + D \longrightarrow n + n + \pi^+ , \qquad (2.1.2)$$

$$\gamma + D \longrightarrow p + p + \pi^- . \qquad (2.1.3)$$

The hard-core and soft-core potentials of Reid yield the properties of the deuteron, in particular, the binding energy, the electric quadrupole moment, the D-state probability and the asymptotic D to S wave ratio, accurately.

The process of photoproduction of neutral and charged pions from deuterium has been studied by many authors[3], based

+ K.Ananthanarayanan and K.Srinivasa Rao, Nuo.Cimento 44, 31 (1966)
++ K.Srinivasa Rao, R.Parthasarathy and V.Devanathan, to be submitted to Nuo.Cimento.

1) L.Hulthen and M.Sugawara, Hand buch der Physik 39, 1 (1957).
2) R.V.Reid Jr., Ann.Phys. 50, 411 (1968).
3) G.F.Chew and H.W.Lewis, Phys.Rev. 84, 779 (1951);
W.Lax and H.Feshbach, Phys.Rev. 88, 509 (1952);
Y.Saito, Y.Watanabe and Y.Yamaguchi, Prog.Theor.Phys. 7, 103 (1952);
J.Chappelear, Phys.Rev. 99, 254 (1955).

on the impulse approximation (Appendix.B) using a phenomenological approach, assuming the single nucleon photoproduction transition operator to be of the form ($\underline{\sigma}.\underline{K}+L$), where $\underline{K}$ and L represent the spin-dependent and spin-independent parts of the amplitude. In these calculations, the explicit forms of $\underline{K}$ and L were not considered, since these calculations were performed before the advent of the CGLN amplitudes. More recently, expressions for the differential cross section were derived for photoproduction of neutral[4] and charged[5] pions, using the impulse approximation and the CGLN amplitudes. Ericson and Schaerf[6] studied the process of photoproduction of neutral pions from deuterons at an incident photon energy of 500 Mev and found that a D-state admixture of

$$P_D = (7.5 \pm 0.6)\ \%$$

had to be assumed to fit their experimental data. Here, we analyse the differential and total cross sections for neutral and charged pion photoproduction from the deuteron, for lower incident photon energies for which the effects of the second pion-nucleon resonance can be more reasonably neglected, in the impulse approximation using the CGLN amplitudes and deuteron radial wave functions[1,2] which

---

4) Alladi Ramakrishnan, V.Devanathan and G.Ramachandran, Nucl.Phys. 24, 163 (1961).

5a) V.Devanathan and G.Ramachandran, Nucl.Phys.23, 312(1961).

5b) V.Devanathan and K.Ananthanarayanan,Nuo.Cimento 32,723(1964).

6) B.F.Ericson and C.Schaerf, Phys.Rev.Letts. 11, 432 (1963).

depend upon the D-state admixture (^{p}D), the hard-core radius (r_c) and the triplet effective range (ρ).

2. The existence of a small but finite quadrupole moment for the deuteron shown by Rabi and co-workers[7] and the deviation of the deuteron magnetic moment from the simple sum of the proton and neutron magnetic moments can be accounted for by assuming that the force between the neutron and proton is partly central and partly due to a non-central, tensor, force. The very existence of a non-central force implies that the ground state of the deuteron can no longer be regarded as a pure S-state (L=0, S=1, J=1) and that there is a D-state (L=2, S=1, J=1) admixture in the ground state of the deuteron. It should be noted that parity conservation does not allow the admixture of even and odd orbital angular momentum states and hence we have to choose a linear combination of S and D states for the ground state of the deuteron.

The Generalized Pauli principle requires the antisymmetry of the overall wave function with respect to the interchange of nucleons. Therefore, the ground state wave function of the deuteron can be written as:

$$\Psi_M^{(J=1)} = \frac{(2\pi)^{-3/2}}{r} \eta_0(1,2) \left[u(r)\, Y_0^0(\hat{r})\, {}^3\chi_M(1,2) + \right.$$

$$\left. + \sum_{M'} C(121; M', M-M', M)\, Y^2_{M-M'}(\hat{r})\, {}^3\chi_{M'}(1,2) \right], \qquad (2.2.1)$$

---

7) J.M.B.Kellogg, I.I.Rabi, N.F.Ramsey Jr., and J.R.Zacharias, Phys.Rev. 55, 318 (1939); ibid 57, 677 (1940).

where ${}^3\chi_M$ denotes the triplet spin eigon functions, $Y_m^\ell(\hat{r})$ denotes the normalized spherical harmonic which is the orbital angular momentum eigen function with $\hat{r} = r/|r|$, $\eta_o(1,2) = \frac{1}{\sqrt{2}}[p(1)n(2) - p(2)n(1)]$ denotes the isosinglet part, and u(r) and w(r) are, respectively, the S-and D-state radial wave functions with the normalization condition:

$$\int_0^\infty [u^2(r) + w^2(r)]\, dr = 1 . \qquad (2.2.2)$$

The Hulthen-Sugawara wave function:

Phenomenological deuteron wave functions have been constructed by Hulthen and Sugawara[1], assuming suitable functional forms containing several parameters and adjusting these so as to fit the existing empirical information on the neutron-proton system. The empirical facts which can be used for this purpose are the deuteron binding energy E, the quadrupole moment Q, the D-state probability P_D and, in addition, the deuteron effective range[8], $\rho(-E,-E)$. The deuteron binding energy is used to determine the correct asymptotic behaviour. They assume the following empirical values of the deuteron constants:

$$E = 2.226 \text{ Mev}, \qquad (2.2.3)$$

$$Q = 2.738 \times 10^{-27} \text{cm}^2, \qquad (2.2.4)$$

$$P_D = 3\%, 4\%, 5\% , \qquad (2.2.5)$$

and the following two values of $\rho(-E, -E)$:

$$\rho(-E, -E) = 1.704 \text{ fm. and } 1.734 \text{ fm.} \qquad (2.2.6)$$

---

8) H.A.Bethe, Phys.Rev. 76, 41 (1949).

This is all the empirical information which can be extracted from the low energy data. With regard to the high energy data they allow the possibility for a hard core radius to be introduced, which they fix as:

$$x_c \equiv \alpha r_c = 0,\ 0.10,\ 0.13,$$
$$r_c = 0,\ 0.4316\ \text{fm},\ 0.561\ \text{fm} \qquad (2.2.7)$$

where, for the sake of convenience, $x \equiv \alpha r$ is introduced as a unit of length with $\alpha^{-1} = 0.4316$ fm being the deuteron radius for E = 2.226 Mev.

As a simple, but reasonable example, Hulthen and Sugawara assume the following functional forms for the radial wave functions:

$$u(x) = N \cos\epsilon_g \left[1 - e^{-\beta(x-x_c)}\right] e^{-x},$$

$$w(x) = N \sin\epsilon_g \left[1 - e^{-\gamma(x-x_c)}\right] e^{-x} \cdot$$

$$\cdot \left\{1 + \frac{3}{x}(1-e^{-\gamma x}) + \frac{3}{x^2}(1-e^{-\gamma x})^2\right\} \quad \text{for} \quad x = \alpha r \geq x_c ,$$

$$u(x) = w(x) = 0 \quad \text{for} \quad x < x_c , \qquad (2.2.8)$$

where ϵ_g is the mixing parameter in the deuteron ground state and the normalization factor N is given by:

$$N^2 = \frac{2}{1 - \alpha\rho(-E,-E)} = \begin{matrix} 3.0347 \text{ for } \rho = 1.704 \text{ fm} \\ 3.3433 \text{ for } \rho = 1.734 \text{ fm.} \end{matrix} \qquad (2.2.9)$$

In table.1 are given the values of the parameters β , γ and

Table.1

The parameters in the deuteron radial wave functions, Eq.(2.2.8), fitted to all the triplet low energy data[+] and a hard core radius r_c, are given below:

r_c (fm.)	ρ (fm.)	P_D (%)	β	γ	$\sin \epsilon_g$
0.0	1.704	3	4.860	2.494	0.03232
		4	4.751	2.922	0.02928
		5	4.647	3.275	0.02754
	1.734	3	4.741	2.505	0.03192
		4	4.637	2.936	0.02891
		5	4.536	3.289	0.02720
0.4316	1.704	3	8.237	3.155	0.02942
		4	7.961	3.798	0.02666
		5	7.699	4.346	0.02514
	1.734	3	7.933	3.175	0.02901
		4	7.675	3.814	0.02634
		5	7.431	4.364	0.02487
0.561	1.704	3	10.223	3.413	0.02873
		4	9.814	4.144	0.02611
		5	9.433	4.771	0.02471
	1.734	3	9.774	3.436	0.02832
		4	9.397	4.170	0.02577
		5	9.045	4.799	0.02438

[+]Numerical calculation of L.T.Hedin and P.H.L.Conde[9].

sin ϵ_g , obtained from a numerical calculation by Hedin and Conde[9] for various values of x_c, P_D, and ϱ . It has been observed by Hulthen and Sugawara[1] that among the three quantities ϱ , P_D and x_c, the ambiguity arising from is a minor one, while the latter two give rise to big uncertainties in the deuteron wave functions, especially at smaller distances. Further, there is a certain arbitrariness in the particular functional forms chosen for u(x) and w(x), Eq.(2.2.8), by Hulthen and Sugawara.

Reid wave functions:-

Recently, Reid[2] has used local and static phenomenological nucleon-nucleon (NN) hard (infinitely hard) and soft (Yukawa) core potentials to fit Yale and Livermore phase parameters and low energy data. Using a better approach than that of Hamada[10], - who employed the integration method to solve the well-known[1,10] coupled equations for S and D radial wave functions of the deuteron - Reid has calculated the properties of the deuteron - in particular, the quadrupole moment, D-state probability and the asymptotic D to S wave ratio - with his NN potentials. These are summarized in table.2 along with the predicted binding energy of the deuteron, effective range and scattering lengths for his potentials. A comparison of his results with the well-

9) L.T.Hedin and P.H.L. Conde, Reference (1), p.92.
10) T.Hamada, Prog.Theor.Phys. 24, 126 (1960).

Table.2

Triplet effective-range parameters and deuteron properties

Potential	a_t	$\varrho(-E,-E)$	Deuteron properties			
			B.E.(Mev)	$Q(fm^2)$	$P_D(\%)$	A_D/A_S
Reid(HC)	5.397	1.724	2.22464	0.27700	6.4970	0.025900
Reid(SC)	5.390	1.720	2.22460	0.27964	6.4696	0.026223
Experimental	5.396	1.726	2.22452	0.278	4.0-7.0	0.026

established experimental results (also shown in table.2) clearly reveals that his hard-core (Hc) and sof-core(Sc) potentials yield the deuteron properties within the accuracy to which they are known. Reid's hard-core and soft-core deuteron wave functions are given in table.3.

3. NEUTRAL PION PHOTOPRODUCTION FROM DEUTERON:

The matrix element of the transition amplitude for the photoproduction of neutral pions from deuterons in the impulse approximation can be written as follows:

$$\langle f | T | i \rangle = \langle f | \sum_{j=1,2} t_j \exp(i \underline{k} \cdot \underline{r}_j) | i \rangle, \qquad (2.3.1)^{+}$$

where $\underline{k} = \underline{\nu} - \underline{\mu}$ is the momentum transfer, $\underline{\nu}$ being the momentum of the incident photon and $\underline{\mu}$ that of the outgoing pion, $\underline{r}_j$ is the position vector of the j-th nucleon, and $|i\rangle$ and $|f\rangle$, the initial and final states of the deuteron, are given by

$$| i \rangle = \Psi_M \qquad (2.3.2)$$

$$| f \rangle = \Psi_{M'} . \exp(i\underline{K}.\underline{R}) \qquad (2.3.3)$$

where Ψ_M is given by (2.2.2) and $\underline{R} = \frac{1}{2}(\underline{r}_1 + \underline{r}_2)$. The single nucleon amplitude t_j for the neutral pion photoproduction can be written in the iso-spin space as:

+ We apologize for using i in two different senses in this expression: i is used to denote both the initial state, $|i\rangle$, and to denote the value $\sqrt{-1}$ in $\exp(i\underline{k}.\underline{r}_j)$.

Table.3

Deuteron wave functions of Reid[+]

Hard Core			Soft Core		
x	u(x)	w(x)	x	u(x)	w(x)
3.83830 -1	0.0	0.0	1.000 -2	0.0	0.0
4.46330 -1	1.2676 -1	5.9692 -2	4.125 -2	3.3373 -5	1.0850 -5
5.08830 -1	2.3528 -1	1.0804 -1	7.250 -2	2.3901 -4	8.4073 -5
5.71330 -1	3.2091 -1	1.4290 -1	1.350 -1	2.7621 -3	1.0369 -3
6.33830 -1	3.8556 -1	1.6615 -1	1.975 -1	1.2737 -2	4.9642 -3
7.58830 -1	4.6726 -1	1.8845 -1	2.600 -1	3.6062 -2	1.4446 -2
8.83830 -1	5.0777 -1	1.9205 -1	3.225 -1	7.5359 -2	3.0795 -2
1.00883 0	5.2478 -1	1.8663 -1	3.850 -1	1.2847 -1	5.3157 -2
1.13383 0	5.2827 -1	1.7705 -1	4.475 -1	1.8993 -1	7.8995 -2
1.25883 0	5.2376 -1	1.6575 -1	5.100 -1	2.5349 -1	1.0525 -1
1.38383 0	5.1441 -1	1.5397 -1	5.725 -1	3.1390 -1	1.2933 -1
1.63383 0	4.8801 -1	1.3123 -1	6.350 -1	3.6770 -1	1.4958 -1
1.88383 0	4.5719 -1	1.1102 -1	6.975 -1	4.1317 -1	1.6529 -1
2.38383 0	3.9436 -1	7.9259 -2	7.600 -1	4.4992 -1	1.7645 -1
2.88383 0	3.3672 -1	5.7106 -2	8.850 -1	4.9953 -1	1.8710 -1
3.38383 0	2.8636 -1	4.1749 -2	1.010 0	5.2406 -1	1.8654 -1
3.88383 0	2.4310 -1	3.1002 -2	1.135 0	5.3166 -1	1.7946 -1

(continued on next page)

Table.3(continued)

Hard Core			Soft Core		
x	u(x)	w(x)	x	u(x)	w(x)
4.38383 0	2.0620 -1	2.3366 -2	1.260 0	5.2864 -1	1.6910 -1
4.88383 0	1.7484 -1	1.7851 -2	1.385 0	5.1926 -1	1.5742 -1
5.38383 0	1.4821 -1	1.3802 -2	1.510 0	5.0621 -1	1.4553 -1
5.88383 0	1.2563 -1	1.0783 -2	1.760 0	4.7505 -1	1.2314 -1
6.38383 0	1.0648 -1	8.5013 -3	2.010 0	4.4200 -1	1.0373 -1
7.38383 0	7.6489 -2	5.4035 -3	2.510 0	3.7864 -1	7.3859 -2
8.38383 0	5.4943 -2	3.5156 -3	3.010 0	3.2249 -1	5.3293 -2
9.38383 0	3.9465 -2	2.3277 -3	3.510 0	2.7399 -1	3.9077 -2
			4.010 0	2.3251 -1	2.9115 -2
			4.510 0	1.9719 -1	2.2016 -2
			5.010 0	1.6718 -1	1.6871 -2
			5.510 0	1.4172 -1	1.3079 -2
			6.010 0	1.2012 -1	1.0243 -2
			7.010 0	8.6290 -2	6.4412 -3
			8.010 0	6.1983 -2	4.1575 -3
			9.010 0	4.4523 -2	2.7363 -3

+Each entry is followed by its exponent to the base 10.

$$t = t_p\left(\frac{1+\tau_z}{2}\right) - t_n\left(\frac{1-\tau_z}{2}\right)$$

$$= \frac{1}{2}(t_p + t_n) + \frac{1}{2}(t_p - t_n)\tau_z \,, \qquad (2.3.4)$$

where t_p and t_n are the amplitudes for the process $\gamma + p \longrightarrow p + \pi^0$ and $\gamma + n \longrightarrow n + \pi^0$, respectively.

Using the antisymmetry of $|i\rangle$ and $|f\rangle$ for the simultaneous interchange of the nucleon indices in all the spin, isospin and configuration spaces, we can write (2.3.1) as

$$\langle f \mid T \mid i \rangle = 2 \langle f \mid t_2 \exp(i\underline{k}.\underline{r}_2) \mid i \rangle \qquad (2.3.5)$$

Noting the vanishing of the matrix element of τ_z between states of zero isospin, we have

$$\langle f \mid T \mid i \rangle = \langle f \mid (t_p(2)+t_n(2)) \exp(i\underline{k}.\underline{r}_2) \mid i \rangle \qquad (2.3.6)$$

Using the expression (2.3.2) and (2.3.3) for $|i\rangle$ and $|f\rangle$ and the following Rayleigh expansion:

$$\exp(i\underline{k}\cdot\underline{r}) = 4\pi \sum_{\ell=0}^{\infty} \sum_{m=-\ell}^{+\ell} i^{\ell} (-1)^m Y_m^{\ell}(\hat{k}) Y_{-m}^{\ell}(\hat{r})\, j_{\ell}(kr), \qquad (2.3.7)$$

we have for the matrix element (2.3.6):

$$\langle f \mid T \mid i \rangle = \langle \Psi_{M'} \mid (t_p(2) + t_n(2)) \exp(i\,\underline{k}\cdot(\underline{r}_2 - \underline{R})) \mid \Psi_M \rangle$$

$$= \langle \Psi_{M'} \mid (t_p(2) + t_n(2)) \exp(-\tfrac{i}{2}\,\underline{k}\cdot\underline{r}) \mid \Psi_M \rangle$$

$$= F_{SS}\, t_M^{M'} - F_{SD} \sum_{m_2} C(121; m_2, M-m_2, M)\, Y^2_{M-m_2}(\hat{k})\, t^{M'}_{m_2} +$$

$$+ F_{SD} \sum_{m_2} C(121; m_2, M'-m_2, M')\, Y^2_{M'-m_2}(\hat{k})\, t^{M}_{m_2} +$$

$$+ F_{DD} \sum_{m_2} C(121; m_2, M-m_2, M)\, C(121; m_2, M'-m_2, M')\, t^{M'-M+m_2}_{m_2}\,, \tag{2.3.8}$$

where $r = r_1 - r_2$,

$$F_{SS} = \int_0^\infty u^2(r)\, j_0(\tfrac{1}{2}kr)\, dr, \tag{2.3.9}$$

$$F_{SD} = \int_0^\infty u(r)\, w(r)\, j_2(\tfrac{1}{2}kr)\, dr, \tag{2.3.10}$$

$$F_{DD} = \int_0^\infty w^2(r)\, j_0(\tfrac{1}{2}kr)\, dr, \tag{2.3.11}$$

$$t_M^{M'} = \langle {}^3\chi_{M'} |\, (t_p(2) + t_n(2)) \,|\, {}^3\chi_M \rangle . \tag{2.3.12}$$

and $\hat{k} = \underline{k} / |\underline{k}|$. Here, we have omitted the terms proportional to the negligible elements $\int_0^\infty w^2(r)\, j_\ell(\tfrac{1}{2}kr)dr$ for $\ell = 2$ and $\ell = 4$.

The integrals F_{SS}, F_{SD} and F_{DD} were evaluated numerically taking for the radial wave functions u(r) and w(r) the expressions given in (2.2.6), for various values of the parameters x_c, P_D and β.

In Table.4 we give the values of F_{SS}, F_{SD} and F_{DD} for a set of values of k. From Table.2 it is clear that, for both the Hulthen-Sugawara and Reid wave functions F_{SD} and F_{DD} are small when compared with F_{SS}, so that the error involved in neglecting the terms containing F_{SD} and F_{DD} will be very small. Thus the effect of the D-state admixture is taken into account only in the normalization and the scale of the S-state wave function. In Fig.1, we have plotted the Hulthen-Sugawara and Reid(HC) S-state radial wave functions along with $j_o(\frac{1}{2}kr)$ for $k = 2fm^{-1}$. We notice that while there is complete overlap between Hulthen-Sugawara wave function and $j_o(r)$, the Reid wave function has a lesser overlap with $j_o(r)$. This accounts for F_{SS} being much smaller in the case of the Reid wave function as can be seen from table.4.

Therefore, neglecting the terms containing F_{SD} and F_{DD} in (2.3.8), we have

$$\langle f | T | i \rangle = \langle {}^3\chi_{M'} | (t_p(2) + t_n(2)) | {}^3\chi_M \rangle F_{SS} . \qquad (2.3.13)$$

Using the CGLN amplitudes (1.2.2) and (1.2.3) we can write

$$t_p(2) + t_n(2) = i\, \underline{\sigma}.\underline{K} + L , \qquad (2.3.14)$$

where

$$\underline{K} = \frac{4\pi e f}{\sqrt{\mu_o \nu_o}} \left[\underline{\mu} \times (\underline{\nu} \times \underline{\epsilon}) \lambda \eta^{+-} + \frac{(\underline{\mu}\cdot\underline{\epsilon})\underline{\mu}}{2M\mu_o} \right] , \qquad (2.3.15)$$

Table.4

The nuclear form factors for deuteron as a function of the momentum transfer k, in the centre-of-momentum system are given here. The Hulthen and Sugawara wave functions correspond to the set of parameters $P_D = 3\%$, $r_c = 0$ and $\varrho = 1.704$ fm.

	k (fm^{-1})	F_{SS}	F_{SD}	F_{DD}
Hulthen-Sugawara wave functions	0.191	0.9482	0.2994×10^{-1}	0.3084×10^{-3}
	1.037	0.5891	-0.3256×10^{-2}	0.2079×10^{-4}
	1.454	0.4012	-0.2767×10^{-2}	0.149×10^{-4}
	2.048	0.2705	-0.2016×10^{-2}	0.837×10^{-5}

	k (fm^{-1})	Soft-core	Hard-core		
		F_{SS}	F_{SS}	F_{SD}	F_{DD}
Reid wave functions	0.1976	0.62992	0.63651	0.9083×10^{-3}	0.4501×10^{-1}
	1.0388	0.37574	0.38094	0.1593×10^{-1}	0.3609×10^{-1}
	1.6825	0.20997	0.21471	0.2506×10^{-1}	0.2636×10^{-1}
	2.0492	0.14550	0.15034	0.2766×10^{-1}	0.2114×10^{-1}

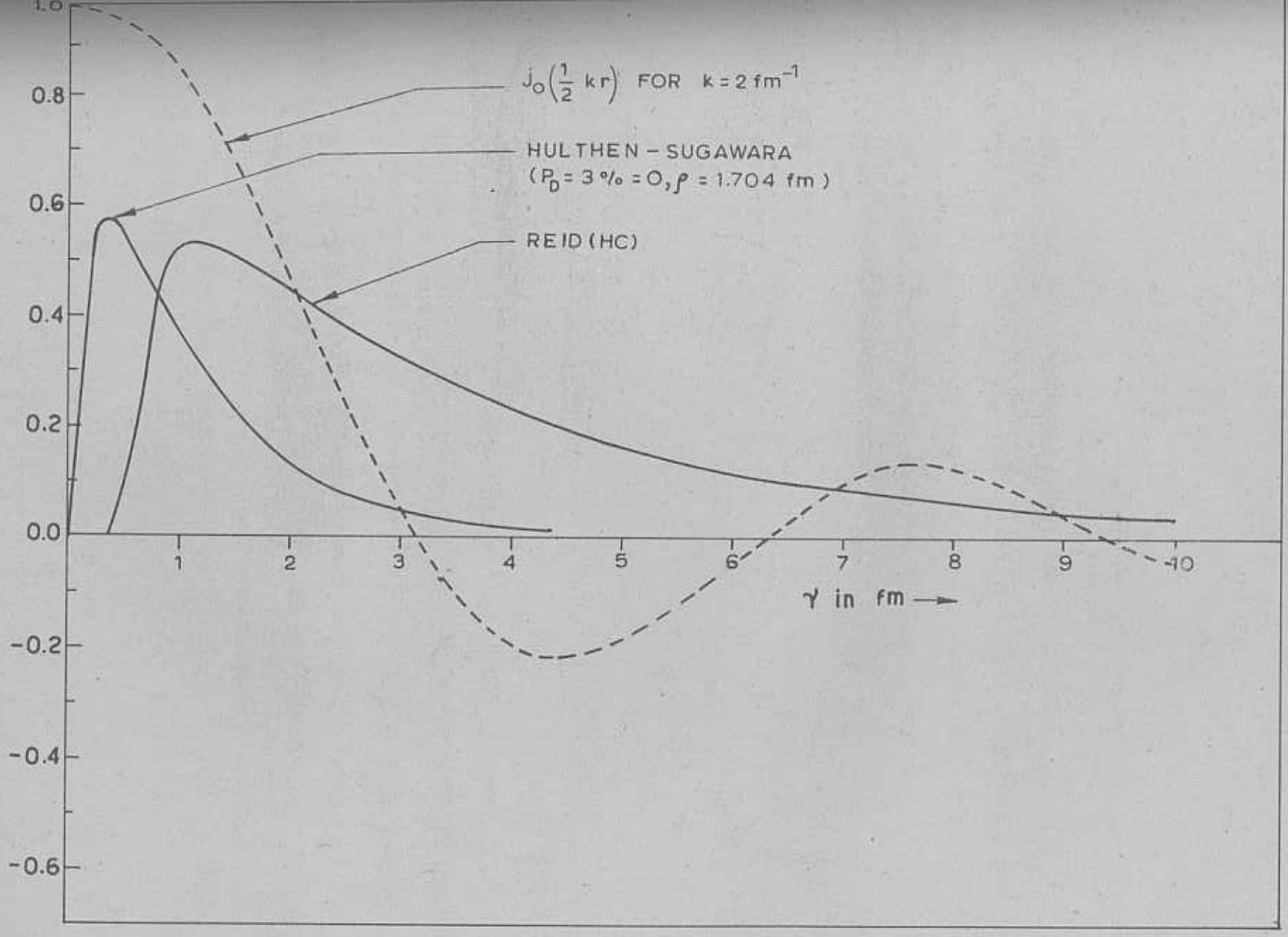

Fig.1. Hulthen-Sugawara and Reid (HC) S-state radial wave functions along with $j_0(\frac{1}{2}kr)$ for $k = 2\ fm^{-1}$.

and

$$L = \frac{4\pi e f}{\sqrt{\mu_0 \nu_0}} \underline{\mu} \cdot (\underline{\nu} \times \underline{\epsilon}) \lambda h^{++}. \qquad (2.3.16)$$

All the symbols which occur in (2.3.15) and (2.3.16) have been explained in section 2. of Chapter.1. We take the small phase shifts δ_{11} and δ_{13} (= δ_{13}) also into account.

Squaring, summing over final states and averaging over the initial spin states and the incident photon polarizations we obtain

$$|Q|^2 = \frac{1}{6} \sum_{M, M', \epsilon} |\langle f | T | i \rangle|^2$$

$$= \frac{16\pi^2 e^2 f^2}{\mu_0 \nu_0} \left[\mu^2 \lambda^2 \nu^2 \{ (1+\cos^2\theta) |h^{+-}|^2 + \right.$$

$$\left. + \tfrac{3}{2} \sin^2\theta |h^{++}|^2 + \frac{\mu^4 \sin^2\theta}{2M^2 \mu_0^2 \nu^2} \right] |F_{SS}|^2. \qquad (2.3.17)$$

If we make the justifiable assumption that the recoil deuteron receives only momentum but no appreciable energy, the differential cross section can be written as:

$$\frac{d\sigma}{d\Omega} = (2\pi)^{-2} \mu \mu_0 |Q|^2. \qquad (2.3.18)$$

Though F_{SD} and F_{DD} are neglected, the D-state probability exhibits itself through F_{SS}.

As the recoil energy is less in the centre-of-momentum system, the static model calculation for $d\sigma/d\Omega$ is done in the centre-of-momentum system and then the cross section is transformed to the laboratory system using the well-known transformation[11]:

$$\left(\frac{d\sigma}{d\Omega}\right)_{Lab} = \frac{(1+\gamma^2+\gamma\cos\theta)^{3/2}}{1+\gamma\cos\theta}\left(\frac{d\sigma}{d\Omega}\right)_{c.m.} \qquad (2.3.19)$$

where θ is the centre-of-momentum scattering angle and $\gamma = m_\pi / M$. The scattering angle θ_{lab} in the laboratory system is related to $\theta_{c.m.}$ by the following relation:

$$\tan\theta_{lab} = \frac{\sin\theta_{c.m.}}{\gamma+\cos\theta_{c.m.}} . \qquad (2.3.20)$$

Numerical calculations have been made for the differential cross section for neutral pion photoproduction from deuteron for various incident photon energies using the Hulthen-Sugawara and Reid wave functions. Some of the results for the differential cross sections for the reaction (2.1.1) at the photon energy of 280 Mev, using (2.3.18), obtained with the Hulthen-Sugawara wave functions, are presented in Figs.2, 3 and 4 along with the experimental results of Davis and Corson[12] and Rosengren and Baron[13], while the results

11) L.I.Schiff, "Quantum mechanics", McGraw-Hill Book Company, Inc.(1955), p.99.
12) H.L.Davis and D.R.Corson, Phys.Rev.99, 273 (1955).
13) J.W.Rosengren and N.Baron, Phys.Rev. 101, 410 (1956).

obtained with Reid wave functions are plotted in Figs.5,6 and 7.

In Fig.2, $(d\sigma/d\Omega)_{Lab}$ is plotted against θ_{Lab} for $P_D = 0\%$, 3%, 4% and 5%, $x_c = 0 (r_c = 0)$ and $\rho = 1.704$ fm. We notice that the differential cross section is in better agreement with experimental results for $P_D = 5\%$ than for $P_D = 0\%$, 3% and 4%.

In Fig.3, $(d\sigma/d\Omega)_{Lab}$ is plotted against θ_{Lab} for $P_D = 5\%$, $x_c = 0$, 0.1 and 0.13 ($r_c = 0$, 0.4136 fm. and 0.561 fm) and $\rho = 1.704$ fm. We observe that the differential cross section is in better agreement with experimental results for $r_c = 0.561$ fm. than for $r_c = 0$ or 0.4316 fm.

In Fig.4, $(d\sigma/d\Omega)_{Lab}$ is plotted against θ_{Lab} for $P_D = 5\%$, $x_c = 0.13$ ($r_c = 0.561$ fm) and $\rho = 1.704$ fm and 1.734 fm. We find that the cross section is in better agreement with experimental results for $\rho = 1.734$ fm. than for $\rho = 1.704$ fm. For the sake of comparison the cross section for $P_D = r_c = 0$ and $\rho = 1.734$ fm. is also plotted in this figure.

From Figs.2,3 and 4 we conclude that while the Hulthen-Sugawara wave function for the deuteron, which includes D-state admixture and hard-core radius, decreases the cross section at all angles, the agreement with experimental results is better at backward angles.

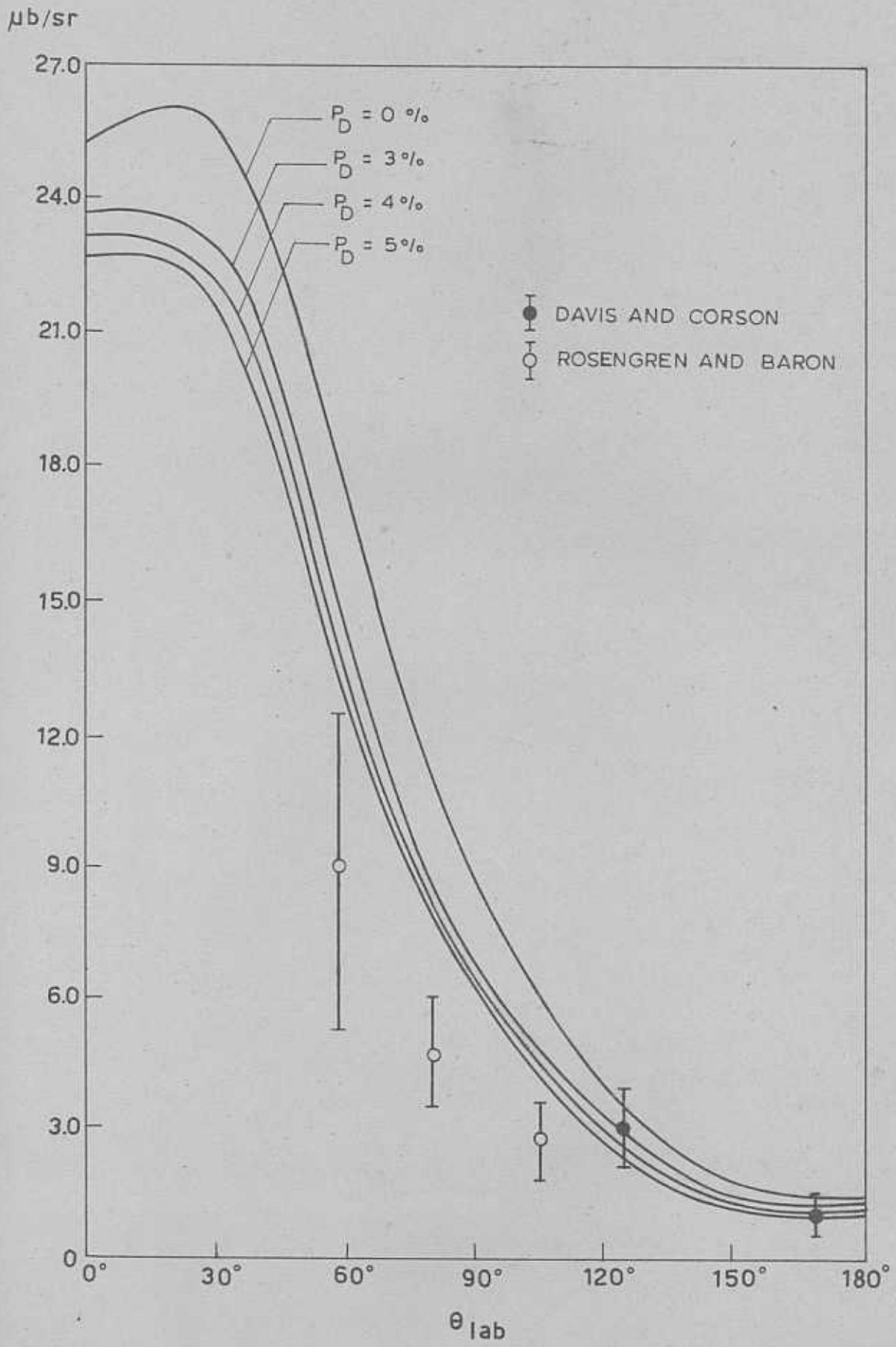

FIG.2. $\left(\frac{d\sigma}{d\Omega}\right)_{lab}$ For $\gamma + D \longrightarrow D + \pi^o$ At $E_\gamma^{lab} = 280$ meV with $\rho = 1.704 \times 10^{-13}$ cm; $\chi_c = 0$.

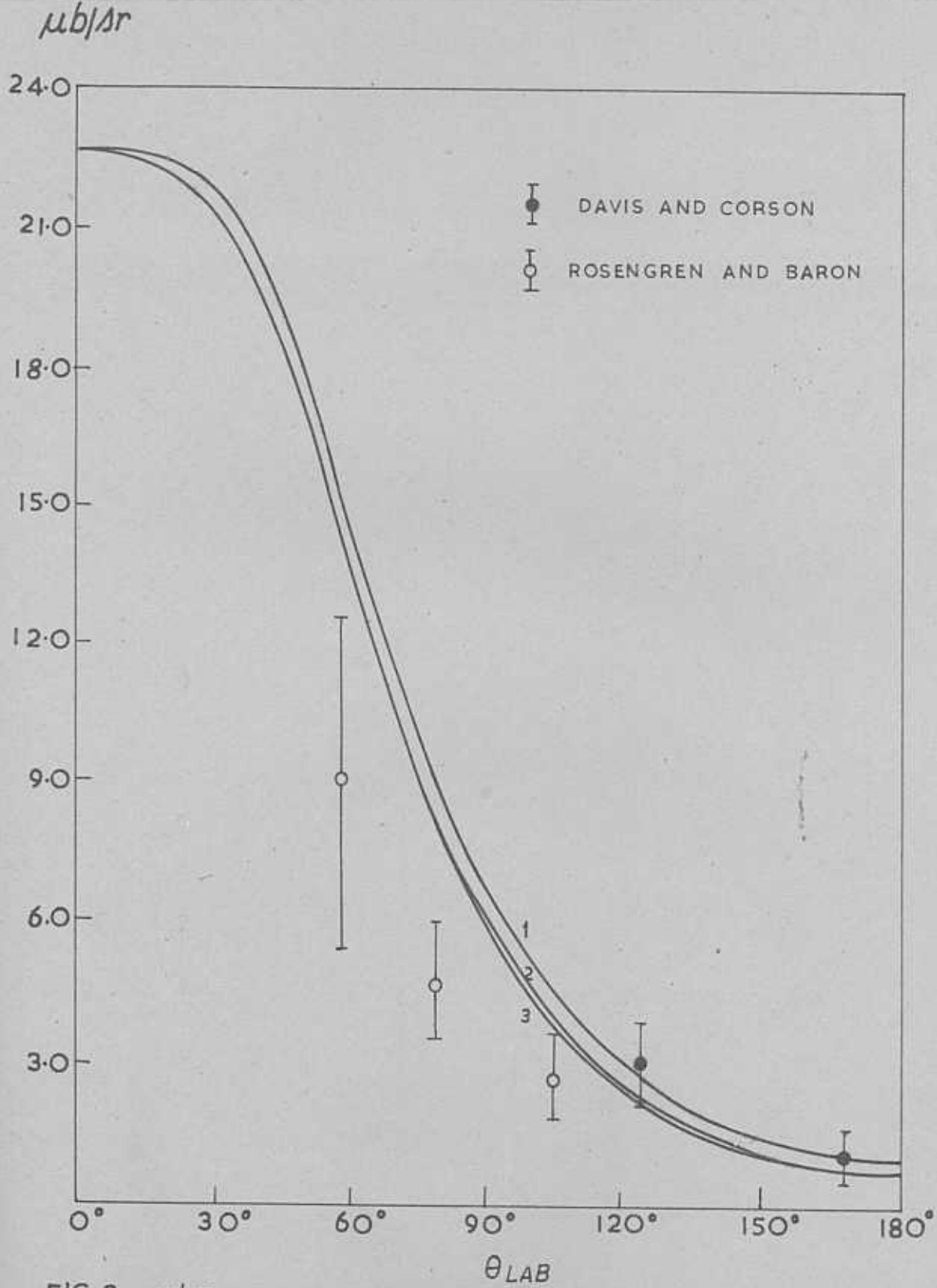

FIG. 3. $\left(\frac{d\sigma}{d\Omega}\right)_{LAB}$ FOR $\gamma + D \rightarrow D + \pi^{\circ}$ AT $E_{\gamma}^{LAB} = 280$ mev

WITH $\rho = 1{\cdot}704 \times 10^{-13}$ cm

$P_D = 5\%$ (1) $x_c = 0$ (2) $x_c = 0{\cdot}10$

(3) $x_c = 0{\cdot}13$

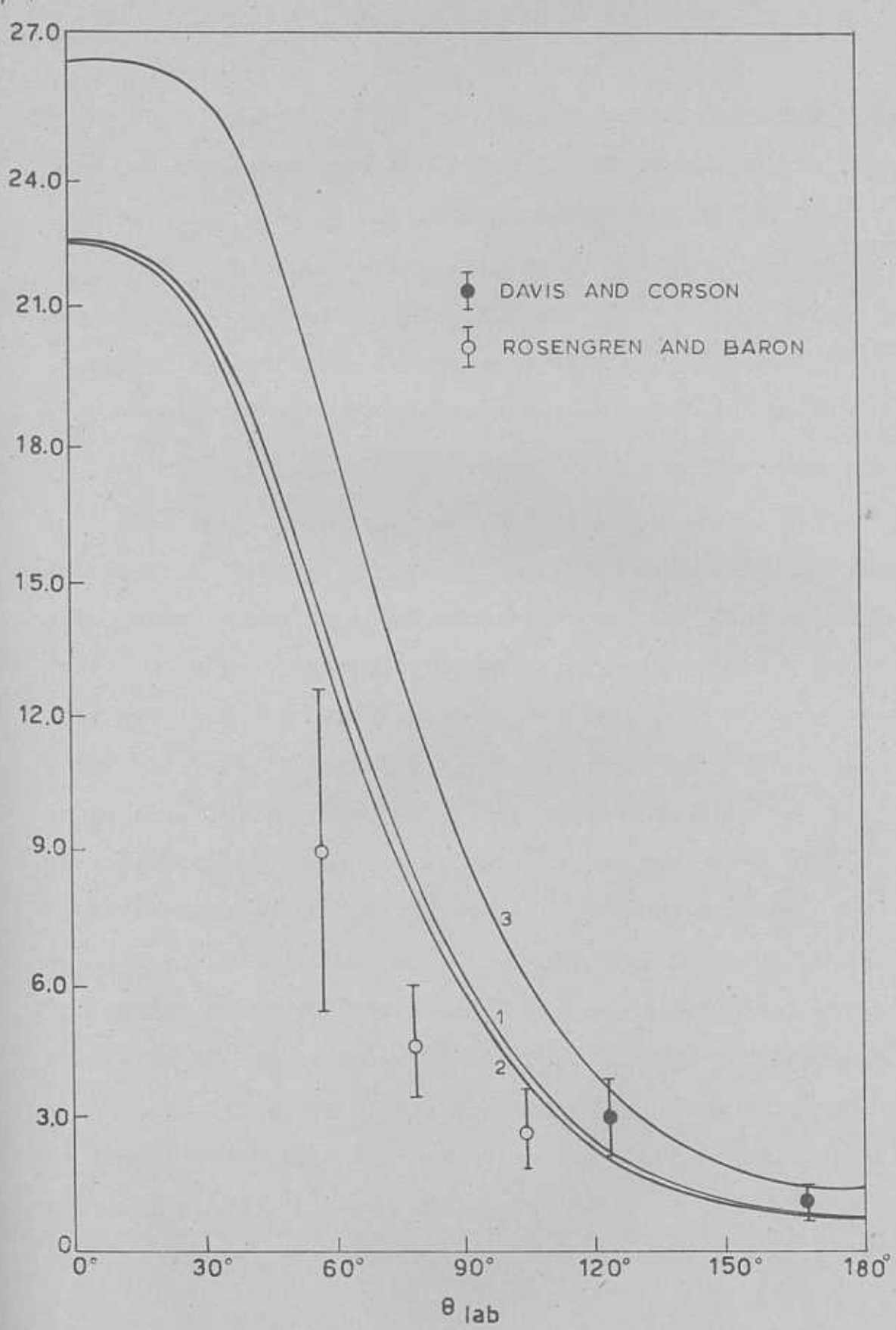

FIG. 4. $\left(\frac{d\sigma}{d\Omega}\right)_{lab}$ For $\gamma + D \longrightarrow D + \pi^0$ at $E_\gamma^{lab} = 280$ meV

(1) $P_D = 5\%$, $\chi_c = 0.13$, $\rho = 1.704 \times 10^{-13}$ cm

(2) $P_D = 5\%$, $\chi_c = 0.13$, $\rho = 1.734 \times 10^{-13}$ cm

(3) $P_D = 0\%$, $\chi_c = 0$, $\rho = 1.734 \times 10^{-13}$ cm

In Fig.5, $(d\sigma/d\Omega)_{Lab}$, obtained with the Reid hard-core and soft-core wave functions for the deuteron, is plotted against θ_{Lab} for an incident photon energy of 280 Mev, along with the experimental results of Davis and Corson[12], Rosengren and Baron[13], and Wolfe et. al.[14]. The cross sections obtained with Hulthen-Sugawara wave functions for P_D = 0% and 5%, r_c = 0.561 fm. and ϱ = 1.734 fm are also plotted for the sake of comparison. It is interesting to note that there is a large difference (of almost a factor of 2) between our theoretical results obtained with Hulthen-Sugawara wave function and Reid wave functions for the deuteron. But there is no appreciable difference between the cross sections obtained with the Reid hard core and soft core deuteron wave functions. It is interesting to note that the Reid wave functions, derived ffom realistic nucleon-nucleon potentials, lead to results which are in much better agreement with experiment, both at forward and backward angles, than the results obtained with the phenomenological wave functions - the choice of whose functional forms has a certain arbitrariness - of the deuteron constructed by Hulthen and Sugawara.

In Fig.6, we have shown the angular distribution of the differential cross sections for the reaction (2.1.1) obtained using Reid hard core wave functions for various

---

14) B.Wolfe, A.Silverman and J.W.DeWire, Phys.Rev.99,268(1955).

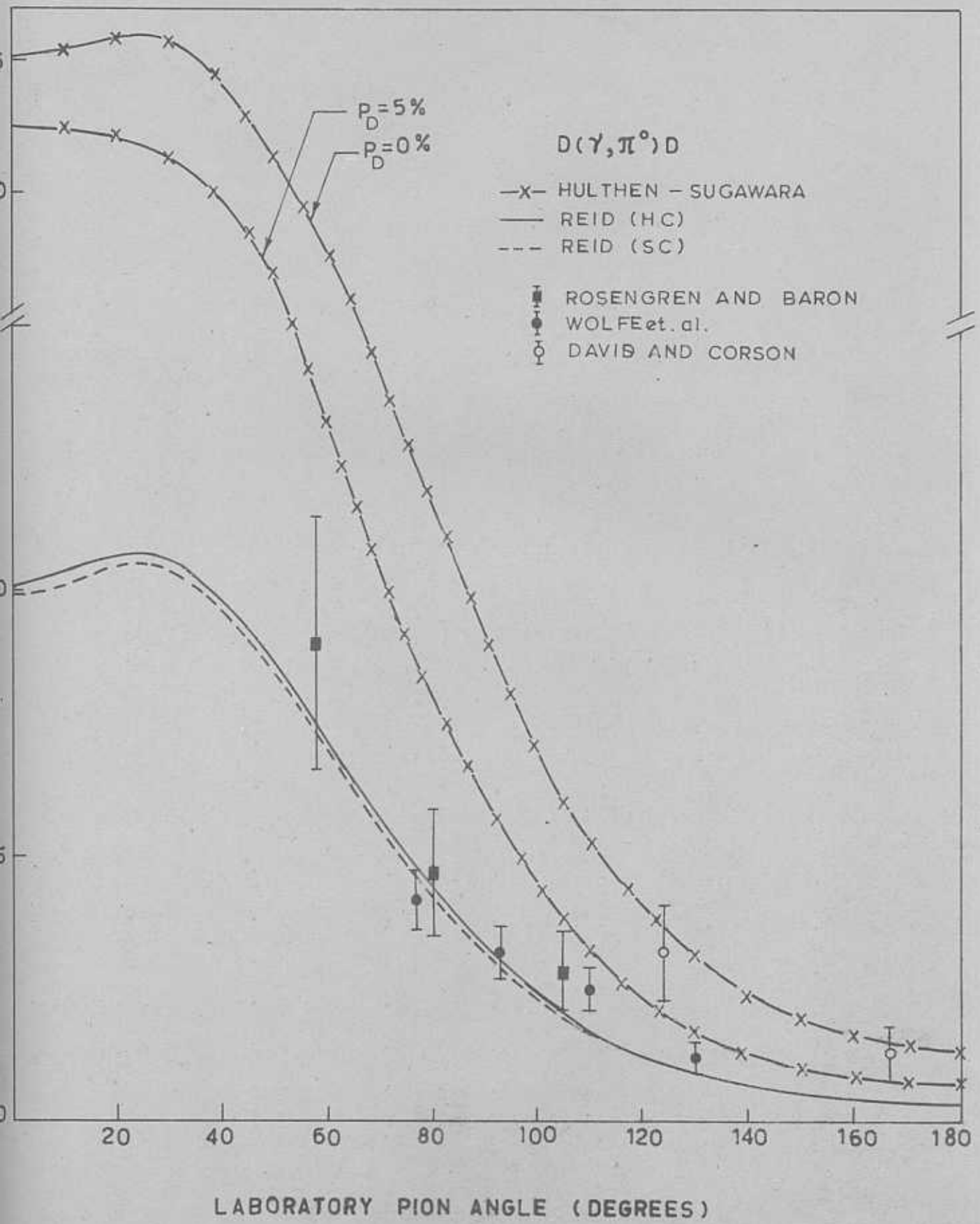

Differential cross section for D(γ ,π^0)D obtained with Reid(HC) and SC) wave function at an incident photon energy of 280 Mev.

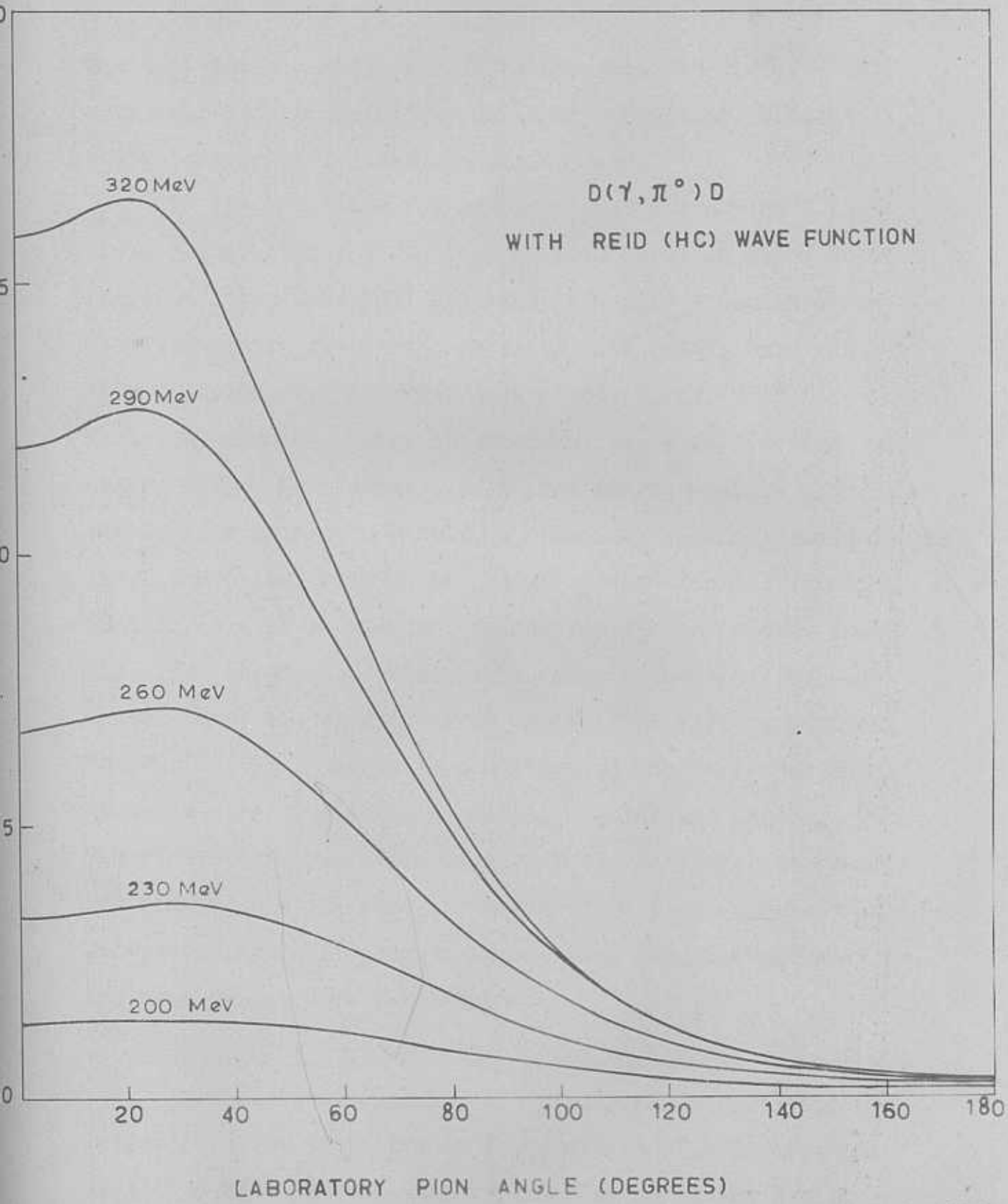

Fig.6. Differential cross sections for D(γ ,π°)D obtained using Reid(HC) wave function for various incident photon energies.

incident photon energies. We notice that the differential cross sections increase rapidly with increasing incident photon energy in the forward angles only.

In Fig.7 we show the energy dependence of the total cross section for the reaction (2.1.1) obtained using Hulthen (Eq.(2.4.18)), Reid (HC) and Reid (SC) wave functions. We find that while the curves obtained with Reid's hard and soft core deuteron wave functions are almost alike, they lie significantly below the curve obtained Hulthen wave function which has $P_D = r_c = 0$. Further, as in the single nucleon case, the total cross section exhibits, a prominant peaking around 320 Mev.

Thus, the differential cross section for the reaction (2.1.1) is weakly dependent on the D-state component itself, since F_{SD} and F_{DD} are negligible, and in the specific model chosen here, the cross section, being directly proportional to $|F_{SS}|^2$, is found to be sensitive to the choice of the deuteron wave functions, especially at forward angles. We therefore feel that measurements of the differential cross section for neutral pion photoproduction from deuterons at forward angles will provide interesting information about the deuteron radial wave function.

4. CHARGED PION PHOTOPRODUCTION FROM DEUTERONS.

The reactions (2.1.2) and (2.1.3) are necessarily inelastic since there are no bound states of a di-neutron or a di-proton system. The matrix element Q is taken between the initial and final nuclear states of the operator:

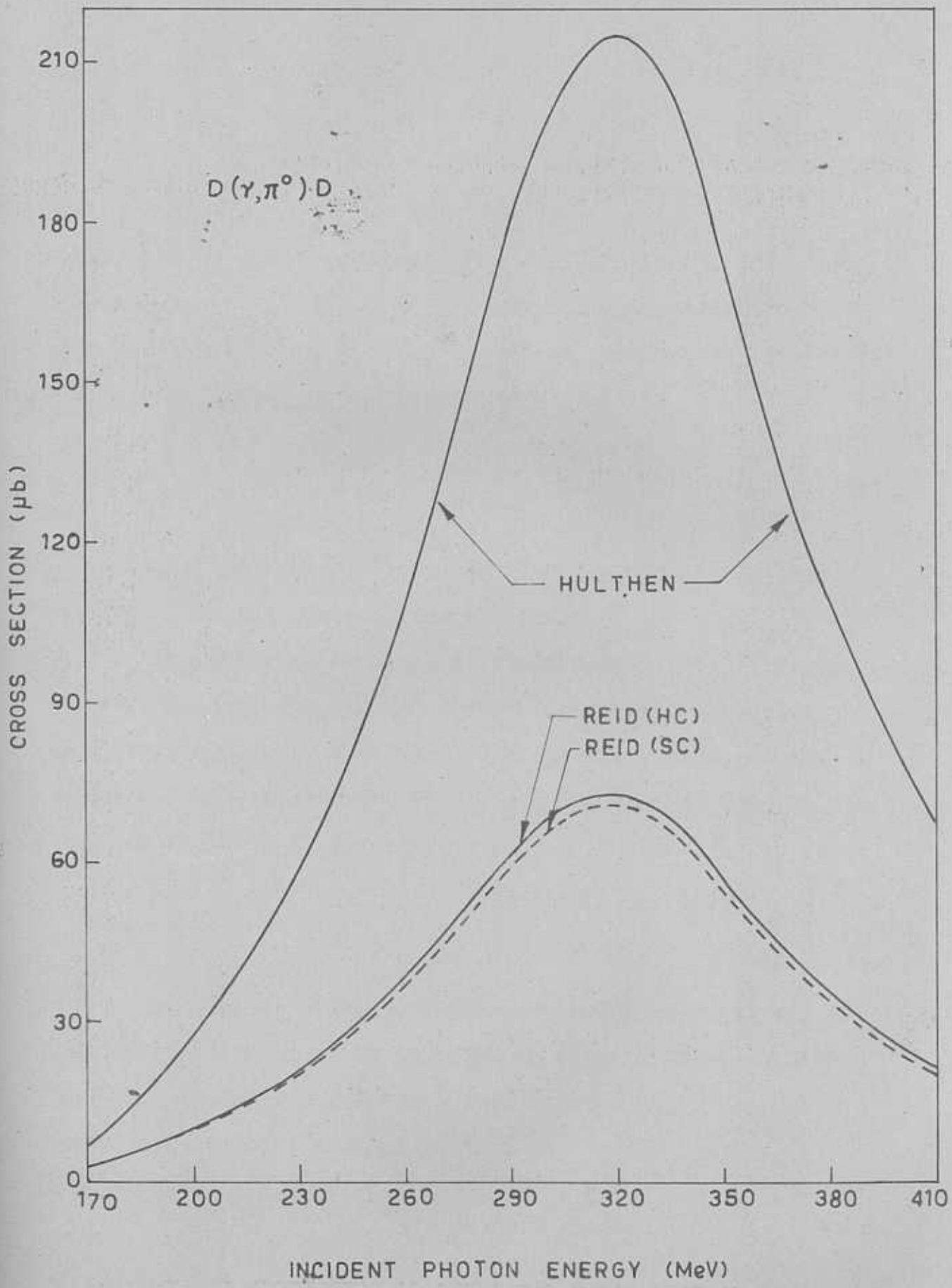

Fig.7. Energy dependence of the total cross section for $D(\gamma,\pi^{o})D$ obtained using Hulthen, Reid (HC) and Reid (SC) wave functions.

$$T = t_1 + t_2 ,$$

$$t_j = (\underline{\sigma}_j \cdot \underline{K} + L)\, \tau_j^{\mp} \exp(i\underline{k}\cdot\underline{r}_j) . \qquad (2.4.1)$$

where, for $\underline{K}$ and L, we choose the CGLN amplitudes defined in Chapter.1, $\underline{\sigma}_j$, $\tau_j^{\mp}$ and $\underline{r}_j$ are the spin, isobaric spin and position vector of the j^{th} nucleon, respectively. Further, $\tau^{\mp}$ is defined in the conventional way as:

$$\tau^{\mp} = \frac{1}{2}(\tau_x \mp i\tau_y) , \qquad (2.4.2)$$

τ^- being the isobaric spin operator for π^+ photoproduction, while τ^+ is the operator for π^- case.

From our study of elastic photoproduction of neutral pions from deuteron, we found that the effect of D-state admixture shows up only through the normalization and the scale of the S-state wave function. So, we take the deuteron initial state to be given by:

$$|i\rangle = (2\pi)^{-3/2} \frac{u(r)}{r}\, {}^3\chi_m\, Y_0^0\, \eta_0 . \qquad (2.4.3)$$

The final nuclear state consists of two neutrons (in the π^+ photoproduction case) or two protons (in the π^- case) with relative momentum $\underline{k}$ and Pauli principle requires separate consideration of two final states, one that is symmetric and one that is antisymmetric in space:

$$|f_e\rangle = (2\pi)^{-3/2}\, u_{f,e}(\underline{k}\cdot\underline{r})\, {}^1\chi_0\, \eta^1_{\mp 1} \exp(i\underline{k}\cdot\underline{R}) , \qquad (2.4.4)$$

$$|f_o\rangle = (2\pi)^{-3/2}\ u_{f,o}(\underline{k}\cdot\underline{r})\,{}^3\chi_m\,\eta^1_{\mp 1}\ \exp(i\underline{k}\cdot\underline{R}), \qquad (2.4.5)$$

where $u_{f,e}(\underline{k}.\underline{r})$ and $u_{f,o}(\underline{k}.\underline{r})$ are the symmetric (even) and antisymmetric (odd) radial wave functions of the two nucleons; $\underline{R} = \frac{1}{2}(\underline{r}_1 + \underline{r}_2)$ is the centre-of-mass coordinate; $\underline{r}=\underline{r}_1 - \underline{r}_2$ the relative coordinate; ${}^3\chi_m$ is the triplet spin function, m being the z component of the total spin; and $\eta^1_{\mp 1}$ is the isobaric triplet function, which is explicitly:

η^1_{-1} = p(1) p(2) for π^- photoproduction case, and

η^1_{+1} = n(1)n(2) for π^+ photoproduction case.

The integration over $\underline{R}$ leads to the requirement of conservation of momentum. The matrix elements for the symmetric and antisymmetric case become, respectively,

$$Q_e = \frac{1}{\sqrt{2}}\ \langle {}^1\chi_o\,|\,(\underline{\sigma}_1 - \underline{\sigma}_2)\cdot\underline{K}\ |\,{}^3\chi_m\rangle\ E, \qquad (2.4.5)$$

$$Q_o = \frac{1}{\sqrt{2}}\ \langle {}^3\chi_{m'}|\,(\underline{\sigma}_1 + \underline{\sigma}_2)\cdot\underline{K}\ |\,{}^3\chi_m\rangle\ O, \qquad (2.4.6)$$

where

$$E = \int u^*_{f,e}\,(\underline{k}\cdot\underline{r})\cos\left(\tfrac{1}{2}\underline{k}\cdot\underline{r}\right)\frac{u(r)}{r}\,d\underline{r}, \qquad (2.4.7)$$

$$O = \int u^*_{f,o}\,(\underline{k}\cdot\underline{r})\sin\left(\tfrac{1}{2}\underline{k}\cdot\underline{r}\right)\frac{u(r)}{r}\,d\underline{r}. \qquad (2.4.8)$$

Squaring, summing over final states, averaging over initial spin states and averaging over photon polarizations, we obtain:

$$|Q|^2 = |Q_e|^2 + |Q_o|^2, \qquad (2.4.9)$$

where

$$|Q_e|^2 = \frac{1}{3}\frac{1}{2}\sum_m |\langle {}^1\chi_o |(\underline{\sigma}_1 - \underline{\sigma}_2)\cdot \underline{K}\,|{}^3\chi_m\rangle E|^2$$

$$= \frac{1}{3}\,2\,|\underline{K}|^2 |E|^2,$$

$$|Q_o|^2 = \frac{1}{3}\frac{1}{2}\sum_{m,m'} |\langle {}^3\chi_{m'}|(\underline{\sigma}_1 + \underline{\sigma}_2)\cdot \underline{K}\,|{}^3\chi_m\rangle O|^2$$

$$= \frac{1}{3}\,2\,(2|\underline{K}|^2 + 3|L|^2)\,|O|^2,$$

with $|\underline{K}|^2 = \frac{1}{2}(|\underline{K}|^2_{\epsilon_x} + |\underline{K}|^2_{\epsilon_y})$ and $|L|^2 = \frac{1}{2}(|L|^2_{\epsilon_x} + |L|^2_{\epsilon_y})$, the subscripts ϵ_x and ϵ_y correspond to the photon polarizations.

Devanathan and Ramachandran[5a] have obtained explicit expressions for the meson spectrum in terms of pion-nucleon phase shifts and the overlap integrals of Lax and Feshbach[15]. Alladi Ramakrishnan et. al.[16] have shown that calculations become very much simplified if the binding energy of the deuteron is neglected and the "closure" approximation is used for the integration of the final relative momentum of the two-nucleon system(+). The resulting "closure" matrix element

15) Lax M. and Feshbach H., Phys.Rev. 88, 509 (1952).
16) Alladi Ramakrishnan, V.Devanathan and K.Venkatesan, Nucl.Phys. 29, 680 (1962).
(+) In the closure approximation $\int |E|^2\, dk_o = \frac{1}{2}(1+I)$ and $\int |O|^2\, dk_o = \frac{1}{2}(1-I)$ where $\underline{k}_o = \underline{k}/2$ and the integral I is given by (2.4.13).

given by[15,16]:

$$|Q|^2 = \frac{1}{2}\left[2\left(|\underline{K}|^2 + |L|^2\right) - \frac{2|\underline{K}|^2 + 6|L|^2}{3} I\right] \qquad (2.4.12)$$

where

$$I = \int \cos(\underline{k}\cdot\underline{r}) \left[\frac{u(r)}{r}\right]^2 d\underline{r} \qquad (2.4.13)$$

has a first term exactly in agreement with the corresponding free nucleon matrix element while the second "two-particle" term contains the interference integral I. The differential cross section can be written as:

$$\frac{d\sigma}{d\Omega} = (2\pi)^{-2} \frac{\mu\mu_0}{2}\left(Z^{\pm} - \frac{Z^{\pm} + 4|L|^2}{3} I\right), \qquad (2.4.14)$$

where

$$Z^{\pm} = 2\left(|\underline{K}|^2 + |L|^2\right), \qquad (2.4.15)$$

Z^+ corresponds to π^+ production and Z^- corresponds to π^- production. The explicit expressions for $Z^{\pm}$ and $|L|^2$ are given below:

$$Z^{\pm} = \frac{8\pi^2 e^2 f^2}{\mu_0 v_0}\left\{\frac{2}{(1+\mu g_M)^2}\left[1 - \frac{2\mu^2 \sin^2\theta}{(k^2+1)^2}\right] +\right.$$

(continued.)

$$+\frac{1}{1+\mu_0/M}\left[4\frac{\nu\lambda}{3\mu}A\left(\frac{\mu\nu\sin^2\theta}{k^2+1}-\cos\theta\right)+\right.$$

$$\left.\pm 4\alpha\left\{\mu\nu\cos\theta-\mu_0^2+\frac{\mu^2\sin^2\theta}{k^2+1}(\mu_0^2-\nu^2)\right\}\right]+$$

$$+\left(\frac{\nu\lambda}{3\mu^2}\right)^2\left[(A^2+B^2)(1+\cos^2\theta)+(C^2+D^2)\sin^2\theta\right]+$$

$$\pm\alpha\frac{2\nu\lambda}{3\mu}A\left[2\mu_0^2\cos\theta-\mu\nu(1+\cos^2\theta)\right]+$$

$$+\alpha^2\left[\mu^2\nu^2(1+\cos^2\theta)+2\mu_0^2(\mu_0^2-2\mu\nu\cos\theta)\right]+$$

$$+H_-\left\{\frac{1}{1+\mu_0/M}\frac{2\mu^2\sin^2\theta}{M\mu_0}\left[\frac{2}{k^2+1}(\mu^2-\mu\nu\cos\theta)-1\right]+\right.$$

$$\left.+\frac{\mu^4\sin^2\theta}{M^2\mu_0^2}-2\alpha\frac{\mu_0\mu^2}{M}\sin^2\theta\right\}\Bigg\}$$

(2.4.16)

where the upper sign is for π^+ production and the lower sign is for π^- production, $H_- = 0$ for π^+ production and $H_- = 1$ for π^- production,

$$A = \cos\delta_{11}\sin\delta_{11} - \cos\delta_{13}\sin\delta_{13} - \cos\delta_{31}\sin\delta_{31} + \cos\delta_{33}\sin\delta_{33},$$

$$B = \sin^2\delta_{11} - \sin^2\delta_{13} - \sin^2\delta_{31} + \sin^2\delta_{33},$$

$$C = \cos\delta_{11}\sin\delta_{11} + 2\cos\delta_{13}\sin\delta_{13} - \cos\delta_{31}\sin\delta_{31} - 2\cos\delta_{33}\sin\delta_{33},$$

$$D = \sin^2\delta_{11} + 2\sin^2\delta_{13} - \sin^2\delta_{31} - 2\sin^2\delta_{33},$$

$$\alpha = \frac{\mu_p + \mu_n}{2M\mu_0}, \qquad \lambda = \frac{\mu_p - \mu_n}{4Mf^2},$$

and

$$|L|^2 = \frac{8\pi^2 e^2 f^2}{\mu_0 v_0} \; 2\left(\frac{v\lambda}{3\mu^2}\right)^2 (C^2 + D^2) \sin^2\theta . \qquad (2.4.17)$$

The expressions (2.4.16) and (2.4.17) are different from those obtained by Devanathan and Ananthanarayanan[5b] in that we have taken into account all the p-wave pion-nucleon phase-shifts (viz. δ_{11}, δ_{13}, δ_{31} and δ_{33}) instead of taking into account only the dominant δ_{33} phase shift. Devanathan and Ananthanarayanan[5b] have calculated the cross sections for charged pions photoproduction from deuterons assuming the deuteron wave function to be represented by the Hulthen function

$$u(r) = \left[\frac{\alpha}{2\pi(1-\alpha\rho_1)}\right]^{1/2} (e^{-\alpha r} - e^{-\beta r}) \qquad (2.4.18)$$

with $\alpha = 0.3274$, $\beta = 2.068$ and $\rho_1 = 1.231$. Using (2.4.18) they obtain the following analytical expression for the interference integral I;

$$I = \left[\frac{2\alpha}{(1-\alpha\rho_1)k}\right]\left[\tan^{-1}\left(\frac{k}{2\alpha}\right) + \tan^{-1}\left(\frac{k}{2\beta}\right) - 2\tan^{-1}\left(\frac{k}{\alpha+\beta}\right)\right]. \qquad (2.4.19)$$

In the present study we use instead of the Hulthen form (2.4.18) for the deuteron wave function, the Reid wave functions discussed in section.2 of this Chapter, and numerically integrate the interference integral I.

Numerical calculations for various incident photon energies have been made using expression (2.4.14) for the differential cross section of the positive and negative pion photoproduction from deuteron in the centre-of-momentum system and then the cross section is transformed to the laboratory system with the help of (2.3.19). Some of the results obtained with the Hulthen wave function (2.4.18) and the Reid hard core (HC) wave functions are presented in Figures 8, 9 and 10.

In Fig.8, $(d\sigma/d\Omega)_{Lab}$ for the reaction (2.1.2) is plotted against θ_{Lab} for incident photon energies of 200 and 230 Mev along with the experimental results of Beneventano et.al.[17].

In Fig.9, $(d\sigma/d\Omega)_{Lab}$ for the reaction (2.1.3) is plotted against θ_{Lab} for incident photon energies of 200 and 230 Mev along with the experimental results of Beneventano et.al.[17].

In Fig.10 the total cross sections for π^+ and π^- photoproduction obtained using Hulthen and Reid wave functions are plotted as a function of the incident photon energy.

From figures 8 and 9 we observe that the differential cross sections for the photoproduction of π^+ and π^- are almost the same at low angles but differ widely at large angles in accordance with the observations of Beneventano et.al.[17].

---

17) M.Beneventano, G.Bernardini, G.Stoppini and L.Tau, Nuo. Cimento 10, 1109 (1958).

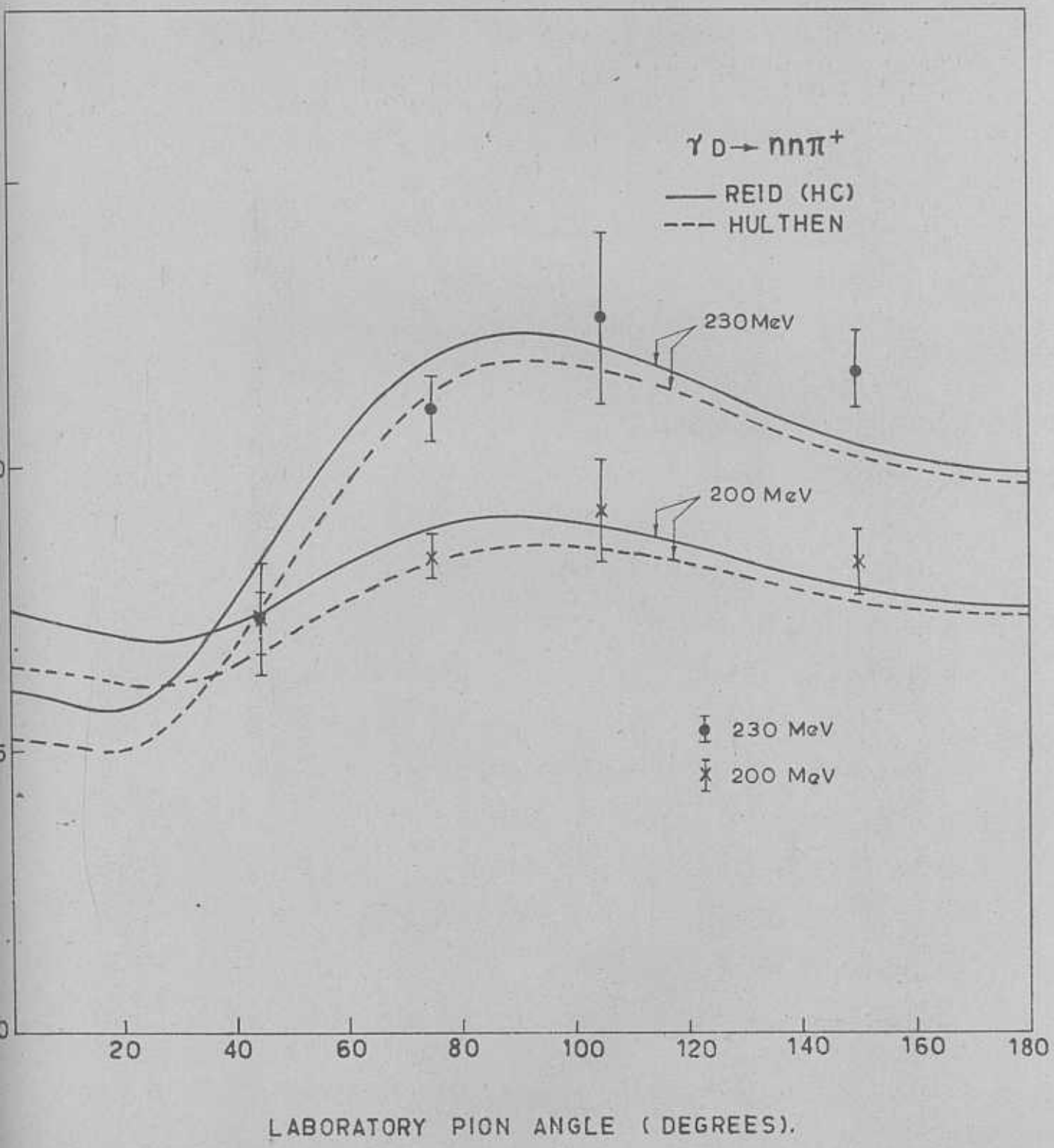

Fig.8. Differential cross sections for $\gamma D \longrightarrow nn\pi^+$ at incident photon energies of 200 Mev and 230 Mev obtained using Hulthen and Reid (HC) wave functions.

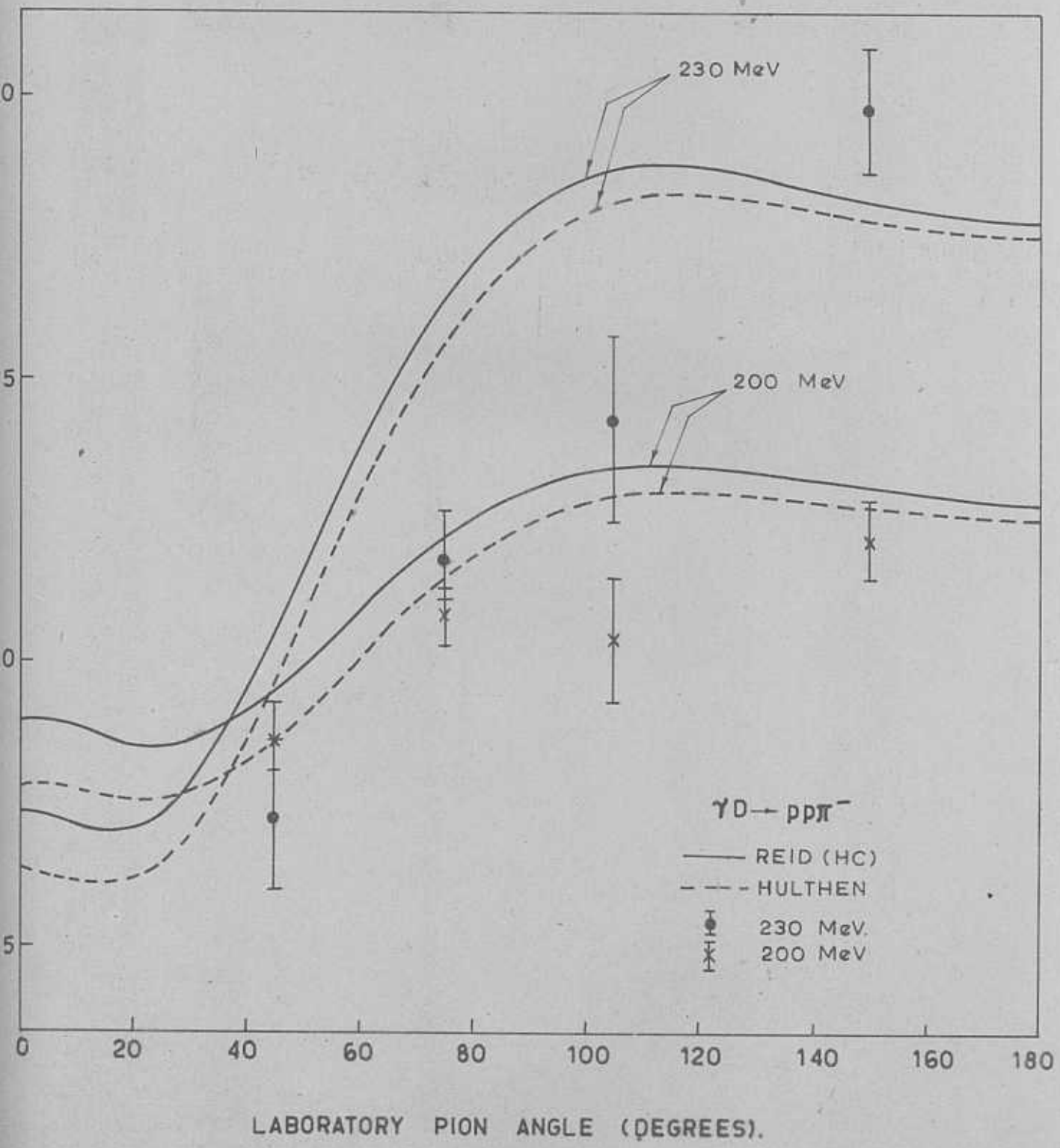

Fig.9. Differential cross sections for $\gamma d \longrightarrow pp\pi^-$ at incident photon energies of 200 Mev and 230 Mev obtained using Hulthen and Reid (HC) wave functions.

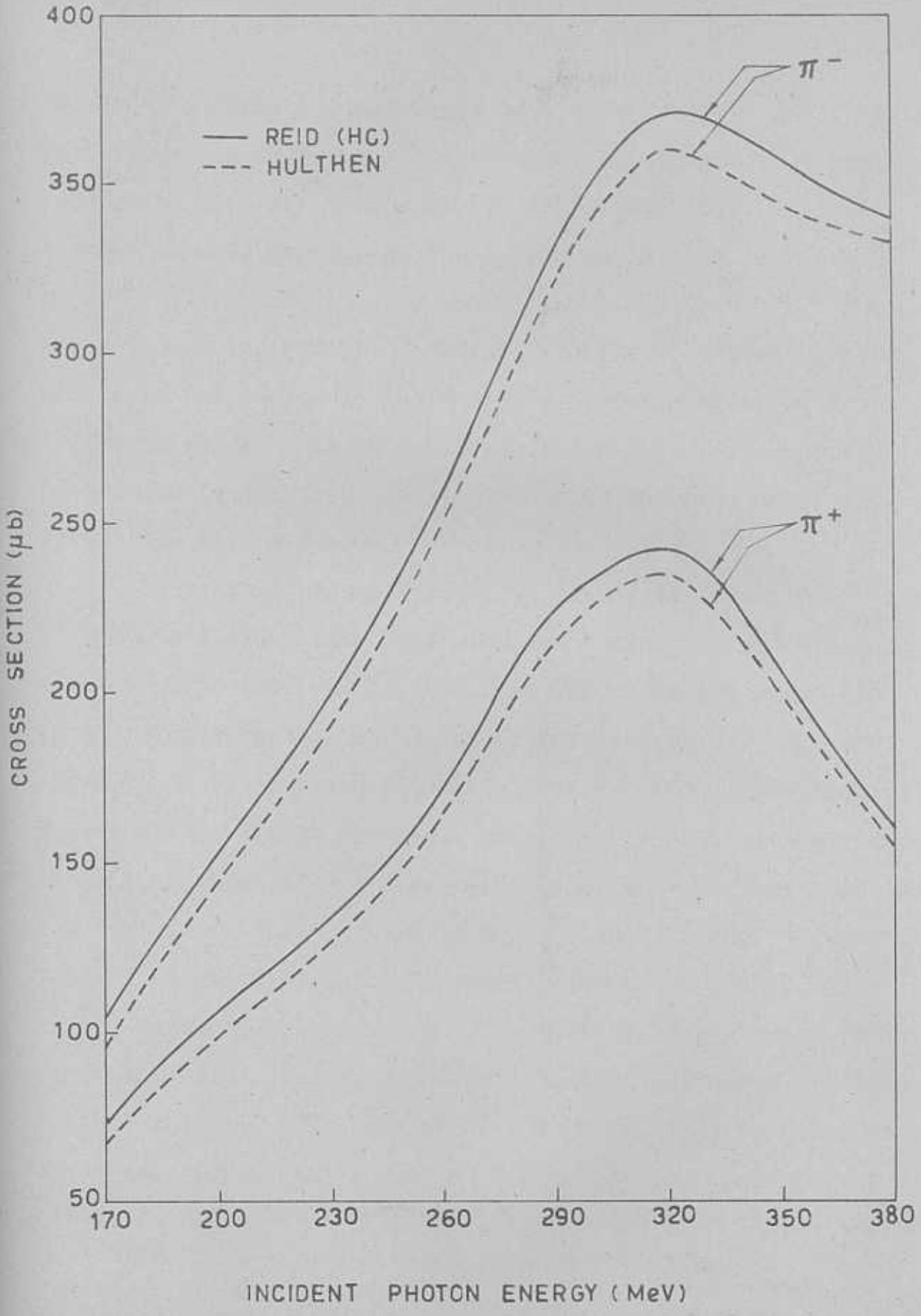

Fig.10. Energy dependence of the total cross sections for π^+ π^- photoproduction from the deuteron obtained using Hulthen and Reid (HC) wave functions.

We also find that the agreement between our theory and experiment is much better for π^+ photoproduction than for π^- photoproduction from the deuteron. Further, since the integral multiplies only the two-particle term in (2.4.14) - instead of the whole expression for $d\sigma/d\Omega$ as in the case of π^0 photoproduction - the effect of D-state admixture, or, rather the effect of the choice of the deuteron wave function, on the differential, as well as total cross sections for $\pi^\pm$ photoproduction is not very significant as in the case of π^0 photoproduction from deuteron.

In table.5, the differential cross sections for π^- and π^+ photoproduction from deuterons and their ratios, obtained with the Reid (HC) and Hulthen wave functions are given along with the experimental ratios of Beneventano et.al.[17]. The theoretical ratios obtained with the Reid (HC) and Hulthen wave functions are almost the same. The experimental ratios increase with increasing angle and we notice that this is reproduced by our theory and there is a reasonably good agreement between our theory and the experimental results of Beneventano et. al.

In Table.6, the total cross sections for π^- and π^+ photoproduction from deuterons and their ratios are given for both the Hulthen and Reid (HC) wave functions for various incident photon energies. Experimental data of Baldin[18], available in the photon energy range 156 Mev to 181 Mev, are also given. We find that there is a good agreement between our theory and the experimental results of Baldin.

18) A.Baldin, Nuo.Cimento 8, 567 (1958).

Differential cross sections for the photoproduction of negative and positive pions and their ratios obtained using Hulthen and Reid (HC) wave functions are given here along with the experimental ratios of Beneventano et.al.

Incident photon energy(Mev)	θ_{Lab} (degrees)	Differential cross section in $\mu b/sr$.						
		Hulthen wave function			Reid(HC) wave function			Experimental
		$\frac{d\sigma(\pi^-)}{d\Omega}$	$\frac{d\sigma(\pi^+)}{d\Omega}$	$\frac{d\sigma(\pi^-)}{d\sigma(\pi^+)}$	$\frac{d\sigma(\pi^-)}{d\Omega}$	$\frac{d\sigma(\pi^+)}{d\Omega}$	$\frac{d\sigma(\pi^-)}{d\sigma(\pi^+)}$	$\frac{d\sigma(\pi^-)}{d\sigma(\pi^+)}$
180	45	8.05	6.27	1.28	8.8	6.85	1.28	1.35 ± 0.12
	75	9.2	6.67	1.38	9.8	7.15	1.37	1.41 ± 0.10
	106	9.6	6.5	1.48	10.1	6.87	1.47	1.47 ± 0.11
	150	9.35	5.87	1.593	9.65	6.05	1.595	--
200	45	9.7	7.55	1.285	10.6	8.5	1.248	1.25 ± 0.12
	75	15.65	11.2	1.397	16.4	11.85	1.384	1.28 ± 0.09
	106	18.1	11.7	1.547	18.65	12.1	1.541	1.14 ± 0.15
	150	17.8	10.18	1.749	18.1	10.37	1.746	1.46 ± 0.12
230	45	8.64	6.75	1.28	9.5	7.42	1.28	0.96 ± 0.21
	75	11.5	8.35	1.377	12.25	8.9	1.376	1.07 ± 0.08
	106	13.0	8.5	1.53	13.45	8.9	1.511	1.32 ± 0.10
	150	12.75	7.67	1.663	13.1	7.8	1.68	1.67 ± 0.13

Table.6

Total cross sections (in μb) for the photoproduction of negative and positive pions from deuterons and their ratios obtained with Hulthen and Reid wave functions are given below.

Incident photon energy(Mev)	Reid(HC) wave function			Hulthen wave function		
	$\sigma(\pi^-)$	$\sigma(\pi^+)$	$\sigma(\pi^-)/\sigma(\pi^+)$	$\sigma(\pi^-)$	$\sigma(\pi^+)$	$\sigma(\pi^-)/\sigma(\pi^+)$
165	90.84	65.59	1.385	84.67	61.03	1.388
180	121.07	85.47	1.417	113.73	80.03	1.420
200	151.488	104.23	1.457	143.58	98.34	1.460
230	198.43	133.20	1.489	190.03	126.80	1.498
260	259.32	173.06	1.498	250.08	165.75	1.509
290	331.94	222.83	1.489	321.45	214.19	1.501
320	371.18	243.82	1.523	360.53	234.92	1.535
350	352.17	206.45	1.705	343.54	199.54	1.722
380	339.44	160.11	2.119	333.03	155.47	2.141

Experimental Data of Baldin[18] for the total cross section of the π^- photoproduction reaction from deuteron are:

Photon energy(Mev) :	156.5	163.5	170	181
$\sigma(\pi^-)$ in μb :	46 $\pm$ 6	64 $\pm$ 8	90 $\pm$ 10	110 $\pm$ 17

PART. II

PHOTOPRODUCTION OF CHARGED PIONS FROM CERTAIN CLOSED-SHELL NUCLEI

CHAPTER 3

PHOTOPRODUCTION OF POSITIVE PIONS FROM ^{16}O:

(i) CONFIGURATION MIXING AND THE PRODUCTION MECHANISM+

1. In this chapter, we take up the study of photoproduction of positive pions from Oxygen, which is a doubly closed "magic" nucleus, and attempt to remove the ambiguity in nuclear structure, as much as possible, to gain an insight into the mechanism of photoproduction of pions from nuclei. We study the reaction $^{16}O(\gamma,\pi^+)^{16}N$, for which experimental results of Meyer, Walters and Hummel[1] are available. We do not discuss the case of negative pion photoproduction from Oxygen, viz. $^{16}O(\gamma,\pi^-)^{16}F$, since, in this case, the final nuclear state cannot be easily identified and further even the ground state of ^{16}F is not stable against nucleon emission[2].

Explicitly, the reaction which we study is:

$$\gamma + {}^{16}O(J = 0^+, T=0) \longrightarrow \pi^+ + {}^{16}N(J^P=0^-,1^-,2^-,3^-;T=1) \quad (3.1.1)$$

in which the final nuclear states are the four bound states of ^{16}N, observed experimentally. To eliminate the nuclear structure uncertainty, as much as possible, we note that

---

+ V.Devanathan, M.Rho, K.Srinivasa Rao and S.C.K.Nair, Nucl. Phys. B2, 329 (1967).

1) R.A.Meyer, W.B.Walters and J.P.Hummel, Phys.Rev.138, B1421 (1965).

2) F.Ajzenberg-Selove and T.Lauritzen, Nucl.Phys.11, 1 (1959).

the process (3.1.1) or equivalently its inverse reaction - viz. radiative pion capture by ^{16}O which has been studied theoretically by Anderson and Eisenberg[3] is expected to have similar matrix elements[4] as the muon capture process:

$$\mu^- + {}^{16}O(J^P = 0^+; T=0) \longrightarrow \nu_\mu + {}^{16}N(J^P = 0^-, 1^-, 2^-, 3^-; T=1) \qquad (3.1.2)$$

since the initial and final nuclear states are the same in both the reactions (3.1.1) and (3.1.2).

We assume the ground state of ^{16}O to be spherical(+) and for the low lying, bound, odd-parity states of ^{16}N we use wave functions obtained from the following nuclear models:

(i) the independent particle model,

(ii) the particle-hole models and

(iii) the quasi-particle model of Migdal[5].

Of these, the quasi-particle model of Migdal is known to yield[6] reasonably accurate matrix elements for the process (3.1.2).

In our study, we use the impulse approximation for the transition amplitude. This amounts to neglecting off-the-energy shell production of pions and, although a serious limitation, it will not affect our results to any great extent

---

3) D.K.Anderson and J.M.Eisenberg, Phys.Letts.22, 164 (1966).
4) J.Delrome and T.E.O.Ericson, Phys.Letts.21, 98 (1966).
+) In this Chapter ground state correlations are taken into account only in an approximate way.
5) A.B.Migdal, Proceedings of the International School of Physics "Enrico Fermi", Course 36, edited by C.Bloch, Academic Press, New York (1966).
6) M.Rho, Phys.Rev.Letts. 18, 671 (1967); Phys.Rev.161,955(1967).

since we confine our consideration to the low-lying states of the final nucleus. Further, near the threshold of pion production, at which the neglecting of the off-the-energy shell effects is most serious, the gauge term ($i\underline{\sigma}.\underline{\varepsilon}$) alone gives the dominant contribution and since this term is independent of the kinematics, one may apply the correct kinematics of the problem by taking into account the excitation energy of the final nucleus[3].

On comparing our theoretical total cross sections with available experimental results[1] we find that though the smooth variation of the cross section as a function of photon energy is reproduced, there is still a definite discrepancy (about a factor of two) between theory and experiment. This discrepancy can be attributed to the following sources of uncertainty: (a) the production mechanism and/or (b) the impulse approximation. To eliminate the discrepancy between theory and experiment we invoke Butler's[7] mechanism of surface production of pions and we find that we can bring the theoretical results in agreement (both in magnitude and in shape) with experimental results.

2. The comparatively high energy which is required in closed-shell nuclei to raise a particle to the next unoccupied shell led Wilkinson[8], in 1956, to suggest that the

---

7) S.T.Butler, Phys.Rev.87, 1117 (1952).
8) D.H.Wilkinson, Physica 22, 1039 (1956), Phys.Rev.Letts.3, 388 (1959).

odd-parity states of ^{16}O can be described in terms of independent particle-hole excitations. This was followed by the pioneering work of Elliott and Flowers[9] who introduced, with great success, the effect of the residual interaction between the particle-hole configurations and restricted the diagonalization of the residual two-body force to the subspace of configurations with one particle-hole pair of energy $1\hbar\omega$. This approximation is referred to as the Tamm-Dancoff Approximation or TDA. The particle-hole model of nuclear excitations was then extended by Gillet and Vinh-Mau[10] to include in a simple way excitations of more than one particle-hole pair, at the cost of violating somewhat the Pauli exclusion principle. This approximation is referred to as the Random Phase Approximation or RPA. Duck[11], Erickson, Sens and Rood[12], and Gillet and Jenkins[13] have used the particle-hole wave functions in their studies of the muon capture process (3.1.2) and find that the partial muon capture rates obtained with these wave functions are not in good agreement with the experimental values for the same. Rho[6] applied the quasi-particle model of Migdal[14]

9) J.P.Elliott and B.H.Flowers, Proc.Roy.Soc.A242, 57(1957).
10) V.Gillet and N.Vinh-Mau, Nucl.Phys. 54, 321 (1964).
11) I.Duck, Nucl.Phys. 35, 27 (1962).
12) T.Ericson, J.C.Sens and H.P.C.Rood, Nuo.Cim.34, 52 (1964).
13) V.Gillet and D.A.Jenkins, Phys.Rev. 140, B32 (1965).
14) A.B.Migdal, Nucl.Phys. 57, 29 (1966).

to the study of partial muon capture rates in ^{16}O, in the frame-work of the particle-hole configurations. Using the effective coupling constants for the quasi-particle amplitudes which give the magnetic moments, the β-decay rates and other nuclear properties correctly, Rho[6] obtained the partial muon capture rates in ^{16}O within experimental accuracy. In this section, we briefly discuss some aspects of the nuclear wavefunctions which we have used in our study of the process (3.1.1).

The cross section for the reaction (3.1.1) has been measured by Meyer et.al.[1] for the incident photon energy upto about 290 Mev. Their experiment selects the transitions to the lowest 2^-, 0^-, 3^- and 1^- states of ^{16}N with isobaric spin 1, which ultimately decay by β-emission, whereas the other higher excited states of ^{16}N decay by nucleon emission.[2] The experimenters[1] measured the 6.14 Mev γ rays in ^{16}O. Figure 1 shows the photon induced transitions $^{16}O(0^+) \longrightarrow {}^{16}N(2^-, 0^-, 3^-, 1^-)$ and their subsequent decays.

The Independent particle Model (IPM) envisages a pure configuration for the excited states of the nucleus while the particle-hole models allow configuration mixing. The particle-hole wave function, in the TDA, in the j-j coupling scheme, is of the form[10-13]:

$$|J_f M_f T M_T\rangle = \sum_{\substack{p,h \\ m_p, m_h, \tau_p, \tau_h}} X^{J_f}_{p,h} (-1)^{j_h+m_h} C(j_p j_h J_f ; m_p m_h M_f) (-1)^{1/2+\tau_h} \times C(\tfrac{1}{2}\tfrac{1}{2}T ; \tau_p \tau_h M_T) a^+_{p m_p \frac{1}{2} \tau_p} a_{h,-m_h \frac{1}{2},-\tau_h} |0\rangle, \quad (3.2.1)$$

where h (hole) is used to denote a typical occupied state characterized by the set of quantum numbers (n_h, ℓ_h, j_h), p(particle) is used to denote a typical unoccupied state characterized by the set of quantum numbers (n_p, ℓ_p, j_p), the ket $|0\rangle$ is the Hartree-Fock ground state and the $X^{J_f}_{p,h}$ are the configuration mixing coefficients associated with the particle-hole configurations with the normalization:

$$\sum_{p,h} \left(X^{J_f}_{p,h} \right)^2 = 1 . \qquad (3.2.2)$$

In Eq.(3.2.1), the C's are the Clebsch-Gordon coefficients(+) and a^+(a) denote the creation (annihilation) operators specified by the labels on them. Further,

$$a^+_h |0\rangle = a_p |0\rangle = 0. \qquad (3.2.3)$$

For, the state h being already occupied in $|0\rangle$, $a^+_h |0\rangle$ violates the exclusion principle and hence it is zero; while the state p being absent from $|0\rangle$, cannot be annihilated by a_p and hence $a_p|0\rangle$ is zero. The Fermion nature of the nucleons is guaranteed by the following standard anticommutation relations.

$$\{a^+_\alpha , a^+_\beta\} = \{a_\alpha , a_\beta\} = 0,$$

$$\text{and} \quad \{a_\alpha , a^+_\beta\} = \delta_{\alpha\beta} . \qquad (3.2.4)$$

In the TDA, as mentioned earlier, the diagonalization of the residual interaction is in the subspace of the

(+) We follow the notation of M.E.Rose for the angular momentum coefficients: M.E.Rose, "Elementary Theory of Angular momentum", John Wiley and Sons, New York, 1957.

$1\hbar\omega$ particle-hole excitations. Wave functions in this approximation have been derived from two different potentials by Elliott and Flowers[9] and by Gillet and Vinh Mau[10]. The potential used by the former was the Rosenfeld mixture, while the potential parameter used by the latter was found from a least squares search carried over nine well-identified energy levels of ^{16}O. The nuclear potential used was of the form:

$$V(r) = f(\frac{r}{\mu})\, V\,(W + BP_\sigma - HP_\tau + MP_\sigma P_\tau) \qquad (3.2.5)$$

where P_σ and P_τ are the spin and isobaric-spin exchange operators, $f(\frac{r}{\mu})$ is a radial form factor, V is the potential depth, μ is the range of the force and W,B,H and M are the four possible types of exchange potentials. In terms of the parameters: $\theta = M-W$ and $\eta = M+W-B-H$ with $M+W+B+H = 1$, the different characteristics of the potentials used by Elliott and Flowers[9] and Gillet[15] are as given below:

Author(s)	V (Mev)	b (fm.)	μ/b	H	θ	η
Elliott and Flowers[9]	-40	1.8	0.9	-0.26	1.06	0.6
Gillet[15]	-40	1.75	1.0	0.4	0	0.4

Both potentials were found to yield overall good fits for the energies but they were found to affect the small

15) V.Gillet, Proceedings of the International School of Physics "Enrico Fermi", Course 36, edited by C.Bloch, Academic Press, New York (1966).

components of the nuclear wave functions appreciably.

In the Random Phase Approximation, Gillet and Vinh-Mau[10] have taken into account the probability amplitude for exciting the nuclear state by annihilation of a particle-hole pair in the ground state. While in the TDA there can be only one particle-hole pair at a given time, any odd number of particle-hole pairs may exist at a given time in the RPA. The particle-hole wave function of the excited state, in the RPA, in the j-j coupling scheme, is given by:

$$
\begin{aligned}
|J_f M_f T M_T\rangle = \sum_{\substack{p,h \\ m_p, m_h, \tau_p, \tau_h}} \Big\{ & X^{J_f}_{p,h} (-1)^{j_h + m_h} C(j_p j_h J_f ; m_p m_h M_f) \times \\
& \times (-1)^{\frac{1}{2} + \tau_h} C(\tfrac{1}{2}\tfrac{1}{2} T ; \tau_p \tau_h M_T) a^{+}_{p m_p \frac{1}{2} \tau_p} a_{h, -m_h \frac{1}{2}, -\tau_h} + \\
& + Y^{J_f}_{p,h} (-1)^{j_p + m_p} C(j_h j_p J_f ; m_h m_p M_f) \times \\
& \times (-1)^{\frac{1}{2} + \tau_p} C(\tfrac{1}{2}\tfrac{1}{2} T ; \tau_h \tau_p M_T) a^{+}_{h m_h \frac{1}{2} \tau_h} a_{p, -m_p \frac{1}{2}, -\tau_p} \Big\} |0\rangle
\end{aligned}
\tag{3.2.6}
$$

where $X^{J_f}_{p,h}$ and $Y^{J_f}_{p,h}$ may be interpreted as probability amplitudes for reaching the excited state when creating or annihilating a particle-hole (ph) pair in the ground state with the normalization:

$$
\sum_{p,h} \left\{ \left(X^{J_f}_{p,h} \right)^2 - \left(Y^{J_f}_{p,h} \right)^2 \right\} = 1 . \tag{3.2.7}
$$

If the ket $|0\rangle$ in Eq.(3.2.5) were a strict closed-shell state, then $a^{+}_{h}\, a_{p}\, |0\rangle$ term should be zero by virtue of

Eq.(3.2.3). But, if the exact ground state departs from the ideal closed-shell state, then $a_h^+ a_p |0\rangle$ term will be non-vanishing. Thus, the RPA introduces some of the ground state correlations. Gillet and Vinh-Mau[10] have computed the particle-hole wave functions, in both the TDA and RPA approximations, for ^{16}O.

Gillet and Jenkins[13] studied the partial muon capture rates between the 0^+ ground state of ^{16}O and the 2^-, 0^-, 1^- and 3^- low-lying T=1 bound states of ^{16}N as a function of C_p, the induced pseudo-scalar coupling constant of weak interactions, with the particle-hole wave functions obtained by Elliott and Flowers[9] and by Gillet and Vinh-Mau[10]. They found the muon capture rates to be very sensitive to the admixture of states. The theoretically calculated $0^+ \longrightarrow 2^-$ transition rate went through a minimum value of 1.2×10^4 sec^{-1} as C_p was increased. and this value is higher than the experimentally measured value[16] of $(0.63 \pm 0.07) \times 10^4$ sec^{-1}. Rho[6] showed that this discrepancy between theory and experiment can be successfully eliminated by the quasi-particle model of Migdal[5]. In the theory for finite Fermi systems developed by Migdal[5,17], multi-particle collisions - which are normally neglected in the shell model- are (properly) taken into account by considering the collision of only two quasi-particles at a time.

16) R.Cohen, S.Devons and A.Kanaris, Phys.Rev.Letts.11, 134 (1963); Nucl.Phys.57, 255 (1964).
17) A.B.Migdal, Nucl.Phys.57, 29 (1964).

For this purpose, the single particle transition operator, as well as the quasi-particle interaction are renormalized. For the T=1 states, the residual interaction between quasi-particles is given, in the momentum representation, by the amplitude[11,12]:

$$\Gamma(\underline{p}_1,\underline{p}_2) = V_0(\underline{\tau}_1\cdot\underline{\tau}_2)\sum_k (f_k' + g_k'\underline{\sigma}_1\cdot\underline{\sigma}_2)P_k\left(\frac{\underline{p}_1\cdot\underline{p}_2}{p_F^2}\right), \quad (3.2.8)$$

where $V_0 = \partial\epsilon_F/\partial\rho$, ϵ_F is the Fermi energy, p_F is the Fermi momentum, ρ is the nuclear matter density, $P_k(\frac{\underline{p}_1\cdot\underline{p}_2}{p_F^2})$ is the Legendre polynomial, f_k' and g_k' are dimensionless coupling constants for spin-independent and spin-dependent T=1 amplitudes determined from magnetic moments, electric quadrupole moments, β-decay ft values, total muon capture rates, isotope shifts, etc., of various nuclei. Assuming that higher harmonics decrease sufficiently fast, one may restrict the values of k to 0 and 1. The expression (3.2.8) for $\Gamma(\underline{p}_1, \underline{p}_2)$ is the most fundamental ansatz in the quasi-particle interaction theory for finite Fermi systems. Apart from the renormalization of the single particle transition operator and the method of determining the effective force $\Gamma(\underline{p}_1, \underline{p}_2)$, the method of Migdal seems to be in the same spirit as the TDA or RPA when only particle-hole configurations are considered. The four nuclear coupling constants f_0', g_0', f_1' and g_1' are determined from experiments. For the strength normalization Migdal et. al. take:

$$V_0 = 4\pi \times 35 \text{ Mev fm}^3. \qquad (3.2.9)$$

This value has been used by Bunatyan[18] in his study of the total muon capture rates in ^{16}O and ^{40}Ca. The comparison with magnetic moments[19] yields:

$$g_0' = 0.50, \qquad (3.2.10)$$

which value is found to be consistent with the Gamow-Teller matrix elements in β-decay[20] and the axial-vector matrix elements in total muon capture rates[19]. The comparison with electric quadrupole moments[5,17] yields:

$$0.35 \leq f_0' \leq 0.40. \qquad (3.2.11)$$

The momentum dependent Migdal amplitudes f_1' and g_1' were not found to effect the muon capture rates and Rho[6] deduces them to be negative, qualitatively. To take into account the renormalization due to complicated quasi-particle configurations, Migdal defines an effective charge e(t) for an operator t. From magnetic moments[19] Migdal deduces for the operator $\underline{\sigma}$, which occurs in Eq.(3.2.8),

$$e(\underline{\sigma}) = 0.9 \text{ for } \Delta T = 1 \text{ transitions.} \qquad (3.2.12)$$

This means that for T=1, one should replace the operator $\underline{\sigma}$ by:

$$\underline{\sigma} \longrightarrow e(\underline{\sigma})\,\underline{\sigma} = 0.9\,\underline{\sigma} \qquad (3.2.13)$$

For the operator p, the effective charge is assumed to be,

---

18) G.G.Bunatyan, Soviet Jour.Nucl.Phys.(English Transl.)2, 619 (1966); ibid 3, 613(1966); V.M.Novikov and M.G.Urin, ibid 3, 302 (1966).

19) A.B.Migdal, Nucl.Phys.75, 441 (1966); Soviet Phys.JETP (English Transl.) 19, 1136 (1964).

20) A.B.Migdal and V.A.Khodel, Soviet.Jour.Nucl.Phys.(English Transl.) 2, 20 (1966).

$e(\underline{p}) \approx 1$. On this basis the operator $\underline{\sigma}.\underline{p}$ has the effective charge $e(\underline{\sigma}.\underline{p}) = e(\underline{\sigma}) = 0.9$. Using the above mentioned values of the constants Rho[6] computed the normalized wave functions for the 0^-, 1^-, 2^- and 3^-, T=1 states of ^{16}O. For example, for the 2^-, T=1 state he has:

$$|2^-,T=1> = 0.932\,|1d_{5/2}\,1p^{-1}_{1/2}> + 0.34|1d_{5/2}\,1p^{-1}_{3/2}> +$$
$$+ 0.099\,|1d_{3/2}\,1p^{-1}_{3/2}> + 0.047|1d_{3/2}\,1p^{-1}_{1/2}> +$$
$$+ 0.057|2s_{1/2}\,1p^{-1}_{3/2}> \qquad (3.2.14)$$

which is to be compared with the particle-hole wave function of Gillet and Vinh-Mau[10] in the TDA, given below:

$$|2^-,T=1> = 0.983|1d_{5/2}\,1p^{-1}_{1/2}> + 0.174|1d_{5/2}\,1p^{-1}_{3/2}> +$$
$$+ 0.035|1d_{3/2}\,1p^{-1}_{3/2}> + 0.007|1d_{3/2}\,1p^{-1}_{1/2}> +$$
$$+ 0.054|2s_{1/2}\,1p^{-1}_{3/2}> \qquad (3.2.15)$$

On comparison, we notice that Eq.(3.2.14) has the same sign as, but more mixing than Eq.(3.2.15). The greater mixing in the first two configurations of Eq.(3.2.14) along with the effective charge for the operators, correctly accounts for the discrepancy which existed earlier between theory and experiment for the $0^+ \longrightarrow 2^-$ muon capture rate in ^{16}O. This is a remarkable success for the quasi-particle theory of Migdal. Rho[6] finds that besides predicting the partial muon capture

rates in ^{16}O within experimental accuracy, Migdal theory also yields a satisfactory fit of the transverse form factor for the inelastic electron scattering process:

$e^- + {}^{16}O(0^+) \longrightarrow e^- + {}^{16}O(2^-)^*$.

For the process $^{16}O(\gamma,\pi^+)^{16}N$ only the T=1 states of the final nucleus will contribute. The wave functions for the four low-lying, T=1, bound states of ^{16}N are taken from the wave functions for the analogous levels in ^{16}O (see Fig.1) under the assumption of good isobaric spin. The wave function amplitudes X and Y which occur in Eqs.(3.2.1) and (3.2.6) for the low-lying states of ^{16}N as given by the various particle-hole models discussed above are given in Table.1.

3. The transition operator for photoproduction of charged pions from a bound nucleon is given by:

$$t = t(\gamma + N \longrightarrow N + \pi^{\pm}) = (\underline{\sigma}.\underline{K}+L)\{\exp(i\underline{k}.\underline{r})\}\,\tau^{\mp} \qquad (3.3.1)$$

where $\tau^{\mp}$ is the isobaric spin operator, $\underline{K}$ and L are the spin-dependent and spin-independent parts of the amplitude given by Eqs.(1.2.17) and (1.2.18) of Chapter.1, $\underline{k} = \underline{\nu} - \underline{\mu}$ is the momentum transfer to the nucleon, $\underline{\nu}$ and $\underline{\mu}$ being the incident photon and outgoing pion momenta and $\underline{r}$ is the position vector of the nucleon. In order to enable us to write the transition operator in spherical tensor notation, we use the unit operator σ_o (=I) in spin-space and redefine $\underline{K}$ and L as

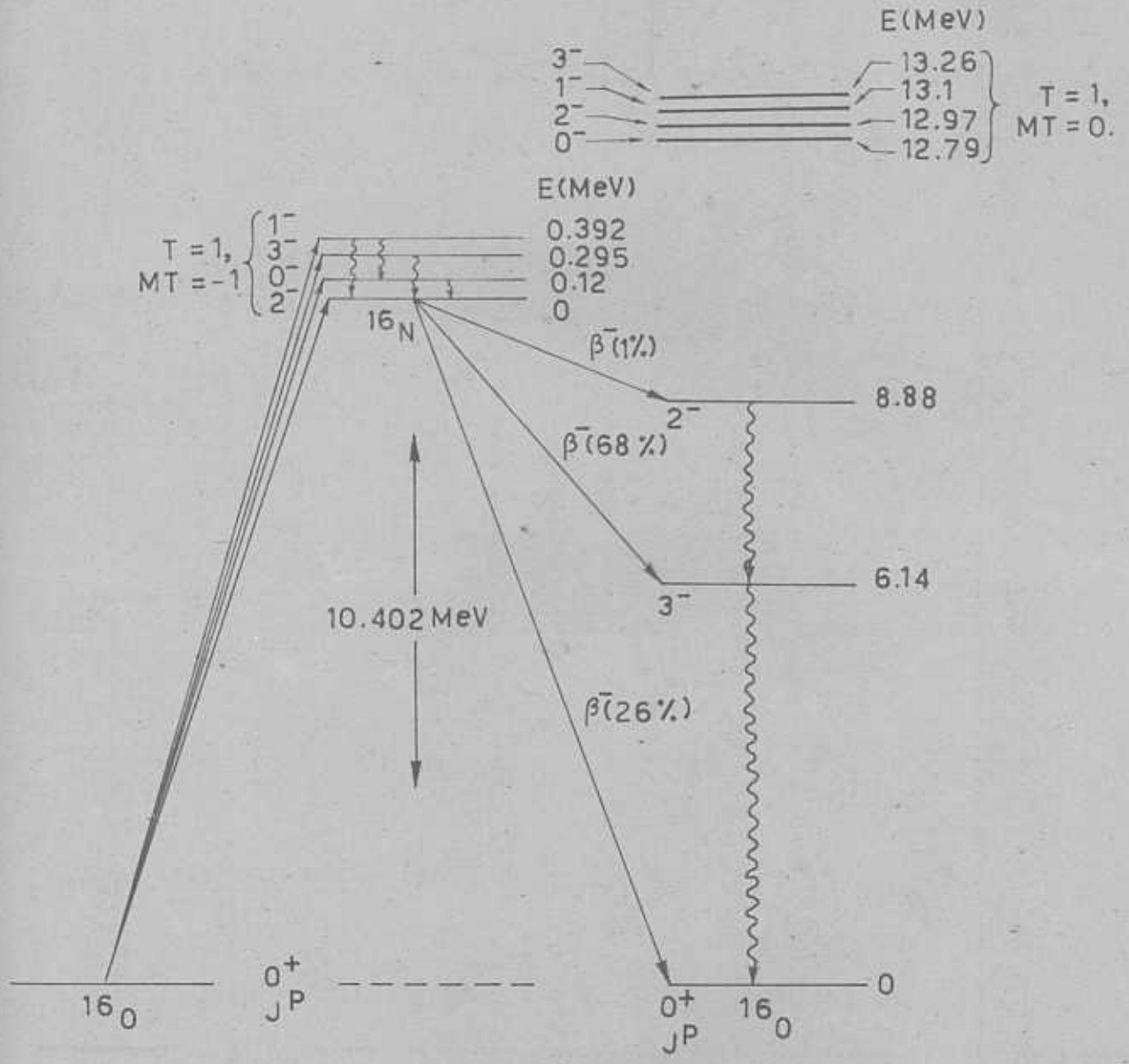

Fig.1. Level scheme for the reaction $^{16}O(\gamma,\pi^+)^{16}N$ and subsequent decays. Solid arrows indicate the β-decays with the branching ratios and wigly arrows the γ de-excitations. The photon induced transitions $^{16}O(0^+) \longrightarrow {}^{16}N(J^\pi)$ are shown on the left. The experiment in ref.1. measures the 6.14 Mev γ rays in ^{16}O. The isobaric analogue levels in ^{16}O are also shown.

Table.1

The wave function amplitudes X and Y for the low-lying states of ^{16}N as given by the Particle-hole models of Elliott and Flowers[15], Gillet and Vinh-Mau[10] and Migdal theory(+), with the proper phases consistent with Eq.(3.2.1). The quantities within brackets denote the amplitudes Y which occur in the RPA.

^{16}N state	Nuclear model	$(1p_{1/2})^{-1}$ $(2s_{1/2})$	$(1p_{1/2})^{-1}$ $(1d_{5/2})$	$(1p_{1/2})^{-1}$ $(1d_{3/2})$	$(1p_{3/2})^{-1}$ $(2s_{1/2})$	$(1p_{3/2})^{-1}$ $(1d_{5/2})$	$(1p_{3/2})^{-1}$ $(1d_{3/2})$
	IPM	1.000	--	--	--	--	--
	EF	1.000	--	--	--	--	-0.050
	GV(TDA)	0.999	--	--	--	--	0.055
0^-	GV(RPA)	0.990	--	--	--	--	0.053
		(-0.012)					(0.012)
	MIGDAL(+)	0.998	--	--	--	--	0.069
	IPM	1.000	--	--	--	--	--
	EF	0.980	--	0.010	-0.160	-0.080	-0.020
1^-	GV(TDA)	0.995	--	-0.008	-0.026	-0.096	-0.020
	GV(RPA)	0.996	--	-0.006	0.026	-0.090	-0.019
		(0.001)		(-0.009)	(-0.012)	(-0.008)	(0.008)
	MIGDAL(+)	0.988	--	0.014	0.054	-0.093	-0.022
	IPM	--	1.000	--	--	--	--
	EF	--	0.980	-0.100	0.060	0.140	0.090
2^-	GV(TDA)	--	0.983	0.007	0.054	0.174	0.035
	GV(RPA)	--	0.985	0.007	0.051	0.166	0.034
			(-0.026)	(-0.001)	(0.009)	(0.020)	(0.015)
	MIGDAL(+)	--	0.932	0.047	0.057	0.340	0.099
	IPM	--	1.000	--	--	--	--
	EF	--	0.980	--	--	-0.180	0.060
3^-	GV(TDA)	--	0.998	--	--	-0.062	-0.011
	GV(RPA)	--	0.999	--	--	-0.059	-0.010
			(0.000)			(-0.004)	(0.029)
	MIGDAL(+)	--	0.936	--	--	-0.245	-0.078

(+) V. Devanathan, M.Rho, K.Srinivasa Rao and S.C.K.Nair, Nucl.Phys.B2, 329 (1969).

$\underline{K}^1$ and K^0. Using the Rayleigh expansion for $\exp(i\underline{k}.\underline{r})$ given by Eq.(2.3.7) we have for the transition operator:

$$t = \tau^{\mp} \sum_{n=0,1} (\underline{\sigma}^n . \underline{K}^n)\, 4\pi \sum_{\ell=0}^{\infty} \sum_{m=-\ell}^{+\ell} i^{\ell} (-1)^m Y_m^{\ell}(\hat{r}) Y_{-m}^{\ell}(\hat{k})\, j_{\ell}(kr)$$

$$= \tau^{\mp} \sum_{n} \sum_{\mu=\pm 1,0} (-1)^{\mu} \sigma_{\mu}^{n} K_{-\mu}^{n}\, 4\pi \sum_{\ell} \sum_{m} i^{\ell} (-1)^m Y_m^{\ell}(\hat{r}) Y_{-m}^{\ell}(\hat{k})\, j_{\ell}(kr).$$

Separating the angular and radial parts and forming the tensor products of the operators in pairs[21], we obtain:

$$t = \tau^{\mp}\, 4\pi \sum_{n,\mu,\ell,m} (-1)^{\mu+m}\, i^{\ell}\, j_{\ell}(kr) \cdot$$

$$\cdot \sum_{\lambda, m_\lambda} C(\ell n \lambda; \mu\, m\, m_\lambda)\, (Y^{\ell}(\hat{r}) \times \sigma^n)^{\lambda}_{m_\lambda} \cdot$$

$$\cdot \sum_{\lambda', m'_\lambda} C(\ell n \lambda'; -\mu, -m, -m'_\lambda)\, (Y^{\ell}(\hat{k}) \times K^n)^{\lambda'}_{-m'_\lambda} .$$

Substituting $\mu+m = m_\lambda$ and using the symmetry property of the Clebsch-Gordon coefficient:

$$C(\ell n \lambda'; -\mu, -m, -m'_\lambda) = (-1)^{\ell+n-\lambda'} C(\ell n \lambda; \mu\, m\, m_\lambda)$$

we note that we can perform the summation over the projection quantum numbers μ and m which yields due to the orthogonality property for the Clebsch-Gordon coefficients:

$$t = \tau^{\mp}\, 4\pi \sum_{n,\ell} \sum_{\lambda, m_\lambda} i^{\ell} (-1)^{\ell+n-\lambda} (-1)^{m_\lambda}\, j_{\ell}(kr) \cdot$$

$$\cdot (Y^{\ell}(\hat{r}) \times \sigma^n)^{\lambda}_{m_\lambda}\, (Y^{\ell}(\hat{k}) \times K^n)^{\lambda}_{-m_\lambda}$$

$$= \tau^{\mp} \sum_{\lambda, m_\lambda} t^{\lambda}_{m_\lambda} \qquad (3.3.2)$$

---

21) V.Devanathan and G.Ramachandran, Nucl.Phys.38, 654 (1962); Ibid.42, 25 (1963); Ibid 66, 595 (1965).

with

$$t^{\lambda}_{m_\lambda} = 4\pi \sum_{n,\ell} i^{\ell} (-1)^{\ell+n-\lambda} (-1)^{m_\lambda} j_\ell(kr) \cdot$$

$$\cdot (Y^{\ell}(\hat{r}) \times \sigma^{n})^{\lambda}_{m_\lambda} (Y^{\ell}(\hat{k}) \times K^{n})^{\lambda}_{-m_\lambda} . \qquad (3.3.3)$$

Using the impulse approximation, the transition operator between any two nuclear states can be written as a superposition of single nucleon transition operators (3.3.2). Thus, the nuclear transition operator is given by:

$$\mathcal{T} = \sum_{n=1}^{A} t_n = \sum_{n=1}^{A} \Big(\sum_{\lambda, m_\lambda} t^{\lambda}_{m_\lambda} \tau^{\mp} \Big)_n \qquad (3.3.4)$$

where A is the mass number of the nucleus. The nuclear transition operator, Eq.(3.3.3), becomes in the occupation number representation:

$$\mathcal{T} = \sum_{\alpha,\beta} \langle \alpha | \sum_{\lambda, m_\lambda} t^{\lambda}_{m_\lambda} \tau^{\mp} | \beta \rangle \, a^{+}_{\alpha} a_{\beta} \qquad (3.3.5)$$

where α and β are the single particle states, $a^{+}(a)$ is the creation (annihilation) operator for a nucleon.

4. We now proceed to evaluate the transition matrix element of the operator $\mathcal{T}$ given by Eq.(3.3.5) between an initial closed shell state and a final T=1 particle-hole state given, in the TDA, by Eq.(3.2.1).

$$Q = \langle J_f M_f 1 M_T \mid \mathcal{T} \mid 0 \rangle$$

$$= \sum_{\substack{p,h \\ m_p, m_h, \tau_p, \tau_h}} X^{J_f}_{p,h} (-1)^{j_h + m_h} C(j_p j_h J_f ; m_p m_h M_f) (-1)^{\frac{1}{2} + \tau_h} \cdot$$

$$\cdot C(\tfrac{1}{2}\tfrac{1}{2}1 ; \tau_p \tau_h M_T) \sum_{\alpha,\beta} \langle \alpha \mid \sum_{\lambda, m_\lambda} t^{\lambda}_{m_\lambda} \tau^{\mp} \mid \beta \rangle \cdot$$

$$\cdot \langle 0 \mid a^{+}_{h_s - m_h \frac{1}{2} s - \tau_h} a_{p m_p \frac{1}{2} \tau_p} a^{+}_{\alpha} a_{\beta} \mid 0 \rangle .$$

In the evaluation of the matrix element $\langle 0 \mid a^{+}_{h} a_{p} a^{+}_{\alpha} a_{\beta} \mid 0 \rangle$, repeated use is made of Eq.(3.2.4) to take a_p and a^{+}_{h} to the extreme right and finally the result Eq.(3.2.3) is applied to omit the terms in which a_p or a^{+}_{h} occurs next to the ket $|0\rangle$. Using this technique we get:

$$Q = \sum_{\substack{p,h \\ m_p, m_h, \tau_p, \tau_h}} X^{J_f}_{p,h} (-1)^{j_h + m_h} C(j_p j_h J_f ; m_p m_h M_f) (-1)^{\frac{1}{2} + \tau_h} \cdot$$

$$\cdot C(\tfrac{1}{2}\tfrac{1}{2}1 ; \tau_p \tau_h M_T) \langle p\, m_p \tfrac{1}{2} \tau_p \mid t^{\lambda}_{m_\lambda} \tau^{\mp} \mid h_s - m_h \tfrac{1}{2} s - \tau_h \rangle .$$

For the case of positive pion (π^+) photoproduction, the isobaric spin operator is τ^- and in spherical tensor notation:

$$\tau^- = \frac{1}{\sqrt{2}} \tau^1_{-1} .$$

Separating the spin and isobaric-spin parts of the matrix element, we have:

$$Q = \sum_{\substack{p,h,m_p,m_h \\ \tau_p,\tau_h,\lambda,m_\lambda}} X^{J_f}_{p,h} (-1)^{j_h + m_h} C(j_p j_h J_f ; m_p m_h M_f) \langle p\, m_p \mid t^{\lambda}_{m_\lambda} \mid h_s - m_h \rangle \cdot$$

$$\cdot \frac{1}{\sqrt{2}} (-1)^{\frac{1}{2} + \tau_h} C(\tfrac{1}{2}\tfrac{1}{2}1 ; \tau_p \tau_h M_T) \langle \tfrac{1}{2} \tau_p \mid \tau^1_{-1} \mid \tfrac{1}{2} - \tau_h \rangle$$

Applying the Wigner-Eckart theorem(+) we have:

$$Q = \sum_{p,h,\lambda,m_\lambda} X^{J_f}_{p,h} \langle p \| t^\lambda \| h \rangle \sum_{m_p,m_h} (-1)^{j_h+m_h} C(j_p j_h J_f ; m_p m_h M_f) \cdot$$

$$\cdot C(j_h \lambda j_p ; -m_h m_\lambda m_p) \frac{1}{\sqrt{2}} \langle \tfrac{1}{2} \| \tau^1 \| \tfrac{1}{2} \rangle \sum_{\tau_p,\tau_h} (-1)^{\frac{1}{2}+\tau_h} C(\tfrac{1}{2}\tfrac{1}{2}1; \tau_p \tau_h M_T) C(\tfrac{1}{2}1\tfrac{1}{2}; -\tau_h, -1, \tau_p) .$$

Using now the symmetry properties of the Clebsch-Gordon coefficients, their orthogonality property and

$$\langle \tfrac{1}{2} \| \tau^1 \| \tfrac{1}{2} \rangle = \sqrt{3} ,$$

we finally get:

$$Q = \delta_{J_f,\lambda} \delta_{M_f,m_\lambda} \delta_{M_T,-1} \sum_{p,h} X^{J_f}_{p,h} \frac{[j_p]}{[J_f]} \langle p \| t^\lambda \| h \rangle , \qquad (3.4.1)$$

where we use the notation $[J]$ for $(2J+1)^{1/2}$. This expression reduces to one term in the independent particle model (IPM) for which $X^{J_f}_{p,h} = 1$. Eq.(3.4.1) can be written in an explicit form by using Eq.(3.3.3) for the transition operator, as:

$$Q = 4\pi \sum_{p,h,n,\ell} i^\ell (-1)^{\ell+n-J_f} \frac{[j_p]}{[J_f]} X^{J_f}_{p,h} (-1)^{M_f} \langle j_\ell(kr) \rangle_{p,h} \cdot$$

$$\cdot (Y^\ell(\hat{k}) \times K^n)^{J_f}_{-M_f} \langle p \| (Y^\ell(\hat{r}) \times \sigma^n)^{J_f} \| h \rangle ,$$

(3.4.2)

where $\langle j_\ell(kr) \rangle_{p,h}$ is the radial integral involving the spherical Bessel function $j_\ell(kr)$ between the particle and hole states:

(+) We follow the statement of this theorem as given by M.E.Rose, "Elementary Theory of Angular Momentum", John Wiley and sons, New York (1957). Viz. $\langle j'm' | O^\lambda_{m_\lambda} | jm \rangle = c(j \lambda j ; m\, m_\lambda\, m') \langle j' \| O^\lambda \| j \rangle$ where $\langle j' \| O^\lambda \| j \rangle$ is the reduced matrix element.

$$\langle j_\ell(kr)\rangle_{p,h} = \langle j_\ell(kr)\rangle_{n_p\ell_p, n_h\ell_h}$$

$$= \int_0^\infty R^*_{n_p\ell_p}(r)\, j_\ell(kr)\, R_{n_i\ell_i}(r)\, r^2\, dr, \qquad (3.4.3)$$

where $R_{n\ell}(r)$ is the harmonic oscillator wave function used to describe the radial wave functions of the single particle states. In the present study of the reaction $^{16}O(\gamma,\pi^+)^{16}N$, only the configurations $(1p)^{-1}(1d)$ and $(1p)^{-1}(2s)$ occur, and the radial integrals for these cases can be evaluated analytically (see Appendix.C) to give the results:

$$\langle j_1(kr)\rangle_{1P,1d} = \left(\frac{2}{5}\right)^{1/2} \frac{kb}{12}(10-k^2b^2)\exp(-k^2b^2/4), \qquad (3.4.4)$$

$$\langle j_3(kr)\rangle_{1P,1d} = \left(\frac{2}{5}\right)^{1/2} \frac{k^3b^5}{12}\exp(-k^2b^2/4), \qquad (3.4.5)$$

and

$$\langle j_1(kr)\rangle_{1P,2S} = \frac{kb}{12}(k^2b^2-4)\exp(-k^2b^2/4). \qquad (3.4.6)$$

The reduced matrix element in Eq.(3.4.2) is evaluated[7] by making use of standard relations as:

$$\langle p \| (Y^\ell(\hat{r}) \times \sigma^n)^{J_f} \| h\rangle \equiv \langle \ell_p \tfrac{1}{2} j_p \| (Y^\ell(\hat{r}) \times \sigma^n)^{J_f} \| \ell_h \tfrac{1}{2} j_h\rangle$$

$$= [\ell_p][1/2][j_h][J_f] \begin{Bmatrix} \ell_h & \ell & \ell_p \\ 1/2 & n & 1/2 \\ j_h & J_f & j_p \end{Bmatrix} \cdot$$

$$\cdot \langle \ell_p \| Y^\ell(\hat{r}) \| \ell_h\rangle \langle \tfrac{1}{2} \| \sigma^n \| \tfrac{1}{2}\rangle \cdot$$

(3.4.7)

where

$$\langle \ell_p \| Y^{\ell}(\hat{r}) \| \ell_h \rangle = \frac{[\ell_h][\ell]}{\sqrt{4\pi}\,[\ell_p]}\, C(\ell_h \ell \ell_p; 000)\,, \qquad (3.4.8)$$

and

$$\langle \tfrac{1}{2} \| \sigma^{n} \| \tfrac{1}{2} \rangle = [n]\,. \qquad (3.4.9)$$

The square of the transition matrix element[+] is given by:

$$\begin{aligned} |Q|^2 &= \sum_{M_f} |\langle J_f M_f\, 1,-1 \,|\, \mathcal{T} \,|\, 0 \rangle|^2 \\ &= 16\pi^2 \sum_{p,h,p',h'} \frac{[j_p][j_{p'}]}{[J_f]^2}\, X^{J_f}_{p,h} \left(X^{J_f}_{p',h'}\right)^* \cdot \\ &\quad \cdot \sum_{n,\ell,n',\ell'} i^{\ell-\ell'} (-1)^{\ell+n-\ell'-n'} \langle j_{\ell}(kr) \rangle_{p,h} \langle j_{\ell'}(kr) \rangle^*_{p',h'} \cdot \\ &\quad \cdot \Big\{ \sum_{M_f} (Y^{\ell}(\hat{k}) \times K^{n})^{J_f}_{-M_f} \left[(Y^{\ell'}(\hat{k}) \times K^{n'})^{J_f}_{-M_f} \right]^* \Big\} \cdot \\ &\quad \cdot \langle p \| (Y^{\ell}(\hat{r}) \times \sigma^{n})^{J_f} \| h \rangle \langle p' \| (Y^{\ell'}(\hat{r}) \times \sigma^{n'})^{J_f} \| h' \rangle^* . \end{aligned} \qquad (3.4.10)$$

The quantity within the flower bracket of Eq.(3.4.10) can be simplified[++] to give:

$$\begin{aligned} &\sum_{M_f} (Y^{\ell}(\hat{r}) \times K^{n})^{J_f}_{-M_f} \left[(Y^{\ell'}(\hat{r}) \times K^{n'})^{J_f}_{-M_f} \right]^* = \\ &= \frac{(-1)^{\ell-\ell'+J_f}}{(4\pi)^{1/2}} [\ell][\ell'][J_f]^2 \sum_{N} \frac{1}{[N]}\, C(\ell\ell' N; 000) \cdot \\ &\quad \cdot W(\ell\ell' n n'; J_f N) \left(Y^{N}(\hat{k}) \cdot (K^{n} \times K^{*n'})^{N} \right). \end{aligned} \qquad (3.4.11)$$

+ Note that the averaging over photon polarizations is taken care of elsewhere-while evaluating the expressions LL^*, $\underline{K}.\underline{K}^*$, etc. in Chapter.1.

++ A phase error in Eq.(7) of G.Ramachandran and V.Devanathan's paper in Nucl.Phys. 66, 595 (1965) has been corrected by V.Devanathan, Nucl.Phys. 87, 397 (1967).

Due to the two reduced matrix elements in Eq.(3.4.10), we have the two parity Clebsch-Gordon coefficients, $C(\ell_h \ell \ell_p ; 000)$ and $C(\ell_h' \ell' \ell_p' ; 000)$, which will be non-zero if and only if

$$\ell_h + \ell + \ell_p \quad \text{and} \quad \ell_h' + \ell' + \ell_p' \quad \text{are even.}$$

In other words, $\ell + \ell'$ must be even, if the product of the above mentioned parity Clebsch-Gordon coefficients is to be non-zero. Further, the parity Clebsch-Gordon coefficient $C(\ell \ell' N ; 000)$ in Eq.(3.4.11) will be non-zero only if:

$$\ell + \ell' + N \text{ is even.}$$

Therefore, it follows that N, the summation index in Eq.(3.4.11) must be even. Furthermore, in the scalar product $(Y^N(\hat{k}).(K^n \times K^{*n'})^N)$, since n and n' can each take only two values 0 and/or 1, it follows that:

$$N = 0,2 \quad \text{and} \quad n = n'.$$

The values of the scalar products are evaluated and the results are given in Table.2.

In the case of the Random Phase Approximation, the transition matrix element of the operator $\mathcal{T}$ given by Eq.(3.3.5) between an initial closed shell state and a final T=1 particle-hole state given by Eq.(3.2.6)is:

$$Q = \delta_{J_f,\lambda}\, \delta_{M_f,m_\lambda}\, \delta_{M_T,-1} \sum_{p,h} \left\{ X^{J_f}_{p,h} \frac{[j_p]}{[J_f]} \langle p \| t^\lambda \| h \rangle + \right.$$

$$\left. + Y^{J_f}_{p,h} \frac{[j_h]}{[J_f]} \langle h \| t^\lambda \| p \rangle \right\}. \qquad (3.4.12)$$

Table.2

The scalar products $(Y^N(\hat{k}).(\underline{K}^n \times \underline{K}^{*n})^N)$, for permitted values of n and N, are given in the table below.

N \ n	0	1
0	$(4\pi)^{-1/2}\ LL^*$	$(12\pi)^{-1/2}\underline{K}.\underline{K}^*$
2	0	$(\frac{15}{8\pi})^{1/2}[\frac{(\underline{k}\cdot\underline{K})(\underline{k}\cdot\underline{K}^*)}{k^2} - \frac{(\underline{K}\cdot\underline{K}^*)}{3}]$

The expressions for $\underline{K}.\underline{K}^*$, LL^* and $(\underline{k}.\underline{K})(\underline{k}.\underline{K}^*)$, for the case of charged pion photoproduction are given explicitly by Eqs.(1.2.22), (1.2.23) and (1.2.24) of Chapter.1.

Squaring and summing over M_f, we obtain:

$$|Q|^2 = \frac{16\pi^2}{[J_f]^2} \sum_{p,h,p',h'} \Big\{ [j_p][j_{p'}]\, X^{J_f}_{p,h} (X^{J_f}_{p',h'})^* M_{1,1} +$$

$$+ [j_p][j_{h'}]\, X^{J_f}_{p,h} (Y^{J_f}_{p',h'})^* M_{1,2} +$$

$$+ [j_h][j_{p'}]\, Y^{J_f}_{p,h} (X^{J_f}_{p',h'})^* M_{2,1} +$$

$$+ [j_h][j_{h'}]\, Y^{J_f}_{p,h} (Y^{J_f}_{p',h'})^* M_{2,2} \Big\} \cdot$$

$$\cdot \sum_{n,\ell,n',\ell'} i^{\ell-\ell'} (-1)^{\ell+n-\ell'-n'} \Big\{ \sum_{M_f} (Y^{\ell}(\hat{k}) \times K^{n})^{J_f}_{-M_f} [(Y^{\ell'}(\hat{k}) \times K^{n'})^{J_f}_{-M_f}]^* \Big\}, \qquad (3.4.13)$$

where

$$M_{1,1} = \langle p \| (Y^{\ell}(\hat{r}) \times \sigma^{n})^{J_f} \| h \rangle \langle p' \| (Y^{\ell'}(\hat{r}) \times \sigma^{n'})^{J_f} \| h' \rangle^* \cdot$$

$$\cdot \langle j_\ell(kr) \rangle_{p,h} \langle j_{\ell'}(kr) \rangle^*_{p',h'}, \qquad (3.4.14)$$

$$M_{1,2} = \langle p \| (Y^{\ell}(\hat{r}) \times \sigma^{n})^{J_f} \| h \rangle \langle h' \| (Y^{\ell'}(\hat{r}) \times \sigma^{n'})^{J_f} \| p' \rangle^* \cdot$$

$$\cdot \langle j_\ell(kr) \rangle_{p,h} \langle j_{\ell'}(kr) \rangle^*_{h',p'}, \qquad (3.4.15)$$

$$M_{2,1} = \langle h \| (Y^{\ell}(\hat{r}) \times \sigma^{n})^{J_f} \| p \rangle \langle p' \| (Y^{\ell'}(\hat{r}) \times \sigma^{n'})^{J_f} \| h' \rangle^* \cdot$$

$$\cdot \langle j_\ell(kr) \rangle_{h,p} \langle j_{\ell'}(kr) \rangle^*_{p',h'}, \qquad (3.4.16)$$

$$M_{2,2} = \langle h \| (Y^{\ell}(\hat{r}) \times \sigma^{n})^{J_f} \| p \rangle \langle h' \| (Y^{\ell'}(\hat{r}) \times \sigma^{n'})^{J_f} \| p' \rangle^* \cdot$$

$$\cdot \langle j_\ell(kr) \rangle_{h,p} \langle j_{\ell'}(kr) \rangle^*_{h',p'}. \qquad (3.4.17)$$

The differential cross section for photoproduction of pions from nuclei is:

$$\frac{d\sigma}{d\Omega} = (2\pi)^{-2}\, \mu\mu_0\, |Q|^2 \qquad (3.4.18)$$

where $|Q|^2$ is given by Eq.(3.4.10) in the case of the particle-hole model with Tamm-Dancoff Approximation and by Eq.(3.4.17) in the case of the particle-hole model with Random Phase Approximation.

5. In the early experiments[1] on photoproduction of charged pions from nuclei, one of the gross features which was observed was that the sum of the π^+ and π^- cross sections exhibited an almost exact $A^{2/3}$ dependence. In order to account for this $A^{2/3}$ dependence, Butler[7] invoked the mechanism of surface production of pions from nuclei. According to Butler's model, all the nucleons in the nucleus do not take part in the production process, but only those which are outside the central core of constant density, i.e. nucleons whose radial coordinates are greater than the constant density nuclear radius 'r_0', take part in the production process. With this model, Butler[7] was not only able to reproduce the desired $A^{2/3}$ dependence but also account for large fractions ($\sim 60 - 70\%$) of the observed cross sections, as well as the correct π^- to π^+ cross section ratios. This idea has been extended by Laing and Moorehouse[22]

22) E.W.Laing and R.G.Moorehouse, Proc.Phys.Soc.A70, 629(1957).

to the shell model treatment of the problem, wherein the nucleus makes a specific transition from an initial to a final state.

Physically, the surface production model amounts to assuming that all or most of the pions produced in the interior of the nucleus are directly, reabsorbed. Since a quantitative calculation of the reabsorption effect is somewhat difficult, we invoke the surface production mechanism to account for the same.

Stated naively, the difference between the volume and surface production models lies in the limits of integration of the radial integral given by Eq.(3.4.3). In the volume production model, the integral has the limits 0 and ∞ , whereas in the surface production model, the limits are r_0 and ∞ . Explicitly,

$$\langle j_\ell(kr) \rangle_{p,h} = \int_a^\infty R^*_{n_p \ell_p}(r)\, j_\ell(kr)\, R_{n_h \ell_h}(r)\, r^2 dr \qquad (3.5.1)$$

where $a = 0$ corresponds to the volume production model, and $a > r_0$ corresponds to the surface production model. It should be noted that the radial integrals, $\langle j_\ell(kr) \rangle_{p,h}$, cannot be evaluated analytically in the case of the surface production model, since the lower limit of the integration is r_0 , the radius of the nucleus. In this case, the radial integrals have to be evaluated numerically. Unfortunately, r_0 is not a well defined quantity because of the diffuse surface

of the nucleus and furthermore the radial integrals are sensitive to the lower limit of the integration r_0.

6. Before discussing in detail the results of the calculations, we can gain an insight by examining the radial integrals $< j_\ell(kr) >_{p,h}$. In Fig.2, the relevant radial integrals $< j_1(kr) >_{1p,1d}$, $< j_3(kr) >_{1p,1d}$ and $< j_1(kr) >_{1p,2s}$ are plotted as a function of pion angle for two different harmonic oscillator length parameter values b = 1.5 fm. and 2.0 fm. These radial integrals are for the volume production model, i.e. $\alpha = 0$. In Fig.3, the same radial integrals are plotted for the surface production model with $r_0 = 2.686$ fm. From these figures, we notice that in general, for forward angles there is little difference between b=1.5 fm. and b=2.0 fm. curves, but this difference becomes appreciable for larger angles. In Fig.4, the same radial integrals are plotted for four different values of the cut-off parameter, viz. $r_0 = 0.0$, 1.6, 1.9 and 2.2 units of pion Compton wavelength. These three figures clearly reveal that the cross sections for the transitions to the 0^- and 1^- states are expected to be smaller than those to the 2^- and 3^- states. For the 0^- and 1^- states, the most important integral is $< j_1(kr)_{1p,2s}$ which has a large cancellation when integrated over pion angles. On the other hand, the radial integrals

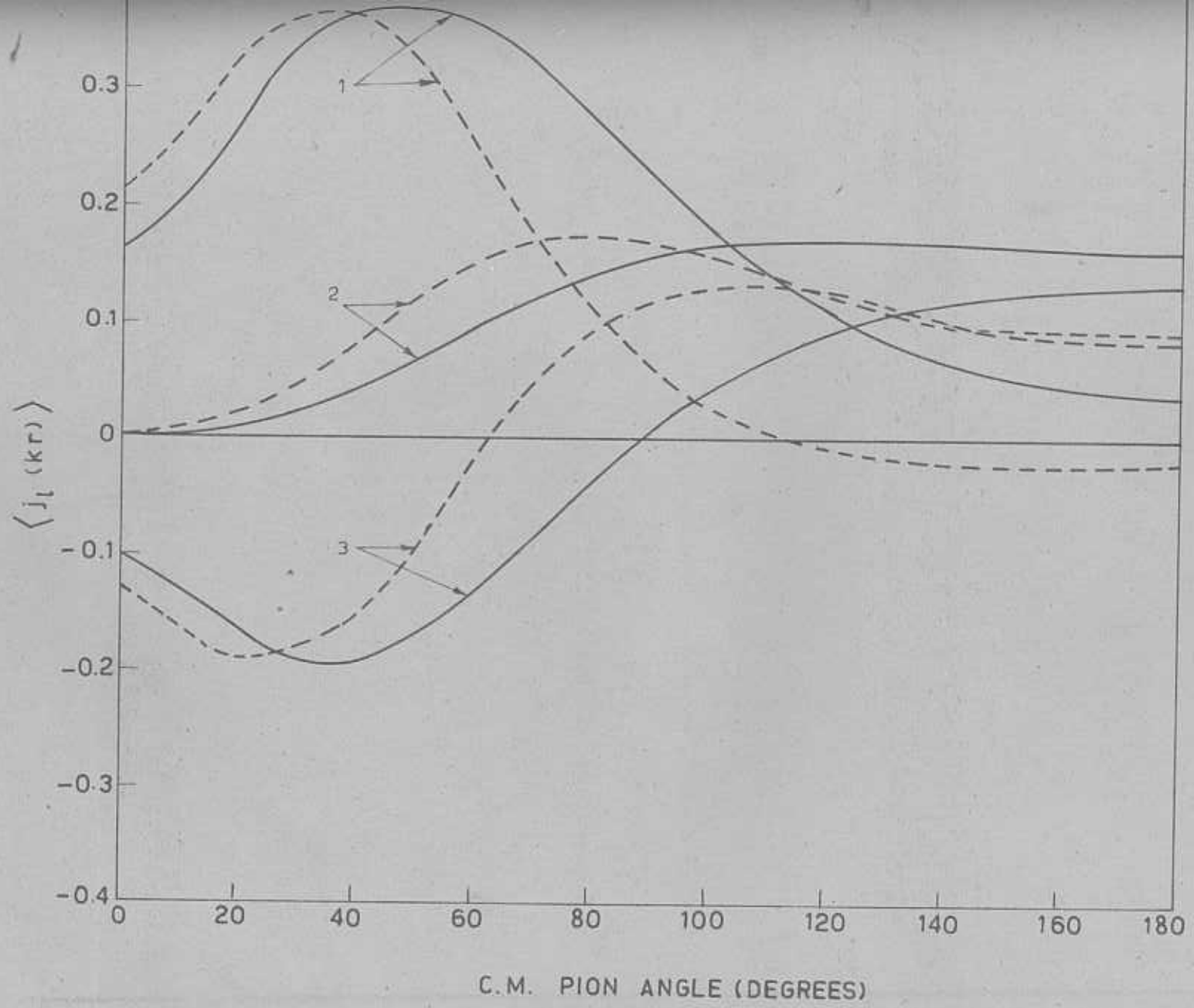

Fig.2. The radial integrals in the volume production model ($r_0 = 0$) as a function of the angle of pion emission. The incident γ-ray energy is taken as 260 Mev. Curves 1,2, and 3 respectively the radial integrals $\langle j_1(kr) \rangle_{1p,1d}$, $\langle j_3(kr) \rangle_{1p,1d}$ and $\langle j_1(kr) \rangle_{1p,2s}$. The solid line curves correspond to b=2 fm. and the dashed line curves to b=1.5 fm.

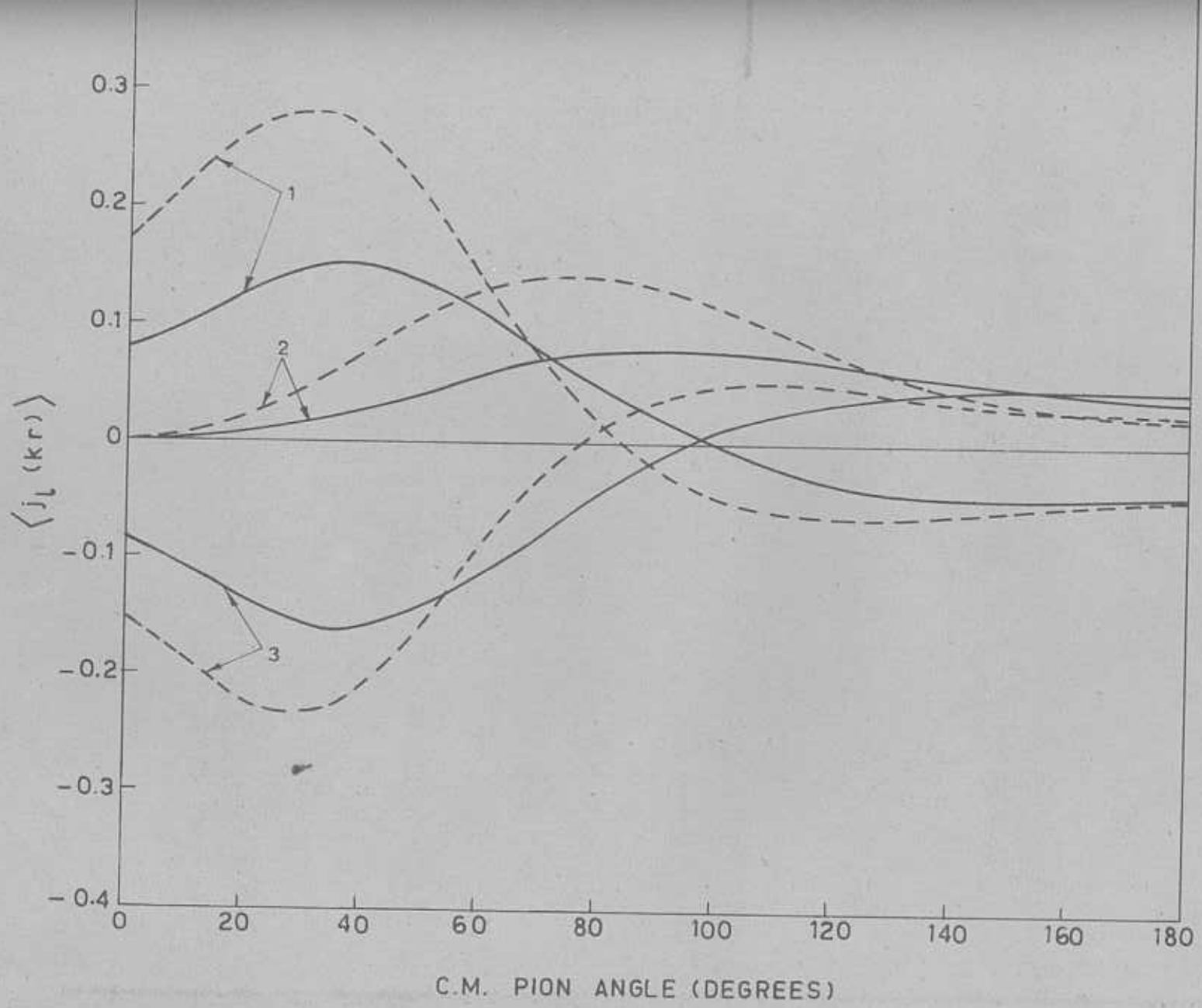

Fig.3. The radial integrals in the surface production model (r_0=2.686 fm.) as a function of the angle of the pion emission. See the caption for Fig.2 for other details.

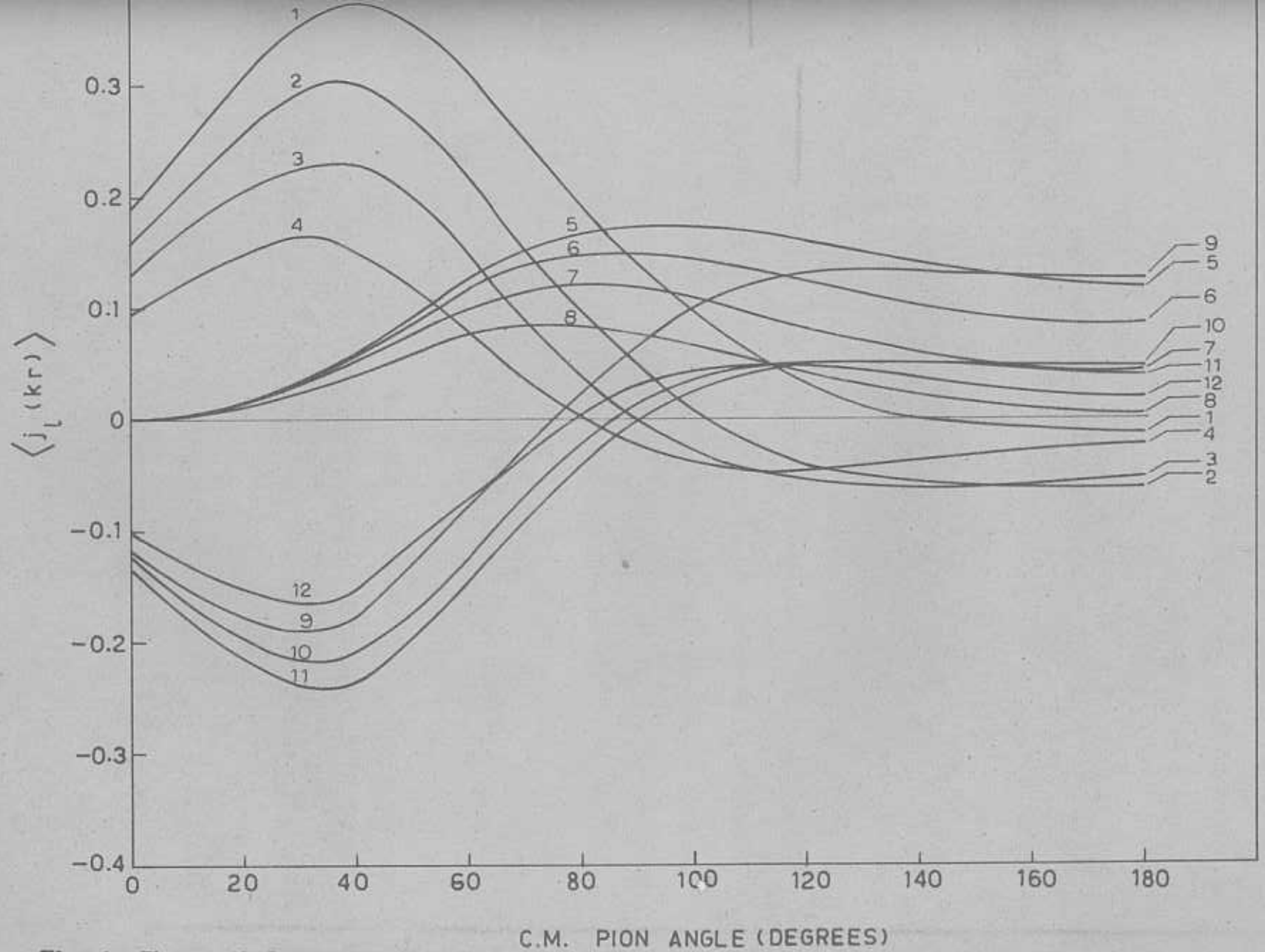

Fig.4. The radial integrals are plotted for four values of the cut-off parameter, γ_0 =0.0, 1.6,1.9 and 2.2 in units of pion Compton wave length. Curves 1,2,3 and 4 correspond to $\langle j_1(kr) \rangle_{1p,1d}$; curves 5,6,7 and 8 correspond to $\langle j_3(kr) \rangle_{1p,1d}$; and curves 9,10,11 and 12 correspond to $\langle j_1(kr) \rangle_{1p,2s}$.

$< j_1(kr)_{1p,1d}$ and $< j_3(kr) >_{1p,1d}$ which play a dominant role for 2^- and 3^- states have a large forward peaking and have negligible or no cancellation by small backward negative components when integrated over the pion angle.

Let us now turn to a discussion of the cross sections. Table.3 gives the cross sections for the reaction $^{16}O(\gamma,\pi^+)^{16}N$ using the volume production model for an incident photon energy of 260 Mev. The effect of the oscillator length parameter 'b' on the cross section has also been studied, and in general found to be none-too-serious, except for the 2^- final state. A careful consideration of the partial transitions and a reference to figures, 3 and 4 will reveal the cause for this. Of the partial transitions that we have considered, the transition to the 2^- state is the only one which includes an interference between two different ℓ terms and this interference term involving the product of the radial integrals $< j_1(kr) >_{1p,1d}$ and $< j_3(kr) >_{1p,1d}$ is very sensitive to the value of the size parameter b.

Table.4 summarizes the results obtained for the cross section with r_o treated as a free parameter and an incident photon energy of 260 Mev. Notice the sensitive dependence of the cross section on r_o. Tables 5 and 6 give the cross sections in the volume production ($r_o = 0$) and surface production ($r_o > 0$) models for various incident photon energies.

Table.3.

Cross sections for the reaction $^{16}O(\gamma,\pi^+)^{16}N$ in the volume production model, for an incident photon energy of 260 Mev, as a function of the harmonic oscillator size parameter b. The nuclear wavefunctions used correspond to the following models for the ^{16}N states: IPM, EF, GV(TDA) and GV(RPA).

^{16}N state	b (fermi)	Cross section in μb.			
		IPM	EF	GV(TDA)	GV(RPA)
0^-	1.50	0.384	0.475	0.314	0.292
	1.76	0.423	0.454	0.406	0.389
	2.00	0.475	0.486	0.475	0.456
1^-	1.50	3.273	3.223	2.853	2.923
	1.76	3.971	4.129	3.717	3.786
	2.00	3.858	3.946	3.622	3.689
2^-	1.50	21.501	14.304	14.210	13.983
	1.76	13.233	8.947	8.817	8.685
	2.00	8.979	6.083	5.974	5.863
3^-	1.50	15.114	13.445	14.142	13.314
	1.76	14.704	12.862	13.742	12.942
	2.00	12.352	10.631	11.531	10.862
Sum of all the above four states	1.50	40.272	31.447	31.519	30.512
	1.76	32.331	26.392	26.682	25.772
	2.00	25.664	21.146	21.602	20.870

Table.4

Cross sections for the reaction $^{16}O(\gamma,\pi^+)^{16}N$ for an incident photon energy of 260 Mev and b=1.76 fm, as a function of the cut-off parameter r_0, $r_0 = 0$ corresponds to the volume production model and $r_0 > 0$ corresponds to surface production model. The nuclear wavefunctions used correspond to the following models for the ^{16}N states: IPM, EF, GV(TDA), GV(RPA) and MIGDAL.

^{16}N state	r_0 (in pion compton wavelength)	Cross section in μb.				
		IPM	EF	GV(TDA)	GV(RPA)	MIGDAL
0^-	0	0.423	0.454	0.406	0.389	0.327
	1.6	0.382	0.461	0.304	0.277	0.231
	1.7	-	-	-	-	0.223
	1.9	0.283	0.330	0.235	0.216	0.180
	2.2	0.145	0.166	0.123	0.114	-
1^-	0	3.971	4.129	3.717	3.786	3.092
	1.6	2.521	1.947	1.71	1.782	1.444
	1.7	-	-	-	-	1.415
	1.9	1.994	1.621	1.433	1.486	1.205
	2.2	1.086	0.915	0.811	0.839	-
2^-	0	13.233	8.947	8.817	8.655	3.769
	1.6	6.502	3.935	3.949	3.960	1.635
	1.7	-	-	-	-	1.342
	1.9	3.511	2.039	2.069	2.090	0.847
	2.2	1.478	0.840	0.855	0.868	-
3^-	0	14.704	12.862	13.742	12.942	8.591
	1.6	10.026	8.692	9.364	8.820	5.882
	1.7	-	-	-	-	5.041
	1.9	5.602	4.800	5.228	4.925	3.304
	2.2	2.191	1.849	2.043	1.925	-
Sum of all the above four states	0	32.331	26.392	26.682	25.771	15.779
	1.6	19.431	15.035	15.327	14.839	9.192
	1.7	-	-	-	-	8.021
	1.9	11.390	8.790	8.965	8.717	5.537
	2.2	4.900	3.770	3.832	3.744	-

Table.5

Cross sections for the reaction $^{16}O(\gamma,\pi^+)^{16}N$ in the volume production ($r_o=0$) and surface production ($r_o>0$) models, with b=1.76 fm for various incident photon energies. The nuclear wavefunctions used correspond to the following models for the ^{16}N states: IPM, EF, GV(TDA) and GV(RPA).

Incident Photon energy (Mev)	(in pion compton wavelength)	Cross section in μb.(Sum of $0^-,1^-,2^-,3^-$ states of ^{16}N) IPM	EF	GV(TDA)	GV(RPA)
	0	31.849	21.010	21.006	-
165	1.6	24.048	16.998	16.384	-
	1.9	15.024	11.108	10.508	-
	2.2	6.911	5.334	4.969	-
	0	36.702	25.528	24.826	24.353
180	1.6	26.140	19.135	17.823	17.604
	1.9	15.673	12.007	11.008	10.872
	2.2	6.937	5.551	5.042	4.970
	0	34.807	25.321	24.615	24.004
200	1.6	23.795	17.914	16.857	16.541
	1.9	13.990	10.994	10.237	10.038
	2.2	6.125	5.002	4.635	4.536
	0	33.594	27.093	26.419	25.545
230	1.6	21.053	16.682	16.168	15.682
	1.9	12.441	10.013	9.682	9.413
	2.2	5.550	4.490	4.334	4.228

(continued on next page)

Table.5 (continued)

Incident photon energy (Mev)	r_o (in pion compton wavelength)	Cross section in μb.(Sum of $0^-,1^-,2^-,3^-$ states of ^{16}N)			
		IPM	EF	GV(TDA)	GV(RPA)
	0	32.331	26.392	26.682	25.771
260	1.6	19.431	15.035	15.327	14.839
	1.9	11.390	8.790	8.965	8.717
	2.2	4.900	3.770	3.832	3.746
	0	33.007	25.818	27.757	26.845
290	1.6	19.350	14.124	15.315	14.845
	1.9	11.116	8.084	8.735	8.512
	2.2	4.679	3.424	3.672	3.594
	0	33.580	24.716	28.011	27.153
320	1.6	19.699	13.735	15.387	14.954
	1.9	11.302	7.952	8.791	8.587
	2.2	4.897	3.514	3.822	3.746
	0	29.033	20.855	23.657	22.974
350	1.6	17.353	12.117	13.278	12.934
	1.9	10.135	7.215	7.749	7.582
	2.2	4.538	3.303	3.486	3.422
	0	21.880	15.970	17.377	16.889
380	1.6	13.390	9.625	10.048	9.802
	1.9	7.959	5.841	5.982	5.859
	2.2	3.608	2.700	2.726	2.679

Table.6

Cross sections for the reaction $^{16}O(\gamma,\pi^+)^{16}N$ in the volume production ($r_o = 0$) and surface production ($r_o > 0$) models, for b = 1.76 fm and various incident photon energies. The nuclear wave function used corresponds to the MIGDAL theory model.

Incident photon energy (Mev)	r_o (in pion compton wavelength)	Cross section in μb for ^{16}N states				
		0^-	1^-	2^-	3^-	Sum of all the four states
165	0	1.959×10^{-5}	0.631	2.865	0.303	3.699
	1.6	4.598×10^{-5}	1.345	1.700	0.264	3.309
	1.7	4.456×10^{-5}	1.313	1.446	0.248	3.007
	1.9	3.673×10^{-5}	1.098	0.953	0.205	2.256
180	0	0.011	0.830	6.827	1.729	9.447
	1.6	0.035	2.664	3.736	1.461	7.896
	1.7	0.034	2.592	3.112	1.354	7.092
	1.9	0.027	2.116	1.955	1.083	5.181
200	0	0.028	0.947	7.066	3.910	11.951
	1.6	0.096	2.308	3.467	3.174	9.045
	1.7	0.091	2.239	2.817	2.893	8.040
	1.9	0.070	1.802	1.678	2.216	5.766
230	0	0.132	2.101	5.157	6.973	14.363
	1.6	0.152	1.652	3.226	5.163	9.198
	1.7	0.150	1.611	1.789	4.546	8.096
	1.9	0.117	1.348	1.071	3.179	5.715

(continued on next page)

Table.6 (continued)

Incident photon energy (Mev)	r_o (in pion compton wavelength)	Cross section in μb for ^{16}N states				
		0^-	1^-	2^-	3^-	Sum of all the four states
260	0	0.327	3.092	3.769	8.591	15.779
	1.6	0.231	1.444	1.635	5.882	9.192
	1.7	0.223	1.415	1.342	5.041	8.021
	1.9	0.180	1.205	0.847	3.304	5.536
290	0	0.563	3.910	3.088	9.991	17.552
	1.6	0.332	1.427	1.473	6.388	9.620
	1.7	0.322	1.399	1.233	5.368	8.322
	1.9	0.265	1.188	0.796	3.389	5.638
320	0	0.669	4.198	3.049	10.355	18.271
	1.6	0.400	1.511	1.588	6.342	9.841
	1.7	0.388	1.480	1.333	5.294	8.495
	1.9	0.322	1.251	0.854	3.338	5.765
350	0	0.517	3.430	3.023	8.224	15.194
	1.6	0.339	1.405	1.610	4.960	8.314
	1.7	0.330	1.376	1.346	4.154	7.206
	1.9	0.276	1.163	0.859	2.668	4.966
380	0	0.298	2.314	2.679	5.374	10.665
	1.6	0.222	1.131	1.417	3.263	6.033
	1.7	0.216	1.107	1.183	2.755	5.261
	1.9	0.183	0.937	0.756	1.808	3.684

In Fig.5, the theoretical partial volume production cross sections for the reaction $^{16}O(\gamma,\pi^+)^{16}N$ calculated in the four models - IPM, EF, GV(RPA) and MIGDAL - are plotted as a function of the incident photon energy. Only the ones corresponding to the MIGDAL model are expected to be free of the uncertainty due to nuclear structure, since Migdal theory has been found to give satisfactory results both for muon capture and inelastic electron scattering[12]. It is interesting to compare the results of IPM with MIGDAL for the dominant transitions to the 2^- and 3^- states of ^{16}N. Take, as an example, the case where the incident photon energy is 260 Mev. Just as in the muon capture process where a correct account of nuclear correlations reduces the capture rate to the 2^- state by a factor of about 4 from the IPM value, a reduction of the same order is obtained also in the pion photoproduction case. A less drastic reduction is found for the 3^- state: i.e., $(\sigma_{IPM} - \sigma_{MIGDAL}) / \sigma_{IPM} \approx 0.42$ but this is consistent with that observed in the muon capture process, viz. $(\Lambda_{IPM} - \Lambda_{MIGDAL}) / \Lambda_{IPM} \approx 0.46$. There are however some significant differences between the muon capture process and the pion photoproduction process. In the former, the transition to the 3^- state is highly forbidden, but in the latter, the matrix element becomes large because of the large momentum transfer involved. This accounts for the fact

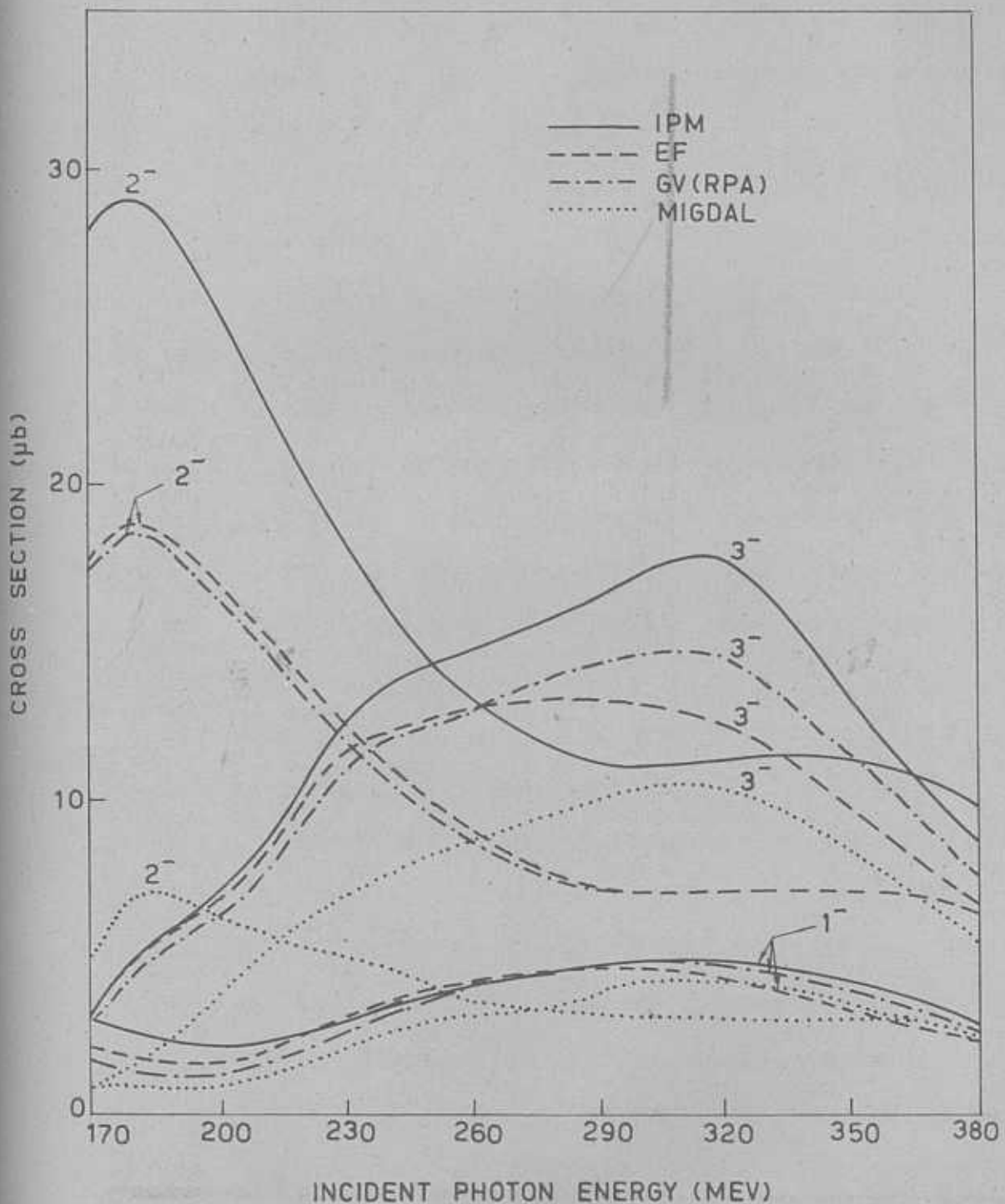

Fig.5. Partial cross sections for the reaction $^{16}O(\gamma,\pi^+)^{16}N$ for the final nuclear states 1^-, 2^- and 3^- obtained assuming volume production of pions with b=1.76 fm for the IPM, EF, GV(RPA) and MIGDAL models.

that the $0^+ \longrightarrow 3^-$ partial cross section contributes almost 50% to the total cross section in the case of the pion photoproduction process. One can see from Fig.5 that the estimate given above would also hold for other photon energies. Further, from Fig.5 it is clear that of the four final states of ^{16}N we have taken into account, the greater part of the cross section comes from 2^- and 3^- states which have the dominant particle-hole configuration $(1p_{1/2})^{-1}\ (1d_{5/2})$ while the contribution from the 1^- state is small and that for the 0^- state is negligible and hence not shown in the figure. Thus, our results indicate the relative importance of the final states of the nucleus as against the expectation of Meyer et.al.[5] that the cross section would depend more on the number of states available rather than on the specific details of the states involved.

In Figures 6,7,8 and 9, the volume and surface production cross sections for the reaction $^{16}O(\gamma,\pi^+)^{16}N$ are plotted as a function of the incident photon energy, with the final nucleus in any one of the four low-lying bound states of ^{16}N whose wave functions are given by the IPM, EF, GV (TDA and RPA) and MIGDAL models, respectively. From Fig.8, we find that the TDA and RPA results do not differ very much from each other and further that the RPA cross sections are slightly lesser than the TDA cross sections. Thus, we find that the ground state correlations taken into

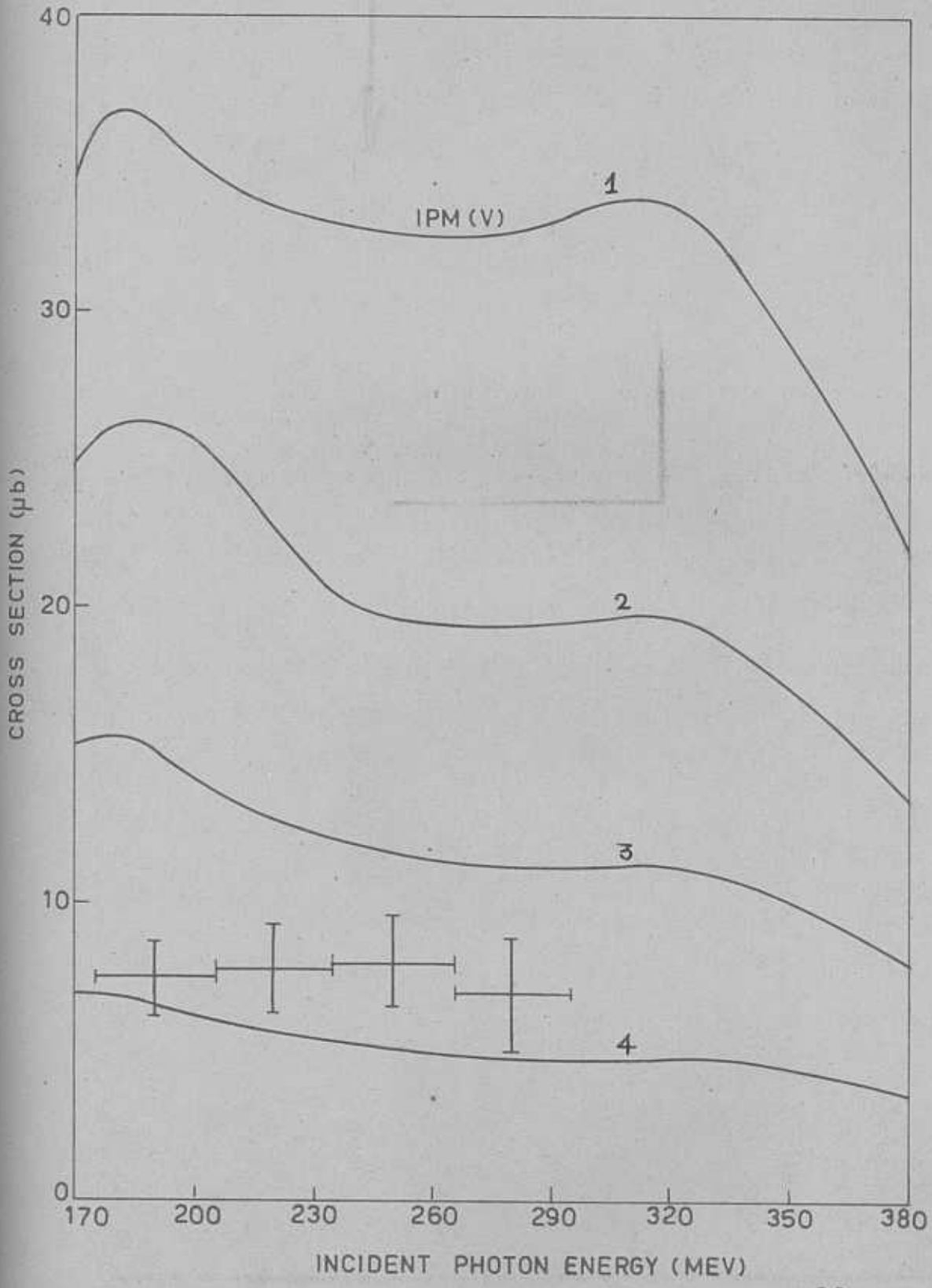

Fig.6. Total cross section for the reaction $^{16}O(\gamma,\pi^+)^{16}N$ obtained assuming the IPM model curves 1,2,3 and 4 correspond to r_o =0.0, 2.262 fm, 2.686 fm and 3.111 fm, respectively. b=1.76 fm. The experimental results are from ref.1.

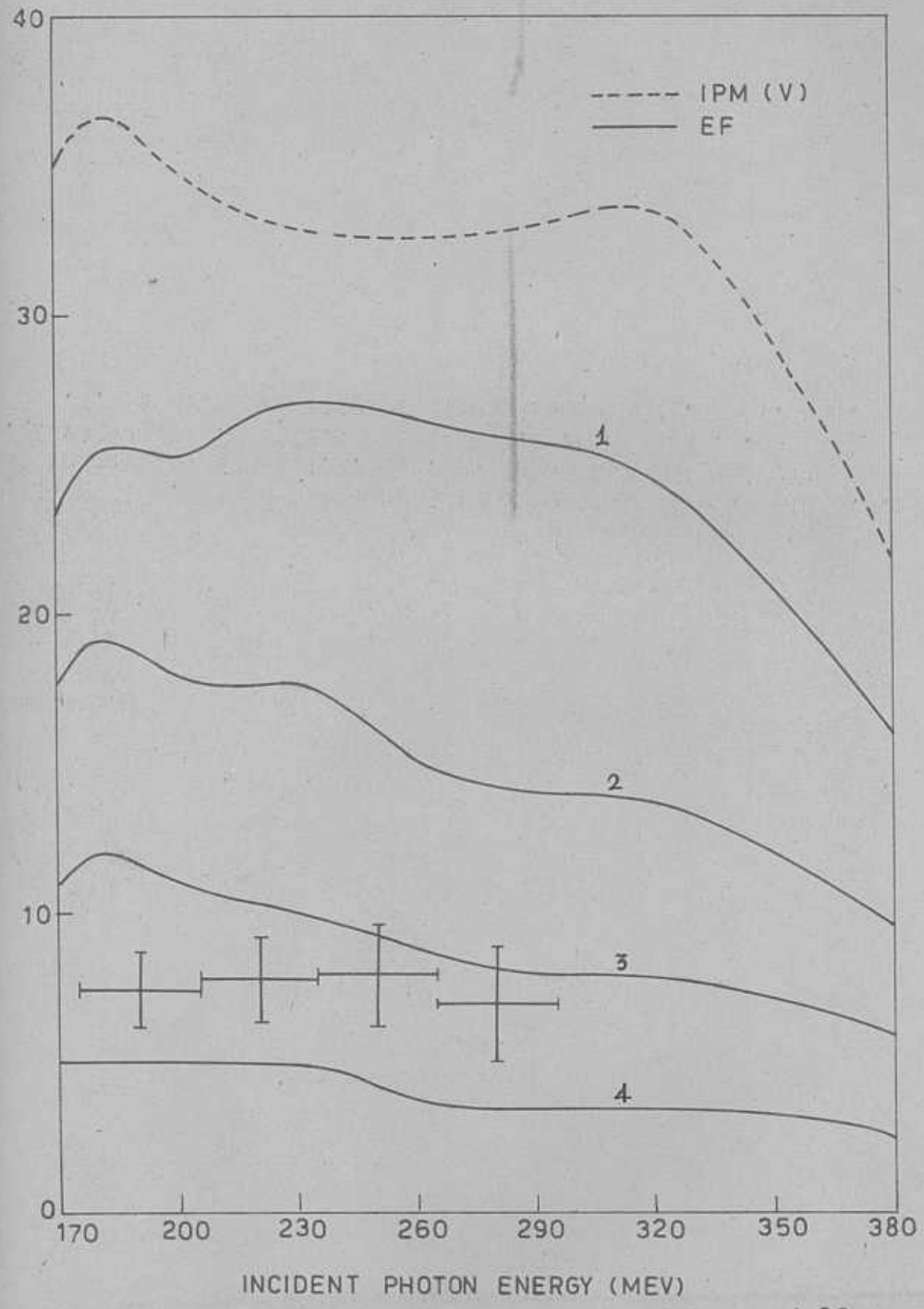

Fig.7. Total cross section for the reaction $^{16}O(\gamma,\pi^+)^{16}N$ obtained assuming the EF model. Curves 1,2,3 and 4 correspond to r_0 = 0.0, 2.262 fm, 2.686 fm and 3.111 fm, respectively. b=1.76 fm. The experimental results are from ref.1.

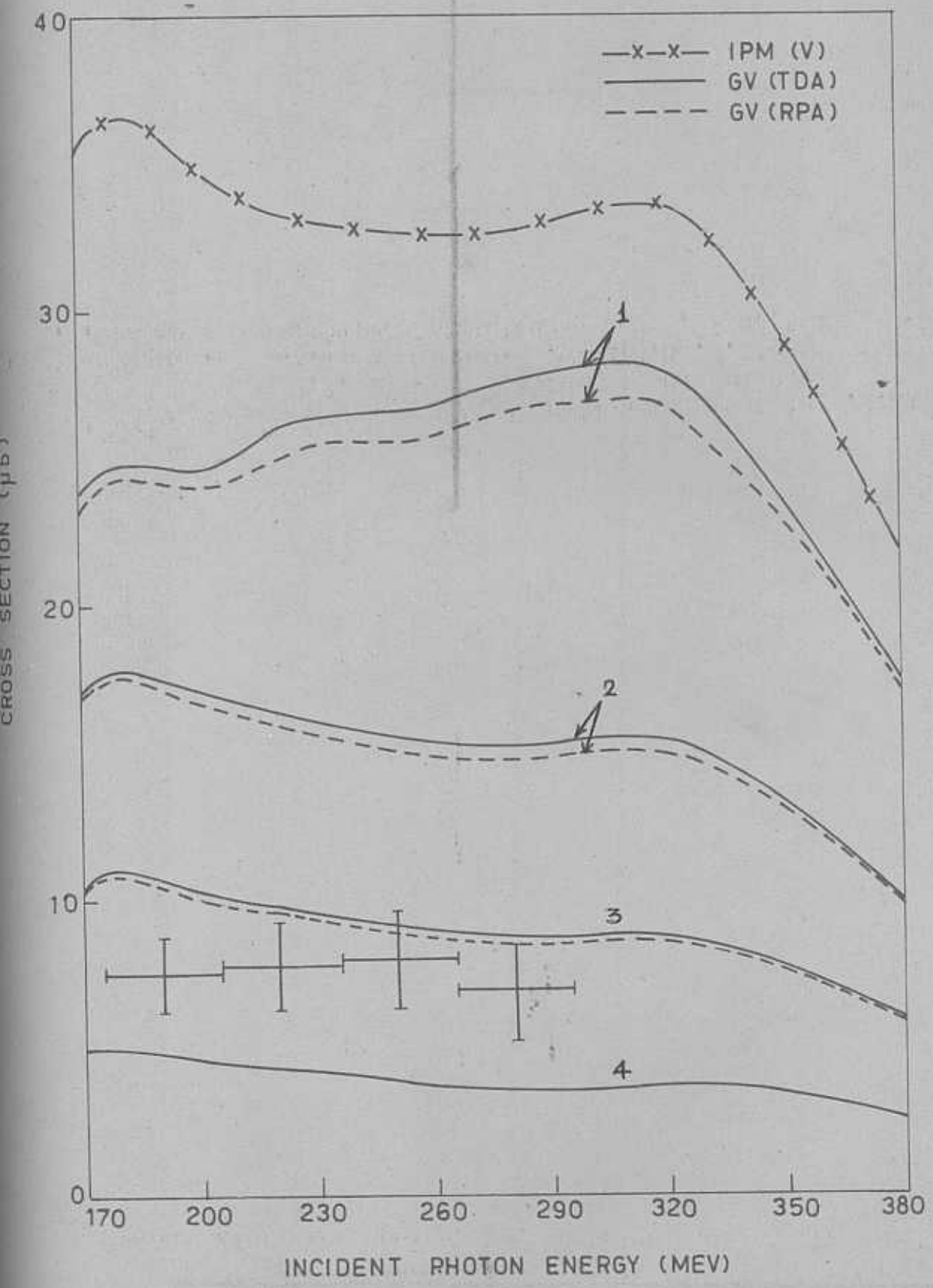

Fig.8. Total cross section for the reaction $^{16}O(\gamma,\pi^+)^{16}N$ obtained assuming the GV(TDA) and GV(RPA) models. Curves 1,2,3 and 4 correspond to r_0=0.0, 2.262 fm, 2.686 fm and 3.111 fm, respectively. b=1.76 fm. The experimental results are from ref.1.

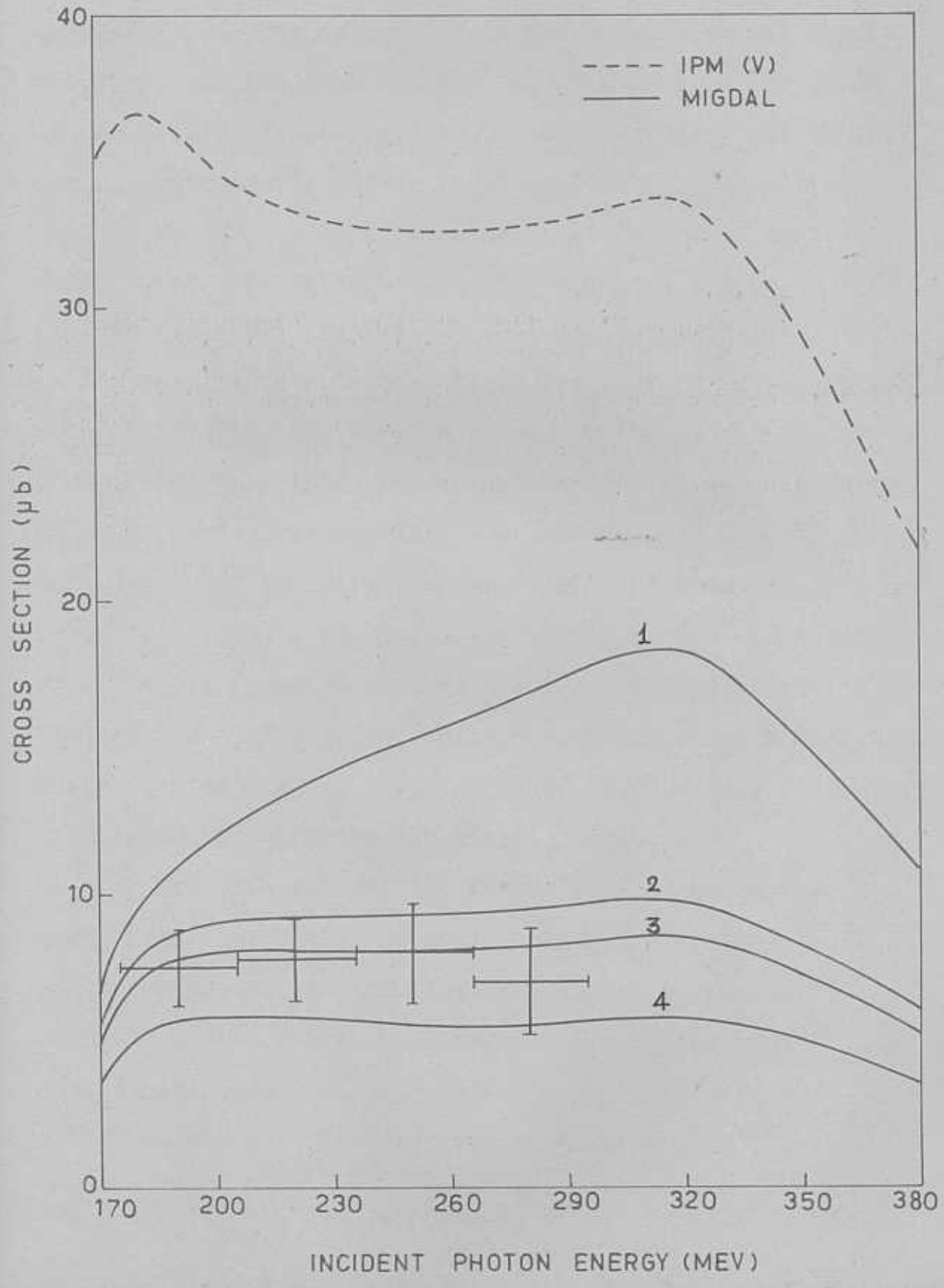

Fig.9. Total cross section for the reaction $^{16}O(\gamma, \pi^+)^{16}N$ obtained assuming the MIGDAL model. Curves 1,2,3 and 4 corr-espond to r_0 =0.0, 2.262 fm, 2.404 fm and 2.686 fm, respectively. b=1.76 fm. The experimental results are from ref.1.

account by the RPA do not affect the cross sections significantly. In the next chapter, we will take up the study of the effect of two-particle-two-hole correlations in the ground state of ^{16}O on the reaction (3.1.1). We notice that in Figs.6,7 and 8, the cross section curves obtained with r_0 =2.2 in units of pion Compton wave length (r_0 =3.1108 fm.) lie below the experimental results. It is interesting to note that the cross section curves obtained with Gillet-Vinh Mau wave functions in the Tamm-Dancoff(TDA) and Random Phase (RPA) Approximations for r_0=1.9 in units of pion Compton wavelength (r_0 =2.686 fm) are in very good agreement with the experimental results of Meyer et.al[1] (see Fig.8). But, in Fig.9, the cross section curve obtained with = 1.9 in units of pion Compton wavelength lies below the experimental results, while that obtained with r_0=1.7 in units of pion Compton wave length (r_0=2.4038 fm.) is in very good agreement with the experimental results.

If we were to take the Butler surface production mechanism[7] seriously, we should choose r_0 = 2.686 fm. which corresponds to the root-mean-square radius of ^{16}O consistent with the charge distribution measurement[23]. We should also take the value of the oscillator parameter fitted to the Stanford electron scattering data[24], viz.

---

23) L.R.B.Elton, "Nuclear Sizes", Oxford University Press, London (1961).

24) R.Hofstadter and R.Herman, "High Energy Electron Scattering", Stanford University Press (1960).

b = 1.76 fm. Thus, we find that the RPA wave functions of Gillet-Vinh Mau, in the surface production model with r_0 and b determined by electron scattering data reproduce the experimental cross sections of Meyer, Walters and Hummel[1]. As noted earlier, this value of r_0 yields a theoretical curve, for MIGDAL wavefunctions, which is now too low compared with the experimental results. However, as shown in Fig.9, a suitable adjustment of r_0 (= 2.40 fm. or 1.7 in units of pion Compton wave length) brings the theoretical results to a good agreement with the experimental results both in magnitude and shape; but, this is only of qualitative value because of other effects neglected here.

In Fig.10, a comparison is made of the total cross sections for $^{16}O(\gamma,\pi^+)^{16}N$ obtained with the IPM, RPA and MIGDAL wave functions for the low-lying bound states of ^{16}N. The solid line curves and dashed line curves correspond respectively to the results obtained using volume (V) and surface (S) production of pions. While curves IPM(S) and RPA(S) are obtained with r_0=2.686 fm., MIGDAL(S) has been obtained with r_0=2.403 fm.

The total cross sections given in Figs.6,7,8,9 and 10 are almost constant in the energy range 180-320 Mev, although the cross sections to discrete final states are energy-dependent as shown in Fig.5. It is, however, found that the

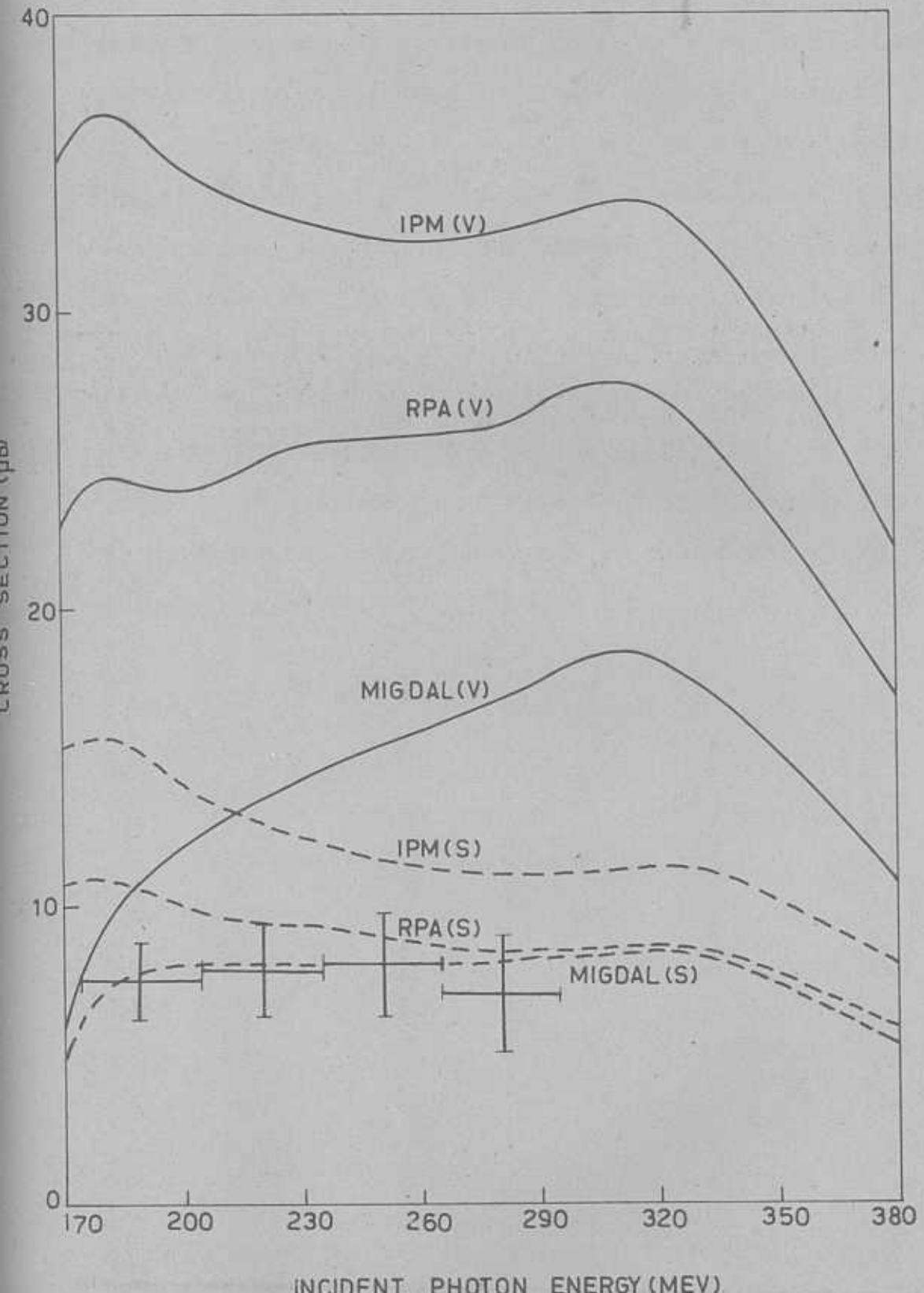

.10. Total cross section for the reaction $^{16}O(\gamma,\pi^+)^{16}N$. The solid
dashed line curves correspond respectively to the results obtained
ng the volume(V) and surface (S) production of pions. Curves IPM(S)
RPA(S) are obtained with γ_0 =2.686 fm and MIGDAL(S) is obtained with
=2.403 fm. b=1.76 fm. The experimental results are from ref.1.

total cross section decreases beyond the (3,3) resonance region and also near the threshold for pion photoproduction.

In conclusion, we see that the configuration mixing models (EF, GV and MIGDAL) play a large role but they fail to eliminate the discrepancy between theory and experiment in the case of $^{16}O(\gamma,\pi^+)^{16}N$. Here, we have shown that this discrepancy can be eliminated successfully, if we attribute it entirely to the production mechanism. More definite information can be obtained if the partial cross sections to the low-lying bound states of ^{16}N, analogous to partial muon capture rate measurements[29,30], are also measured experimentally.

29) A.Astbury et.al., Nuovo Cimento 33, 1020 (1964).
30) R.Cohen, S.Devons and A.Kanaris, Phys.Rev.Letts.11, 134 (1963) and Nucl.Phys.57, 255 (1964).

CHAPTER 4

PHOTOPRODUCTION OF POSITIVE PIONS FROM ^{16}O: (ii) EFFECT OF GROUND STATE CORRELATIONS+

1. Two series of positive parity levels in ^{16}O which obey rotational band systematics were observed, in 1964, by Carter et. al.[1]. Brown and Green[2] proposed a model in which these two bands are considered as mixtures of "deformed" two-particle, two-hole (2p-2h) and four-particle, four-hole (4p-4h) states with the usual spherical shell model ground state. Several theoretical studies[2,3,4] have been made to estimate the amount of deformed components in the ground state wave function of ^{16}O. Recently, Purser et.al.[5] made a direct measurement of the 2p-2h admixtures in the ground state wave function of ^{16}O by investigating the pick-up reactions $^{16}O(d,t)^{15}O$ and $^{16}O(d,^{3}He)^{15}N$ at a deuteron energy of 20 Mev. Their results confirm the existence of such pair excitations with intensities comparable to those predicted by Brown and Green[2]. Assuming an ^{16}O ground state containing

---

+ K.Srinivasa Rao and V.Devanathan , to appear in Phys.Letts.

1)E.B.Carter, G.E.Mitchell and R.H.Davis, Phys.Rev.133, B1421 and B1434 (1964).

2)G.E.Brown and A.M.Green, Nucl.Phys.75, 401 (1966); ibid 85, 87 (1966).

3)T.E.England, Nucl.Phys.72, 68 (1965).

4)A.P.Zucker, B.Buck and J.B.McGrory, Phys.Rev.Letts.21,39(1968).

5)K.H.Purser, W.P.Alford, D.Cline, H.W.Fulbright, H.E.Gove and M.S.Krick, Nucl.Phys. A132, 75 (1969).

2p-2h components, Walker[6] and Green and Rho[7] have shown that several theoretical-experimental discrepancies, for muon capture and photo-disintegration on ^{16}O, can be resolved.

In Chapter.3, we have made a detailed study of the reaction $^{16}O(\gamma,\pi^+)^{16}N$ assuming the ^{16}O ground state to be a closed shell state, as well as one which contains long-range correlations introduced via the RPA. On comparing our results with the available experimental data, we found that there still remained a factor of two discrepancy which we attributed to the production mechanism. Our intention here is to ascertain whether some of the phenomenology resorted to therein (viz. the surface production mechanism and the phenomenology brought in through Migdal theory) can be eliminated by explicitly taking into account the 2p-2h admixture to the ground state wave function of ^{16}O.

2. As discussed above, the ground state wave function of ^{16}O contains in addition to the op-oh component, 2p-2h, 4p-4h, etc. components. We shall assume in the present study

---

6) G.E.Walker, Phys.Rev. 174, 1290 (1968).
7) A.M.Green and M.Rho, Nucl.Phys.A130, 112 (1969) and A.M.Green, T.K.Dahlblom, A.Kallio and M.Rho, Phys.Letts. 31B, 189 (1970).

that it can be approximated by:

$$|0^+, g.s.\rangle = \alpha\,|0p\text{-}0h\rangle + \beta\,|(1d^2_{5/2})_{J=0,T=1}\,(1p^{-2}_{1/2})_{0,1}\rangle + \gamma\,|(2s^2_{1/2})_{0,1}\,(1p^{-2}_{1/2})_{0,1}\rangle . \qquad (4.2.1)$$

where configurations with particles and holes separately coupled to (J,T) other than J=0, T=1 are neglected, based on the observation by Zamick[8] that they lie much higher in energy and hence their coupling to the |op-oh > state is much weaker. In table.1 are listed the values of the parameters α, β and γ determined by Purser et.al.[5] from an experimental study of the pick-up reactions $^{16}O(d,t)^{15}O$ and $^{16}O(d,{}^3He)^{15}N$.

Table.1

^{16}O model	α	β	γ
I (PS)	1.00	0.00	0.00
II (Expt. $^{16}O(d,t)^{15}O$)	0.87	0.26	0.27
III (Expt. $^{16}O(d,{}^3He)^{15}N$)	0.82	0.54	0.20

Here, (PS) denotes pure shell model wave function popular before the days of nuclear coexistence. It should also be mentioned here that most calculations to date have been done with $\alpha = 1$, $\beta = \gamma = 0$, the exceptional ones being

8) L.Zamick, Phys. Letts. 15, 580 (1965).

those of Walker[6] and Green and Rho[7].

In general, the ground state and low-lying T=1 states of ^{16}N can be considered to be a combination of the usual particle-hole (1p-1h) states with three-particle, three-hole (3p-3h) configuration admixtures, to be consistent with the choice of the ground state (4.2.1). Walker[6] claims, using a method of generating the ^{16}N states from a deformed ground state, that the 3p-3h mixing can be as large as the 2p-2h mixing of the ground state. On the other hand, Green and Rho[7] have argued, on both theoretical and empirical grounds, that the 3p-3h configurations are insignificant in the ^{16}N quartet states. Therefore, we take the ground state and low lying T=1 states of ^{16}N to be described simply by 1p-1h combinations. The ^{16}N wave functions used in the present study are shown in table.2. Three of the five model wave functions, shown in table.2, viz. Independent Particle Model (IPM) wave function, Elliott and Flowers[9] wave function (EF) and Gillet-Vinh Mau[10] wave function(GV), have been discussed already in section.2 of Chapter.3. The Kuo wave functions, shown in this table, have been calculated with matrix elements derived from the realistic Hamada-Johnston potential without and with

---

9) J.P.Elliott and B.H.Flowers, Proc.Roy.Soc.A242, 57 (1957).
10) V.Gillet and N.Vinh Mau, Nucl.Phys.54, 321 (1964).

Table.2. Wave functions for 0^-, 1^-, 2^- and 3^-, T=1 states of ^{16}N.

J^π	Model	$2s_{1/2}\,1p_{1/2}^{-1}$	$1d_{5/2}\,1p_{1/2}^{-1}$	$1d_{3/2}\,1p_{3/2}^{-1}$	$2s_{1/2}\,1p_{3/2}^{-1}$	$1d_{5/2}\,1p_{3/2}^{-1}$	$1d_{3/2}\,1p_{3/2}^{-1}$
	IPM	1.000	--	--	--	--	--
	EF	1.000	--	--	--	--	0.055
0^-	GV	0.999	--	--	--	--	-0.05
	KUO	0.998	--	--	--	--	0.059
	KUO(S)	0.997	--	--	--	--	0.076
	IPM	1.000	--	--	--	--	--
	EF	0.980	--	0.010	-0.160	-0.080	- 0.020
1^-	GV	0.995	--	-0.008	0.026	-0.096	- 0.020
	KUO	0.974	--	0.082	-0.110	-0.177	0.017
	KUO(S)	0.975	--	0.073	0.064	-0.198	0.009
	IPM	--	1.000	--	--	--	--
	EF	--	0.980	-0.100	-0.060	0.140	0.090
2^-	GV	--	0.983	0.007	0.054	0.174	0.035
	KUO	--	0.973	-0.087	0.002	0.201	0.074
	KUO(S)	--	0.962	-0.097	0.048	0.226	0.106
	IPM	--	1.000	--	--	--	--
	EF	--	0.980	--	--	0.180	0.060
3^-	GV	--	0.998	--	--	-0.062	-0.011
	KUO	--	0.965	--	--	-0.263	-0.023
	KUO(S)	--	0.942	--	--	-0.329	-0.073

IPM = Independent Particle Model, EF=Elliott and Flowers wave function[9],
GV = Gillet-Vinh Mau wave function in the Tamm-Dancoff Approximation[10], KUO=Kuo wave function calculated with Hamada-Johnston potential without screening correction,
KUO(S) = Kuo wave function with screening correction.

screening corrections(+) - we denote these by KUO and KUO(S), respectively - and these have been taken from table.2 of ref.7.

3. The 2p-2h state is given by[6]:

$$|2p\text{-}2h,(n_1\ell_1 j_1)^2_{J=0,T=1}(n_2\ell_2 j_2)^{-2}_{0,1}\rangle = \frac{1}{2}\sum_{m_1,m_1'}\sum_{m_2,m_2'}\sum_{T_z,T_z'}\sum_{\tau_1,\tau_1'}\sum_{\tau_2,\tau_2'}(-1)^{T_z}\times$$

$$\times C(j_1 j_1 0; m_1 m_1' 0)\, C(j_2 j_2 0; -m_2 -m_2' 0)\, C(\tfrac{1}{2}\tfrac{1}{2}1; \tau_1\tau_1' T_z)\times$$

$$\times C(\tfrac{1}{2}\tfrac{1}{2}1; -\tau_2 -\tau_2' T_z')\, C(110; T_z T_z' 0)\, a^+_{j_1 m_1 \frac{1}{2}\tau_1}\, a^+_{j_1 m_1' \frac{1}{2}\tau_1'}\times$$

$$\times a_{j_2 m_2 \frac{1}{2}\tau_2}\, a_{j_2 m_2' \frac{1}{2}\tau_2'}\,|0\rangle\,, \qquad (4.3.1)$$

where the ket $|0\rangle$ is the (Hartree-Fock) closed shell state, $(n_1\ \ell_1\ j_1)^2$ denotes the two-particle (occupied) state and $(n_2\ \ell_2\ j_2)^{-2}$ denotes the two-hole (unoccupied) states, C's are the Clebsch-Gordon coefficients and a^+(a) the creation (annihilation) operators defined in section.2 of Chapter.3. Using the property of the Clebsch-Gordon coefficient:

$$C(jj0; m\,m'0) = \delta_{m',-m}\,\frac{(-1)^{j-m}}{[j]} \qquad (4.3.2)$$

we have for (4.3.1):

$$|2p\text{-}2h;(n_1\ell_1 j_1)^2_{0,1}(n_2\ell_2 j_2)^{-2}_{0,1}\rangle = \frac{1}{2\sqrt{3}}\,\frac{(-1)^{j_1+j_2}}{[j_1][j_2]}\sum_{m_1,m_2}(-1)^{m_2-m_1+1}\times$$

$$\times\sum_{\tau_1,\tau_1',\tau_2,\tau_2',T_z} C(\tfrac{1}{2}\tfrac{1}{2}1;\tau_1\tau_1' T_z)\, C(\tfrac{1}{2}\tfrac{1}{2}1;\tau_2\tau_2' T_z)\, a^+_{j_1 m_1 \frac{1}{2}\tau_1}\, a^+_{j_1,-m_1 \frac{1}{2}\tau_1'}\times$$

$$\times a_{j_2,-m_2 \frac{1}{2}\tau_2}\, a_{j_2 m_2 \frac{1}{2}\tau_2'}\,|0\rangle\,. \qquad (4.3.3)$$

(+) Core polarization corrections to particle-hole matrix elements are referred to as "screening" corrections.

The final particle-hole nuclear state, in the Tamm-Dancoff Approximation, in the j-j coupling scheme is given by (3.2.1). The nuclear transition operator, for photoproduction of pions, in the occupation number representation is given by (3.3.5). In Chapter.3, we have derived the expression for the matrix element:

$$Q(\text{op-oh}) = \langle J_f M_f\, 1\, M_T \mid \mathcal{T} \mid \text{op-oh} \rangle. \tag{3.4.1}$$

We will now derive an expression for the matrix element:

$$Q(2p-2h) = \langle J_f M_f\, 1\, M_T \mid \mathcal{T} \mid 2p\text{-}2h, (n_1 \ell_1 j_1)^2_{0,1} (n_2 \ell_2 j_2)^{-2}_{0,1} \rangle, \tag{4.3.4}$$

where $M_T = -1$ for T=1 states of ^{16}N. Using (4.3.3), (3.2.1) and (3.35) we have:

$$\begin{aligned} Q(2p-2h) = {} & \frac{1}{2\sqrt{3}} \frac{(-1)^{j_1+j_2}}{[j_1][j_2]} \sum_{\substack{p,h \\ m_p, m_h, \tau_p, \tau_h}} X^{J_f}_{p,h} (-1)^{j_h+m_h} (-1)^{\frac{1}{2}+\tau_h} C(j_p j_h J_f; m_p m_h M_f) \times \\ & \times C(\tfrac{1}{2}\tfrac{1}{2}1; \tau_p \tau_h M_T) \sum_{m_1,m_2} (-1)^{m_2-m_1+1} \sum_{\tau_1,\tau_1',\tau_2,\tau_2'} C(\tfrac{1}{2}\tfrac{1}{2}1; \tau_1 \tau_1' T_z) \times \\ & \times C(\tfrac{1}{2}\tfrac{1}{2}1; \tau_2 \tau_2' T_z) \sum_{\alpha,\beta} \langle \alpha \mid t^{\lambda}_{m_\lambda} \tau^- \mid \beta \rangle \times \\ & \times \langle 0 \mid a^+_{j_h,-m_h\frac{1}{2},-\tau_h} a_{j_p m_p \frac{1}{2} \tau_p} a^+_\alpha a_\beta a^+_{j_1 m_1 \frac{1}{2} \tau_1} a^+_{j_1,-m_1\frac{1}{2}\tau_1'} a_{j_2,-m_2\frac{1}{2}\tau_2} a_{j_2 m_2 \frac{1}{2} \tau_2} \mid 0 \rangle. \end{aligned} \tag{4.3.5}^{+}$$

In the evaluation of the matrix element

$$\langle 0 \mid a^+_h a_p a^+_\alpha a_\beta a^+_1 a^+_1 a_2 a_2 \mid 0 \rangle \tag{4.3.6}$$

+Note that α and β which occur in expressions (4.3.5) and (4.3.6) are the single particle states of the transition operator, refer Eq.(3.3.5), in the occupation number representation. In all other expressions, in this Chapter, α and β represent the parameters which occur in Eq.(4.2.1).

repeated use is made of (3.2.4) to take a_p and a_h^+ to the extreme right and finally the result (3.2.3) is applied to omit the terms in which a_p or a_h^+ occurs next to the ket $|\,0\,\rangle$. This procedure gives rise to the following four non-vanishing terms:

$$-\delta_{\alpha;j_2,-m_2\frac{1}{2}\tau_2}\,\delta_{\beta;j_1m_1\frac{1}{2}\tau_1}\,\delta_{pm_p\frac{1}{2}\tau_p;j_1,-m_1\frac{1}{2}\tau_1'}\,\delta_{h,-m_h\frac{1}{2},-\tau_h;j_2m_2\frac{1}{2}\tau_2'}\,, \qquad (4.3.6a)$$

$$+\delta_{\alpha;j_2,-m_2\frac{1}{2}\tau_2}\,\delta_{\beta;j_1,-m_1\frac{1}{2}\tau_1'}\,\delta_{pm_p\frac{1}{2}\tau_p;j_1m_1\frac{1}{2}\tau_1}\,\delta_{h,-m_h\frac{1}{2},-\tau_h;j_2m_2\frac{1}{2}\tau_2'}\,, \qquad (4.3.6b)$$

$$+\delta_{\alpha;j_2m_2\frac{1}{2}\tau_2'}\,\delta_{\beta;j_1m_1\frac{1}{2}\tau_1}\,\delta_{pm_p\frac{1}{2}\tau_p;j_1,-m_1\frac{1}{2}\tau_1'}\,\delta_{h,-m_h\frac{1}{2},-\tau_h;j_2,-m_2\frac{1}{2}\tau_2}\,, \qquad (4.3.6c)$$

$$-\delta_{\alpha;j_2m_2\frac{1}{2}\tau_2'}\,\delta_{\beta;j_1,-m_1\frac{1}{2}\tau_1'}\,\delta_{pm_p\frac{1}{2}\tau_p;j_1m_1\frac{1}{2}\tau_1}\,\delta_{h,-m_h\frac{1}{2},-\tau_h;j_2,-m_2\frac{1}{2}\tau_2}\,. \qquad (4.3.6d)$$

Substituting (4.3.6a) for the matrix element (4.3.6) in (4.3.5) we find that we have to evaluate the term:

$$I = \frac{1}{2\sqrt{3}}\,\frac{(-1)^{j_1+j_2}}{[j_1][j_2]}\,X^{J_f}_{j_1j_2}\sum_{\substack{m_1,m_2\\ \tau_1,\tau_2,\tau_1',\tau_2',T_z}}(-1)^{m_2-m_1+1}(-1)^{j_2-m_2+1}(-1)^{\frac{1}{2}-\tau_2'}\times$$

$$\times\; C(j_1j_2J_f;-m_1,-m_2M_f)C(\tfrac{1}{2}\tfrac{1}{2}1;\tau_1\tau_1T_z)\,C(\tfrac{1}{2}\tfrac{1}{2}1;\tau_2\tau_2'T_z)\,C(\tfrac{1}{2}\tfrac{1}{2}1;\tau_1'\tau_2',-1)\times$$

$$\times\;\langle j_2,-m_2\tfrac{1}{2},-\tau_2\,|\,t^{\lambda}_{m_\lambda}\tau^-\,|\,j_1m_1\tfrac{1}{2}\tau_1\rangle\;\delta(p,1)\,\delta(h,2)\,,$$

where the Kronecker delta product $\delta(p,1)\;\delta(h,2)$ is zero unless the two particles (holes) of the 2p-2h initial state component have the same $(n\ell j)$ quantum numbers as the particle (hole) of the 1p-1h final state. Separating the

spin and isospin parts:

$$\langle j_2,-m_2\,\tfrac{1}{2},-\tau_2|\, t^{\lambda}_{m_\lambda}\tau^{-}\,|\, j_1 m_1 \tfrac{1}{2}\tau_1\rangle = \langle j_2,-m_2|\, t^{\lambda}_{m_\lambda}\,|\, j_1 m_1\rangle \frac{1}{\sqrt{2}}\langle \tfrac{1}{2},-\tau_2|\,\tau^{1}_{-1}\,|\,\tfrac{1}{2}\tau_1\rangle$$

and using the Wigner-Eckart theorem, we have:

$$I = \frac{1}{2\sqrt{3}}\frac{(-1)^{j_1+j_2}}{[j_1][j_2]}\, X^{J_f}_{j_1 j_2} \sum_{m_1,m_2}(-1)^{m_2-m_1} C(j_1 j_2 J_f;-m_1,-m_2 M_f)\times$$

$$\times\, C(j_1\lambda j_2; m_1 m_\lambda,-m_2)\langle j_2\|t^{\lambda}\|j_1\rangle \frac{1}{\sqrt{2}} \sum_{\tau_1,\tau_2,\tau_1',\tau_2',T_z}(-1)^{\frac{1}{2}-\tau_2'} C(\tfrac{1}{2}\tfrac{1}{2}1;\tau_1'\tau_2',-1)\times$$

$$\times\, C(\tfrac{1}{2}\tfrac{1}{2}1;\tau_1,-1,-\tau_2)\, C(\tfrac{1}{2}\tfrac{1}{2}1;\tau_1\tau_1' T_z)\, C(\tfrac{1}{2}\tfrac{1}{2}1;\tau_2\tau_2' T_z)\langle\tfrac{1}{2}\|\tau^{1}\|\tfrac{1}{2}\rangle\,\delta(p,1)\,\delta(h,2).$$

From the Clebsch-Gordon coefficients for isospin, we find - due to the additive property of their projections - that we must have:

$$\tau_1 = \tau_2 = 1/2 \quad \text{and} \quad \tau_1' = \tau_2' = -1/2 \text{ and hence } T_z = 0.$$

Now using the values:

$$C(\tfrac{1}{2}\tfrac{1}{2}1;\tfrac{1}{2}\tfrac{1}{2}1) = C(\tfrac{1}{2}\tfrac{1}{2}1;-\tfrac{1}{2},-\tfrac{1}{2},-1) = 1,$$

$$C(\tfrac{1}{2}\tfrac{1}{2}1;\tfrac{1}{2},-\tfrac{1}{2}0) = C(\tfrac{1}{2}\tfrac{1}{2}1;-\tfrac{1}{2}\tfrac{1}{2}0) = \frac{1}{\sqrt{2}},$$

$$\langle\tfrac{1}{2}\|\tau^{1}\|\tfrac{1}{2}\rangle = [1],$$

$$C(j_1 j_2 j_3; m_1 m_2 m_3) = (-1)^{j_1-m_1}\frac{[j_3]}{[j_2]}\, C(j_1 j_3 j_2;\, m_1,-m_3,-m_2),$$

and the orthogonality property of Clebsch-Gordon coefficients, we get,

$$I = \frac{1}{2}(-1)^{2j_2-\lambda+1}\frac{[j_2]}{[\lambda]}\langle j_2\|t^{\lambda}\|j_1\rangle\,\delta_{J_f,\lambda}\,\delta_{M_f,m_\lambda}\frac{(-1)^{j_1+j_2}}{2\sqrt{3}\,[j_1][j_2]}X^{J_f}_{j_1 j_2}\,\delta(p,1)\delta(h,2)$$

$$= \frac{1}{4\sqrt{3}}\frac{(-1)^{j_1+j_2+J_f}}{[j_1][J_f]}\, X^{J_f}_{j_1 j_2}\langle j_2\|t^{J_f}\|j_1\rangle\,\delta(p,1)\,\delta(h,2), \qquad (4.3.7)$$

since $(2j_2+1)$ is always even. Following a similar procedure it can be easily shown that the three other terms (4.3.6b), (4.3.6c) and (4.3.6d) lead to exactly the same result (4.3.7). Therefore, the sum of the four non-vanishing terms yield the result:

$$Q(2p\text{-}2h) = \frac{1}{\sqrt{3}} \frac{(-1)^{j_1+j_2+J_f}}{[j_1][J_f]} X^{J_f}_{j_1 j_2} \langle j_2 \| t^{J_f} \| j_1 \rangle \delta(p,1)\delta(h,2)$$

$$= \frac{1}{\sqrt{3}} \frac{(-1)^{j_1+j_2+J_f}}{[j_p][J_f]} X^{J_f}_{j_p j_h} \langle j_h \| t^{J_f} \| j_p \rangle . \tag{4.3.8}$$

From (4.2.1) it is clear that we consider only two possible 2p-2h states, viz. $1d^2_{5/2}\, 1p^{-2}_{1/2}$ and $2s^2_{1/2}\, 1p^{-2}_{1/2}$. Hence, the matrix element for π^+ photoproduction is:

$$Q = \langle f | \sum_k (t^{\lambda}_{m_\lambda})_k \tau^- | 0^+, \text{g.s.} \rangle$$

$$= \alpha Q(0p\text{-}0h) + \beta Q(1d^2_{5/2}\, 1p^{-2}_{1/2}) + \gamma Q(2s^2_{1/2}\, 1p^{-2}_{1/2})$$

$$= \alpha \sum_{p,h} \frac{[j_p]}{[J_f]} X^{J_f}_{p,h} \langle p \| t^{J_f} \| h \rangle +$$

$$+ \frac{\beta}{\sqrt{18}} \frac{(-1)^{J_f+1}}{[J_f]} X^{J_f}_{1d_{5/2},1p_{1/2}} \langle 1p_{1/2} \| t^{J_f} \| 1d_{5/2} \rangle +$$

$$+ \frac{\gamma}{\sqrt{6}} \frac{(-1)^{J_f+1}}{[J_f]} X^{J_f}_{2s_{1/2},1p_{1/2}} \langle 1p_{1/2} \| t^{J_f} \| 2s_{1/2} \rangle . \tag{4.3.9}$$

Notice that when we put $\alpha = 1$, $\beta = \gamma = 0$ in (4.3.9) we get back to our result of Chapter.3, Eq.(3.4.1). Let us now examine how the 2p-2h terms enter into the partial

cross sections in the case of the Independent Particle Model (IPM).

In the IPM, for $J_f^P = 0^-$ and 1^-, we know that the dominant component is for $^2s_{1/2}\ ^1p^{-1}_{1/2}$ as shown in Table.2. So, for these states we have:

$$Q^{J_f^P=0^-,1^-}_{IPM} = \alpha\frac{[1/2]}{[J_f]}\langle 2s_{1/2}\|t^{J_f}\|1p_{1/2}\rangle + \frac{\gamma}{\sqrt{6}}\frac{(-1)^{J_f+1}}{[J_f]}\langle 1p_{1/2}\|t^{J_f}\|2s_{1/2}\rangle \quad (4.3.10)$$

From Eqs.(3.4.7), (3.4.8) and (3.4.9) we have, in general, (for the case of photoproduction of pions) for the reduced matrix element:

$$\langle p\|(Y^\ell(\hat{r})\times\sigma^n)^{J_f}\|h\rangle = \langle \ell_p \tfrac{1}{2} j_p\|(Y^\ell(\hat{r})\times\sigma^n)^{J_f}\|\ell_h \tfrac{1}{2} j_h\rangle$$

$$= \frac{1}{\sqrt{4\pi}}[\ell_h][1/2][j_h][\ell][n][J_f]C(\ell_h\ell\ell_p;000)\begin{Bmatrix}\ell_h & \ell & \ell_p\\ 1/2 & n & 1/2\\ j_h & J_f & j_p\end{Bmatrix} \quad (4.3.11)$$

and

$$\langle h\|(Y^\ell(\hat{r})\times\sigma^n)^{J_f}\|p\rangle = \frac{1}{\sqrt{4\pi}}[\ell_p][1/2][j_p][\ell][n][J_f]C(\ell_p\ell\ell_h;000)\begin{Bmatrix}\ell_p & \ell & \ell_h\\ 1/2 & n & 1/2\\ j_p & J_f & j_h\end{Bmatrix}$$

$$= \frac{1}{\sqrt{4\pi}}[\ell_p][1/2][j_p][\ell][n][J_f](-1)^\ell\frac{[\ell_h]}{[\ell_p]}C(\ell_h\ell\ell_p;000)(-1)^\delta\begin{Bmatrix}\ell_h & \ell & \ell_p\\ 1/2 & n & 1/2\\ j_h & J_f & j_p\end{Bmatrix}$$

$$= \frac{1}{\sqrt{4\pi}}[\ell_h][1/2][j_p][\ell][n][J_f](-1)^{\ell+\delta}C(\ell_h\ell\ell_p;000)\begin{Bmatrix}\ell_h & \ell & \ell_p\\ 1/2 & n & 1/2\\ j_h & J_f & j_p\end{Bmatrix} \quad (4.3.12)$$

where in (4.3.12) we have used the symmetry properties of the Clebsch-Gordon coefficient and the 9-j symbol. The following relationship exists between $\langle p\|t^{J_f}\|h\rangle$ and

$\langle h \| t^{J_f} \| p \rangle$ matrix elements:

$$\langle h \| (Y^{\ell}(\hat{r}) \times \sigma^{n})^{J_f} \| p \rangle = \frac{[j_p]}{[j_h]} (-1)^{\ell+s} \langle p \| (Y^{\ell}(\hat{r}) \times \sigma^{n})^{J_f} \| h \rangle, \tag{4.3.13}$$

where $s = \ell_p + 1/2 + j_p + \ell_h + 1/2 + j_n + \ell + n + J_f$. For the particular case which occurs in (4.3.10) we have:

$$\begin{aligned} \langle 1p_{1/2} \| t^{J_f} \| 2s_{1/2} \rangle &= \frac{[1/2]}{[1/2]} (-1)^{\ell+3+\ell+n+J_f} \langle 2s_{1/2} \| t^{J_f} \| 1p_{1/2} \rangle \\ &= (-1)^{n+J_f+1} \langle 2s_{1/2} \| t^{J_f} \| 1p_{1/2} \rangle, \end{aligned} \tag{4.3.14}$$

since $2\ell+2$ is always even, ℓ being an integer. Therefore, (4.3.10) becomes:

$$\begin{aligned} Q_{IPM}^{J_f^P = 0^-, 1^-} &= \left\{ \alpha [1/2] + \frac{\gamma}{\sqrt{6}} (-1)^{n+J_f+1} (-1)^{J_f+1} \right\} \frac{1}{[J_f]} \langle 2s_{1/2} \| t^{J_f} \| 1p_{1/2} \rangle \\ &= \left(\alpha + \frac{(-1)^n \gamma}{\sqrt{12}} \right) \frac{[1/2]}{[J_f]} \langle 2s_{1/2} \| t^{J_f} \| 1p_{1/2} \rangle \end{aligned} \tag{4.3.15}$$

where n can take the two values 0 and/or 1. The expression for the reduced matrix element in (4.3.15) is given by (4.3.11). We notice that for the $^2s_{1/2}\,{}^1p^{-1}_{1/2}$ case, the parity Clebsch-Gordon coefficient is: $C(1\ell\,0;000)$ and hence the index can take only one value: $\ell = 1$. Using this fact, when we look at the 9-j symbol $\begin{Bmatrix} 1 & 1 & 0 \\ 1/2 & n & 1/2 \\ 1/2 & J_f & 1/2 \end{Bmatrix}$ we gather that (i) for $J_f^P = 0^-$, n can take only the value one

and (ii) for $J_f^P = 1^-$, n can take both the values 0 and 1.

Similarly, for $J_f^P = 2^-$ and 3^-, we know that the dominant component in IPM is $^1d_{5/2}\ ^1p^{-1}_{1/2}$. Arguing on the same lines as for $J_f^P = 0^-$ and 1^- states, we get:

$$Q^{J_f^P=2^-,3^-}_{IPM} = \left(\alpha + \frac{(-1)^n \beta}{6}\right) \frac{[1/2]}{[J_f]} \langle 1d_{5/2} \| t^{J_f} \| 1p_{1/2} \rangle . \qquad (4.3.16)$$

In this case, the parity Clebsch-Gordon coefficient in the reduced matrix element, $C(1\,\ell\,2;000)$, reveals that ℓ can take two values: 1 and 3. In the corresponding 9-j symbol, $(\ell\ n\ J_f)$ will satisfy the triangular conditions (i) in the case of $J_f^P = 2^-$ only with n=1 and (ii) with n=0 and 1 in the case of $J_f^P = 3^-$.

The differential cross section we are interested in is given by:

$$\frac{d\sigma}{d\Omega}(0^+ \to J_f^P) = (2\pi)^{-2} \mu \mu_0 \overline{\sum_{M_f}} |Q^{J_f^P}|^2, \qquad (4.3.17)$$

where $\underline{\mu}$ is the momentum of the outgoing pion ($\mu = |\underline{\mu}|$) and μ_0 is its energy. The sum in Eq.(4.3.17) is over the final spins and the bar over the sum denotes the average over photon polarizations.

In the IPM, the "partial" cross sections for 0^- and 2^- states are given by:

$$\sigma(0^-) = \sigma^{PS}(0^-)\left(\alpha - \frac{\gamma}{\sqrt{12}}\right)^2, \qquad (4.3.18)$$

$$\sigma(2^-) = \sigma^{PS}(2^-)\left(\alpha - \frac{\beta}{6}\right)^2, \qquad (4.3.19)$$

where we have denoted the "partial" cross sections for $0^+ \rightarrow J_f^P$ in the absence of 2p-2h correlations in the ^{16}O ground state by $\sigma^{PS}(J_f^P)$. Since the index n in Eqs.(4.3.15) and (4.3.16) can take both the values 0 and 1, for $J_f^P = 1^-$ and 3^- and since n occurs also in the 9-j symbol, we cannot write explicit expressions for "partial" cross sections to those states, like Eqs. (4.3.18) and (4.3.19). We have already seen in Chapter.3, that the $0^+ \rightarrow 2^-$ transition gives rise to a dominant contribution to the total cross section. Hence, it is interesting to note that the factor $\left(\alpha - \frac{\beta}{6}\right)^2 \approx 0.53$ when $\alpha = 0.82$ and $\beta = 0.54$ as in table.1. Furthermore, this is the same reduction factor which occurs in the expression for the $0^+ \rightarrow 2^-$ partial muon capture rate[7]. Thus, in the IPM, there is a clear cut reduction of the $0^+ \rightarrow 2^-$ photopion production cross section as well as the muon capture rate by almost a factor of two, when we take the 2p-2h correlations in the ^{16}O ground state into account.

4. Numerical calculations have been made for the cross section for π^+ photoproduction from the 0^+ deformed ground state of ^{16}O to the lowest 2^-, 0^-, 3^- and 1^- bound states of ^{16}N in the impulse approximation using the CGLN amplitudes (described in Chapter.1). We have used the harmonic oscillator form for the radial wave functions with b_{osc} = 1.76 fm - consistent with the Stanford elastic electron scattering data.[11)]

In table.3 are shown the cross sections to the individual 0^-, 1^-, 2^-, and 3^- states of ^{16}N and their sum for an incident photon energy of 260 Mev. We notice that among the models used for ^{16}N, the KUO(S) model gives the maximum amount of reduction in the cross section and among the three models for ^{16}O, the model III ($\alpha = 0.82$, $\beta = 0.54$ and $\gamma = 0.20$) gives the maximum amount of reduction in the cross section.

In table.4 are shown the sum of the "partial" cross sections to the 0^-, 1^-, 2^- and 3^- states of ^{16}N for the five nuclear models for ^{16}N and the three ground state wave functions of ^{16}O. for various incident photon energies.

The results of the calculation are shown in Figs.1 to 4. The experimental results are those of Meyer,

---

11) R.Hofstadter and R.Herman, "High Energy Electron Scattering", Stanford University Press (1960).

Table.3. Cross sections for the reaction $^{16}O(\gamma,\pi^+)^{16}N$ for an incident photon energy of 260 Mev and b = 1.76 fm. The nuclear wave functions for ^{16}N states correspond to IPM, EF, GV, KUO and KUO(S) given in table.2 and the ground state wavefunctions for ^{16}O are those in table.1.

Ground state of ^{16}O	Model for ^{16}N states	Cross section in μb. for ^{16}N states				
		0^-	1^-	2^-	3^-	Sum of all four states
I ($\alpha = 1$, $\beta = \gamma = 0$)	IPM	0.443	4.030	13.246	15.133	32.852
	EF	0.478	4.170	8.978	13.128	26.754
	GV	0.424	3.882	8.828	14.135	27.269
	KUO	0.422	4.019	7.992	10.737	23.170
	KUO(S)	0.421	3.957	7.039	8.957	20.374
II ($\alpha = 0.87$, $\beta = 0.27$, $\gamma = 0.26$)	IPM	0.280	2.751	9.015	11.067	23.113
	EF	0.306	2.869	5.825	9.565	18.575
	GV	0.265	2.643	5.706	10.313	18.927
	KUO	0.265	2.759	5.093	7.765	15.882
	KUO(S)	0.263	2.711	4.393	6.436	13.803
III ($\alpha = 0.82$, $\beta = 0.54$, $\gamma = 0.20$)	IPM	0.257	2.490	7.059	9.510	19.316
	EF	0.281	2.593	4.262	8.188	15.324
	GV	0.245	2.393	4.161	8.841	15.630
	KUO	0.244	2.494	3.624	6.599	12.961
	KUO(S)	0.243	2.452	3.023	5.432	11.150

Table.4. Cross sections for the reaction $^{16}O(\gamma,\pi^+)^{16}N$ for b = 1.76 fm. and various incident photon energies. The nuclear wavefunctions used for ^{16}N correspond to IPM, EF, GV, KUO and KUO(S) given in table.2 and the ground state wavefunctions of ^{16}O are given in table.1

Incident photon energy(Mev)	^{16}O g.s. wave function model	Cross section in μb. for models of ^{16}N				
		IPM	EF	GV	KUO	KUO(S)
165	I	31.831	20.998	20.996	18.192	14.992
	II	21.510	13.413	13.382	11.326	8.953
	III	17.116	10.002	9.959	8.177	6.119
180	I	36.525	25.459	25.112	21.991	18.400
	II	24.789	16.526	16.229	13.945	11,288
	III	19.775	12.428	12.142	10.172	7.871
200	I	35.528	26.643	25.887	22.861	19.421
	II	24.198	17.556	16.970	14.761	12.221
	III	19.256	13.445	12.897	10.999	8.803
230	I	33.243	26.848	26.218	22.997	19.897
	II	22.883	18.132	17.618	15.257	12.966
	III	18.566	14.396	13.913	11.774	9.890
260	I	32.852	26.754	27.269	23.170	20.374
	II	23.113	18.575	18.927	15.882	13.803
	III	19.316	15.324	15.630	12.961	11.150

continued on next page.

Table.4 continued.

Incident photon energy(Mev)	^{16}O g.s. wave function model	Cross section in μb. for models of ^{16}N				
		IPM	EF	GV	KUO	KUO(S)
290	I	34.651	26.773	29.238	23.723	21.177
	II	25.012	19.166	21.023	16.872	14.962
	III	21.540	16.374	18.023	14.344	12.661
320	I	34.651	25.301	29.032	22.838	20.523
	II	25.507	18.455	21.284	16.594	14.847
	III	22.252	16.004	18.527	14.360	12.797
350	I	28.829	20.699	23.659	18.684	16.709
	II	21.158	15.029	17.275	13.509	12.019
	III	18.328	12.902	14.903	11.552	10.231
380	I	21.686	15.818	17.354	14.088	12.437
	II	15.624	11.211	12.370	9.910	8.674
	III	13.309	9.412	10.642	8.263	7.144
420	I	15.627	11.727	12.345	10.308	9.013
	II	11.070	8.146	8.606	7.083	6.117
	III	9.284	6.709	7.114	5.772	4.927

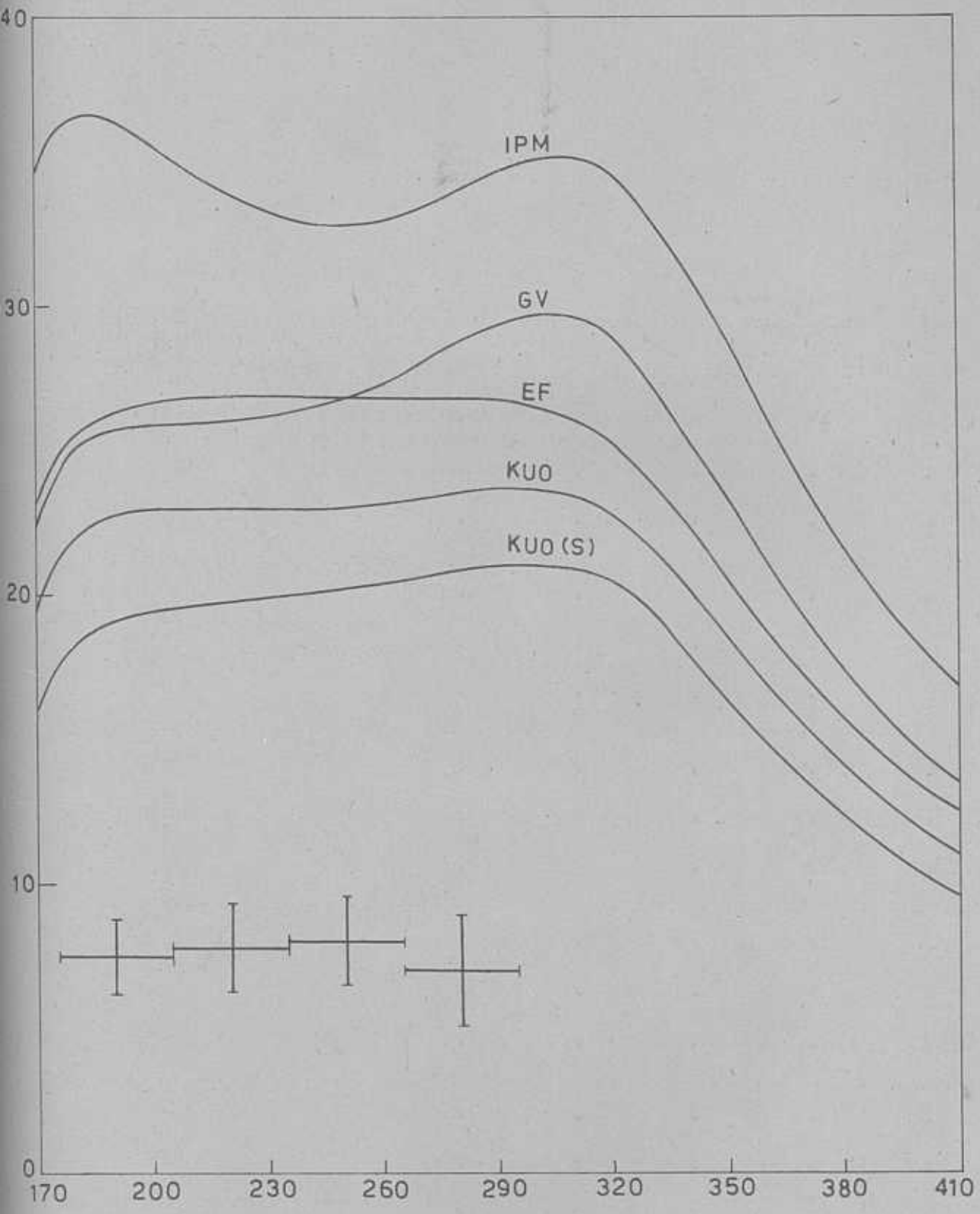

Fig.1. Total cross section for the reaction $^{16}O(\gamma,\pi^+)^{16}N$ obtained using model I of table.1 for the ground state of ^{16}O. The nuclear models used for ^{16}N states are: IPM, EF, GV, KUO and KUO(S). The experimental results are from ref.12.

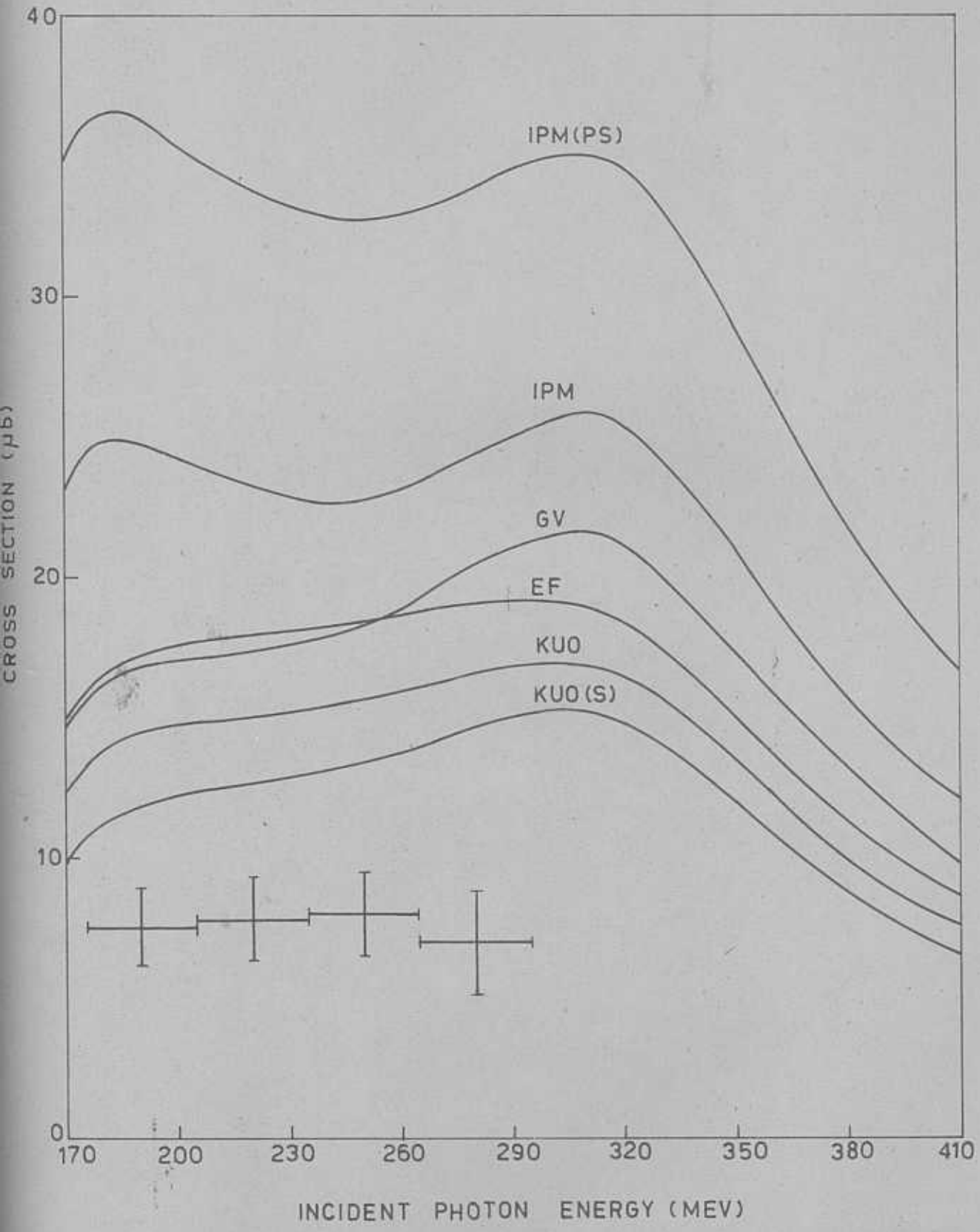

Fig.2. Total cross section for the reaction $^{16}O(\gamma,\pi^+)^{16}N$ obtained using model II of table.1 for the ground state of ^{16}O. The nuclear models used for ^{16}N states are: IPM, EF, GV, KUO and KUO(S). The curve IPM(PS) is also shown for the sake of comparison. The experimental results are from ref.12.

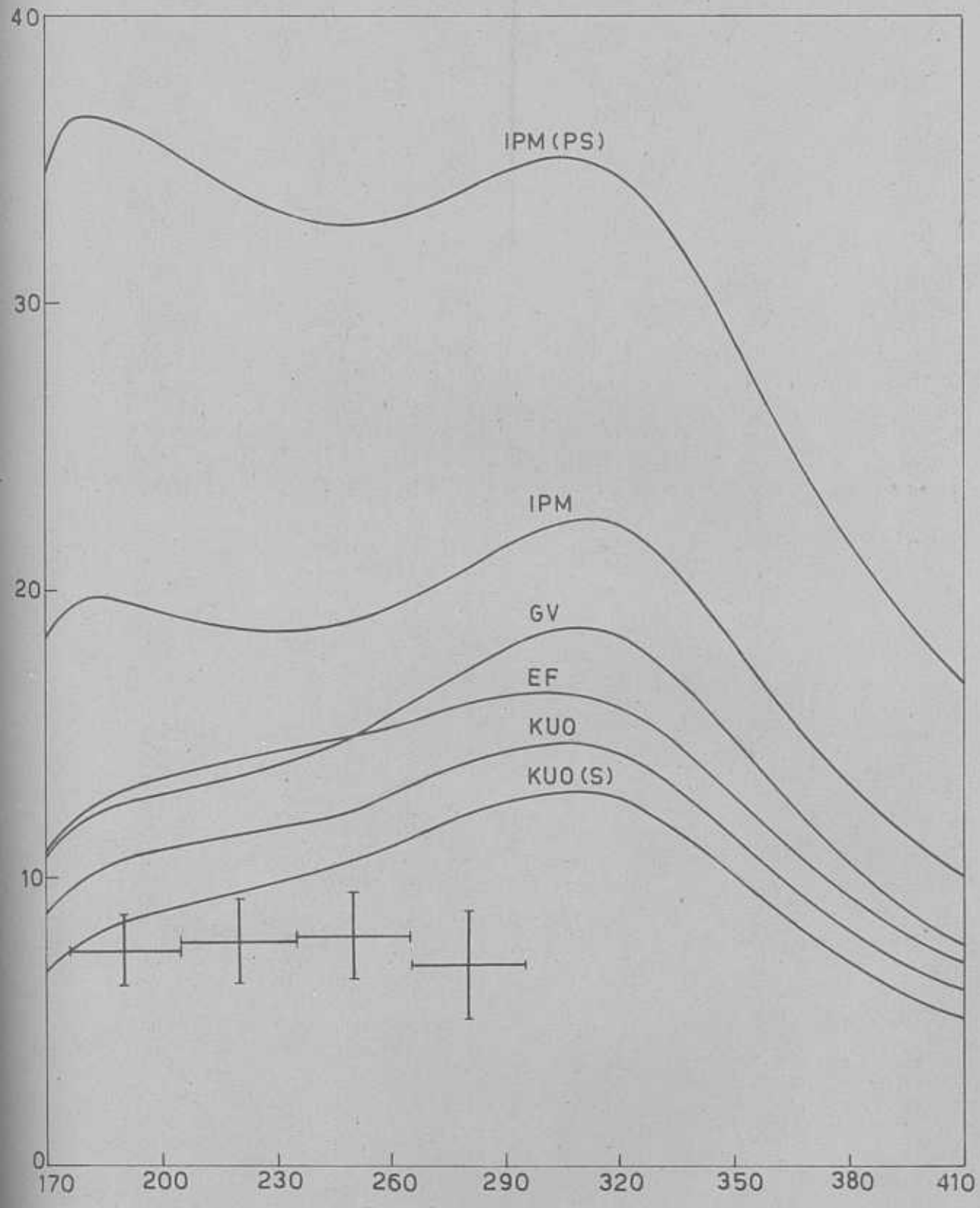

Fig.3. Total cross section for the reaction $^{16}O(\gamma,\pi^+)^{16}N$ obtained using model III of table.1 for the ground state of ^{16}O. The nuclear models used for ^{16}N states are: IPM, EF, GV, KUO and KUO(S). The curve IPM(PS) is also shown for the sake of comparison. The experimental results are from ref.12.

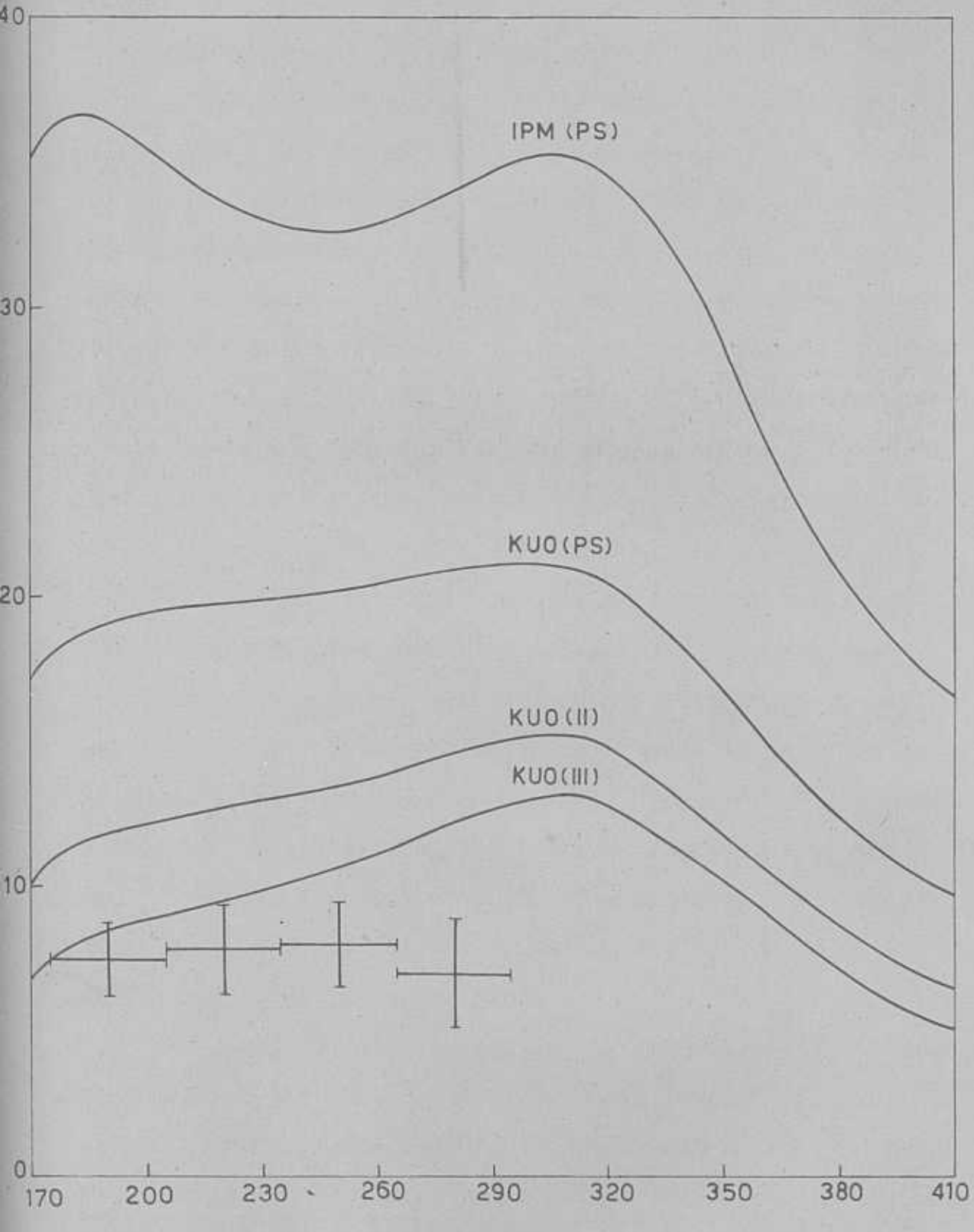

.4. Total cross section for the reaction $^{16}O(\gamma,\pi^+)^{16}N$ obtained using Kuo wave function with screening corrections for the states of ^{16}N the three models of table.1 for the ground state of ^{16}O. The curve (PS) is also shown for the sake of comparison. The experimental ults are from ref.12.

Walters and Hummel[12]. The curves are for the total cross section, which is a sum of the "partial" cross sections to the lowest 0^-, 1^-, 2^- and 3^- bound states of ^{16}N, which are stable against nucleon emission. While Fig.1 shows the cross section curves obtained in the case of a pure shell model wave function of ^{16}O, Figs.2 and 3 show the curves for the two deformed ground state wave functions of ^{16}O given by II and III of table.1, respectively. Fig.4 projects the results obtained with the "screened" wave function for ^{16}N states and for the three possibilities for the ground state wave function of ^{16}O, enumerated in table.1.

We draw the following conclusion from our results: Without invoking the phenomenological surface production mechanism, we find that a better agreement between theory and experiment for the photoproduction of π^+ from $^{16}O(0^+,g.s.)$ leading to the four bound states of $^{16}N(J_f^P : 0^-, 1^-, 2^-$ and $3^-)$ can be obtained using the Kuo wave function with "screening" for ^{16}N states together with the deformed ground state wave function of ^{16}O obtained by Purser et.al.[5] from an analysis of the $^{16}O(d,{}^3He)^{15}N$ experiment.

We would now like to mention two possible effects which might modify the conclusion drawn above. One is the possible effect of short-range correlations which we analyse in detail in the next chapter. The other is the effect of final state

---

12) R.A.Meyer, W.B.Walters and J.P.Hummel, Phys.Rev.138, B1421 (1965).

interactions, that is, the interaction of the outgoing pion with the residual nucleus. A way to treat this effect would be to use an optical model potential for the outgoing pion and use the solutions of the Schrodinger equation instead of the plane wave for the pion, as done in all the studies described in this thesis. We intend investigating this problem in the near future. In this connection, we would like to quote the results of an earlier study of Saunders[13]. He finds that around 250 Mev incident photon energy, the final state interaction is much more significant for neutral pion photoproduction than for charged pion photoproduction. In one particular case of charged pion photoproduction, viz., $^{88}Sr(\gamma, \pi^-)^{88}Y$, he shows the effect to be of some importance only in the forward angles ($< 30^{\circ}$) and there too the reduction in the differential cross section is at most of the order of 20-25 % .

---

12) L.M.Saunders, B7, 293 (1968).

CHAPTER 5

PHOTOPRODUCTION OF POSITIVE PIONS FROM ^{16}O: (iii) EFFECT OF SHORT-RANGE CORRELATIONS+

1. In this Chapter, we present an investigation made to find the effect of the short-range correlations between nucleons upon the differential cross section for photoproduction of π^+ from ^{16}O, leading to any one of the four final T=1 states ($J^P = 0^-$, 1^-, 2^- and 3^-) of ^{16}N. It is usually accepted that the nucleon-nucleon interaction contains a hard-core, that is, the interaction becomes strongly repulsive at short distances in the relative coordinate of two nuclear particles. But the short-range correlations induced by such a hard-core are neglected in most shell model calculations even though the correlation corrections are expected to become increasingly important as one considers nuclear phenomena at high momentum transfers. Da Providencia and Shakin[1] have shown, following Villars[2], how short-range correlations can be introduced into the nuclear wave function using a unitary model operator e^{iS}, where S is a hermitian two-body operator. If we

---

+ V.Devanathan, "Symposia in Theoretical Physics and Mathematics", Plenum Press, Vol.(1969).
K.Srinivasa Rao and V.Devanathan (to be published).

1) J.Da Providencia and C.M.Shakin, Ann.Phys.30, 95 (1964).

2) F.Villars, "Proceedings of the International School of Physics", 'Enrico Fermi' - Course.23, 1961". Academic Press, New York, (1963); F.Coester and H.Kummel, Nucl. Phys.17, 477 (1960).

denote the usual shell model wave function by Φ , then the wave function which contains short-range correlations induced by the unitary operator e^{iS} can be written as:

$$\Psi = e^{iS}\Phi \ , \ S^{+} = S \qquad (5.1.1)$$

Da Providencia and Shakin[1] find the corrections to the matrix elements of the dipole transition operator for particle-hole states to be small. They have also shown[3] that the presence of short-range correlations cause a significant modification of electron scattering form factors at high momentum transfer ($q \approx 3$ fm^{-1}). There are many studies[4] of the influence of short-range dynamical nucleon-nucleon correlations on elastic electron and nucleon scattering cross sections and these provide a strong evidence for the existence of correlations. Another important step in clarifying the correlation structure of nuclei is the study of the ground state energy. This has been done directly using the Jastrow[5] method by Dabrowski[6] to get the binding energy of ^{16}O nucleus. In the preliminary results which we have obtained in the study of the effect of short-range correlations in $^{16}O(\gamma,\pi^{+})^{16}N$, we have made use of the form of the correlation function

---

3) J.Da Providencia and C.M.Shakin, Nucl.Phys.65, 54 (1965).
4) For example, C.Ciofi Degli Atti, ISS 68/24, Instituto Superiore di Sanita, Laboratori di Fisica, contains a list of references.
5) R.Jastrow, Phys.Rev.98, 1479 (1955); F.Iwamoto and H.Yamada, Prog.Theor.Phys. 17, 543 (1957).
6) J.Dabrowski, Proc.Phys.Soc. 71, 658 (1958); ibid 72, 499 (1958).

chosen by Dabrowski.

2. The model operator which introduces short-range correlations is written as e^{iS}. If we make the important assumption that the short-range correlations are the same in the ground state and the excited states of the system, then we need only a single model operator to correlate the shell model wave functions. On the basis of this assumption it becomes possible to calculate the physical quantities using uncorrelated shell model states if one uses a set of transformed operators, $\tilde{O}$, related to the standard operator, O, by:

$$\tilde{O} = e^{-iS} \; O \; e^{iS} \qquad (5.2.1)$$

where O is the transition operator for single nucleon positive photopion production, viz:

$$O = (\underline{\sigma}\cdot\underline{k} + L)\{\exp(i\underline{k}\cdot\underline{r})\}\tau^- = \sum_n (\sigma_n \cdot K_n)\tau^- \exp(i\underline{k}\cdot\underline{r}) \qquad (5.2.2)$$

where $\sigma_1 = \underline{\sigma}$, $n = 0,1$, $\sigma_0 = I$, $K_1 = \underline{K}$ is the spin-flip part of the CGLN amplitude, $K_0 = L$ is the spin-non-flip part, $\underline{k} = \underline{\nu} - \underline{\mu}$ is the momentum transfer to the nucleon with $\underline{\nu}$ and $\underline{\mu}$ being the momenta of the photon and pion, respectively, and τ^- is the isobaric spin operator. The transform of a one-body operator contains a one-body part, a two-body part,

etc.,

$$\tilde{O} = \tilde{O}^{(1)} + \tilde{O}^{(2)} + \cdots \qquad (5.2.3)$$

where

$$\tilde{O}^{(1)} = \sum_{\alpha,\beta} a^{+}_{\alpha} \langle \alpha | O | \beta \rangle a_{\beta} , \qquad (5.2.4)$$

and

$$\tilde{O}^{(2)} = \tfrac{1}{2} \sum_{\alpha,\beta,\gamma,\delta} a^{+}_{\alpha} a^{+}_{\beta} [\langle \alpha\beta | e^{iS}(O_1+O_2)e^{iS} | \gamma\delta \rangle - \langle \alpha\beta | (O_1+O_2) | \gamma\delta \rangle] a_{\delta} a_{\gamma}, \qquad (5.2.5)$$

where $a^{+}(a)$ are the creation (annihilation) operators for fermions, defined in section.2 of Chapter.3. Here, we are interested in calculating the magnitude of the corrections due to the presence of the correlation correction operator, $\tilde{O}^{(2)}$. The calculation of the one-body part of the operator $\tilde{O}$, viz. $\tilde{O}^{(1)}$, between the pure shell model ground state of ^{16}O and the particle-hole state of ^{16}N has already been carried out explicitly in Chapter.3 and the result is given by Eq.(3.4.2). Here, we will denote this one-body matrix element by M_1.

Before defining the behaviour of the model operator e^{iS} in the space spanned by the two-particle wave functions, we recall the transformation which takes us from motion of two particles about a common center to a description of the

relative and center-of-mass motion of the two particles. This transformation can be written in the notation of Moshinsky[7] as:

$$|n_1 \ell_1, n_2 \ell_2, LM\rangle = \sum_{n\ell, N\mathcal{L}} \{n\ell, N\mathcal{L}, L | n_1\ell_1, n_2\ell_2, L\} \, |n\ell, N\mathcal{L}, LM\rangle \tag{5.2.6}$$

where $(n\ell)$ are the quantum numbers of the relative motion and $(N\,\mathcal{L})$ are the quantum numbers associated with the center-of-mass motion. The operator e^{iS} is assumed to have a simple representation in the relative and center-of-mass system:

$$[e^{iS}]^{(2)} = \sum_{\substack{n\ell, N\mathcal{L}, LM \\ SS_z, TT_z}} |\widetilde{n\ell}, N\mathcal{L}, LM, SS_z, TT_z\rangle\langle n\ell, N\mathcal{L}, LM, SS_z, TT_z| \tag{5.2.7}$$

The operator $[e^{iS}]^{(2)}$ is the two-body part of the model operator e^{iS} and we restrict ourselves to matrix elements of the model operator between two-particle states. Further, the simplifying assumption that the correlations are the same in singlet and triplet spin and isobaric spin states is made in Eq.(5.2.7).

The bra and ket in Eq.(5.2.7) are identical in all quantum numbers except $(n\,\ell)$. While $(n\,\ell)$ corresponds to a state of relative motion governed by a wave function of the harmonic oscillator form, the state $(\widetilde{n\,\ell})$ that replaces $(n\ell)$

7) M.Moshinsky and T.A.Brody, "Tables of Transformation brackets", Monografias del Instituto de Fisica, Mexico,(1960). We use Moshinsky's notation for the radial quantum number throughout this Chapter.

via the unitary transfomation has short-range correlations. Since e^{iS} is a unitary operator, we must insure that the correlated radial wave functions, which we denote by $\tilde{R}_{nl}$, have the same completeness and orthonormal properties as the harmonic oscillator radial wave functions R_{nl}. This is guaranteed if we assume (for $l = 0$):

$$\tilde{R}_{no}(r) = \frac{f(r)}{\sqrt{N_{no}}} R_{no}(r) \qquad (5.2.8)$$

where f(r) is the correlation function and

$$N_{no} = \int_0^\infty f^2(r) R_{no}^2(r) r^2 dr \qquad (5.2.9)$$

is the factor which normalizes the correlation function. We have assumed, in writing (5.2.8), the existence of short-range correlations only in S-states ($l=0$), for the sake of simplicity. For the correlation function, f(r), we choose the form employed by Dabrowski[6] in his variational calculation on the binding energy of ^{16}O; viz.

$$f(r) = 0 \qquad \text{for } r \leq c ,$$
$$f(r) = 1-\exp\left\{-\beta\left[\left(\frac{r}{c}\right)^2-1\right]\right\} \qquad \text{for } r > c \qquad (5.2.10)$$

where β and c are two parameters. For $c = 0.2$ fm and $\beta = 0.75$, Dabrowski obtains for the binding energy, E, a value of -199 Mev and for r_o, a value of 0.86 fm; while for $c = 0.6$ fm and $\beta = 2.0$, he obtains E = -64.7 Mev and $r_o = 1.4$ fm. The experi-

mental values of E and r_0 are -127.56 Mev and 1.2 fm, respectively.

We now return to the evaluation of the matrix element of the two-body part of the model operator, Eq.(5.2.5), between the pure shell model ground state of ^{16}O and the particle-hole state of ^{16}N, defined by Eq.(3.2.1), without configuration mixing. We consider the Moshinsky transformation:

$$\underline{r} = \frac{1}{\sqrt{2}}(\underline{r}_1 - \underline{r}_2) \quad , \quad \underline{R} = \frac{1}{\sqrt{2}}(\underline{r}_1 + \underline{r}_2). \tag{5.2.11}$$

This definition of $\underline{r}$ has an advantage over the more usual one in that the harmonic oscillator wave functions have the same form in both the coordinate systems. In these new coordinates, the two-body operator constructed from two one-body operators becomes:

$$\begin{aligned} O_1 + O_2 &= \sum_{n=0,1} \{ (\sigma_{1n} \cdot K_n)\, \tau_1^- \exp(i\underline{k}\cdot\underline{r}_1) + \\ &\qquad + (\sigma_{2n} \cdot K_n)\, \tau_2^- \exp(i\underline{k}\cdot\underline{r}_2) \} \\ &= 16\pi^2 \sum_n \sum_{l_r, l_R} \sum_{m_r, m_R} i^{l_r + l_R} (-1)^{m_r + m_R + \mu} \\ &\quad \cdot j_{l_r}\left(\frac{k}{\sqrt{2}} r\right) j_{l_R}\left(\frac{k}{\sqrt{2}} R\right) Y^{l_r}_{m_r}(\hat{r})\, Y^{l_r}_{-m_r}(\hat{k})\, Y^{l_R}_{m_R}(\hat{R})\, Y^{l_R}_{-m_R}(\hat{k})\, K^n_{-\mu} \\ &\quad \cdot \left[(\sigma_1)^n_\mu\, \tau_1^- + (-1)^{l_r} (\sigma_2)^n_\mu\, \tau_2^- \right] \end{aligned} \tag{5.2.12}$$

where we have used the Rayleigh expansion given by Eq.(2.3.7),

Now, making use of

(i) $$Y^{l_r}_{-m_r}(\hat{k})\,Y^{l_R}_{-m_R}(\hat{k}) = \sum_{\lambda,m_\lambda} \frac{[l_r][l_R]}{\sqrt{4\pi}\,[\lambda]}\, C(l_r l_R \lambda; -m_r,-m_R,-m_\lambda)\cdot$$

$$\cdot\; C(l_r l_R \lambda; 000)\; Y^{\lambda}_{-m_\lambda}(\hat{R})$$

with $[l] = \sqrt{2l+1}$,

(ii)

$$Y^{l_r}_{m_r}(\hat{r})\,Y^{l_R}_{m_R}(\hat{R}) = \sum_{\lambda',m'_\lambda} C(l_r l_R \lambda'; m_r m_R m_{\lambda'})\,(Y^{l_r}(\hat{r}) \times Y^{l_R}(\hat{R}))^{\lambda'}_{m'_\lambda},$$

and the orthogonality property for Clebsch-Gordon coefficients, we get after simplifications:

$$O_1 + O_2 = 16\pi^2 \sum_{\substack{n,l_r,l_R\\ \lambda,\Lambda}} i^{l_r+l_R}(-1)^{l_r+l_R+n-\Lambda}(-1)^{m_\Lambda}\cdot$$

$$\cdot\; \frac{[l_r][l_R]}{\sqrt{4\pi}\,[\lambda]}\, C(l_r l_R \lambda; 000)\, j_{l_r}\!\left(\tfrac{k}{\sqrt{2}}r\right) j_{l_R}\!\left(\tfrac{k}{\sqrt{2}}R\right)\cdot$$

$$\cdot\; (Y^{\lambda}(\hat{k}) \times K^n)^{\Lambda}_{-m_\Lambda} \Big\{ \big[(Y^{l_r}(\hat{r}) \times Y^{l_R}(\hat{R}))^{\lambda} \times \sigma_1^n \big]^{\Lambda}_{m_\Lambda} \tau_1^- +$$

$$+ (-1)^{l_r} \big[(Y^{l_r}(\hat{r}) \times Y^{l_R}(\hat{R}))^{\lambda} \times \sigma_2^n \big]^{\Lambda}_{-m_\Lambda} \tau_2^- \Big\} \qquad (5.2.13)$$

If we denote by M_z the two-body matrix element,

$\langle j_p j_h\; JM\; TM_T \mid \tilde{O}^{(2)} \mid 0^+, \text{g.s.} \rangle$, then

$$\tilde{M}_2 = \sum_{\substack{m_p,m_h,\tau_p,\tau_h\\ n_c,l_c,j_c}} C(j_p j_h J;\, m_p,-m_h\, M)\,(-1)^{j_h-m_h}(-1)^{\frac{1}{2}-\tau_h}\, C(\tfrac{1}{2}\tfrac{1}{2}T;\, \tau_p,-\tau_h\, M_T)\cdot$$

$$\cdot \big[\langle pc \mid \{ e^{-iS}(O_1+O_2)e^{iS} - (O_1+O_2) \} \mid hc \rangle +$$

$$- \langle pc \mid \{ e^{-iS}(O_1+O_2)e^{iS} - (O_1+O_2) \} \mid ch \rangle \big] \qquad (5.2.14)$$

where the sum over $(n_c\ \ell_c\ j_c)$ refers to a sum over the occupied orbits of ^{16}O core - $1s_{1/2}$, $1p_{3/2}$ and $1p_{1/2}$ and p,h and c in the bra and ket states stand for the complete set of quantum numbers of the respective nucleons. The isobaric spin part is evaluated first. Now, to evaluate the angular momentum part, we find it advantageous to go over to the combined space of the two-particle total angular momentum - i.e. we couple j_h and j_c to J_i and j_p and j_c to J_f - and then go over to the L-S coupling scheme by means of the LS-jj transformation:

$$|\, j_1\, j_2\, J\, M\rangle = \sum_{L,S} [L][S][j_1][j_2] \begin{Bmatrix} \ell_1 & \tfrac{1}{2} & j_1 \\ \ell_2 & \tfrac{1}{2} & j_2 \\ L & S & J \end{Bmatrix} |LSJM\rangle \cdot \quad (5.2.15)$$

Further, using standard relations, we get for the reduced matrix elements:

$$\langle j_p\, j_c\, J_f \,\|\, [(Y^{\ell_r}(\hat{r}) \times Y^{\ell_R}(\hat{R}))^{\lambda} \times \sigma_1^{\,n}\,]^{J} \,\|\, j_h\, j_c\, J_i\rangle =$$

$$= \sum_{\substack{L_i, S_i \\ L_f, S_f}} \sum_{\substack{n_i \ell_i, N_i \mathcal{L}_i \\ n_f \ell_f, N_f \mathcal{L}_f}} (-1)^{S_i - S_f} [j_p][j_h][j_c]^2 [L_i][S_i]^2 [L_f]^2 [S_f]^2 \times$$

$$\times [\tfrac{1}{2}][n]\, W(\tfrac{1}{2}\,\tfrac{1}{2}\,n\,S_f;\, S_i\,\tfrac{1}{2}) \begin{Bmatrix} \ell_p & \tfrac{1}{2} & j_p \\ \ell_c & \tfrac{1}{2} & j_c \\ L_f & S_f & J_f \end{Bmatrix} \begin{Bmatrix} \ell_h & \tfrac{1}{2} & j_h \\ \ell_c & \tfrac{1}{2} & j_c \\ L_i & S_i & J_i \end{Bmatrix} \begin{Bmatrix} L_i & \lambda & L_f \\ S_i & n & S_f \\ J_i & J & J_f \end{Bmatrix} \times$$

$$\times \langle n_i \ell_i, N_i \mathcal{L}_i, L_i \,|\, n_h \ell_h, n_c \ell_c, L_i\rangle (-1)^{\ell_c + \mathcal{L}_f} \times$$

$$\times \langle n_f \ell_f, N_f \mathcal{L}_f, L_f \,|\, n_p \ell_p, n_c, \ell_c, L_f\rangle \times$$

$$\times \langle \ell_f\, \mathcal{L}_f\, L_f \,\|\, (Y^{\ell_r}(\hat{r}) \times Y^{\ell_R}(\hat{R}))^{\lambda} \,\|\, \ell_i\, \mathcal{L}_i\, L_i\rangle, \quad (5.2.16)$$

and

$$\langle l_f \mathcal{L}_f L_f \| (Y^{l_r}(\hat{r}) \times Y^{l_R}(\hat{R}))^{\lambda} \| l_i \mathcal{L}_i L_i \rangle =$$

$$= \frac{1}{4\pi} [L_i][\lambda][l_i][l_r][\mathcal{L}_i][l_R] C(l_i l_r l_f; 000)\, C(\mathcal{L}_i l_R \mathcal{L}_f; 000) \times$$

$$\times \begin{Bmatrix} l_i & l_r & l_f \\ \mathcal{L}_i & l_R & \mathcal{L}_f \\ L_i & \lambda & L_f \end{Bmatrix} . \qquad (5.2.17)$$

Using these expressions for the reduced matrix elements, it is now straight forward to evaluate Eq.(5.2.14) and we get the following final result for the correlated two-body matrix element $\tilde{M}_2$:

$$\tilde{M}_2 = \sqrt{4\pi} \sum_{n} \sum_{l_r, l_R, \lambda} \sum_{J_i, J_f} \sum_{l_c, j_c} \sum_{\substack{L_i, S_i \\ L_f, S_f}} \sum_{\substack{n_i l_i, N_i \mathcal{L}_i \\ n_f l_f, N_f \mathcal{L}_f}} i^{l_r + l_R} (-1)^{l_r + l_R + n} \times$$

$$\times (-1)^{l_c + \mathcal{L}_f} (-1)^{S_i - S_f} (-1)^{J_f + j_h - j_c} [j_p][j_h][j_c]^2 [L_i]^2 [S_i]^2 [J_i]^2 \times$$

$$\times [L_f]^2 [S_f]^2 [J_f]^2 [l_i][\mathcal{L}_i][l_r]^2 [l_R]^2 [1/2][n]\, C(l_r l_R \lambda; 000) \times$$

$$\times C(l_i l_r l_f; 000)\, C(\mathcal{L}_i l_R \mathcal{L}_f; 000)\, W(J_f j_p J_i j_h; j_c J)\, W(\tfrac{1}{2}\tfrac{1}{2} S_f n; S_i \tfrac{1}{2}) \times$$

$$\times \begin{Bmatrix} l_p & 1/2 & j_p \\ l_c & 1/2 & j_c \\ L_f & S_f & J_f \end{Bmatrix} \begin{Bmatrix} l_h & 1/2 & j_h \\ l_c & 1/2 & j_c \\ L_i & S_i & J_i \end{Bmatrix} \begin{Bmatrix} L_i & \lambda & L_f \\ S_i & n & S_f \\ J_i & J & J_f \end{Bmatrix} \begin{Bmatrix} l_i & l_r & l_f \\ \mathcal{L}_i & l_R & \mathcal{L}_f \\ L_i & \lambda & L_f \end{Bmatrix} \cdot$$

$$\times \langle n_i l_i, N_i \mathcal{L}_i, L_i | n_h l_h, n_c l_c, L_i \rangle \langle n_f l_f, N_f \mathcal{L}_f, L_f | n_p l_p, n_c l_c, L_f \rangle \cdot$$

$$\times [2 - (-1)^{l_c + l_h + \mathcal{L}_i} \{1 + (-1)^{l_r + S_i - S_f}\}] \times$$

$$\times (-1)^M (Y^{\lambda}(\hat{k}) \times K^n)^J_M \langle j_{l_R}(\tfrac{k}{\sqrt{2}} R) \rangle_{N_f \mathcal{L}_f, N_i \mathcal{L}_i} \langle j_{l_r}(\tfrac{k}{\sqrt{2}} r) \rangle_{\widetilde{n_f l_f}, \widetilde{n_i l_i}} , \qquad (5.2.18)$$

where

$$\langle j_{l_R}(\tfrac{k}{\sqrt{2}}R)\rangle_{N_f\mathcal{L}_f,N_i\mathcal{L}_i} = \int_0^\infty \mathcal{R}_{N_f\mathcal{L}_f}(R)\, j_{l_R}(\tfrac{k}{\sqrt{2}}R)\, \mathcal{R}_{N_i\mathcal{L}_i}(R)\, R^2 dR, \quad (5.2.19)$$

$$\langle j_{l_r}(\tfrac{k}{\sqrt{2}}r)\rangle_{\widetilde{n_f l_f},\widetilde{n_i l_i}} = \int_0^\infty [\,\widetilde{\mathcal{R}}_{n_f l_f}(r)\, j_{l_r}(\tfrac{k}{\sqrt{2}}r)\, \widetilde{\mathcal{R}}_{n_i l_i}(r) - \mathcal{R}_{n_f l_f}(r)\, j_{l_r}(\tfrac{k}{\sqrt{2}}r)\, \mathcal{R}_{n_i l_i}(r)]\, r^2 dr. \quad (5.2.20)$$

In Eq.(5.2.18), the only term that depends on magnetic quantum number, M, is

$$(-1)^M (Y^\lambda(\hat{k}) \times K^n)^J_M \quad (5.2.21)$$

In the expression for the differential cross section, the products of matrix elements $M_1M_1^*$, $M_2\widetilde{M}_2^*$, $M_1\widetilde{M}_2^*$ and $M_1^*\widetilde{M}_2$ occur and they contain the term (5.2.21) bilinearly with a summation over M. Explicitly this term is of the form:

$$\sum_M (Y^\lambda(\hat{k}) \times K^n)^J_M [(Y^{\lambda'}(\hat{k}) \times K^{n'})^J_M]^* \quad (5.2.22)$$

and the result for this summation is given by Eq.(3.4.11) of Chapter.3.

The differential cross section, we are interested in, is given by

$$\frac{d\sigma}{d\Omega} = (2\pi)^{-2} \mu\mu_0 [M_1M_1^* + M_1\widetilde{M}_2^* + M_1^*\widetilde{M}_2 + \widetilde{M}_2\widetilde{M}_2^*]. \quad (5.2.23)$$

8. The rather large number of quantum numbers which are to be summed over in the expression (5.2.18) for $\tilde{M}_2$, makes the numerical calculation tedious, in the absence of any restrictions on the quantum numbers. One restriction which we have introduced is to consider S-wave correlations only. This implies that the quantum numbers l_i and l_f can take the values:

$$l_i = l_f = 0 \; ; \; l_i = 0, l_f \neq 0 \text{ and } l_i \neq 0, \; l_f = 0 .$$

Since the core-particle ($n_c l_c$) can belong to either a 0s or a 0p-shell only and since we consider the odd-parity states of ^{16}N to be assigned to a configuration which has a proton-hole ($n_h l_h$) in the 0p-shell and a neutron-particle ($n_p l_p$) in the 0d or 1s-shell, we find, by looking up the tables for Moshinsky transformation brackets[7] that:

l_i or l_f can take values ≤ 3 when n_i or n_f is 0,
and l_i or l_f can take values ≤ 1 when n_i or n_f is 1.
These conditions together with the restriction to S-wave correlations reduces the number of integrals of the type (5.2.20), which have to be numerically integrated, to 11 only.

Based on the observation that integrals of the type (5.2.19) become smaller and smaller in magnitude, for a given pair of harmonic oscillator wave functions, with increasing order of the spherical Bessel function $j_{l_R}(\frac{k}{\sqrt{2}}R)$, we restrict the quantum number l_R to $l_R \leq 3$. This restriction reduces the number of radial integrals of the type (5.2.19), which have to

be analytically integrated, to 29. These are the only two justifiable restrictions which we make in our present study.

Before looking at the cross sections, we deem it fit to discuss about the radial wave functions $\tilde{R}_{n0}(r)$ for n=0 and 1. In table 1 the usual normalized harmonic oscillator wave functions $R_{00}(r)$ and $R_{10}(r)$ are given together with the normalized correlated wave functions $\tilde{R}_{00}(r)$ and $\tilde{R}_{10}(r)$ for the two sets of values of the parameters β and c which occur in the expression (5.2.10) for the correlation function f(r), for various values of the radial coordinate r. Fig.1 is the corresponding plot of the above mentioned four wave functions for β =2.0, c = 0.6 fm and b = 1.76 fm. From the figure it is clear that $R_{00}(r)$ and $R_{10}(r)$ differ somewhat from $\tilde{R}_{00}(r)$ and $\tilde{R}_{10}(r)$ only near the origin due to the existence of the hard-core radius parameter c = 0.6 fm.

In Fig.2 the momentum transfer ($\underline{k} = \underline{\nu} - \underline{\mu}$, in fm^{-1}) is plotted as a function of the center-of-mass pion angle for various incident photon energies. We notice that larger momentum transfers occur only at the backward angles. We choose the energy of the incident photon to be 260 Mev in our preliminary study.

Even a fast Computer like CDC 3600, took as much as 50 minutes time to compute "partial" differential cross sections at 260 Mev incident photon energy with the ^{16}N states described by the simple Independent Particle Model (IPM) configurations -

wave functions.

$$\tilde{R}_{no}(r) = \frac{f(r)}{\sqrt{N_{no}}} R_{no}(r) \quad \text{where} \quad N_{no} = \int_0^\infty f^2(r) R_{no}^2(r) r^2 dr$$

$$f(r) = 0 \quad \text{for} \quad r \le c$$

$$= 1 - \exp[-\beta \{(\tfrac{r}{c})^2 - 1\}] \quad \text{for} \quad r > c .$$

r	R_{00}	$\tilde{R}_{00}$		R_{10}	$\tilde{R}_{10}$	
		$\beta=2, c=0.6$fm	$\beta=0.75, c=0.2$fm		$\beta=2, c=0.6$fm	$\beta=0.75, c=0.2$fm
0.0	0.6434	0.0	0.0	0.788	0.0	0.0
0.5	0.6179	0.0	0.6077	0.7161	0.0	0.7051
1.0	0.5475	0.5144	0.5491	0.5262	0.4848	0.5284
1.5	0.4475	0.4328	0.4488	0.2826	0.2681	0.2838
2.0	0.3373	0.3263	0.3383	0.05748	0.05451	0.05772
2.5	0.2346	0.2269	0.2353	-0.09917	-0.09405	-0.09958
3.0	0.1505	0.1456	0.1509	-0.1727	-0.1638	-0.1734
3.5	0.0891	0.0862	0.0893	-0.1785	-0.1693	-0.1793
4.0	0.0486	0.0470	0.0488	-0.1455	-0.138	-0.1461

(continued on next page)

Table.1.(continued)

r	R_{00}	$\tilde{R}_{00}$		R_{10}	$\tilde{R}_{10}$	
		$\beta=2, c=0.6$fm	$\beta=0.75, c=0.2$fm		$\beta=2, c=0.6$fm	$\beta=0.75, c=0.2$fm
4.5	0.0245	0.0237	0.0246	-0.1007	-0.0955	-0.1011
5.0	0.0114	0.0110	0.0114	-0.06102	-0.05788	-0.06128
5.5	0.0049	0.0047	0.0049	-0.03289	-0.0312	-0.03303
6.0	0.0019	0.0019	0.0019	-0.01592	-0.0151	-0.01599
6.5	0.0007	0.00068	0.0007	-0.006964	-0.006604	-0.006993
7.0	0.0002363	0.0002286	0.000237	-0.002763	-0.002620	-0.002774
7.5	0.00007332	0.0000709	0.00007354	-0.0009974	-0.0009459	-0.001002
8.0	0.00002099	0.0000203	0.00002105	-0.0003283	-0.0003114	-0.003297
8.5	0.000005541	0.00000536	0.000005558	-0.00009874	-0.00009365	-0.00009916
9.0	0.00000135	0.000001305	0.000001354	-0.00002716	-0.00002576	-0.00002728
9.5	0.000000303	0.000000293		-0.000006842	-0.0000064[illegible]9	

$(0p_{1/2})^{-1}(1s_{1/2})$ for $J^p = 0^-$ and 1^- states and $(0p_{1/2})^{-1}(0d_{5/2})$ for $J^p = 2^-$ and 3^- states. In table.2 we give the theoretical differential cross sections obtained with the correlation function parameters $\beta = 2.0$, $c = 0.6$ fm and the harmonic oscillator size parameter $b = 1.76$ fm. Fig.3 shows these cross sections--solid and dashed line curves have been obtained without and with short-range correlations.

The maximum momentum transfer involved is 1.9 fm^{-1} for an incident photon energy of 260 Mev (see Fig.2), and we find from Fig.3 that the correlation corrections are not as yet the dominant feature in our study of π^+ photoproduction from ^{16}O. This is in conformity with the finding of Providencia and Shakin[3] that the short-range correlation studied via the process of inelastic electron scattering, cause a significant modification of the electron scattering form factor only for $q \approx 3$ fm^{-1}. We conjecture that for larger incident photon energies (say, around 400 Mev) these correlation corrections may become more important. In any case, a definite conclusion about the effect of short-range correlations on photopion production cross sections can be drawn only when experimental angular distributions of the cross sections are available.

Table 1. Effect of correlations on the differential cross section for elastic scattering of 260 Mev with b=1.76 fm, c=0.6 fm and β =2.0.

Center-of-mass differential cross section in μb/sr without and with correlations

$\theta_{c.m.}$ (degrees)	$J^P=0^-$		$J^P = 1^-$		$J^P = 2^-$		$J^P = 3^-$	
	Without	With	Without	With	Without	With	Without	With
0	0.0	0.0	0.1323	0.2091	0.5001	0.5823	0.00015	0.0012
20	0.0105	0.0169	0.2864	0.4357	1.1560	1.3060	0.0044	0.0105
40	0.0563	0.0934	0.3985	0.5746	2.4395	2.6547	0.1123	0.1521
60	0.0253	0.0518	0.1030	0.1687	2.5515	2.6031	0.6661	0.7405
80	0.0083	0.0038	0.0361	0.0214	1.2928	1.1645	1.5741	1.5589
100	0.0555	0.0207	0.3250	0.1300	0.4228	0.4727	1.8896	1.9946
120	0.0560	0.0604	0.5278	0.5461	0.1139	0.0737	1.6802	1.6943
140	0.0281	0.0288	0.5505	0.5540	0.0293	0.0141	1.3058	1.2789
160	0.0069	0.0069	0.5112	0.5131	0.0072	0.0022	1.0421	1.0049
180	0.0	0.0	0.4910	0.4915	0.0026	0.0007	0.9536	0.9133

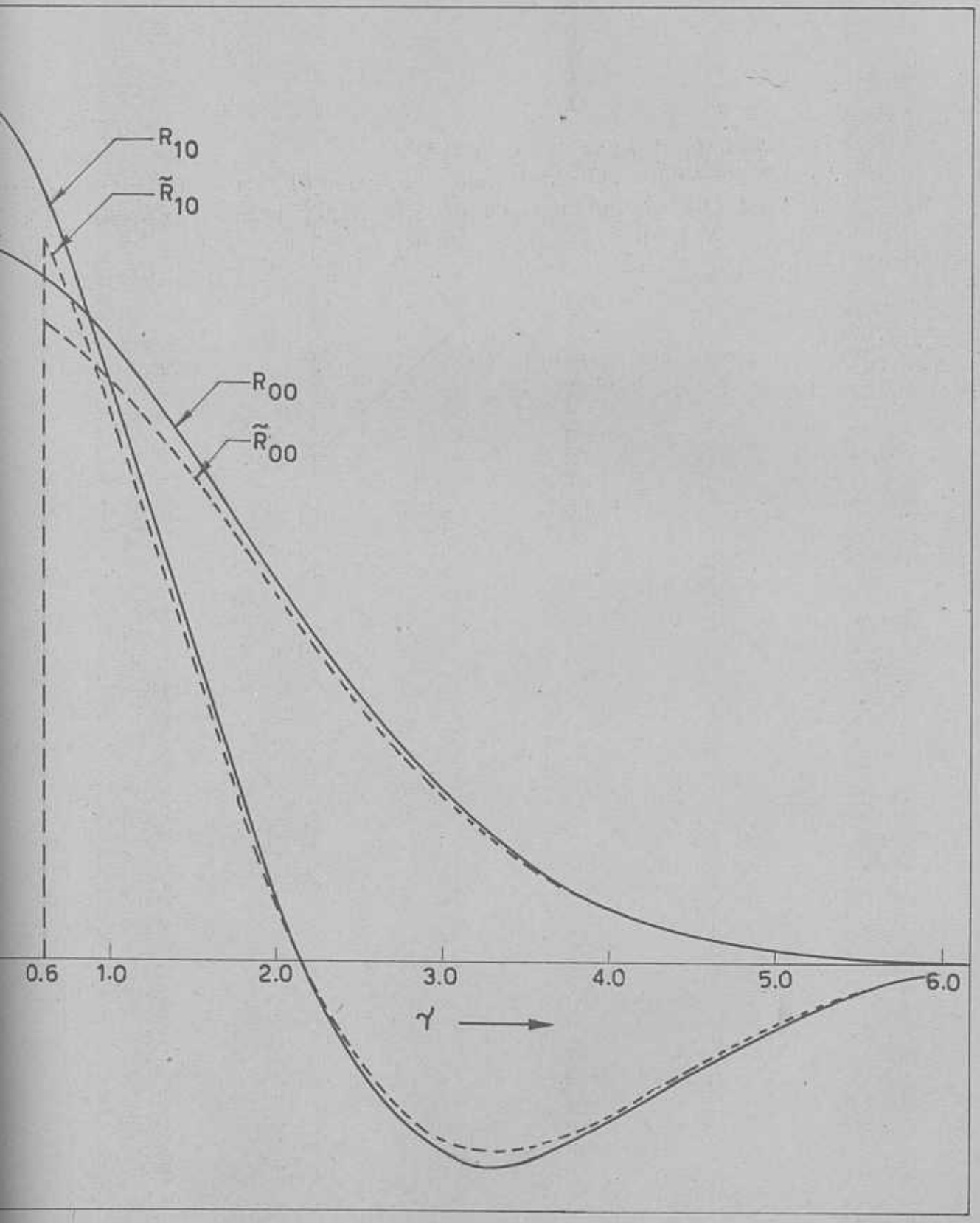

g.1. Correlated and uncorrelated harmonic oscillator radial wave nctions with b=1.76 fm are shown here. The dotted curve is obtained ing the correlation function of Dabrowski[6] with β =2.0 and C=0.6 fm.

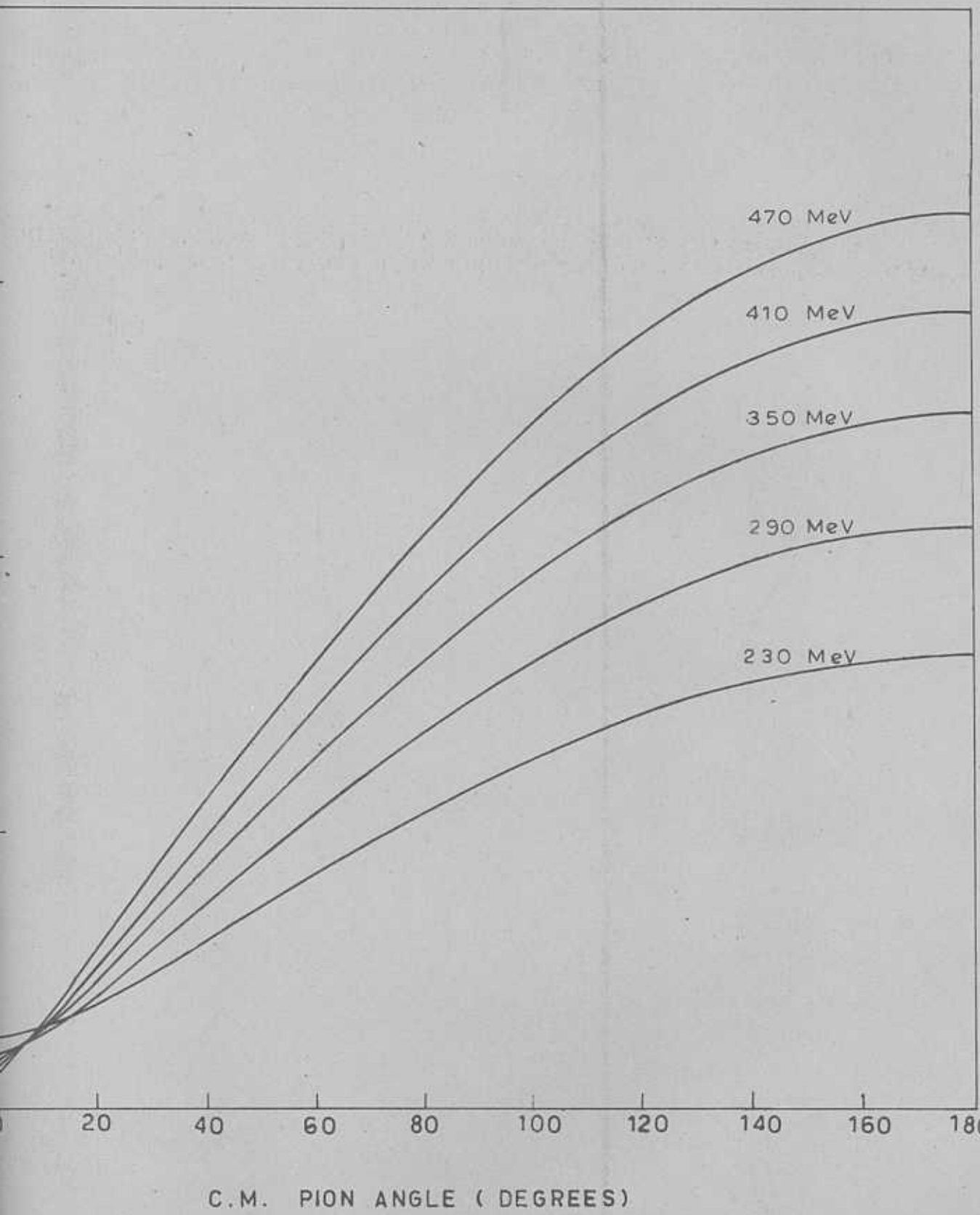

Fig.2. The momentum transfer (fm^{-1}) is plotted here as a function of the c.m. of pion angle for various incident photon energies.

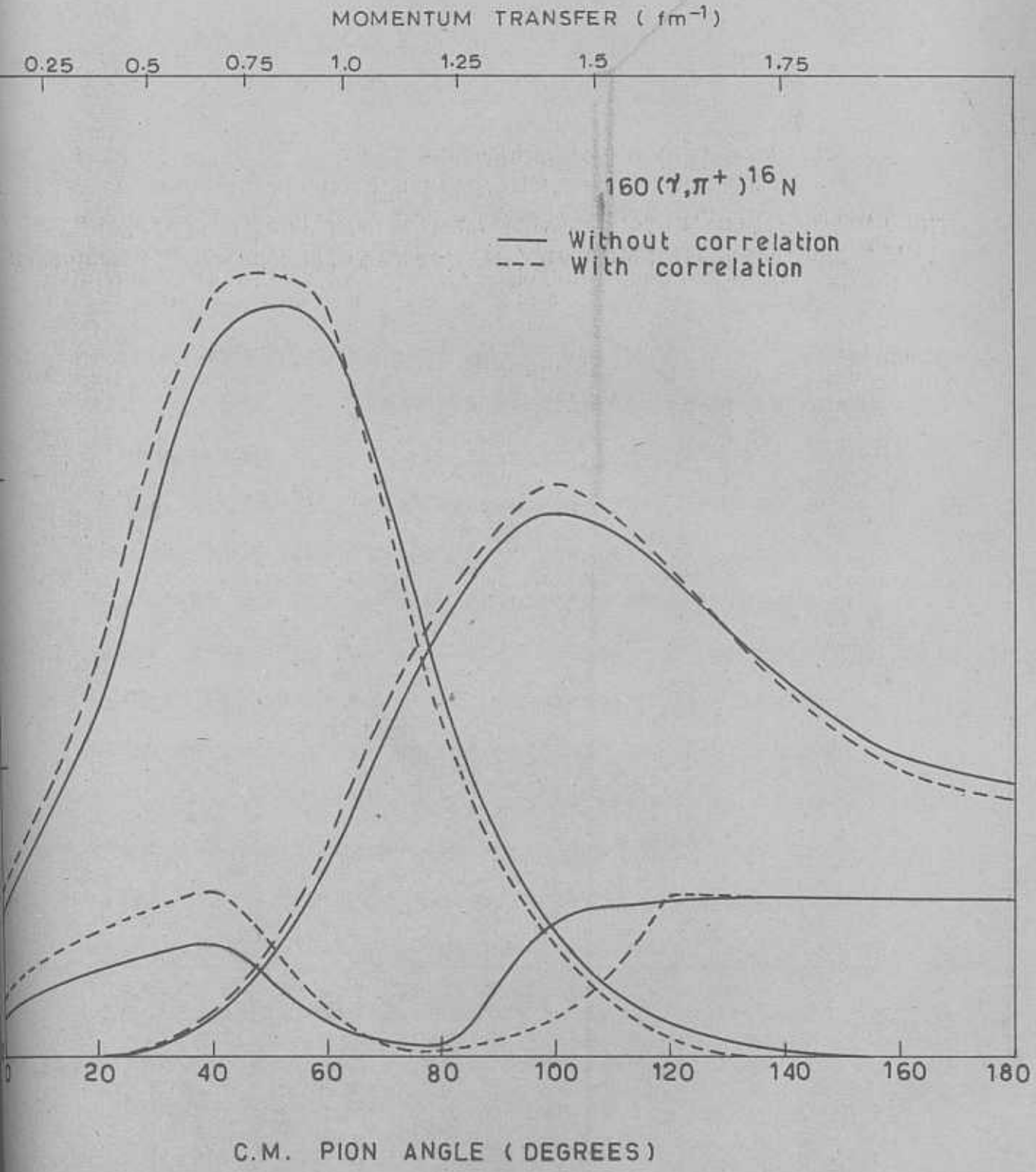

g.3. The differential cross sections for $^{16}O(\gamma,\pi^+)^{16}N$ with and ithout short-range correlations for an incident photon energy of 260 Mev. 1.76 fm. Correlation function parameters $\beta=2.0$ and $c=0.6$ fm.

CHAPTER 6

PHOTOPRODUCTION OF POSITIVE PIONS FROM ^{16}O: (iv) ANALOGS OF GIANT RESONANCES(+)

1. So far, in Chapters 3,4 and 5, we were concerned with some aspects of the process of photoproduction of π^+ from $^{16}O(0^+, g.s.)$ leading to the four low-lying bound states, with $J^P = 0^-, 1^-, 2^-, 3^-$, of ^{16}N. Here we present a study of the cross sections to the higher excited states of ^{16}N which decay by nucleon emission, in order to make a rough estimate of their relative strength.

Originally, giant resonances have been seen in photonuclear reactions[1] and these were explained by Goldhaber and Teller[2] as collective $\Delta T = 1$ dipole vibrations of protons vs. neutrons. These are now referred to as isospin (1) resonances and additional collective modes, referred to as spin-isospin (si) and spin(s) resonances, have since been introduced[3]. The isospin giant quadrupole resonance was first mentioned by Dreschel[4] and by Ligensa et.al.[5] and there is some experimental evidence for their existence.[6] The spin-isospin resonances (S=1) give rise to

(+) K.Srinivasa Rao, to be published.

1) D.H.Wilkinson, Ann.Rev. of Nucl.Sci.9, 1 (1959). References to original papers can be found in this review article.
2) M.Goldhaber and E.Teller, Phys.Rev.74, 1046 (1948).
3) W.Wild, Bayr.Akad.Wiss.Math.-Nat.Kl.18, 371 (1956); see also H.Uberall, Phys.Rev.137, B502 (1965).
4) D.Dreschel, Nucl.Phys.78, 465 (1966).
5) R.Ligensa, W.Reiner and M.Danos, Phys.Rev.Letts.16,364(1966).
6) R.J.J.Stewart, R.C.Morrison and D.E.Frederick, Phys.Rev.Lett. 23, 323 (1969).

states with $J^p = 0^-, 1^-, 2^-$ in the dipole ($L=1^-$) case and to states with $J^p = 1^+, 2^+, 3^+$ in the quadrupole ($L=2^+$) case. In T=0 nuclei (e.g. ^{16}O and ^{12}C) these giant multipole resonances form a T=1 super multiplet whose $T_z = \pm 1$ components exist in neighbouring nuclei. These, $T_z = \pm 1$, analogs of the giant resonances are excited in reactions containing $\tau^{\mp}$, such as:

Muon Capture, e.g. $\mu^- + {}^{16}O \longrightarrow {}^{16}N_{g.res.} + \nu_\mu$, (6.1.1)

Radiative Pion Capture, e.g.: $\pi^- + {}^{16}O \longrightarrow {}^{16}N_{g.res.} + \gamma$, (6.1.2)

Pion photoproduction, e.g.: $\gamma + {}^{16}O \longrightarrow {}^{16}N_{g.res.} + \pi^+$. (6.1.3)

Kelly, McDonald and Überall[7] argue that, since the momentum transfer in pion photoproduction can be varied by varying the angle at which the pion is observed, unlike in capture reactions in which the momentum transfer is fixed, photopion production is perhaps a superior tool for the study of analog giant resonances compared to muon or radiative pion capture. They show that, in the case of the reaction (6.1.3), spin-isospin dipole resonances can be produced predominantly at forward pion angles, whereas the quadrupole resonances appear strongly at large angles, thereby making it possible to experimentally identify these two types of si resonances.

---

7) F.J.Kelly, L.J.McDonald and H.Überall, Nucl.Phys.A139, 329 (1969).

They have made use of (i) a generalized Goldhaber-Teller model which is a collective model; (ii) only the dominant part of the CGLN transition amplitude[8]; and (iii) the surface production mechanism to simulate the effects of final-state interactions. In this Chapter, we make a study of the energy dependence of the total cross sections due to transitions to the above mentioned giant multipole resonance states by making use of (i) the Independent-Particle shell model, (ii) the complete CGLN transition amplitudes which include a certain amount of isospin strength and (iii) the two-particle-two-hole (2p-2h) correlations in the ground state of ^{16}O which we found, in Chapter.4, brought theory into better agreement with experiment so far as transitions to the low-lying bound states of ^{16}N were concerned.

2. Goldhaber and Teller have noted that the electric dipole coupling of a nucleus with radiation is almost entirely accounted for by a collective oscillation of the nucleus, the so-called "giant dipole resonance". They presented an intuitive and simple picture of this resonance in terms of protons and neutrons surging in the opposite directions back and forth through the nucleus. While this hydrodyhamical model has been further developed by several authors[9], Wilkinson[10] has attempted to account for the

8) G.F.Chew, M.L.Goldberger, F.E.Low and Y.Nambu, Phys.Rev. 106, 1345 (1957).
9) H.Steinwedel and J.H.D.Jensen, Z.Naturforsch 5a, 413 (1950); J.Fujita, Prog.Theor.Phys.16, 112 (1956); S.Gallone and U.L.Businaro, Nuo.Cim. 1, 1285 (1955).
10) D.H.Wilkinson, Physica 22, 1039 (1956); Ann.Rev.of Nucl.Sci. 9, 1 (1959).

photonuclear effect entirely on the basis of single particle excitations. Brink[11] has pointed out that the collective and Independent Particle Models (IPM) are actually not so far apart and that the wave function for the state of the nucleus which is excited by the dipole radiation is the same in both models. It consists of a coherent sum of many single-particle excitations thereby acquiring collective properties.

A great number of nuclear levels actually contribute to the photon-absorption but they all cluster around the first excited state of the idealized giant resonance state. Hence, we sum over all states of a given J^p in our independent-particle mode (IPM) study. Even though some of these higher excited states are the collective states with a large admixture of configurations, we have used the simple IPM for calculation in order to make a rough estimate of their relative importance. In table.1 we give the IPM configurations which we expect would have contributed to an individual giant resonance state. The calculational details are the same as those given in Chapter.3. We take the ground state wave function of ^{16}O to contain two-particle-two-hole components in addition to the op-oh component, as discussed in Chapter.4. Explicitly, the ground state wave function of ^{16}O can be approximated by:

---

11) D.M.Brink, Nucl.Phys.4, 215 (1957).

Table.1

IPM configurations which would have contributed to individual giant resonance (g.res.) states.

^{16}N g.res. state J^p	IPM configurations
0^-	$(1p_{3/2})^{-1}(1d_{3/2})$
1^-	$(1p_{1/2})^{-1}(1d_{3/2}),(1p_{3/2})^{-1}(1d_{5/2}),(1p_{3/2})^{-1}(2s_{1/2}),$ $(1p_{3/2})^{-1}(1d_{3/2}).$
2^-	$(1p_{1/2})^{-1}(1d_{3/2}),(1p_{3/2})^{-1}(1d_{5/2}),(1p_{3/2})^{-1}(2s_{1/2}),$ $(1p_{3/2})^{-1}(1d_{3/2}).$
1^+	$(1s_{1/2})^{-1}(2s_{1/2}),(1s_{1/2})^{-1}(1d_{3/2}),(1p_{1/2})^{-1}(2p_{3/2}),$ $(1p_{1/2})^{-1}(2p_{1/2}),(1p_{3/2})^{-1}(1f_{5/2}),(1p_{3/2})^{-1}(2p_{3/2}),$ $(1p_{3/2})^{-1}(2p_{1/2}).$
2^+	$(1s_{1/2})^{-1}(1d_{5/2}),(1s_{1/2})^{-1}(1d_{3/2}),(1p_{1/2})^{-1}(1f_{7/2}),$ $(1p_{1/2})^{-1}(2p_{3/2}),(1p_{3/2})^{-1}(1f_{7/2}),(1p_{3/2})^{-1}(1f_{5/2}),$ $(1p_{3/2})^{-1}(2p_{3/2}),(1p_{3/2})^{-1}(2p_{1/2}).$
3^+	$(1s_{1/2})^{-1}(1d_{5/2}),(1p_{1/2})^{-1}(1f_{7/2}),(1p_{1/2})^{-1}(1f_{5/2}),$ $(1p_{3/2})^{-1}(1f_{7/2}),(1p_{3/2})^{-1}(1f_{5/2}),(1p_{3/2})^{-1}(2p_{3/2}).$

$$|0^+, g.s.\rangle = \alpha\,|0p-0h\rangle + \beta\,|(1d^2_{5/2})_{J=0,T=1}(1p^{-2}_{1/2})_{0,1}\rangle + \\ + \gamma\,|(2s^2_{1/2})_{0,1}(1p^{-2}_{1/2})_{0,1}\rangle, \qquad (6.2.1)$$

where the values of α, β and γ have been experimentally determined by Purser et.al.[12] from an analysis of the reactions $^{16}O(d,t)^{15}O$ and $^{16}O(d,{}^3He)^{15}N$. These values have been given in Table.1 of Chapter.4. Since, the final IPM nuclear states of ^{16}N, for the individual giant multipole states considered in the present Chapter, do not contain $(1p_{1/2})^{-1}(1d_{5/2})$ or $(1p_{1/2})^{-1}(2s_{1/2})$ configurations - which give rise to the low-lying quartet states of ^{16}N viz. 2^-,3^-, 0^- and 1^- - we find that the partial cross sections (in the IPM) for these states are given by:

$$\sigma(J_f^P) = \alpha^2\,\sigma^{PS}(J_f) \qquad (6.2.2)$$

where we have denoted the partial cross section for $0^+ \longrightarrow J_f^P$ in the absence of 2p-2h correlations in the ground state of ^{16}O by $\sigma^{PS}(J_f^\pi)$. $\alpha=1$ corresponds to the assumption of a Pure Shell model (PS) ground state of ^{16}O. The two values of α found by Purser et.al.[12] are 0.87 and 0.82 from their study of the $^{16}O(d,t)^{15}O$ and $^{16}O(d,{}^3He)^{15}N$, respectively. Therefore, it is clear that the cross sections to individual giant multipole resonances will be reduced by a factor of α^2 (0.7569 for $\alpha=0.87$ or 0.6724 for $\alpha=0.82$) due to the

12) K.H.Purser, W.P.Alford, D.Cline, H.W.Fulbright, H.E.Gove and K.S.Krick, Nucl.Phys.A132, 75 (1969).

inclusion of 2p-2h correlations in the ground state wave function of ^{16}O.

3. In table.2 are given the cross sections for the reaction $^{16}O(\gamma,\pi^+)^{16}N$ when the final state is any of the excited states, whose wave functions are described in the simple IPM(see table.1), for an incident photon energy of 260 Mev. These states of ^{16}N can decay by nucleon emission and hence these would not have contributed to the experimental cross sections of Meyer, Walters and Hummel[13]. We notice that these cross sections are very much larger than those obtained in Chapter.3 for the low-lying bound states of ^{16}N.

In table.3 we give the cross sections to individual giant multipole states of ^{16}N, summed over all states of a given J^π, for various incident photon energies, from 180 to 420 Mev.

Fig.1 shows the pion angular distribution for excitation of the individual giant multipole states at an incident photon energy of 200 Mev. We notice that for $\theta > 60^\circ$, the 1^+, 2^+ and 3^+ quadrupole state cross sections exceed the 1^- and 2^- dipole cross sections, so that varying θ allows one to differentiate between the giant multipole resonances. This conclusion has already

13) R.A.Meyer, W.B.Walters and J.P.Hummel, Phys.Rev.138, B1421 (1965).

Table.2

Cross sections for the reaction $^{16}O(\gamma,\pi^+)^{16}N$ when the final state is one of the excited states which decay by nucleon emission. The incident photon energy is 260 Mev.

^{16}N state J^p	Configuration of ^{16}N state in IPM	Cross section in μb.		
		$\alpha=1.0$	$\alpha=0.87$	$\alpha=0.82$
0^-	$(1p_{3/2})^{-1}(1d_{3/2})$	3.531	2.673	2.374
1^-	$(1p_{1/2})^{-1}(1d_{3/2})$	8.508	6.440	5.721
	$(1p_{3/2})^{-1}(1d_{5/2})$	15.315	11.592	10.298
	$(1p_{3/2})^{-1}(2s_{1/2})$	3.192	2.416	2.146
	$(1p_{3/2})^{-1}(1d_{3/2})$	11.007	8.331	7.401
2^-	$(1p_{1/2})^{-1}(1d_{3/2})$	7.755	5.870	5.214
	$(1p_{3/2})^{-1}(1d_{5/2})$	10.560	7.993	7.101
	$(1p_{3/2})^{-1}(2s_{1/2})$	5.753	4.354	3.868
	$(1p_{3/2})^{-1}(1d_{3/2})$	4.609	3.489	3.099
1^+	$(1s_{1/2})^{-1}(2s_{1/2})$	15.477	11.715	10.407
	$(1s_{1/2})^{-1}(1d_{3/2})$	4.891	3.702	3.289
	$(1p_{1/2})^{-1}(2p_{3/2})$	5.472	4.142	3.679
	$(1p_{1/2})^{-1}(2p_{1/2})$	2.020	1.529	1.358
	$(1p_{3/2})^{-1}(1f_{5/2})$	7.922	5.996	5.327
	$(1p_{3/2})^{-1}(2p_{3/2})$	6.515	4.931	4.381
	$(1p_{3/2})^{-1}(2p_{1/2})$	5.472	4.142	3.679

(continued on next page)

Table.2(continued)

^{16}N state J^p	Configuration of ^{16}N state in IPM	Cross section in μb.		
		α=1.0	α=0.87	α=0.82
2^+	$(1s_{1/2})^{-1}(1d_{5/2})$	10.578	8.006	7.113
	$(1s_{1/2})^{-1}(1d_{3/2})$	11.213	8.487	7.540
	$(1p_{1/2})^{-1}(1f_{7/2})$	9.415	7.126	6.331
	$(1p_{1/2})^{-1}(2p_{3/2})$	4.379	3.314	2.944
	$(1p_{3/2})^{-1}(1f_{7/2})$	16.139	12.216	10.852
	$(1p_{3/2})^{-1}(1f_{5/2})$	8.759	6.630	5.890
	$(1p_{3/2})^{-1}(2p_{3/2})$	5.038	3.813	3.388
	$(1p_{3/2})^{-1}(2p_{1/2})$	4.379	3.314	2.944
3^+	$(1s_{1/2})^{-1}(1d_{5/2})$	13.579	10.278	9.131
	$(1p_{1/2})^{-1}(1f_{7/2})$	12.176	9.216	8.187
	$(1p_{1/2})^{-1}(1f_{5/2})$	5.132	3.884	3.451
	$(1p_{3/2})^{-1}(1f_{7/2})$	8.080	6.116	5.433
	$(1p_{3/2})^{-1}(1f_{5/2})$	3.131	2.370	2.105
	$(1p_{3/2})^{-1}(2p_{3/2})$	6.456	4.887	4.341

Table.3.

Cross sections for the reaction $^{16}O(\gamma,\pi^+)^{16}N$ when the final nuclear state is one of the giant resonance states which decays by nucleon emission. The nuclear wavefunctions used correspond to the IPM and $b=1.76$ fm.

Incident photon energy (Mev)	Model for g.s. of ^{16}O (α)	Cross section in μb. due to transition to a giant resonance state					
		0^-	1^-	2^-	1^+	2^+	3^+
165	1	0.075	52.754	30.962	36.364	31.718	25.153
	0.87	0.057	39.930	23.435	27.524	24.008	19.038
	0.82	0.050	35.472	20.819	24.451	21.327	16.913
180	1	0.705	58.623	32.872	52.406	48.152	37.852
	0.87	0.534	44.372	24.881	39.664	36.447	28.650
	0.82	0.474	39.418	22.103	35.236	32.377	25.452
200	1	1.366	51.292	30.367	56.436	54.385	43.948
	0.87	1.034	38.823	22.985	42.716	41.694	33.264
	0.82	0.919	34.489	20.419	37.948	37.039	29.551
230	1	2.426	41.458	28.332	52.626	61.318	47.201
	0.87	1.837	31.379	21.445	39.832	46.411	35.727
	0.82	1.632	27.876	19.050	35.385	41.230	31.738
260	1	3.531	38.022	28.676	47.770	69.900	48.553
	0.87	2.672	28.780	21.706	36.165	52.908	36.750
	0.82	2.374	25.566	19.282	32.121	47.001	32.647

(continued on next page)

Table.3.(continued)

Incident photon energy (Mev)	Model for g.s. of ^{16}O (α)	Cross section in μb. due to transition to a giant resonance state					
		0^-	1^-	2^-	1^+	2^+	3^+
290	1	4.607	40.288	29.580	44.762	80.745	48.238
	0.87	3.487	30.494	22.390	33.880	61.116	36.512
	0.82	3.098	27.090	19.890	30.098	54.293	32.435
320	1	4.717	41.752	27.954	39.927	81.107	42.188
	0.87	3.571	31.604	21.158	30.220	61.390	31.932
	0.82	3.172	28.076	18.796	26.847	54.537	28.368
350	1	3.494	34.619	22.653	31.660	63.071	32.059
	0.87	2.644	26.118	17.147	23.963	47.739	24.266
	0.82	2.349	23.278	15.232	21.288	42.409	21.557
380	1	2.058	25.732	16.961	23.559	42.668	22.849
	0.87	1.557	19.477	12.866	17.832	32.295	17.295
	0.82	1.383	17.303	11.429	15.841	28.690	15.364
420	1	1.250	17.812	12.824	17.868	28.353	17.393
	0.87	0.946	13.482	9.706	13.525	21.461	13.165
	0.82	0.840	11.977	8.622	12.015	19.065	11.695

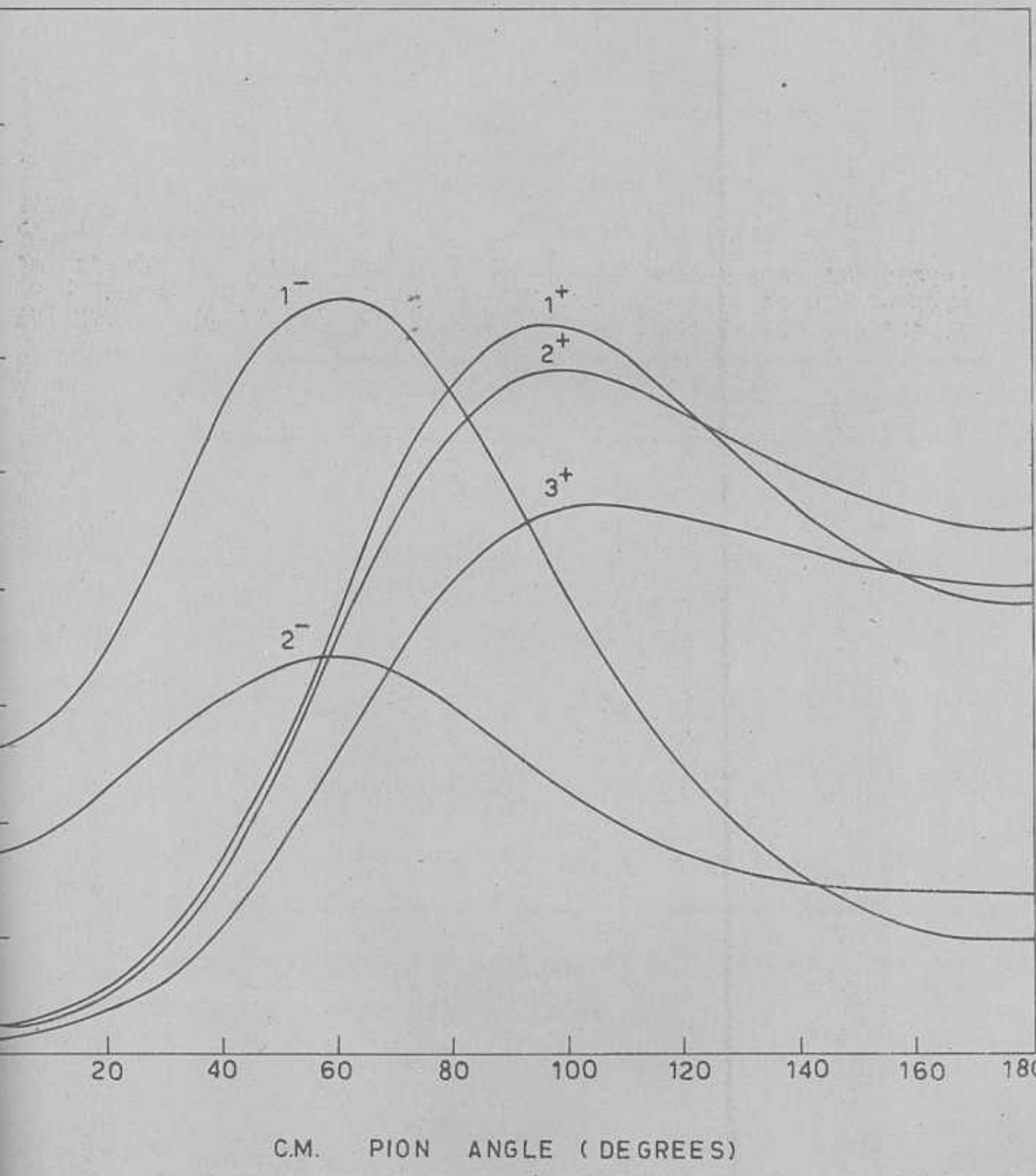

Fig.1. Photopion angular distribution from ^{16}O for 200 Mev photon energy, with excitation of giant resonance states.

Table.4.

Total cross section (in μb) leading to individual giant resonance states for an incident photon energy of 200 Mev.

^{16}N g.res. State	IPM calculation			Kelly et.al's[7] calculation+	
J^p	α=1.0	α=0.87	α=0.82	a_1=0	a_1=2.625 fm.
0^-	1.4	1.06	0.94	2.8	1.1
1^-	51.3	38.82	34.49	31.6	12.6
2^-	30.4	23.00	20.44	49.0	19.7
1^+	56.4	42.68	37.92	13.0	7.9
2^+	54.4	41.17	36.57	48.5	28.8
3^+	43.9	33.22	29.51	64.2	38.1

+The cut-off parameter a_1=0 for volume production and a_1=2.625fm. for surface production of pions.

been drawn by Kelly et.al.[7] on the basis of a generalized Goldhaber-Teller model. In table.4, we compare our results with those of Kelly et.al.[7] for an incident photon energy of 200 Mev. It is interesting to note the large differences which exist between the two different model dependent calculations. We are unable to draw any conclusions due to the absence of experimental data but we notice that the 2p-2h ground state correlations reduce the cross sections only by about 30% while the phenomenological surface production mechanism reduces the cross sections by almost a factor of 2, as is to be expected from our earlier analysis presented in Chapters 3 and 4.

In Fig.2 we have plotted the energy dependence of the cross sections due to excitation of the multipole states. It is interesting to note that the 2^+ state has a large peak at 320 Mev. It stands out from all the other states, so that varying the incident photon energy allows us to differentiate it from the other multipole resonances.

In conclusion we wish to point out that since the cross sections due to excitations of the giant dipole and quadrupole states of ^{16}N in photoproduction of π^+ from ^{16}O are very much larger than those due to excitations to low-lying bound states of ^{16}N, it will be of value to measure these experimentally.

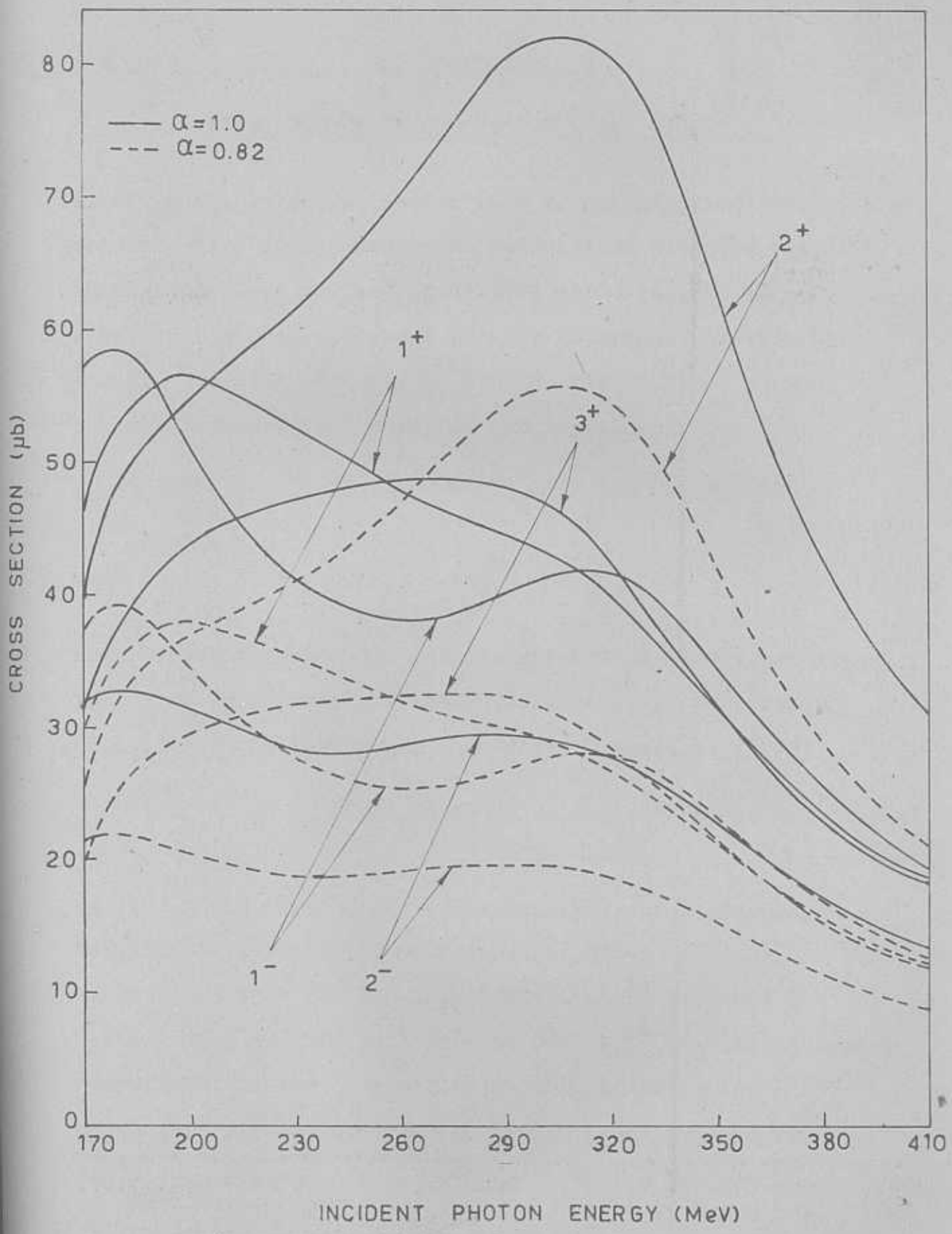

Fig.2. Energy dependence of the total cross section for photopion production from ^{16}O due to excitation of the giant multipole resonance states.

CHAPTER 7

PHOTOPRODUCTION OF CHARGED PIONS FROM ^{12}C(+)

1. In Chapter.3, we showed that by using particle-hole configuration mixing models in conjunction with the purely phenomenological surface production mechanism, we can obtain a reasonably good agreement between theory and experiment for the reaction $^{16}O(\gamma,\pi^+)^{16}N$. In this Chapter, we make a similar theoretical study of the reactions:

$$\gamma + {}^{12}C(J^P=0^+, T=0) \longrightarrow \pi^+ + {}^{12}B(J^P=1^+, 2^+, 2^-, 1^-, 3^-, T=1), \quad (7.1.1)$$

and

$$\gamma + {}^{12}C(J^P=0^+, T=0) \longrightarrow \pi^- + {}^{12}N(J^P=1^+, T=1), \quad (7.1.2)$$

even though experimental results are not available, as yet, for these reactions. Of these two reactions, the former, (7.1.1), is similar to the muon capture process:

$$\mu^- + {}^{12}C(0^+,\ T=0) \longrightarrow \nu_\mu + {}^{12}B(\text{bound } T=1 \text{ states}), \quad (7.1.3)$$

as far as the initial and final nuclear states are concerned. But, in the case of the muon capture process (7.1.3), it has become customary for the experimentalists[1] to quote the partial muon capture rate for the $0^+ \longrightarrow 1^+$ transition from a measurement of the β-activity in ^{12}B, after making a 10% correction for capture leading to the bound excited states.

(+) K.Srinivasa Rao, V.Devanathan and G.N.S.Prasad, submitted to Nucl.Phys.

1) E.J.Maier, R.M.Edelstein and R.T.Siegel, Phys.Rev.133, B663 (1964).

Here, our intention is to study the "partial" photoproduction cross sections from $^{12}C(0^+, g.s.)$ leading to the four bound states $J^P = 1^+, 2^+, 2^-, 1^-, 3^-$ in ^{12}B, as well as π^- photoproduction cross section from $^{12}C(0^+, g.s.)$ leading to the ground state ($J^P = 1^+$) of ^{12}N.

From the experimental point of view, reaction (7.1.1) should turn out to be interesting since ^{12}B is almost uniquely suited for detection by means of the energetic (13.5 Mev end point) β -rays emitted in the radio-active decay back to ^{12}C. The short mean life (29.3 m sec.) for this decay will minimize the time during which a search is to be made for delayed activities and thus minimize the random background. The reaction (7.1.2), on the other hand, should turn out to be interesting since only the ground state of ^{12}N is stable against nucleon emission. Further, as pointed out by March and Walker[2], the (γ,π^-) reaction can be studied much more readily than the (γ,π^+) reaction because the residual nucleus - ^{12}N in the case of reaction (7.1.2) - is a positron emitter and advantage can be taken of the annihilation quanta to use coincidence counting and so eliminate much of the background counting rate. Therefore, we hope that experimental results for reactions (7.1.1) and (7.1.2) will soon be forthcoming.

2. We assume the ground state of ^{12}C to be spherical. In the absence of residual interaction, the two even-parity states of $^{12}B(J^P = 1^+, 2^+, T=1)$ may be assigned to the

---

2) P.V.March and T.G.Walker, Proc.Phys.Soc. 77, 293 (1960).

configuration where there is a proton-hole in $1p_{3/2}$-shell and a neutron particle in the $1p_{1/2}$-shell, while the two odd-parity states of $^{12}B(J^P = 2^-,1^-, T=1)$ may be assigned to the particle-hole configuration $(1p_{3/2})^{-1}(2s_{1/2})$ and the $^{12}B(J^P=3^-)$ state to the configuration $(1p_{3/2})^{-1}(1d_{5/2})$. Similarly the ground state of ^{12}N $(J^P = 1^+,T=1)$ may be assigned to the configuration where there is a neutron-hole in the $1p_{3/2}$-shell and a proton-particle in the $1p_{1/2}$-shell. This scheme is called the Independent Particle Model (IPM) here. In Chapter.3, we have discussed, in detail, the particle-hole configuration mixing calculation of Gillet and Vinh-Mau[3] for ^{16}O. A similar calculation has been performed by them for ^{12}C also, in the Tamm-Dancoff Approximation (TDA) as well as in the Random Phase Approximation (RPA). But since we found in Chapter.3, that the TDA and RPA results do not differ very much from each other in the case of $^{16}O(\gamma,\pi^+)^{16}N$, we use only the wave functions of Gillet and Vinh Mau obtained in the TDA in the present study. We denote this set of wave functions by GV here. As pointed out by Gillet and Vinh Mau, it is difficult at present to give any justification for describing ^{12}C in j-j-coupling scheme other than its simplicity, the similarity of the results with those obtained in a deformed scheme[4], and a posteriori a reasonable agreement

3) V.Gillet and N.Vinh Mau, Nucl.Phys. 54, 321 (1964).
4) S.G.Nilsson, J.Sawicki and N.K.Glendenning, Nucl.Phys. 33, 239 (1962).

with experiment, if any. The wave function amplitudes ($X^{J_f}_{p,h}$ which occur in Eq.(3.2.1) of Chapter.3) for the low-lying states of ^{12}B are given in Table.1. Note that the 1^+ wave function amplitudes given here are applicable to the ground state of ^{12}N also.

For the radial wave functions, we take the harmonic oscillator wave functions with the oscillator strength parameter

$$b = 1.64 \text{ fm}, \qquad (7.2.1)$$

which is in conformity with elastic and most of the inelastic electron scattering data[5]. Since the RPA wave functions of Gillet and Vinh Mau gave correct results[6] for the reaction $^{16}O(\gamma,\pi^+)^{16}N$ when the surface production cut-off parameter r_0 (defined in section.5 of Chapter.3) was chosen to correspond to the root-mean-square (r.m.s) radius of ^{16}O, consistent with the charge distribution measurements, we choose for ^{12}C the r.m.s. radius

$$\langle r^2 \rangle^{1/2} = 2.36 \text{ fm} \qquad (7.2.2)$$

as the value for r_0, consistent with electron scattering data[5].

3. Recently[7], four of the five low-lying bound states of ^{12}B which are stable against nucleon emission have been identified to be the T=1 isobaric multiplets of A=12 nuclei. This identification enables us to take the wave functions for these

---

5)H.Crannel, Phys.Rev.148, 1107 (1966).
6)V.Devanathan, M.Rho, K.Srinivasa Rao and S.C.K.Nair, Nucl. Phys.B2, 329 (1967).
7)F.Ajzenberg-Selove and T.Lauritsen, Nucl.Phys.114, 1 (1968).

Table.1

The wave function amplitudes for the low-lying bound states of ^{12}B in the IPM and GV models are given here. The amplitudes for the 1^+ state of ^{12}N are the same as those for the 1^+ state of ^{12}B.

State J^P	Nuclear Model	$1p^{-1}_{3/2}$ $1p_{1/2}$	$1p^{-1}_{3/2}$ $1f_{7/2}$	$1p^{-1}_{3/2}$ $1f_{5/2}$	$1p^{-1}_{3/2}$ $2p_{3/2}$	$1p^{-1}_{3/2}$ $2p_{1/2}$	$1s^{-1}_{1/2}$ $1d_{5/2}$	$1s^{-1}_{1/2}$ $2s_{1/2}$	$1s^{-1}_{1/2}$ $1d_{3/2}$
1^+	IPM	1.00	--	--	--	--	--	--	--
	GV	1.00	--	0.02	-0.06	-0.06	--	0.01	-0.02
2^+	IPM	1.00	--	--	--	--	--	--	--
	GV	0.99	-0.03	0.06	0.01	-0.04	0.01	--	-0.07

State J^P	Nuclear Model	$1p^{-1}_{3/2}$ $1d_{5/2}$	$1p^{-1}_{3/2}$ $2s_{1/2}$	$1p^{-1}_{3/2}$ $1d_{3/2}$	$1s^{-1}_{1/2}$ $1p_{1/2}$
2^-	IPM	--	1.000	--	--
	GV	-0.460	0.888	-0.021	--
1^-	IPM	--	1.000	--	--
	GV	-0.105	0.991	0.081	-0.008
3^-	IPM	1.00	--	--	--
	GV	1.00	--	--	--

four low-lying bound states of $^{12}B(J^P = 1^+, 2^+, 2^-, 1^-, T=1)$ from the wave functions for the analogous levels in ^{12}C under the assumption of good isobaric spin. The fifth level has not, as yet, been assigned the correct spin-parity, but it is expected[7] to have $J^P \leq 3^+$. From a theoretical point of view, even parity states, other than the lowest lying 1^+ and 2^+ states, can occur only from configurations with a proton-hole in the $1p_{3/2}$-shell and a neutron-particle in the 1f-2p shell. But these states will lie above the negative parity states which arise from configurations with a proton-hole in the $1p_{3/2}$-shell and a neutron-particle in the 1d shell, since the former are $2\hbar\omega$ excitations while the latter are $1\hbar\omega$ excitations. Further, Gillet and Vinh Mau[3] obtain a 3^- state (at 18.5 Mev), which lies lower than the second 2^+ state (at 28.1 Mev) or a second 1^+ state (at 28.5 Mev) and which arises from the configuration $(1p_{3/2})^{-1}(1d_{5/2})$. Due to these considerations, we take the fifth low-lying bound state of ^{12}B to be a 3^- state, in our present calculation. The photon induced transitions $^{12}C(0^+) \longrightarrow {}^{12}B(J^P)$ and their subsequent decays are shown in Fig.1.

In table.2 are given the partial and total cross sections for the reaction $^{12}C(\gamma,\pi^+)^{12}B$ in the case of volume, as well as surface production of pions, using the nuclear models IPM and GV. In table.3 are given the cross sections for the reaction $^{12}C(\gamma,\pi^-)^{12}N$ in the case of volume and

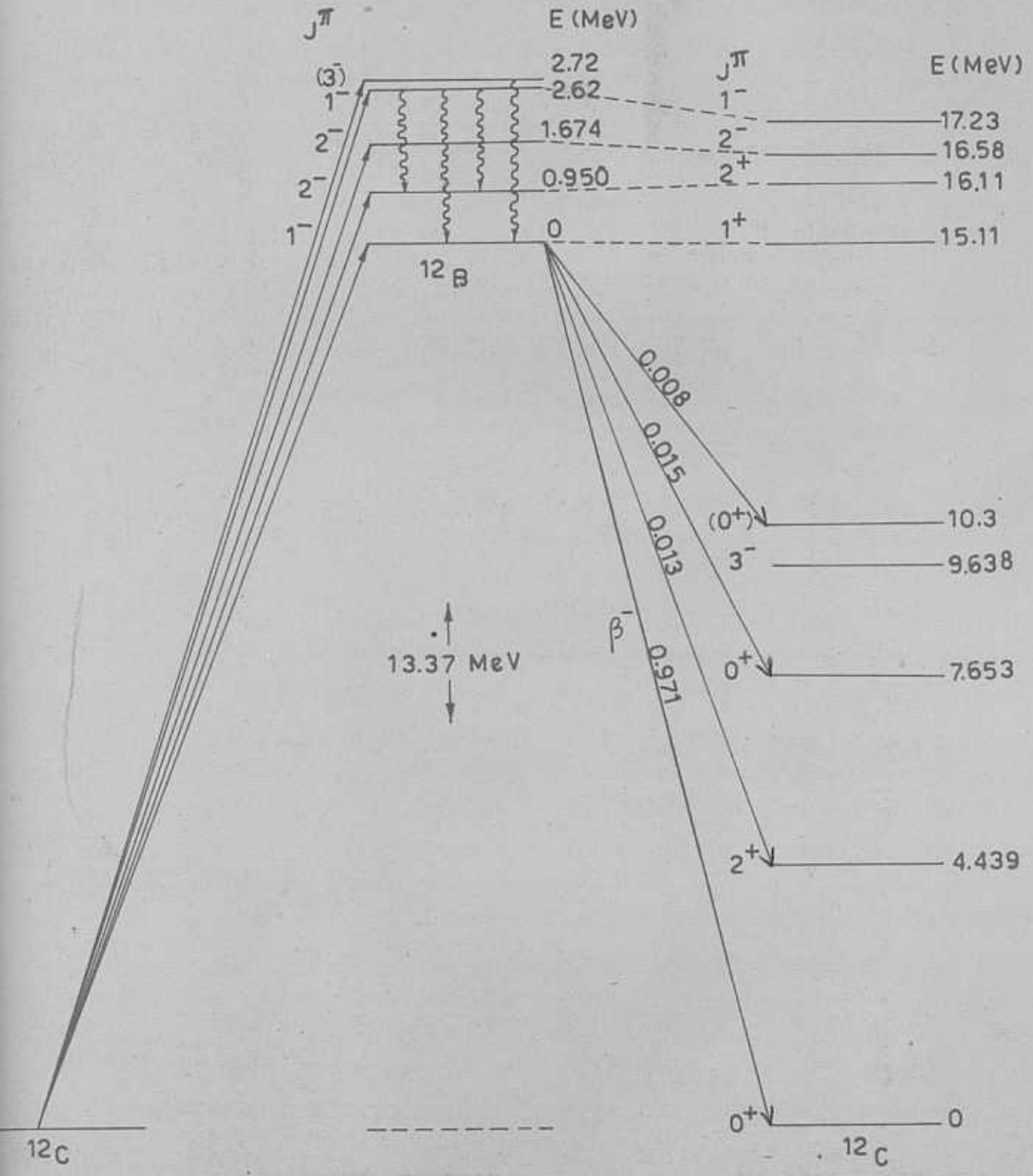

Fig.1. Level scheme for the reaction $^{12}C(\gamma,\pi^+)^{12}B$ and subsequent decays. The photon induced transitions are shown on the left while the β-decays with the branching ratios are shown on the right. Wigly arrows indicate γ de-excitations. Levels which are identified to be T=1 multiplets are connected by dashed lines.

Table.2.

Cross sections for the reaction $^{12}C(\gamma,\pi^+)^{12}B$. The value of the cut-off parameter r_o =0 corresponds to the case of volume production of pions. The nuclear models used are IPM and GV.

Incident photon energy (Mev)	Nuclear Model	r_o (fm)	Cross sections to bound states J^p of ^{12}B(μb)					
			1^+	2^+	2^-	1^-	3^-	Total
180	IPM(V)	0	37.816	11.317	4.747	1.745	0.304	55.93
	IPM(S)	2.36	5.620	4.824	8.447	3.096	0.209	22.196
	GV(V)	0	34.150	11.572	0.623	1.641	0.304	48.29
	GV(S)	2.36	6.432	4.906	1.396	2.934	0.209	15.876
200	IPM(V)	0	30.257	15.439	3.687	1.490	0.899	50.281
	IPM(S)	2.36	4.613	5.734	6.535	2.659	0.585	20.125
	GV(V)	0	27.166	15.699	1.675	1.306	0.899	45.439
	GV(S)	2.36	5.037	5.775	1.060	2.404	0.585	14.861
230	IPM(V)	0	20.089	18.975	3.954	1.811	2.051	46.938
	IPM(S)	2.36	3.567	5.662	4.536	2.273	1.213	17.251
	GV(V)	0	18.021	19.109	3.563	1.579	2.051	44.322
	GV(S)	2.36	3.929	5.592	0.714	1.885	1.213	13.333
260	IPM(V)	0	14.059	21.109	5.464	2.994	4.411	48.037
	IPM(S)	2.36	2.953	5.180	3.804	2.392	2.354	16.683
	GV(V)	0	12.674	21.020	5.138	2.773	4.411	46.017
	GV(S)	2.36	3.220	4.991	0.573	1.830	2.354	12.967

(continued on next page)

Table.2.(continued)

Incident photon energy (Mev)	Nuclear Model	r_0 (fm)	Cross sections to bound states J^P of ^{12}B(μb)					
			1^+	2^+	2^-	1^-	3^-	Total
290	IPM(V)	0	12.994	22.896	6.746	4.834	7.766	55.237
	IPM(S)	2.36	2.935	5.045	3.789	2.841	3.730	18.347
	GV(V)	0	11.881	22.558	5.847	4.627	7.766	52.680
	GV(S)	2.36	3.197	5.015	0.559	2.050	3.730	14.560
320	IPM(V)	0	16.566	21.972	6.573	6.027	9.625	60.763
	IPM(S)	2.36	3.594	4.854	4.015	3.020	4.191	19.666
	GV(V)	0	15.382	21.528	5.049	5.824	9.625	57.408
	GV(S)	2.36	3.968	4.813	0.612	2.179	4.191	15.762
350	IPM(V)	0	18.878	16.879	5.131	5.124	7.652	53.663
	IPM(S)	2.36	3.935	3.947	3.784	2.434	3.078	18.525
	GV(V)	0	17.634	16.565	3.418	4.953	7.652	50.222
	GV(S)	2.36	4.386	3.934	0.600	1.827	3.078	13.824
380	IPM(V)	0	17.466	11.793	3.878	3.535	4.758	41.429
	IPM(S)	2.36	3.584	2.916	3.177	1.697	1.816	13.189
	GV(V)	0	16.338	11.639	2.331	3.413	4.758	38.479
	GV(S)	2.36	4.008	2.928	0.513	1.346	1.816	10.611
410	IPM(V)	0	14.912	8.502	3.118	2.385	2.839	31.721
	IPM(S)	2.36	3.050	2.185	2.597	1.193	1.057	10.081
	GV(V)	0	13.954	8.441	1.803	2.301	2.839	29.338
	GV(S)	2.36	3.414	2.209	0.423	0.996	1.057	8.098

Table.2

Cross sections for the reaction $^{12}C(\gamma,\pi^-)^{12}N$. The value of the cut-off parameter, r_0, in the case of volume (V) and surface (S) production of pions is 0 and 2.36 fm., respectively. The nuclear models used are IPM and GV.

Incident photon energy (Mev)	Cross section in μb.			
	IPM(V)	IPM(S)	GV(V)	GV(S)
180	50.829	7.309	45.701	7.862
200	40.314	5.945	35.972	6.500
230	26.388	4.697	23.519	5.174
260	18.122	3.934	16.250	4.275
290	15.933	3.720	14.491	4.025
320	19.181	4.232	17.723	4.648
350	21.394	4.498	19.900	4.995
380	19.724	4.088	18.376	4.555
410	16.848	3.499	15.702	3.899

surface production mechanisms using the nuclear models IPM and GV.

The method of calculation of the cross sections is the same as that detailed in Chapter.3. In Table.2 and Table.3 the results for reactions (7.1.1) and (7.1.2) respectively are given. Let us therefore discuss our results straightaway.

In Fig.2 are given the theoretical partial cross sections calculated in the two nuclear models, IPM and GV, assuming volume production of pions for the reaction (7.1.1). Fig.3 shows the corresponding theoretical partial cross sections obtained assuming surface production of pions. From Fig.2 we find that among the partial cross sections those which arise from transitions to the 1^+ and 2^+ states are dominant. But in the case of surface production, from Fig.3, we find that all the four partial cross sections become smaller and comparable in magnitude, unlike the muon capture process where the $0^+ \longrightarrow 1^+$ capture rate is 90% of the total capture rate.

Fig.4 shows the total cross section, for $^{12}C(\gamma,\pi^+)^{12}B$, obtained as a sum of the partial cross sections, using the IPM and GV models assuming volume and surface production of pions. We find that though the partial cross sections are energy dependent, as shown in Figs.2 and 3, the total cross section, especially that obtained assuming surface production of pions, reveals a smooth variation of the cross section

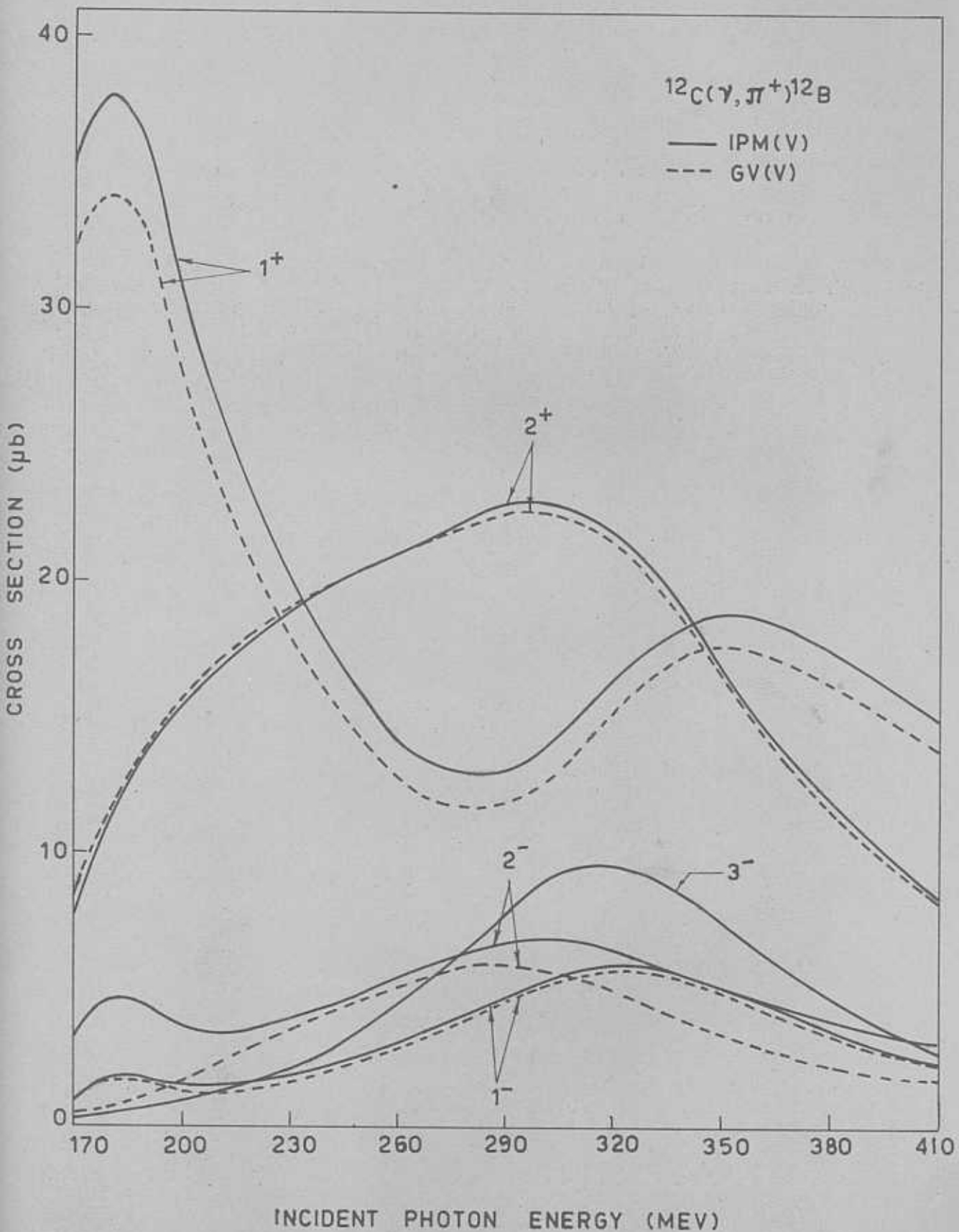

g.2. Cross section for the reaction $^{12}C(\gamma,\pi^+)^{12}N$ for the final clear states $1^+, 2^+, 2^-, 1^-$ and 3^- assuming volume production of pions.

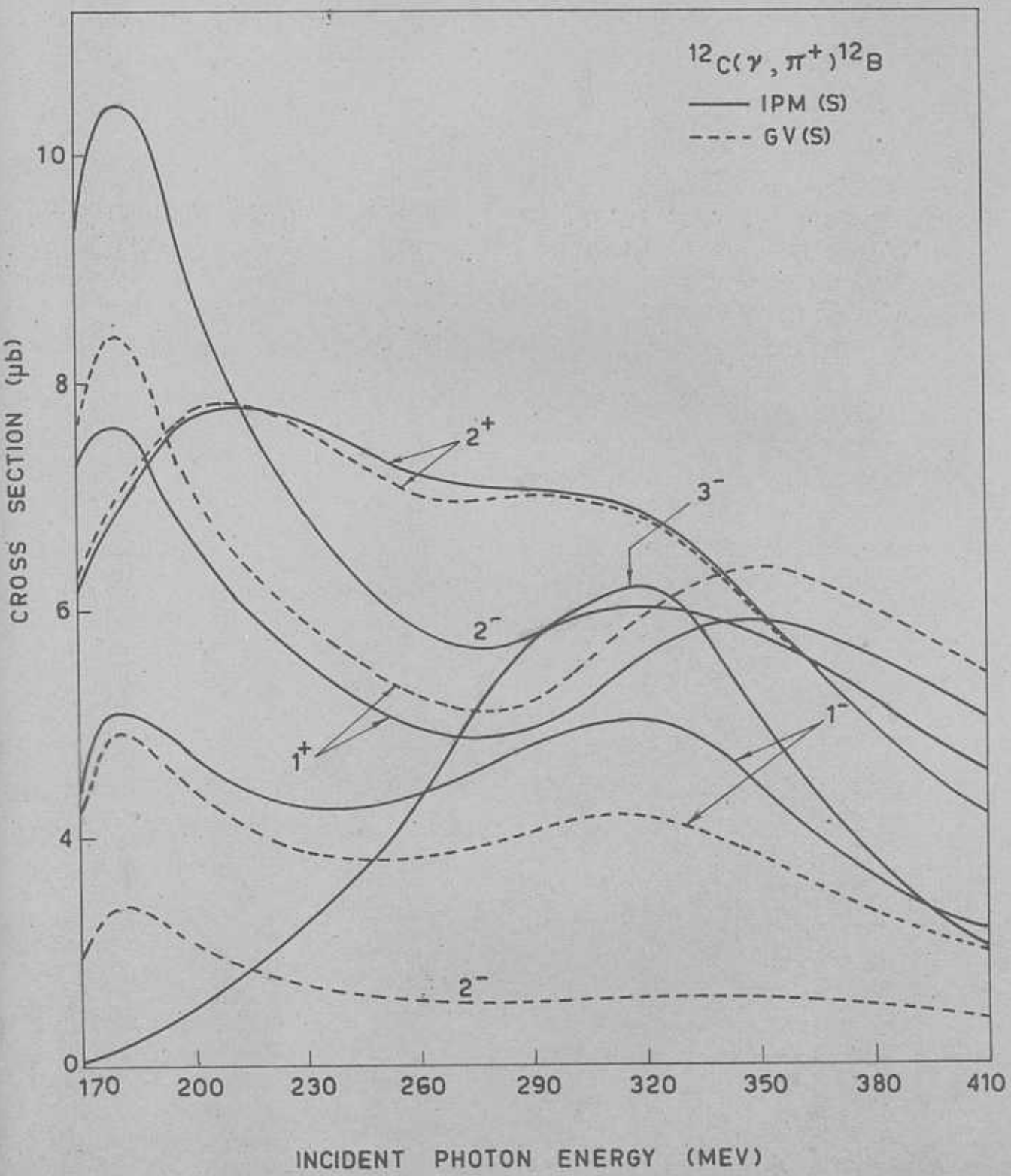

Fig.3. Cross section for the reaction $^{12}C(\gamma, \pi^+)^{12}N$ for the final nuclear states 1^+, 2^+, 2^-, 1^- and 3^- assuming surface production of pions.

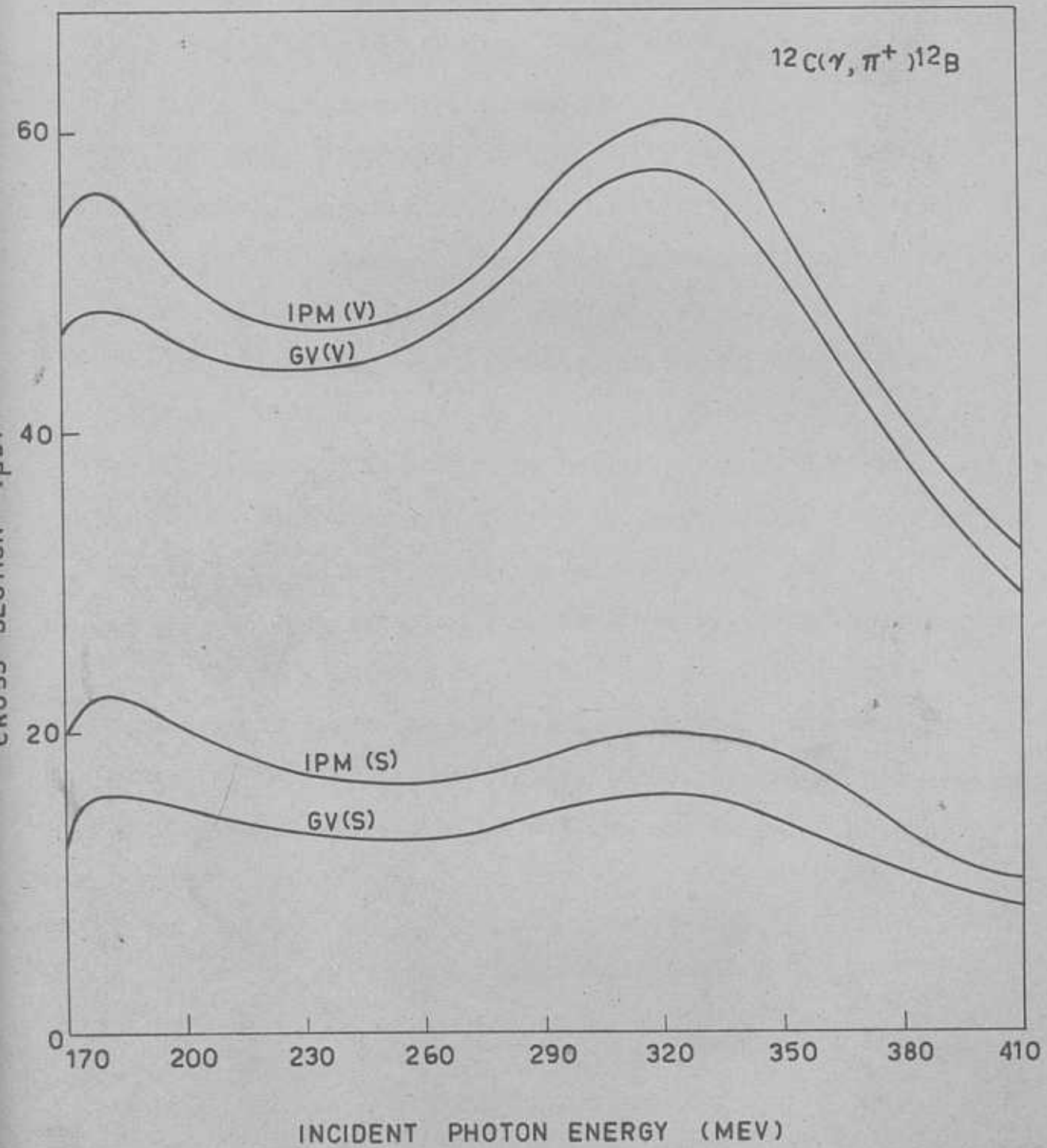

Fig.4. Total cross section for the reaction $^{12}C(\gamma, \pi^+)^{12}B$, assuming volume (V) and surface (S) production of pions. The nuclear models used are IPM and GV.

as a function of the incident photon energy in the 200-350 Mev region, similar to the case of $^{16}O(\gamma,\pi^+)^{16}N$.

Fig.5, shows the cross sections, for the case of negative pion photoproduction from ^{12}C, viz. reaction (7.1.2), leading to the ground state of ^{12}N which alone is stable against nucleon emission, obtained with IPM and GV models assuming volume and surface production of pions. As expected, the cross sections for this reaction turn out to be almost similar to those obtained for the $0^+ \longrightarrow 1^+$ transition in the case of the reaction $^{12}C(\gamma,\pi^+)^{12}B$. Further, the cross section curves obtained in the case of surface production mechanism reveal a smooth variation with incident photon energy, unlike the corresponding ones in the case of the volume production mechanism.

In conclusion we wish to emphasize that the reaction $^{12}C(\gamma,\pi^-)^{12}N$ is most favourable for drawing definite conclusions about the production mechanism, when the experimental results are available, since the only final nuclear state, which is stable against nucleon emission, is the ground state of $^{12}N(J^p = 1^+)$.

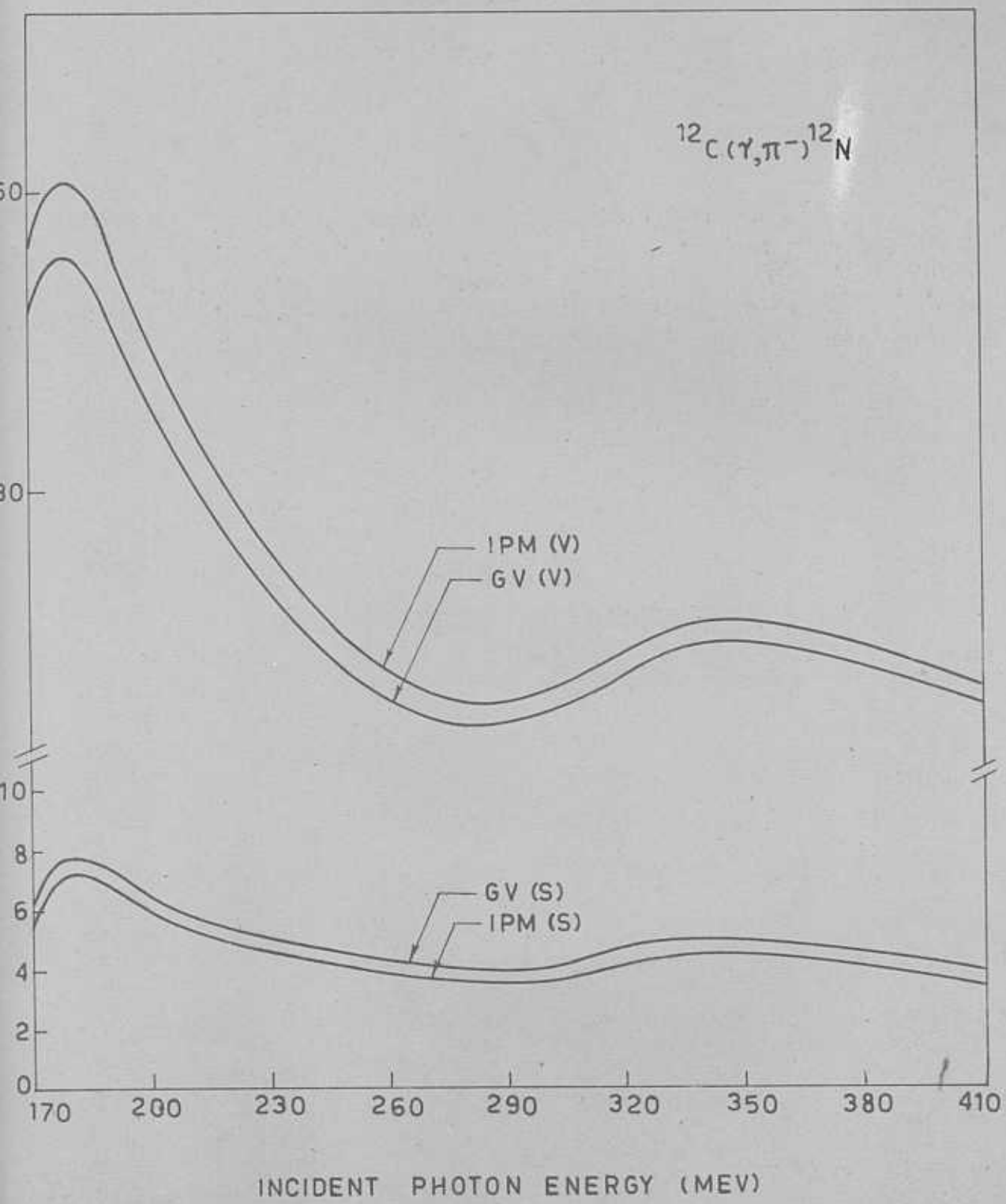

Fig.5. Total cross section for the reaction $^{12}C(\gamma,\pi^-)^{12}N$, assuming volume (V) and surface (S) production of pions. The nuclear models used are IPM and GV.

PART. III

PHOTOPRODUCTION OF CHARGED PIONS FROM CERTAIN NON-CLOSED-SHELL NUCLEI

CHAPTER 8

PHOTOPRODUCTION OF CHARGED PIONS FROM BORON+

1. In Chapter.3, we have made a detailed study[1] of photoproduction of positive pions from Oxygen with a view to obtain information on the pion production mechanism, eliminating as much as possible the uncertainty involved in nuclear structure. It was possible to obtain agreement between theory and experiment by using the surface production mechanism of Butler[2]. As already explained, in section.5 of Chapter.3, we use the phenomenological model of Butler mainly to simulate the effects of final-state interactions.

In this Chapter, we study the reaction cross sections for $^{11}B(\gamma, \pi^+)^{11}Be$ and $^{11}B(\gamma,\pi^-)^{11}C$ in both the volume and surface production models and compare our theoretical results with the experimental results of Hughes and March[3], and Dyal and Hummel[4]. The underlying theory has been outlined in Chapter.3 and we use the impulse approximation, the CGLN single nucleon photopion production amplitudes and the independent particle model wave functions, in the present study.

+ V.Devanathan, K.Srinivasa Rao and R.Sridhar, Phys.Letters. 25B, 456 (1967).

1)V.Devanathan, M.Rho, K.Srinivasa Rao and S.C.K.Nair, Nucl. Phys. B2, 329 (1967).
2)S.T.Butler, Phys.Rev. 87, 1117 (1952).
3)I.S.Hughes and P.V.March, Proc.Phys.Soc. A72, 259 (1958).
4)P.Dyal and J.P.Hummel, Phys.Rev.127, 2217 (1962).

The nucleus ^{11}B has five protons and six neutrons and hence can be considered to have a proton hole in the $1p_{3/2}$ shell. In the case of the reaction:

$$\gamma + {}^{11}_{5}B_{6} \longrightarrow {}^{11}_{4}Be_{7} + \pi^{+} \qquad (8.1.1)$$

each of the three protons in the $1p_{3/2}$ shell of the ^{11}B ground state may take part in the transition to a neutron state in the $1p_{1/2}$ or $2s_{1/2}$ shell in the final state, leaving the other two protons in the $1p_{3/2}$ shell. This is in contrast to the case of the reaction:

$$\gamma + {}^{11}_{5}B_{6} \longrightarrow {}^{11}_{6}C_{5} + \pi^{-} \qquad (8.1.2)$$

which essentially involves a single neutron transition (from a closed $1p_{3/2}$ neutron sub-shell). Further, we realize that the process (8.1.1) is analogous to the muon capture process:

$$\mu^{-} + {}^{11}B \longrightarrow {}^{11}Be^{*} + \nu_{\mu} \qquad (8.1.3)$$

since the same initial and final nuclear states are involved. This muon capture process (8.1.3) has been studied by Rood[5] and we use his analysis in this study. We assume that the wave functions of the nucleons in the filled (sub) shells are not changed in the transition.

We consider transitions to final nuclear states which are bound and subsequently decay by β-emission. There are only two low-lying states ($1/2^{+}$ and $1/2^{-}$) of ^{11}Be which

decay by β-emission[5,6] but there are many possible bound states of ^{11}C, which have not yet been correctly enumerated. The possible bound states of ^{11}C which are stable against nucleon emission[7] are, however, expected to result from the single particle transitions $1p_{3/2} \longrightarrow 1p_{3/2}$, $1p_{1/2}$, $1d_{5/2}$, $2s_{1/2}$ and $1d_{3/2}$.

2. In this section, we follow the analysis of Rood[5] to derive an expression for the matrix element of a one-body operator for the process (8.1.1). The effective part of the initial state has three protons in the $1p_{3/2}$ shell coupled to a total spin $J_i = 3/2$,

$$\text{i.e.} \qquad |i\rangle = |\, j^3\, J_i\, M_i\rangle = |\, (\tfrac{3}{2})^3\, \tfrac{3}{2}\, M_i\rangle \qquad (8.2.1)$$

and the only way to get a final state angular momentum of $J_f = 1/2$ (with the protons in $1p_{3/2}$ shell and one neutron in $1p_{1/2}$ or $2s_{1/2}$ shell) is to couple the two 3/2 angular momenta to an intermediate angular momentum zero, which is then coupled to the angular momentum 1/2 of the third neutron.

$$\text{i.e.} \quad |f\rangle = |\, j^2(0)\, j'\, J_f\, M_f\rangle = |\, (\tfrac{3}{2})^2(0)(1/2)1/2\, M_f\rangle \qquad (8.2.2)$$

Using formula (26.10) of de-Shalit and Talmi[8], we have

---

5) H.P.C.Rood, Nucl.Phys. 87, 367 (1966) and references therein.
6) I.Talmi and I.Unna, Phys.Rev.Letters. 4, 469 (1960).
7) E.W.Laing and R.G.Moorhouse, Proc.Phys.Soc. A70, 629 (1957).
8) A.de-Shalit and I.Talmi, "Nuclear Shell Theory" (Academic Press, New York) 1963. In the text above it is abbreviated as ST.

$$|i\rangle = \sum_{J_1 \text{ even}} [(\tfrac{3}{2})^2(J_1)(\tfrac{3}{2})\tfrac{3}{2}|\}(\tfrac{3}{2})^3\tfrac{3}{2}]\,|(\tfrac{3}{2})^2(J_1)(\tfrac{3}{2})\tfrac{3}{2}M_i\rangle, \tag{8.2.3}$$

where

$$|(\tfrac{3}{2})^2(J_1)(\tfrac{3}{2})\tfrac{3}{2}M_i\rangle = \sum_{m_1,m_2,m_3,M_1} C(\tfrac{3}{2}\tfrac{3}{2}J_1; m_1 m_2 M_1) \cdot \cdot C(J_1\tfrac{3}{2}\tfrac{3}{2}; M_1 m_3 M_i)|\tfrac{3}{2}m_1\rangle|\tfrac{3}{2}m_2\rangle|\tfrac{3}{2}m_3\rangle, \tag{8.2.4}$$

$|\frac{3}{2}\ m\rangle$ being the one-particle harmonic oscillator wave function for the $1p_{3/2}$ shell. Though J_1 in (8.2.3) can take the 'even' values 0 and 2, we do not need the $J_1 = 2$ term since the intermediate angular momentum in (8.2.2) is zero. The coefficient of fractional parentage with $J_1 = 0$ is given by [ST(26.11)a]:

$$[(\tfrac{3}{2})^2(0)(\tfrac{3}{2})\tfrac{3}{2}|\}(\tfrac{3}{2})^3\tfrac{3}{2}] = \frac{1}{\sqrt{6}}. \tag{8.2.5}$$

The properly normalized, antisymmetrized final state wave function is given by [ST(26.3)]:

$$|f\rangle = \frac{1}{\sqrt{3}}\,[\,|(\tfrac{3}{2})^2_{12}(0)(\tfrac{1}{2})_3\tfrac{1}{2}M_f\rangle - |(\tfrac{3}{2})^2_{13}(0)(\tfrac{1}{2})_2\tfrac{1}{2}M_f\rangle + |(\tfrac{3}{2})^2_{23}(0)(\tfrac{1}{2})_1\tfrac{1}{2}M_f\rangle\,], \tag{8.2.6}$$

where

$$|(\tfrac{3}{2})^2_{12}(0)(\tfrac{1}{2})_3\tfrac{1}{2}M_f\rangle = \sum_m C(\tfrac{3}{2}\tfrac{3}{2}0; m,-m\,0)\ C(0\tfrac{1}{2}\tfrac{1}{2}; 0\,M_f M_f) \cdot \cdot |\tfrac{3}{2}m\rangle\,|\tfrac{3}{2},-m\rangle\,|\tfrac{1}{2}M_f\rangle$$
$$= -\sum_m C(\tfrac{3}{2}\tfrac{3}{2}0; m,-m\,0)\,|\tfrac{3}{2}m\rangle\,|\tfrac{3}{2},-m\rangle\,|\tfrac{1}{2}M_f\rangle. \tag{8.2.7}$$

We now wish to evaluate the matrix element:

$$Q = \langle f \mid \sum_{j=1}^{A} t_j \mid i \rangle = 3 \langle f \mid t \mid i \rangle \cdot \qquad (8.2.8)$$

The term $\mid (\frac{3}{2})^2_{12}\ (0)\ (\frac{1}{2})_3\ \frac{1}{2}\ M_f \rangle$ in Eq.(8.2.6) for $\mid f \rangle$ alone contributes to this matrix element, so that

$$Q = 3\,\frac{1}{\sqrt{3}} \langle ((\tfrac{3}{2})^2_{12}(0)(\tfrac{1}{2})_3 \tfrac{1}{2} M_f \mid t \mid (\tfrac{3}{2})^3 \tfrac{3}{2} M_i \rangle . \qquad (8.2.9)$$

Since in (8.2.3), $J_1 = 0$ we have obviously $M_1 = 0$ and because of the orthonormality of the oscillator wave functions, we have:

$$m_1 = -m_2 = m \quad \text{and} \quad m_3 = M_i \ .$$

The contribution to (8.2.9) of the term in $\mid i \rangle$ with $J_1 = 0$ is:

$$Q = \frac{3}{\sqrt{3}}\,\frac{1}{\sqrt{6}} \sum_m C(\tfrac{3}{2}\tfrac{3}{2}\,0;\, m,-m\,0)\, C(\tfrac{3}{2}\tfrac{3}{2}\,0;\, m,-m\,0) \langle \tfrac{1}{2} M_f \mid t \mid \tfrac{3}{2} M_i \rangle \qquad (8.2.10)$$

$$= \frac{1}{\sqrt{2}} \langle \tfrac{1}{2} M_f \mid t \mid \tfrac{3}{2} M_i \rangle ,$$

using the orthogonality property of the Clebsch-Gordon coefficients.

We thus get a $1/\sqrt{2}$ factor compared with the too simple version of the Independent particle shell model which allows only the odd proton to make the transition. This factor exists only for π^+ production process (8.1.1) involving the nuclear transitions $^{11}B \longrightarrow {}^{11}Be^*$. This factor does <u>not</u> exist for π^- production process (8.1.2) involving the

nuclear transitions $^{11}B \longrightarrow {}^{11}C^{*}$, since in this case the effective part of the initial state is a closed shell state with four neutrons in the $1p_{3/2}$ shell coupled to zero angular momentum.

3. The matrix element for the photoproduction of a charged pion from a bound nucleon is given by:

$$Q = \langle l_f \tfrac{1}{2} J_f M_f | (\underline{\sigma}\cdot\underline{K} + L) e^{i\underline{k}\cdot\underline{r}} \tau^{\mp} | l_i \tfrac{1}{2} J_i M_i \rangle \qquad (8.3.1)$$

where the orbital, spin and total angular momenta of the initial and final states are explicitly represented while the radial parts are implicit, $\underline{K}$ and L are the CGLN amplitudes explicitly given for π^+ and π^- photoproduction in section.2 of Chapter.1, the momentum transfer to the bound nucleon is taken into account by $e^{i\underline{k}\cdot\underline{r}}$, $\underline{k}$ being the difference between the momenta of the incident photon ($\underline{\nu}$) and outgoing pion ($\underline{\mu}$), $\underline{r}$ is the position coordinate of the bound nucleon and $\tau^{\mp}$ is the isospin operator for $\pi^{\pm}$ photoproduction. The differential cross section is given by

$$\frac{d\sigma}{d\underline{\mu}\, d\underline{k}} = (2\pi)^{-2} \sum_{M_f} |Q|^2 \, \delta(\underline{\nu} - \underline{\mu} - \underline{k}) \, \delta(\mu_0 - \nu_0)$$

which after integration over $d\underline{k}$ becomes:

$$\frac{d\sigma}{d\Omega} = (2\pi)^{-2} \mu\mu_0 \sum_{M_f} |Q|^2, \qquad (8.3.2)$$

with $\mu_o = \nu_o$, making the assumption that the entire energy of the photon ν_o is given to the outgoing pion. The square of the matrix element, after summing over the final spin states[+] is obtained following the procedure described in detail in section.3 of Chapter 3, as:

$$\sum_{M_f} |Q|^2 = 16\pi^2 \frac{[J_f]^2}{[J_i]^2} \sum_{n,\ell,n',\ell',\lambda} i^{\ell-\ell'} (-1)^{n+\ell+n'+\ell'} \cdot$$

$$\cdot \frac{1}{[\lambda]^2} \left\{ \sum_{m_\lambda} (Y^{\ell}(\hat{k}) \times K^{n})^{\lambda}_{-m_\lambda} [(Y^{\ell'}(\hat{k}) \times K^{n'})^{\lambda}_{-m_\lambda}]^* \cdot \right.$$

$$\cdot \langle \ell_f \tfrac{1}{2} J_f \| (Y^{\ell}(\hat{r}) \times \sigma^{n})^{\lambda} \| \ell_i \tfrac{1}{2} J_i \rangle \cdot$$

$$\left. \cdot \langle \ell_f \tfrac{1}{2} J_f \| (Y^{\ell'}(\hat{r}) \times \sigma^{n'})^{\lambda} \| \ell_i \tfrac{1}{2} J_i \rangle^* \cdot \right.$$

$$\cdot \langle j_\ell(kr) \rangle_{n_i \ell_i, n_f \ell_f} \langle j_{\ell'}(kr) \rangle^*_{n_i \ell_i, n_f \ell_f} \qquad (8.3.3)$$

The expression for the square of the matrix element can be further simplified using Eqs.(3.4.7), (3.4.8), (3.4.9) and (3.4.11) to give:

$$\sum_{M_f} |Q|^2 = (4\pi)^{1/2} [J_f]^2 [1/2]^2 [\ell_i]^2 \sum_{n,\ell_3,\ell',\lambda} i^{\ell-\ell'} (-1)^{\lambda} [\ell]^2 [\ell']^2 [n]^2 [\lambda]^2 \cdot$$

$$\cdot C(\ell_i \ell \ell_f; 000)\, C(\ell_i \ell' \ell_f; 000) \begin{Bmatrix} \ell_i & \ell & \ell_f \\ 1/2 & n & 1/2 \\ J_i & \lambda & J_f \end{Bmatrix} \begin{Bmatrix} \ell_i & \ell' & \ell_f \\ 1/2 & n & 1/2 \\ J_i & \lambda & J_f \end{Bmatrix} \cdot$$

$$\cdot \sum_{N=0,2} \frac{1}{[N]} C(\ell\ell' N; 000) W(\ell\ell' n n; \lambda N) (Y^{N}(\hat{k}) \cdot (K^{n} \times K^{*n})^{N}) \cdot$$

$$\cdot \langle j_\ell(kr) \rangle_{n_i \ell_i, n_f \ell_f} \langle j_{\ell'}(kr) \rangle^*_{n_i \ell_i, n_f \ell_f} , \qquad (8.3.4)$$

[+] Note that averaging over photon polarizations is taken care of elsewhere - while evaluating the expressions LL^*, $\underline{K}.\underline{K}^*$, etc., in Chapter.1.

where $[\,j\,]^2 = (2j+1)$ and

$$\langle j_\ell(kr)\rangle_{n_i l_i, n_f l_f} = \int_a^\infty R_{n_f l_f}(r)\, j_\ell(kr)\, R_{n_i l_i}(r)\, r^2 dr$$

$a = 0$ for volume production and $a = r_0$ for surface production.

In the numerical evaluation we have taken for the harmonic oscillator size parameter b, the value determined in the electron scattering experiments[5,9]:

$$b = (1.55 \pm 0.15) \text{ fm.} \qquad (8.3.5)$$

For the nuclear radius r_0, we have used the values:

$$r_0 = 1.98 \text{ fm, } 2.26 \text{ fm and } 2.55 \text{ fm.} \qquad (8.3.6)$$

Note that the factor $1/\sqrt{2}$ which occurs in the case of π^+ photoproduction (8.1.1), as explained in section.2, has been omitted in Eq.(8.3.1).

Here, we would like to mention the differences which exist between our study of $^{11}B(\gamma,\pi^-)^{11}C$ and that of Laing and Moorehouse[7]. Laing and Moorehouse make the following assumptions: (i) $K_3^2 = (K_1^2 + K_2^2)/2$, which amounts to taking $|Q|^2$ angular independent; (ii) the main contribution to the total cross section arises from S-wave mesons and they take: $K^2+L^2 = c/\nu_0^2$ with $c = 10^{-28}\text{cm}^2$, in agreement with the magnitude of photoproduction at free nucleons; (iii) the values of b and r_0 are taken to be 2.0fm

9) U.Meyer-Berkhout, K.W.Ford and A.E.S.Green, Ann.Phys. 8, 119 (1959).

and 3.16 fm; and (iv) they neglect the difference in the free nucleon photoproduction amplitude of π^+ and π^-.

On the other hand, we take the explicit forms of CGLN for the single nucleon transition operator and use the values of b and r_0 consistent with electron scattering data and also take into account the differences between π^+ and π^- production amplitudes.

4. Numerical calculations for the differential and total cross sections have been made using Eq.(8.3.4) in Eq.(8.3.2). Table.1 gives the cross sections for the process $^{11}B(\gamma,\pi^+)^{11}Be$ in the volume production ($r_0=0$) and surface production (r_0 = 1.98 fm., 2.26 fm. and 2.55 fm.) models, corresponding to three different size parameter values (viz. b = 1.4 fm., 1.55 fm. and 1.7 fm.) consistent with electron scattering data[9], for an incident photon energy of 260 Mev. From the table we find:(i) the cross sections for the single nucleon transitions $1p_{3/2} \longrightarrow 1p_{1/2}$ and $1p_{3/2} \longrightarrow 2s_{1/2}$ are of different orders of magnitude only in the volume production model and that the two cross sections become comparable in their values for surface production models, and
(ii) the dependence of the cross section on the size parameter (b) values is not so pronounced as that on the cut-off parameter (r_0) values.

Table.1.

Cross sections for the reaction $^{11}B(\gamma,\pi^+)^{11}Be$ in the volume production ($r_o = 0$) and surface production ($r_o > 0$) models, for an incident photon energy of 260 Mev, as a function of the harmonic oscillator size parameter b.

r_o (fm)	Single particle transitions	Cross section in μb.		
		b=1.4 fm	b=1.55 fm	b=1.7 fm
0	$1p_{3/2} \rightarrow 1p_{1/2}$	24.428	20.672	17.432
	$1p_{3/2} \rightarrow 2s_{1/2}$	3.494	3.819	4.345
	Sum	27.922	24.491	21.777
1.98	$1p_{3/2} \rightarrow 1p_{1/2}$	6.628	8.330	9.182
	$1p_{3/2} \rightarrow 2s_{1/2}$	5.329	4.463	4.505
	Sum	11.957	12.843	12.687
2.26	$1p_{3/2} \rightarrow 1p_{1/2}$	3.063	4.678	5.869
	$1p_{3/2} \rightarrow 2s_{1/2}$	2.494	3.742	3.425
	Sum	6.557	8.420	9.294
2.55	$1p_{3/2} \rightarrow 1p_{1/2}$	1.121	2.155	3.201
	$1p_{3/2} \rightarrow 2s_{1/2}$	1.794	2.544	2.841
	Sum	2.915	4.699	6.042

Fig.1 gives the calculated cross section for photoproduction of π^+ from ^{11}B assuming volume production of pions with b = 1.55 fm. Fig.2 corresponds to the results obtained assuming surface production of pions with b=1.55 fm. and r_0 = 2.55 fm. In these figures curve 1 gives the total cross section for the transitions to $1/2^+$ and $1/2^-$ and curves 2 and 3 give respectively their separate contributions. The experimental results are those of Dyal and Hummel[4] and we find that the agreement is good for surface production of pions.

Table.2 gives the cross sections for the process $^{11}B(\gamma, \pi^-)^{11}C$ in the volume production (r_0=0) and surface production (r_0 = 1.98 fm., 2.26 fm. and 2.55 fm.) models, corresponding to three different size parameter values (b = 1.4 fm., 1.55 fm. and 1.7 fm.) for an incident photon energy of 260 Mev. Figs.3 and 4 give the results for photoproduction of π^- from ^{11}C assuming volume and surface production of pions, respectively, with b=1.55 fm. and r_0 = 2.55 fm. Curve 1 is obtained by assuming that the final bound states of ^{11}C result from the single particle transitions $1p_{3/2} \longrightarrow 1p_{3/2}$, $1p_{1/2}$, $1d_{5/2}$, $2s_{1/2}$ and $1d_{3/2}$. Curves 2 and 3 correspond to single particle transitions $1p_{3/2} \longrightarrow 1p_{3/2}$, $1p_{1/2}$, $1d_{5/2}$ and $2s_{1/2}$ and $1p_{3/2} \longrightarrow 1p_{3/2}$, $1p_{1/2}$ and $1d_{5/2}$, respectively. The

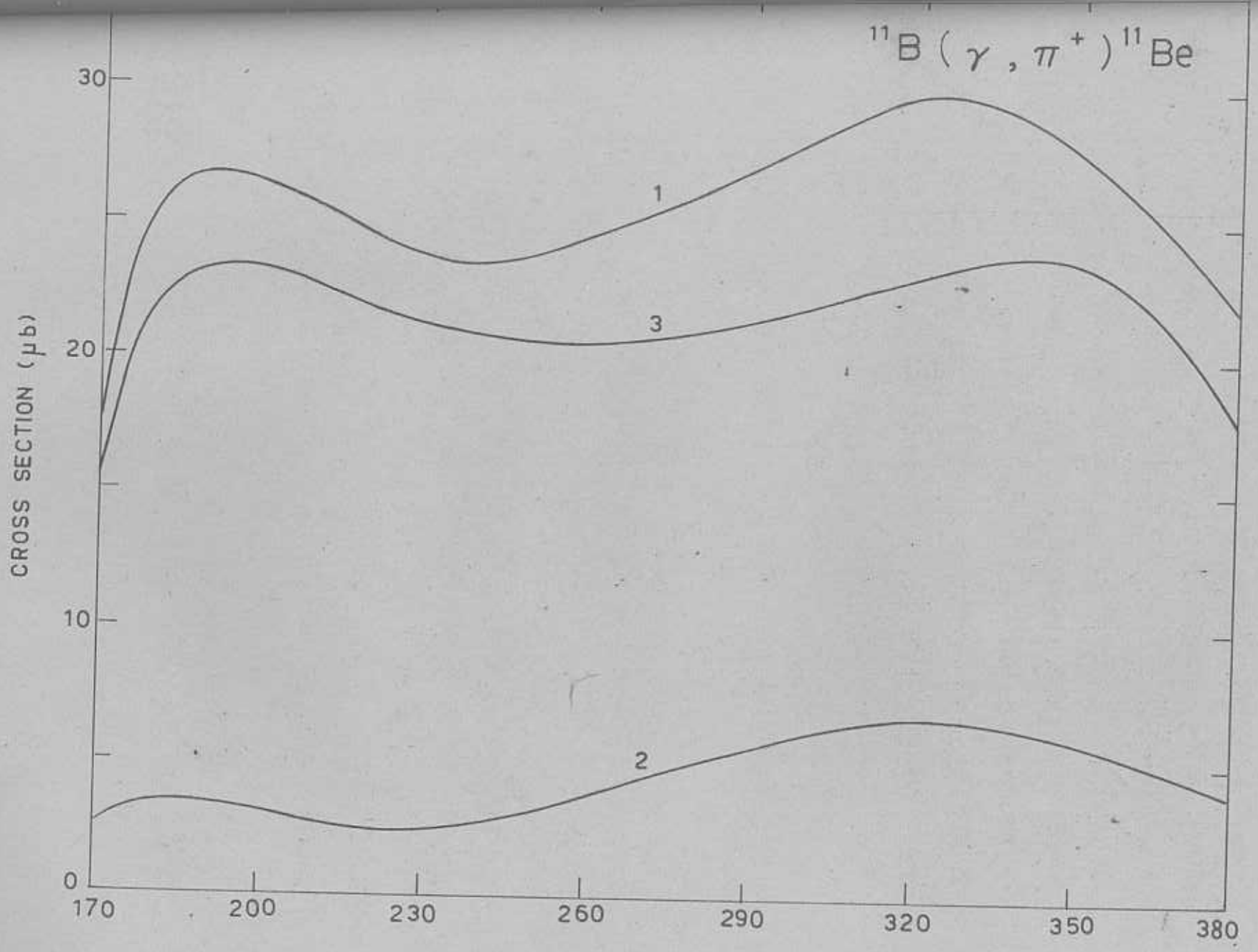

Fig.1. Cross section for the reaction $^{11}B(\gamma,\pi^+)^{11}Be$ assuming volume production of pions with b=1.55fm. Curves 2 and 3 correspond to transitions to 1/2 and 1/2 states, respectively, while curve 1 gives their sum.

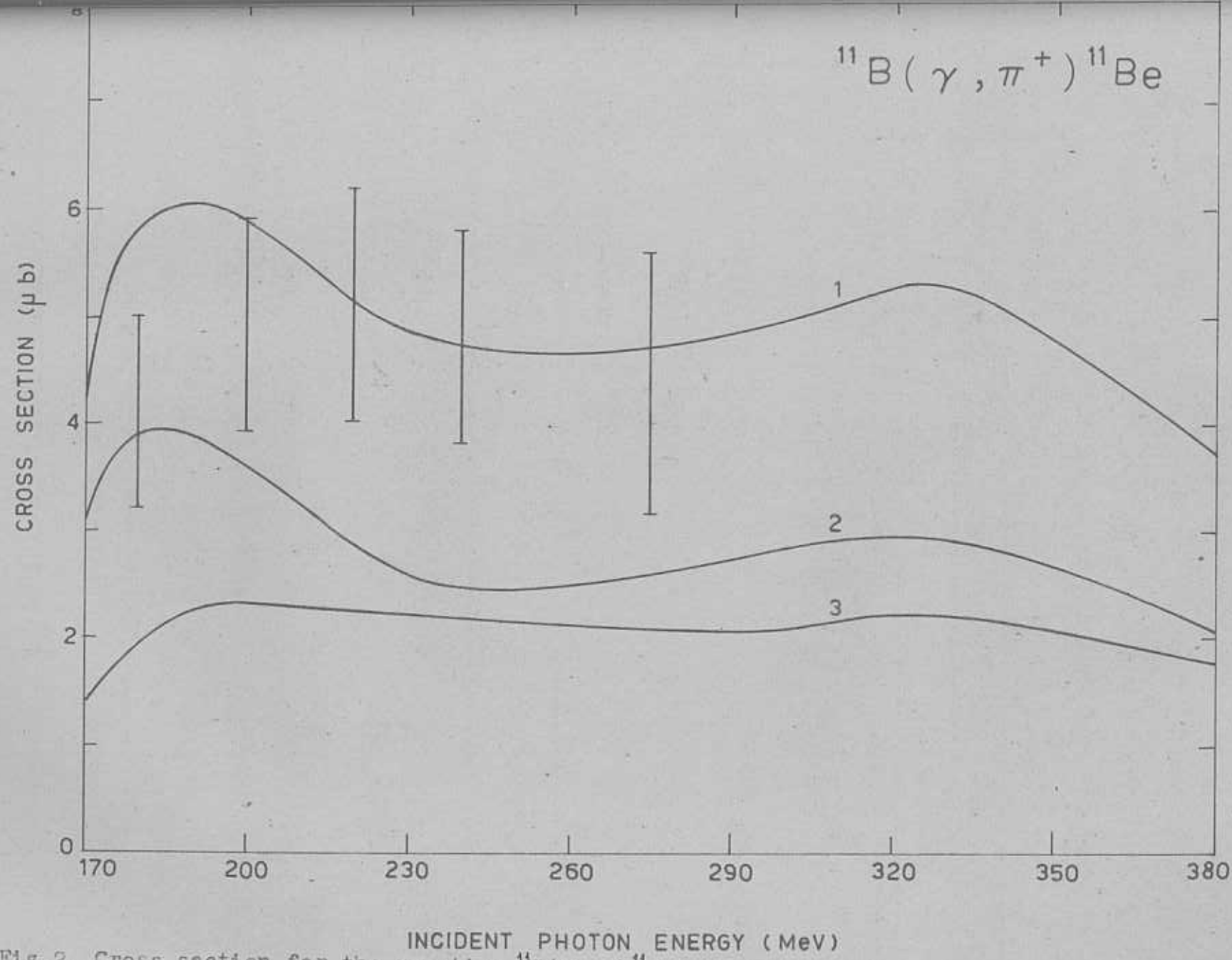

Fig.2. Cross section for the reaction $^{11}B(\gamma,\pi^+)^{11}Be$ assuming surface production of pions with b=1.55 fm. and r_0=2.55 fm. Curves 2 and 3 correspond to transitions to 1/2 and 1/2 states, respectively, while curve 1 gives their sum. The experimental data is from ref.4).

Table.2

Cross section for the reaction $^{11}B(\gamma,\pi^-)^{11}C$ in volume production ($r_0 = 0$) and surface production ($r_0 > 0$) models, for an incident photon energy of 260 Mev. as a function of the harmonic oscillator size parameter b.

r_0 (fm)	Single particle transition	Cross section in μb. b=1.4 fm.	b=1.55fm.	b=1.7fm.
0	$1p_{3/2} \rightarrow 1p_{1/2}$	66.761	55.747	46.300
	$1p_{3/2} \rightarrow 2s_{1/2}$	9.128	10.617	12.447
	$1p_{3/2} \rightarrow 1p_{3/2}$	111.468	94.532	79.307
	$1p_{3/2} \rightarrow 1d_{5/2}$	108.774	93.681	80.304
	$1p_{3/2} \rightarrow 1d_{3/2}$	31.762	69.877	59.374
	Sum	377.893	324.454	277.732
1.98	$1p_{3/2} \rightarrow 1p_{1/2}$	17.854	22.345	24.176
	$1p_{3/2} \rightarrow 2s_{1/2}$	13.074	10.867	8.591
	$1p_{3/2} \rightarrow 1p_{3/2}$	32.202	40.269	43.415
	$1p_{3/2} \rightarrow 1d_{5/2}$	43.475	56.492	58.427
	$1p_{3/2} \rightarrow 1d_{3/2}$	35.730	41.334	42.477
	Sum	147.335	171.307	177.086

continued on next page

Table 2.(ctd.)

r_0 (fm)	Single particle transition	Cross section in μb. b=1.4 fm.	b=1.55fm.	b=1.7fm.
2.26	$1p_{3/2} \rightarrow 1p_{1/2}$	8.179	12.355	15.309
	$1p_{3/2} \rightarrow 2s_{1/2}$	8.551	9.149	8.407
	$1p_{3/2} \rightarrow 1p_{3/2}$	14.916	22.448	27.656
	$1p_{3/2} \rightarrow 1d_{5/2}$	27.321	38.052	44.381
	$1p_{3/2} \rightarrow 1d_{3/2}$	19.859	27.502	31.937
	Sum	78.826	109.306	127.690
2.55	$1p_{3/2} \rightarrow 1p_{1/2}$	2.950	5.608	8.238
	$1p_{3/2} \rightarrow 2s_{1/2}$	4.429	6.302	7.055
	$1p_{3/2} \rightarrow 1p_{3/2}$	5.393	10.198	14.878
	$1p_{3/2} \rightarrow 1d_{5/2}$	12.765	22.013	29.780
	$1p_{3/2} \rightarrow 1d_{3/2}$	9.141	15.712	21.214
	Sum	34.678	59.833	81.165

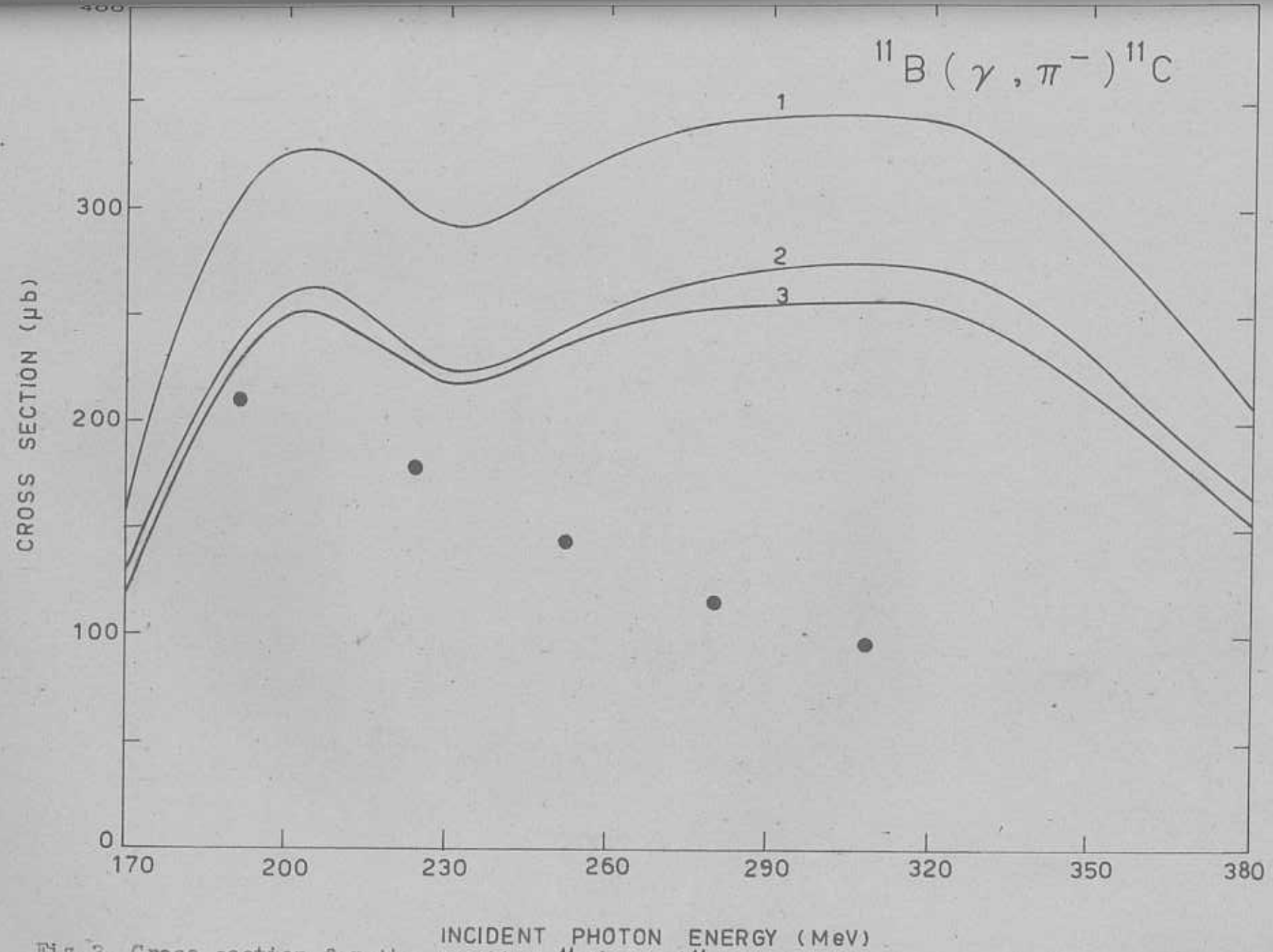

Fig.3. Cross section for the reaction $^{11}B(\gamma,\pi^-)^{11}C$ assuming volume production of pions with b=1.55 fm. Curves 1,2 and 3 correspond to the single particle transitions $1p_{5/2} \rightarrow 1p_{3/2}, 1p_{1/2}, 1d_{5/2}, 2s_{1/2}, 1d_{3/2}$; $1p_{5/2} \rightarrow 1p_{3/2}, 1p_{1/2}, 1d_{5/2}, 2s_{1/2}$ and $1p_{3/2} \rightarrow 1p_{3/2}, 1p_{1/2}, 1d_{5/2}$, respectively.

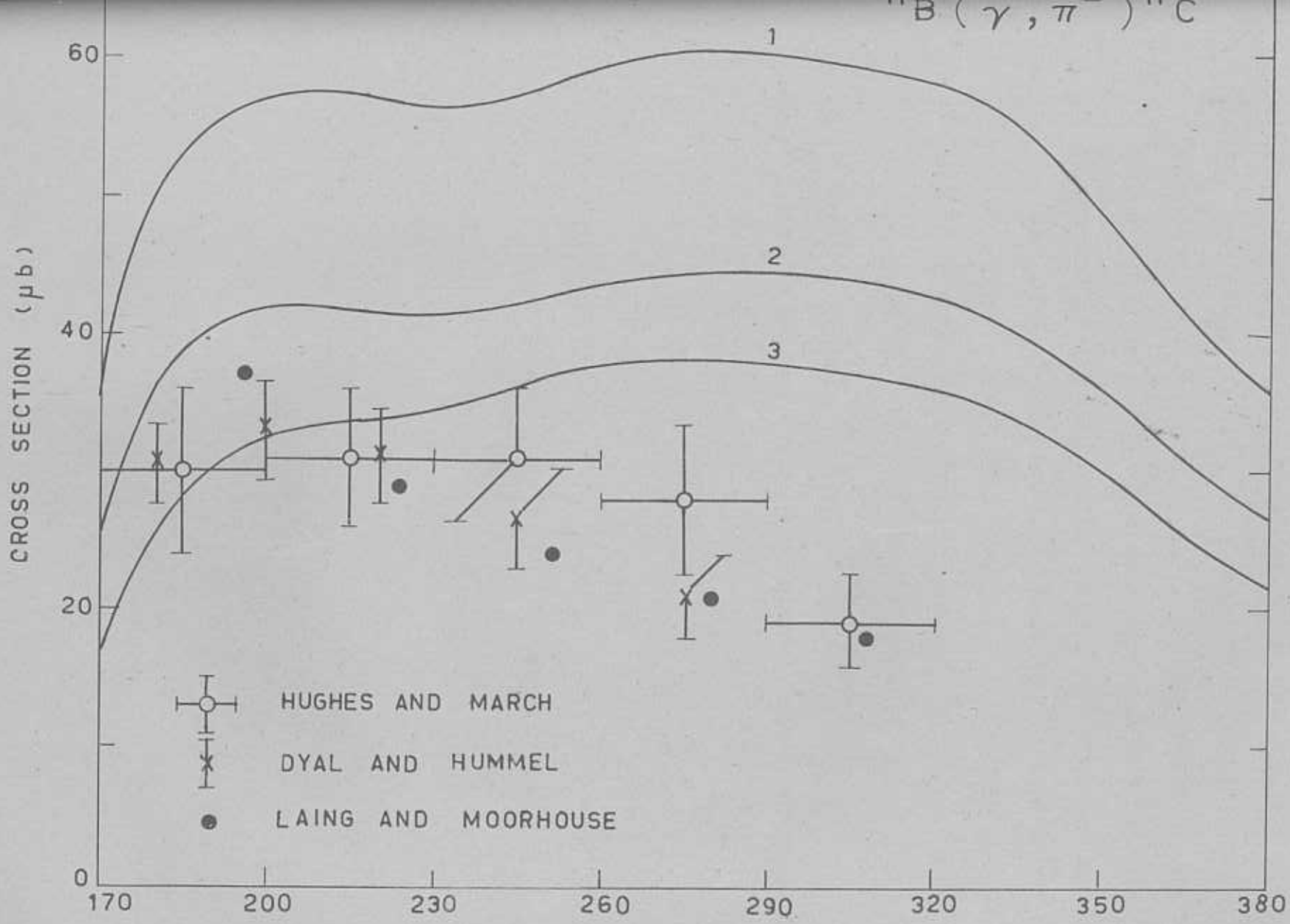

Fig.4. Cross section for the reaction $^{11}B(\gamma,\pi^-)^{11}C$ assuming surface production of pions with b=1.55 fm. and r_0 =2.55 fm. Curves 1,2 and 3 correspond to the single particle transitions $1p_{3/2} \rightarrow 1p_{3/2}$, $1p_{1/2}$, $1d_{5/2}$, $2s_{1/2}$, $1d_{3/2}$; $1p_{3/2} \rightarrow 1p_{3/2}$, $1p_{1/2}$, $1d_{5/2}$, $2s_{1/2}$ and $1p_{3/2} \rightarrow 1p_{3/2}$, $1p_{1/2}$, $1d_{5/2}$, respectively. Experimental data are from ref.3) and ref.4).

experimental data are those of Hughes and March[3] and Dyal and Hummel[4]. The dots correspond to the theoretical values calculated by Laing and Moorehouse[7] and we are of the view that the good agreement which they obtain with the experimental values is fortuitous in the wake of their assumption enumerated in section 3 of this Chapter. We find that our results obtained in the surface production model assuming the bound states of ^{11}C to result from the single particle transitions $1p_{3/2} \longrightarrow 1p_{3/2}$, $1p_{1/2}$ and $1d_{5/2}$ (see curve 2 of Fig.4) are in reasonably good agreement with the experimental results.

CHAPTER 9

PHOTOPRODUCTION OF PIONS FROM ^{27}Al, ^{51}V AND ^{60}Ni (+)

1. We have shown earlier, in Chapter 3 and 8, that a reasonable agreement between theory and experiment can be obtained, in the case of $^{16}O(\gamma,\pi^+)^{16}N$, $^{11}B(\gamma,\pi^+)^{11}Be$ and $^{11}B(\gamma,\pi^-)^{11}C$, if we invoke the phenomenological surface production mechanism for photoproduction of pions from nuclei. In this Chapter, we present a study of the following photoproduction reactions:

$$\gamma + {}^{27}_{13}Al_{14} \longrightarrow {}^{27}_{12}Mg_{15} + \pi^+ , \qquad (9.1.1)$$

$$\gamma + {}^{51}_{23}V_{28} \longrightarrow {}^{51}_{22}Ti_{29} + \pi^+ , \qquad (9.1.2)$$

and

$$\gamma + {}^{60}_{28}Ni_{32} \longrightarrow {}^{60}_{29}Cu_{31} + \pi^- \qquad (9.1.3)$$

for which experimental results are available[1-3]. The aim of the present study is to assess the usefulness of the phenomenological surface production mechanism. Further, in the absence of detailed and conclusive evidence about the number of final states along with their spin-parity assignments, we show that a comparison of a theoretical study of reactions of the type $A(\gamma,\pi^{\pm})B$, in the frame

---

(+) V.Devanathan, G.N.S.Prasad and K.Srinivasa Rao, submitted to Nucl.Phys.

1) W.B.Walters and J.P.Hummel, Phys.Rev.143, 833 (1966). See also ref.2)

2) G.Nydhal and B.Forkman, Nucl.Phys.B7, 97 (1968).

3) P.V.March and T.G.Walker, Proc.Phys.Soc. A77, 293 (1961).

work of the Independent Particle Model (IPM), with the experimental results for the same reactions, enables us to extract some information regarding the low-lying bound states of the final nucleus, B, which are stable against nucleon emission. The underlying theory, based upon the impulse approximation and the single nucleon photoproduction amplitudes of CGLN, used in the present study, has been discussed in detail in the earlier Chapters.

In the case of the three reactions under study, (9.1.1), (9.1.2) and (9.1.3), the allowed final nuclear states are the low-lying bound states which are stable against nucleon emission. Using the shell model description for the initial and final nuclei, we have enumerated in table.1, the possible single nucleon transitions involved in these reactions and the corresponding final states allowed by the Pauli exclusion principle[4].

2. THE REACTION $^{27}Al(\gamma,\pi^+)^{27}Mg$:

Interpreting the surface production mechanism a' la Butler, we take for the cut-off parameter r_0, defined in section 5 of Chapter.3, a value of 2.0 in units of pion Compton wavelength (r_0 = 2.828 fm.) and for the oscillator length parameter b, a value of 1.816 fm. The values of these parameters are taken from Carlson

---

4) A.de-Shalit and I.Talmi, "Nuclear Shell Theory", Academic Press, (1963), sec.24, p.245.

Table.1

Enumeration of final nuclear states allowed by the Pauli exclusion principle

Reaction	Single particle transition	Configuration of final nucleus+	Allowed final nuclear states (all have positive parity)
$^{27}Al(\gamma,\pi^+)^{27}Mg$	$1d_{5/2} \rightarrow 2s_{1/2}$	$(1d_{5/2})_p^4 (2s_{1/2})_n^1$	1/2; 3/2, 5/2; 7/2, 9/2
	$1d_{5/2} \rightarrow 1d_{3/2}$	$(1d_{5/2})_p^4 (1d_{3/2})_n^1$	3/2; 1/2, 3/2, 5/2, 7/2; 5/2, 7/2, 9/2, 11/2
$^{51}V(\gamma,\pi^+)^{51}Ti$	$1f_{7/2} \rightarrow 2p_{3/2}$	$(1f_{7/2})_p^2 (2p_{3/2})_n^1$	3/2; 1/2, 3/2, 5/2, 7/2; 5/2, 7/2, 9/2, 11/2, 13/2; 9/2, 11/2, 13/2, 15/2
	$1f_{7/2} \rightarrow 1f_{5/2}$	$(1f_{7/2})_p^2 (1f_{5/2})_n^1$	5/2; 1/2, 3/2, 5/2, 7/2, 9/2; 3/2, 5/2, 7/2, 9/2, 11/2, 13/2; 7/2, 9/2, 11/2, 13/2, 15/2, 17/2
	$1f_{7/2} \rightarrow 2p_{1/2}$	$(1f_{7/2})_p^2 (2p_{1/2})_n^1$	1/2; 3/2, 5/2; 7/2, 9/2; 11/2, 13/2
$^{60}Ni(\gamma,\pi^-)^{60}Cu$	$2p_{3/2} \rightarrow 2p_{3/2}$	$(2p_{3/2})_n^3 (2p_{3/2})_p^1$	0, 1, 2, 3
	$2p_{3/2} \rightarrow 1f_{5/2}$	$(2p_{3/2})_n^3 (1f_{5/2})_p^1$	1, 2, 3, 4
	$2p_{3/2} \rightarrow 2p_{1/2}$	$(2p_{3/2})_n^3 (2p_{1/2})_p^1$	1, 2

+Closed shell configurations are suppressed in this column for the sake of brevity.

and Talmi[5] who have made calculations on pairing effects in Coulomb energies which have been related by them to the determination of nuclear radii.

In Fig.1, the cross sections for the reaction $^{27}Al(\gamma,\pi^+)^{27}Mg$ have been plotted as a function of the incident photon energy assuming volume production of pions. Fig.2 corresponds to the results obtained assuming surface production of pions. Curves 1 and 2 represent the cross sections corresponding to the single nucleon transitions $1d_{5/2} \longrightarrow 2s_{1/2}$ and $1d_{5/2} \longrightarrow 1d_{3/2}$, respectively. The sum of these two cross sections are represented by curve 3. The experimental results are those of Walters and Hummel[1] and Nydhal and Forkman[2].

The cross sections for this reaction have been measured from threshold upto 700 Mev by Masaike[6] and by Nydhal and Forkman[2] and from threshold upto 300 Mev by Walters and Hummel[1]. While Masaike gives a cross section with a peak value of 120 μb at 250 Mev. Nydhal and Forkman obtained a peak value of 35 μb at 225 Mev and Walters and Hummel obtained a peak value of 13 μb at 220 Mev. The shape of the cross section obtained by Nydhal and Forkman agrees with that obtained by Walters and Hummel but the size of the former is 2.5 times greater

5) B.C.Carlson and I.Talmi, Phys.Rev.96, 436 (1954).
6) A.Masaike, J.Phys.Soc.(Japan) 19, 427 (1964); A.Masaike, Y.Yoshimura, Y.Murata, A.Kusumagi and K.Takamatsu, ibid 18, 1692 (1963).

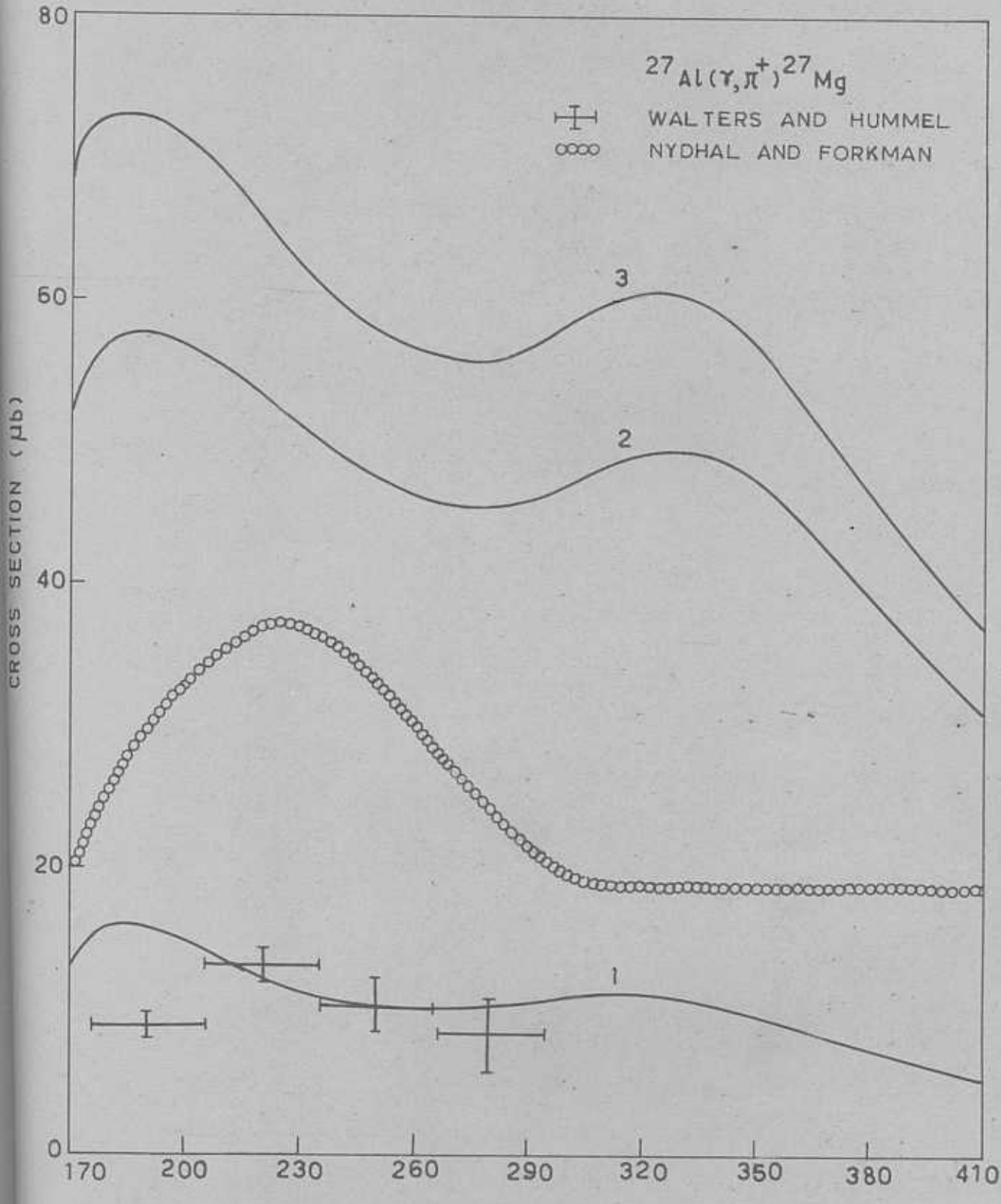

Fig.1. Cross section for the reaction $^{27}Al(\gamma,\pi^+)^{27}Mg$ assuming volume production of pions. Experimental results are those of Walters and Hummel[3] and of Nydhal and Forkman[4].

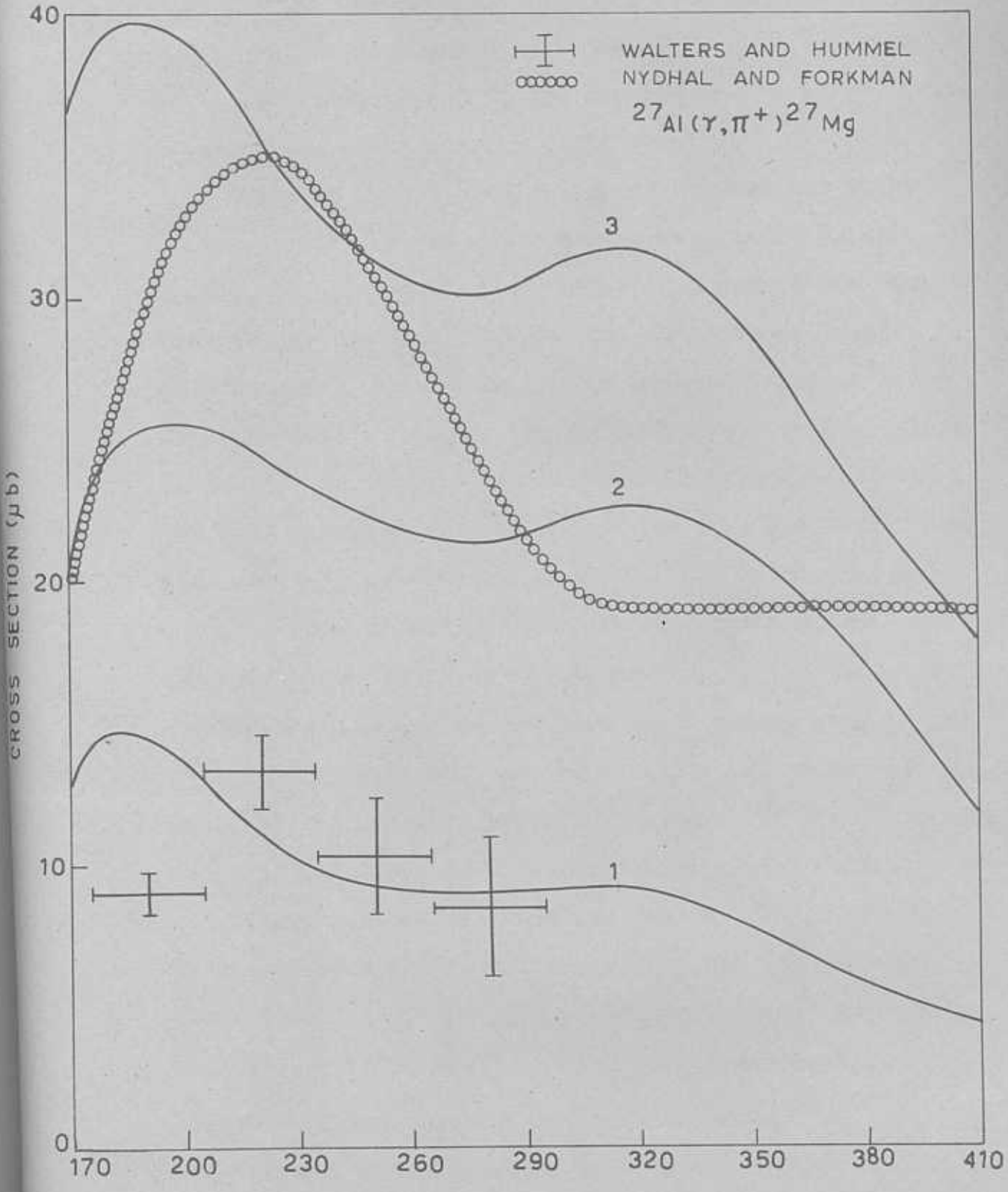

Fig.2. Cross section for the reaction $^{27}Al(\gamma,\pi^+)^{27}Mg$ assuming surface production of pions. Experimental results are those of Walters and Hummel[3] and of Nydhal and Forkman[4].

than that of the latter. Further, both these results are in strong disagreement with those of Masaike. The experimentalists themselves[1,2] are puzzled at the large differences which exist between their results.

There is a very good agreement between our theoretical curve 1 and the experimental results of Walters and Hummel. If the results of Walters and Hummel are correct, then we may conclude that the low-lying bound states of ^{27}Mg which are stable against nucleon emission arise from the single nucleon transition $1d_{5/2} \longrightarrow 2s_{1/2}$ (see table.1). Also, this conclusion is independent of the production mechanism used, since for this particular transition there is no appreciable difference in cross sections obtained from volume and surface production mechanisms. This is essentially due to the overlap of the radial wave functions of 1d and 2s orbitals which cancel away in the region of nuclear size due to nearly equal amount of positive and negative contributions arising from the occurrence of nodal point in the 2s radial wave function.

The experimental cross sections of Nydhal and Forkman lie much above the theoretical curve obtained for the transition $1d_{5/2} \longrightarrow 2s_{1/2}$. So, we included the next higher transition $1d_{5/2} \longrightarrow 1d_{3/2}$ in order to take into account a larger number of final states of ^{27}Mg. In Fig.2, we observe a good agreement between the theoretical curve 3

and the experimental curve of Nydhal and Forkman in the region of 230 Mev and at 400 Mev but there exists a large discrepancy at other energies. Thus, if the results of Nydhal and Forkman are correct, then it follows that in addition to all the final nuclear levels arising from the single nucleon transition $1d_{5/2} \longrightarrow 2s_{1/2}$, being stable against nucleon emission, some (but not all) of the final nuclear levels arising from the transition $1d_{5/2} \longrightarrow 1d_{3/2}$ are also stable against nucleon emission and that these levels should also have contributed to the total cross section observed by them. Further, from our analysis, we can conclude that the experimental results of Masaike exhibit a gross over estimate of the cross section.

3. THE REACTION $^{51}V(\gamma, \pi^+)^{51}Ti$:

Since detailed information about the nature of the level structure of ^{51}Ti is not available, we have computed separately the cross sections for this reaction for the single particle transitions $1f_{7/2} \longrightarrow 2p_{3/2}$, $1f_{5/2}$ and $2p_{1/2}$ with a view to elicit information regarding the possible bound states of ^{51}Ti which are stable against nucleon emission. We assume for the cut-off parameter a value of 2.6 in units of pion Compton wavelength ($\hbar_o$ =3.676 fm) and for the oscillator length parameter b, a value of 2.314 fm. consistent with the electron scattering

results[7].

In Fig.3, the cross sections for the reaction $^{51}V(\gamma,\pi^+)^{51}Ti$ have been plotted as a function of the incident photon energy assuming volume production of pions. Fig.4 corresponds to the results obtained with the surface production mechanism. Curves 1,2 and 3 represent the cross sections due to the individual transitions $1f_{7/2} \longrightarrow 2p_{3/2}$, $1f_{7/2} \longrightarrow 1f_{5/2}$ and $1f_{5/2} \longrightarrow 2p_{1/2}$, respectively. Curve 4 represents the sum of the contributions arising from the transitions $1f_{7/2} \longrightarrow 2p_{3/2}$ and $1f_{5/2}$, while curve 5 represents the sum of all the three transitions. The experimental results are those of Nydhal and Forkman[2] who have measured the cross sections for this π^+ reaction from threshold upto 750 Mev.

Since the curve 1 of Fig.4 lies below the experimental results it follows that all the 14 states enumerated in table.1, as states belonging to ^{51}Ti which arise due to the single particle transition $1f_{7/2} \longrightarrow 2p_{3/2}$, are stable against nucleon emission. But, the fact that the curve 4 lies far above the experimental results implies that in addition to the levels which arise from the transition $1f_{7/2} \longrightarrow 2p_{3/2}$, only a few of the 18 levels which arise

---

7) L.R.B. Elton, "Nuclear Sizes", Oxford University Press, London (1961), see table.2 on page.31.

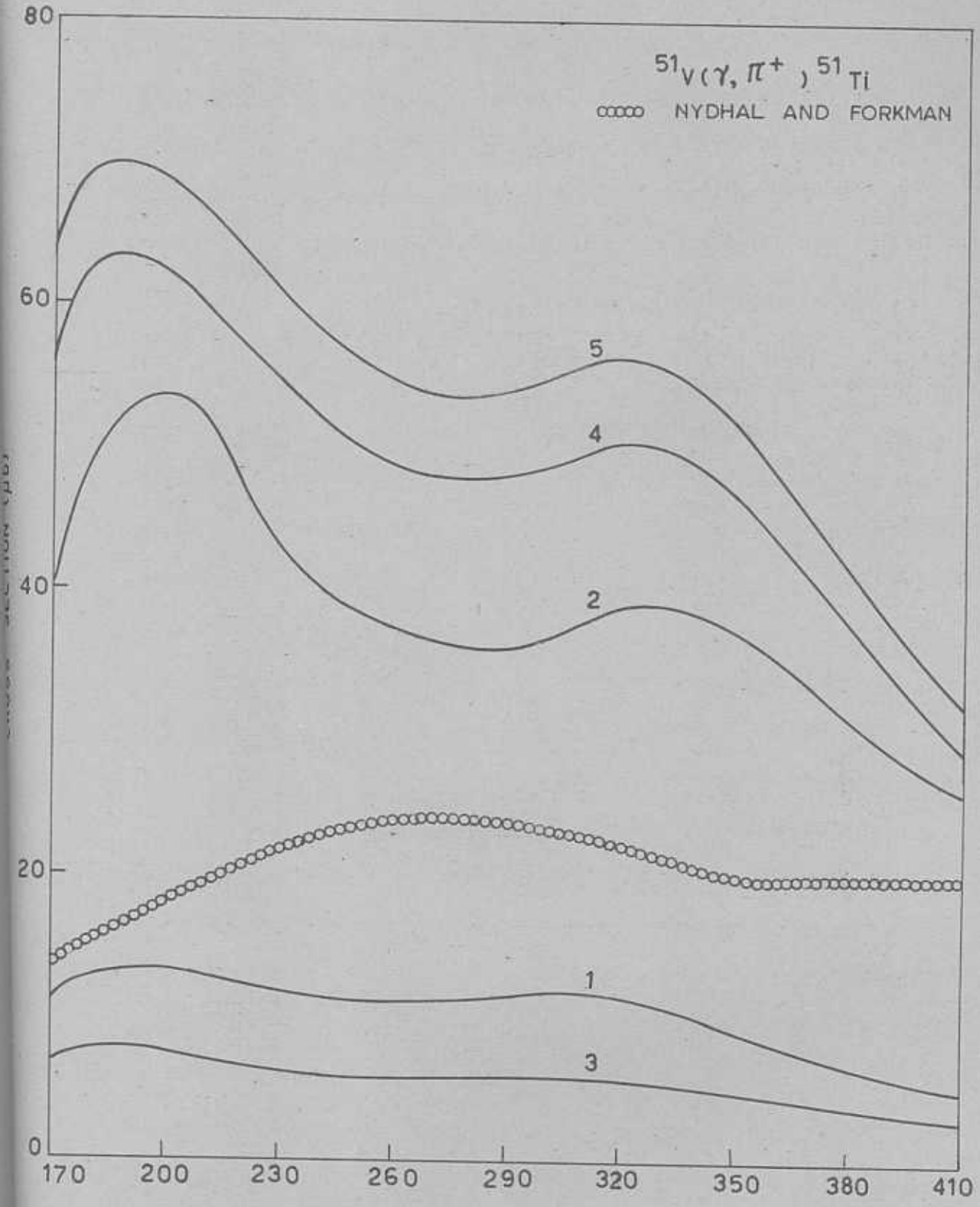

Fig.3.Cross section for the reaction $^{51}V(\gamma, \pi^+)^{51}Ti$ assuming volume production of pions along with the experimental results of Nydhal and Forkman[4].

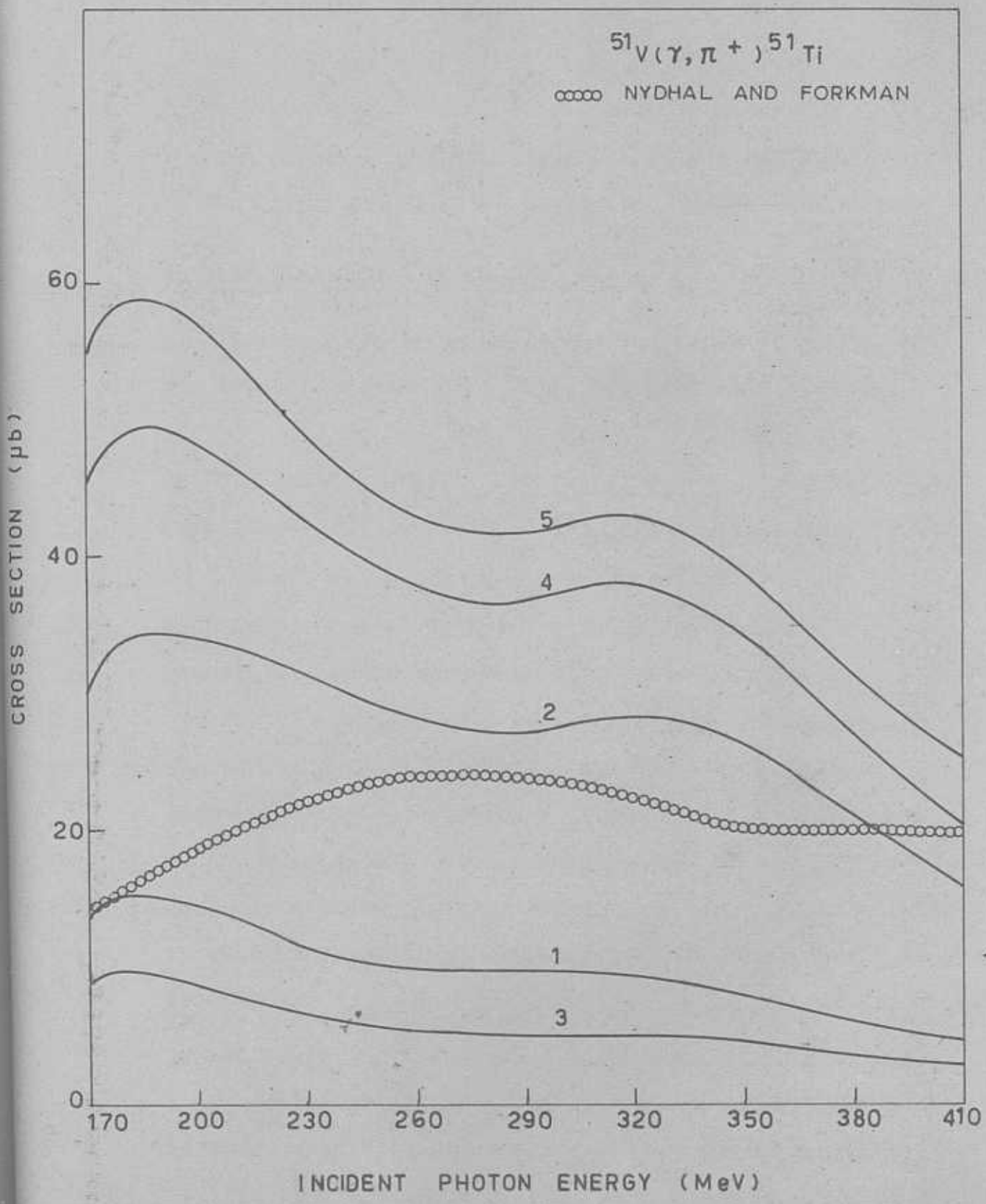

Fig.4. Cross section for the reaction $^{51}V(\gamma,\pi^+)^{51}Ti$ assuming surface production of pions along with the experimental results of Nydhal and Forkman [4].

from the transition $1f_{7/2} \longrightarrow 1f_{5/2}$ should have contributed to the cross section, while it is possible that the rest of the levels of ^{51}Ti may lie above the threshold for nucleon emission and hence might not have contributed to the experimental cross section of Nydhal and Forkman.

4. THE REACTION $^{60}Ni(\gamma,\pi^-)^{60}Cu$:

Since information regarding the detailed nature of the level structure of ^{60}Cu is not available, let us assume that the low-lying states of ^{60}Cu which are stable against nucleon emission result from the single particle transitions $2p_{3/2} \longrightarrow 2p_{3/2}$, $1f_{5/2}$ and $2p_{1/2}$. We take for the cut-off parameter τ_0, a value of 2.6 in units of pion Compton wavelength (τ_0 = 3.676 fm) and for the oscillator length parameter b, a value of 2.34 fm.

In Fig.5, the cross sections for this reaction are plotted as a function of the incident photon energy assuming volume production of pions. Fig.6 corresponds to the results obtained assuming surface production of pions. In these figures, curves 1, 2 and 3 represent the partial cross sections arising from the single particle transitions $2p_{3/2} \longrightarrow 2p_{3/2}$, $2p_{3/2} \longrightarrow 1f_{5/2}$ and $2p_{3/2} \rightarrow 2p_{1/2}$, respectively and the curve 4 represents their sum. The experimental results are those of March and Walker[3]. It is surprising to note from Fig.5 that the experimental results lie much above the theoretical curve obtained in

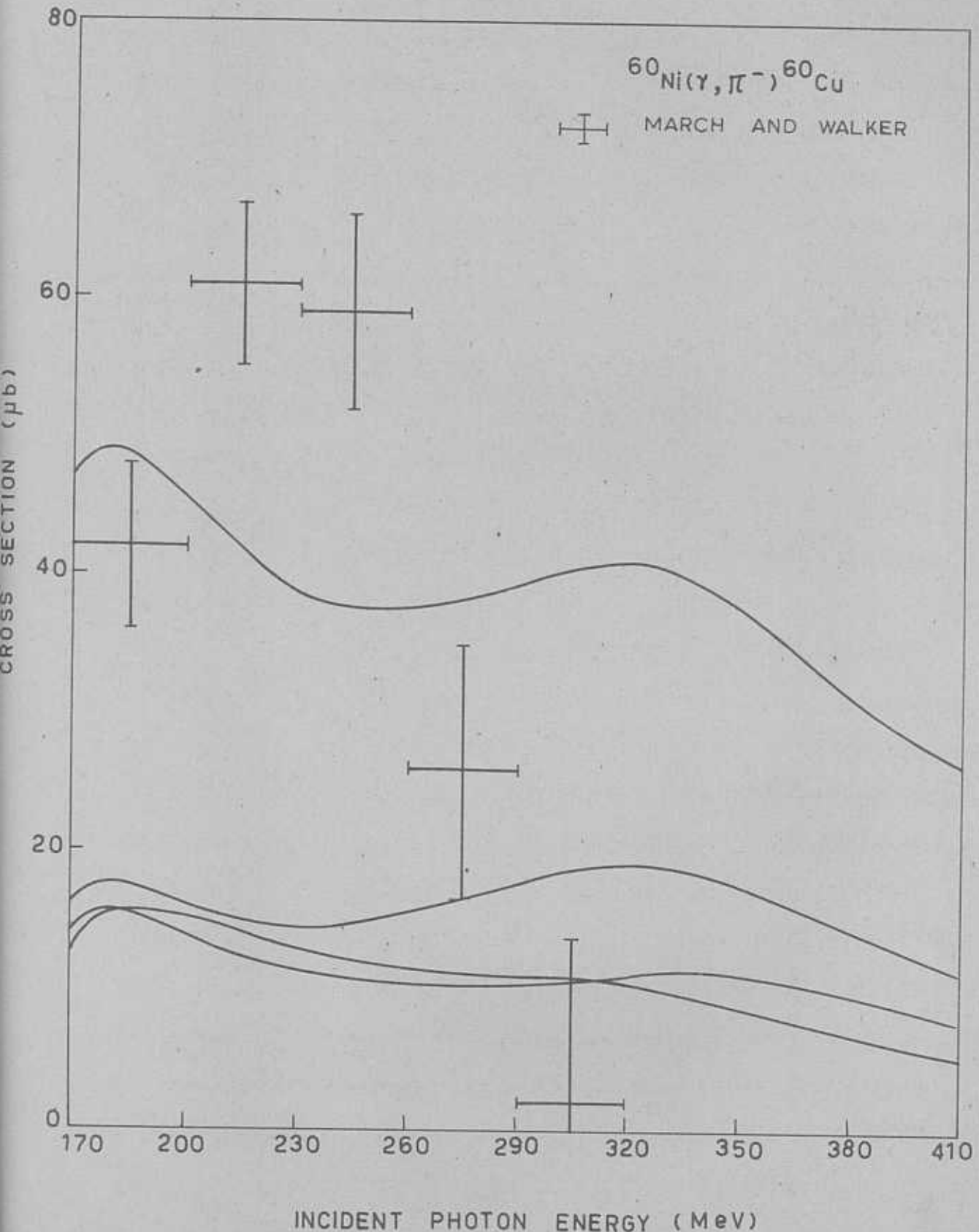

Fig.5. Cross section for the reaction $^{60}Ni(\gamma,\pi^-)^{60}Cu$ assuming volume production of pions along with the experimental results of March and Walker[5].

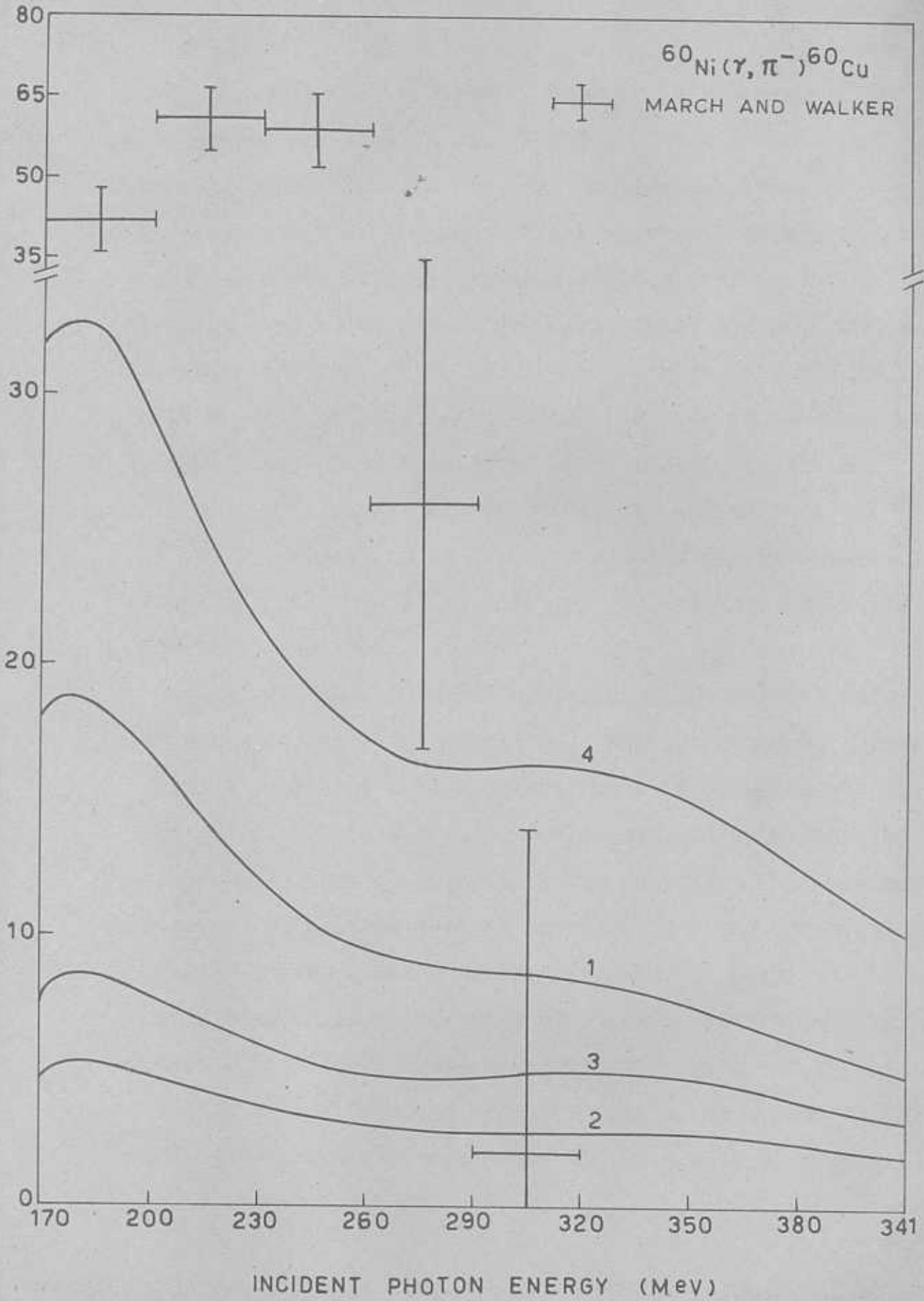

Fig.6. Cross section for the reaction $^{60}Ni(\gamma,\pi^-)^{60}Cu$ assuming surface production of pions along with the experimental results of March and Walker6).

the volume production model. Further, the experimental cross sections seem to reveal a dip in the 290-320 Mev region which is in discord with the general trend of the flattening out of the photopion production cross section around 300 Mev after an initial rapid rise from threshold to some peak value around 200 Mev. Thus, the experimental results of March and Walker are in complete disagreement with our theoretical calculation. In view of the success of our theory with respect to other nuclei, especially $^{16}O(\gamma,\pi^+)^{16}N$ and $^{11}B(\gamma,\pi^+)^{11}Be$, we feel that we will not be in a position to draw any conclusions from our study of $^{60}Ni(\gamma,\pi^-)^{60}Cu$ until new results are available for this reaction.

There is one interesting features which comes out of our study of $^{60}Ni(\gamma,\pi^-)^{60}Cu$. In Figs.5 and 6, curves 1 and 2 represent contributions due to transitions to four final nuclear states, each, while curve 3 represents the contribution due to transitions to only two final nuclear states. We observe that in the case of volume production (Fig.5) curves 2 and 3 are almost alike in shape and magnitude, while in the case of surface production (Fig.6) curve 3 lies above curve 2. Thus, the number of final nuclear states involved does not seem to be important. This conclusion is contrary to the expectation of Meyer

et. al.[8] who assume the cross sections to "depend much more on the total number of states available than on the specific details of the states involved".

8) R.A.Meyer, W.B.Walters and J.P.Hummel, Phys.Rev. 127, 2217 (1962).

Appendix A.

The numerical calculations have all been carried out in the pion-nucleon center-of-mass (c.m.) system, since the photoproduction amplitudes of CGLN are valid only in that system. Here we give the formulae used in our calculations.

Let a γ ray of energy E_γ^l, in the laboratory system, be absorbed by a nucleon and emit a pion. Then, the energy in the c.m. system is:

$$E^c = (M^2 + 2ME_\gamma^l)^{1/2} \tag{A.1}$$

where M is the mass of the nucleon(+). The energy of the photon in the c.m. system is:

$$E_\gamma^c = ME_\gamma^l / E^c. \tag{A.2}$$

The energy of the pion in the c.m. system(+) is:

$$E_\pi^c = \frac{(E^c)^2 - M^2 + 1}{2E^c}. \tag{A.3}$$

The energy of the pion in the laboratory system is:

$$E_\pi^l = \frac{(E^c)^2 - M^2 - 1}{2E^c}. \tag{A.4}$$

The kinetic energy of the pion in the laboratory system is:

$$W_\pi^l = E_\pi^l - 1. \tag{A.5}$$

The c.m. momentum of the pion is:

$$P_\pi^c = [(E_\pi^c)^2 - 1]^{1/2}. \tag{A.6}$$

(+) We use the natural units $\hbar = c = m_\pi = 1$.

By making a comparison between photopion production and pion-nucleon scattering, at the same energy in the c.m. system, it can be shown[1] that the threshold energy for photopion production is:

$$E_o = m_\pi(1+m_\pi/2M) , \qquad (A.7)$$

where m_π is the mass of the pion. Thus, the threshold energy for single nucleon photopion production is 150 Mev for charged and 145 Mev neutral pions.

The energy-dependent pion-nucleon phase shifts upto 700 Mev have been given by Roper, Wright and Feld[2]. The values of the phase-shifts at the required incident photon energies have been calculated using the Lagrange interpolation formula[3] and these are given in Table.1 below(+)

Table.1. Pion-nucleon phase shifts

Incident photon energy(Mev)	W_π^L (Mev)	p-wave phase shifts (degrees)			
		δ_{33}	δ_{11}	δ_{13}	δ_{31}
165	15.14	$0^\circ 55'$	$-0^\circ 32'$	$-0^\circ 36'$	$-0^\circ 73'$
180	30.14	$2^\circ 42'$	$-1^\circ 11'$	$-0^\circ 10'$	$-0^\circ 19'$
200	50.14	$6^\circ 07'$	$-1^\circ 52'$	$-0^\circ 20'$	$-0^\circ 41'$
230	80.14	$13^\circ 52'$	$-2^\circ 14'$	$-0^\circ 39'$	$-1^\circ 22'$
260	110.13	$26^\circ 07'$	$-1^\circ 47'$	$-1^\circ 01'$	$-2^\circ 09'$

table continued on next page.

1) H.A.Bethe and F.de Hoffmann, "Mesons and Fields", Vol.II, Row, Peterson and Company, p.133.
2) L.D.Roper, R.M.Wright and B.T.Feld, Phys.Rev. 138, B190(1965), Table IX.
3) H.Margenau and G.M.Murphy, "The Mathematics of Physics and Chemistry", D.Van Nostrand Company Inc.(1961), p.470.
(+) Except in Chapters1 and 2, the dominant pion-nucleon scattering phase shift δ_{33} alone has been taken into account in the calculations.

Table.1(continued)

Incident photon energy(Mev)	W_π^l (Mev)	p-wave phase shifts (degrees)			
		δ_{33}	δ_{11}	δ_{13}	δ_{31}
290	140.13	45°09'	-0°33'	-1°24'	-3°00'
320	170.13	70°43'	1°23'	-1°48'	-3°53'
350	200.13	95°31'	4°01'	-2°13'	-4°46'
380	230.13	115°19'	7°21'	-2°37'	-5°36'
410	260.13	124°52'	11°32'	-3°01'	-6°19'

The values of some of the constants used in the calculations are given below:

π = 3.14159265,

mass of the pion m_π = 139.5 Mev,

mass of the nucleon M = 938.879 Mev,

magnetic moment of the proton μ_p = 2.79277,

magnetic moment of the neutron μ_n = -1.913155,

the Compton wave length of the pion = 1.414 fm,

the electromagnetic coupling constant e^2 = 1/137, and

the pion-nucleon coupling constant f^2 = 0.08.

Appendix.B.

The Impulse Approximation

According to the impulse approximation, the transition amplitude for the photoproduction of pions from a nucleus can be written as a linear superposition of the individual free nucleon transition amplitudes:

$$\mathcal{T} = \sum_{k=1}^{N} t_k \ , \qquad \text{(B.1)}$$

where N is the mass number of the nucleus. The expression (B.1) neglects the corrections due to multiple scattering, off-the-energy shell matrix elements and the internucleon potential. The following are the assumptions under which the impulse approximation (B.1) is valid:

(i) The incident particle interacts only with one single nucleon at a time.

(ii) The amplitude of the incident wave is not appreciably diminished in crossing the nucleus.

(iii) The binding force has a negligible effect during the interval of strong interaction.

Here we shall summarise the theory of the impulse approximation which was first introduced by Chew[1] and developed by Chew and Wick[2] and Chew and Goldberger[3].

---

1) G.F.Chew, Phys.Rev., 80, 196 (1950).
2) G.F.Chew and G.C.Wick, Phys.Rev., 85, 636 (1952).
3) G.F.Chew and M.L.Goldberger, Phys.Rev., 87, 778 (1952).

We consider a particle incident on a nucleus, its interaction with the individual nucleons of the nucleus being represented by the potential V_k (for interaction with the k^{th} nucleon). If K is the total kinetic energy of the system and U the inter-nucleon potential then the total Hamiltonian for the system can be written as

$$H = K + U + V = H_o + V \tag{B.2}$$

where

$$V = \sum_k V_k$$

The T-matrix for the process is given by the equation

$$T = V + V \frac{1}{E_a + i\eta - H_o} VT$$

$$= V + V \frac{1}{E_a + i\eta - H_o - V} V \tag{B.3}$$

The first form for T in (B.3) is obtained from the S-matrix expansion of Dyson by doing the space and (time-ordered) time integrations separately. The term $i\eta$ in the denominator represents the outgoing wave boundary condition. A limit of $\eta \to o$ is implied in (B.3).

We define the two-particle scattering matrix

$$t_k = V_k \omega_k \tag{B.4}$$

where

$$\omega_k = 1 + \frac{1}{E_\ell + i\eta - K - V_k} V_k . \tag{B.5}$$

Now if B and b are two operators defined by

$$B = \frac{1}{E_a + i\eta - H_o - V} A$$

$$b_k = \frac{1}{E_\ell + i\eta - K - V_k} A$$

where A is any operator, then

$$B = b_k + \frac{1}{E_a + i\eta - H_o - V} \{ [U, b_k] + (V - V_k) b_k \}. \qquad (B.6)$$

This result follows on using the operator identity

$$\frac{1}{X - Y} - \frac{1}{X} = \frac{1}{X - Y} Y \frac{1}{X}.$$

We use (B.6) in (B.3) which we rewrite as

$$T = \sum_{k=1}^{N} \{ V_k + V \frac{1}{E_a + i\eta - H_o - V} V_k \}. \qquad (B.7)$$

From (B.6) and (B.5) we have

$$\frac{1}{E_a + i\eta - H_o - V} V_k = (\omega_k - 1) +$$

$$+ \frac{1}{E_a + i\eta - H_o - V} \{ [U, \omega_k] + (V - V_k)(\omega_k - 1) \}. \qquad (B.8)$$

Substituting (B.8) in (B.7) we finally obtain

$$T = \sum_{k=1}^{N} \{ t_k + V \frac{1}{E_a + i\eta - H_o - V} [U, \omega_k] +$$

$$+ (1 + V \frac{1}{E_a + i\eta - H_o - V})(V - V_k)(\omega_k - 1) \} \qquad (B.9)$$

which may be called the impulse series.

The first term in (B.9) represents the linear superposition of the individual free nucleon amplitudes and it is known, as stated earlier, as the impulse approximation, while the second and third terms denote the correction due to binding energy and the correction due to multiple scattering, respectively. An adequate and workable approximation in many cases is obtained by neglecting the second and third terms of (B.9) and using the correct wave functions for the initial and final states in computing the matrix elements.

Appendix C

In this Appendix we indicate the method of evaluating the radial integrals:

$$\langle j_\ell(kr)\rangle_{n_i\ell_i,n_f\ell_f} = \int_0^\infty \mathcal{R}_{n_f\ell_f}(r)\, j_\ell(kr)\, \mathcal{R}_{n_i\ell_i}(r)\, r^2\, dr, \qquad (C.1)$$

where $\mathcal{R}_{n\ell}(r)$ is the properly normalized single particle harmonic oscillator radial wave function and $j_\ell(kr)$ is a spherical Bessel function of order ℓ. The properly normalized harmonic oscillator radial wave functions[1] are defined by:

$$\mathcal{R}_{n\ell}(r) = N_n \; b^{-\ell-3/2}\, P(r)\, r^\ell \exp\left(-\frac{r^2}{2b^2}\right), \qquad (C.2)$$

where N_n is a normalization constant(+)

$$N_{n\ell} = \left[\frac{2^{n+\ell+1}}{\pi(2n+2\ell-1)!!}\right]^{1/2},$$

b is the oscillator length or size parameter (usually determined from electron scattering experiments), and

$$P(r) = 1 \qquad \text{for } n = 1,$$

$$= \frac{2\ell+3}{2} - \frac{r^2}{b^2} \qquad \text{for } n = 2,$$

$$= \frac{1}{2}\left[\frac{(2\ell+3)(2\ell+5)}{4} - (2\ell+5)\frac{r^2}{b^2} + \frac{r^4}{b^4}\right] \text{ for } n=3.$$

---

1) V.Gillet and D.A.Jenkins, Phys.Rev.140, B32 (1965).

(+) $(2N-1)!! = (2N-1)(2N-3)\ldots(5)(3)(1)$ when N is an integer.

In Table.1, we list some of the normalized harmonic oscillator radial wave functions.

Table.1

Normalized harmonic oscillator radial wave functions

n	ℓ		$R_{n\ell}(r).\exp(r^2/2b^2)$
1	0	(1s)	$(4/(b^3\sqrt{\pi}))^{1/2}$
1	1	(1p)	$(8/(3\,b^3\sqrt{\pi}))^{1/2}\ r/b$
1	2	(1d)	$(16/(15\,b^3\sqrt{\pi}))^{1/2}\ r^2/b^2$
2	0	(2s)	$(8/(3\,b^3\sqrt{\pi}))^{1/2}\ (3/2 - r^2/b^2)$
1	3	(1f)	$(32/(105\,b^3\sqrt{\pi}))^{1/2}\ r^3/b^3$
2	1	(2p)	$(16/(15\,b^3\sqrt{\pi}))^{1/2}\ r(5/2 - r^2/b^2)/b$
1	4	(1g)	$(64/(945\,b^3\sqrt{\pi}))^{1/2}\ r^4/b^4$
2	2	(2d)	$(32/(105\,b^3\sqrt{\pi}))^{1/2}\ r^2(7/2 - r^2/b^2)/b^2$
3	0	(3s)	$(16/(15\,b^3\sqrt{\pi}))^{1/2}(15/4-5\,r^2/b^2+r^4/b^4)/2$
1	5	(1h)	$(128/(10395\,b^3\sqrt{\pi}))^{1/2}\ r^5/b^5$
2	3	(2f)	$(64/(945\,b^3\sqrt{\pi}))^{1/2}\ r^3/b^3$
3	1	(3p)	$(32/(105\,b^3\sqrt{\pi}))^{1/2}\ r(15/4-5r^2/b^2+r^4/b^4)/(2b)$
1	6	(1i)	$(256/(135135\,b^3\sqrt{\pi}))^{1/2}\ r^6/b^6$

The spherical Bessel function, $j_\ell(x)$, is related to the Bessel function of first kind, $J_\ell(x)$, through

$$j_\ell(x) = \left(\frac{\pi}{2x}\right)^{1/2} J_{\ell+1/2}(x) \qquad (C.3)$$

In Table.2, we list some of the spherical Bessel functions[2].

Table.2

Spherical Bessel functions

ℓ	$j_\ell(x)$
0	$\sin x/x$
1	$\sin x/x^2 - \cos x/x$
2	$(3/x^3-1/x)\sin x - 3\cos x/x^2$
3	$(15/x^4-6/x^2)\sin x - (15/x^3 - 1/x)\cos x$
4	$(105/x^5-45/x^3 + 1/x)\sin x - (105/x^4 - 10/x^2)\cos x$
5	$(945/x^6 - 420/x^4 + 15/x^2)\sin x +$ $-(945/x^5 - 105/x^3 + 1/x)\cos x$
6	$(10395/x^7 - 4725/x^5 + 210/x^3 - 1/x)\sin x +$ $-(10395/x^6 - 1260/x^4 + 21/x^2)\cos x$

Evaluation of the radial integral (C.1) involves the use of two basic integrals:

$$\int_0^\infty r^{2n} e^{-r^2/b^2} \cos kr\, dr \quad \text{and} \quad \int_0^\infty r^{2n+1} e^{-r^2/b^2} \sin kr\, dr,$$

which we will denote as I_{2n} and I_{2n+1}, respectively. When $n=0$, we have[3]

$$I_0 = \int_0^\infty e^{-r^2/b^2} \cos kr\, dr = \frac{b\sqrt{\pi}}{2} \exp(-k^2b^2/4), \qquad (C.4)$$

2) Andrew Gray and G.B.Mathews, "A Treatise on Bessel functions and their applications to Physics", Macmillan and Company Limited, (London) 1952, p.17.

3) H.B.Dwight, "Tables of Integrals and other mathematical data", Fourth Edition, The Macmillan Company(N.Y.)1961, p.236, Eqs.861.20 and 861.21.

$$I_1 = \int_0^\infty r\, e^{-r^2/b^2} \sin kr\, dr = \frac{kb^3\sqrt{\pi}}{4} \exp(-k^2b^2/4). \quad \text{(C.5)}$$

Integrating I_{2n} and I_{2n+1} by parts, we derive the following recurrence relations for $n \geq 1$:

$$\begin{aligned} I_{2n} &= \int_0^\infty r^{2n}\, e^{-r^2/b^2} \cos kr\, dr \\ &= \frac{b^2}{2} \left[(2n-1) I_{2n-2} - k I_{2n-1} \right], \end{aligned} \quad \text{(C.6)}$$

$$\begin{aligned} I_{2n+1} &= \int_0^\infty r^{2n+1}\, e^{-r^2/b^2} \sin kr\, dr \\ &= \frac{b^2}{2} \left[2n I_{2n-1} + k I_{2n} \right]. \end{aligned} \quad \text{(C.7)}$$

In table.3, we list the explicit expressions for some of these integrals.

Table.3

N	I_N . $\exp(+k^2b^2/4)/\sqrt{\pi}$
0	$b/2$
1	$kb^3/4$
2	$b^3(1 - k^2b^2/2)/4$
3	$kb^5(3 - k^2b^2/2)/8$
4	$b^5(3-3k^2b^2 + k^4b^4/4)/8$
5	$kb^7(15-5k^2b^2 + k^4b^4/4)/16$
6	$b^7(15-45\, k^2b^2/2 + 15 k^4b^4/4 - k^6b^6/8)/16$
7	$kb^9(105(1-k^2b^2/2) + 21\, k^4b^4/4 - k^6b^6/8)/32$

table.3 continued on next page

Table.3(continued).

N	$I_N \sqrt{\pi} \cdot \exp(+ k^2b^2/4)$
8	$b^9(105(1-2k^2b^2) + 105k^4b^4/2 - 7k^6b^6/2 + k^8b^8/16)/32$
9	$kb^{11}(945(1-2k^2b^2/3)+189k^4b^4/2-9k^6b^6/2+k^8b^8/16)/64$
10	$b^{11}(945(1-5k^2b^2/2)+1575k^4b^4/2-315k^6b^6/4+45k^8b^8/16-k^{10}b^{10}/32)/64$

The radial integral (C.1) for various single particle transitions can now be analytically computed using tables 1,2 and 3. Some of the radial integrals which occur in problems of photoproduction of pions from nuclei are enumerated in table.4.

Table.4

Analytical expressions for radial integrals of the type (C.1)

n_i	l_i	n_f	l_f	l	$< j_l(kr) >_{n_i l_i, n_f l_f} \cdot \exp(+k^2b^2/4)$
1	s	1	s	0	1
1	s	1	p	1	$kb/\sqrt{6}$
1	s	1	d	2	$k^2b^2/\sqrt{60}$
1	s	2	s	0	$k^2b^2/\sqrt{24}$
1	p	1	p	0	$1 - k^2b^2/6$
1	p	1	p	2	$k^2b^2/6$
1	p	1	d	1	$\sqrt{2/5}\ kb(10-k^2b^2)/12$
1	p	1	d	3	$\sqrt{2/5}\ k^3b^3/12$
1	p	2	s	1	$kb(k^2b^2-4)/12$
1	p	1	f	2	$k^2b^2(7-k^2b^2/2)/(6\sqrt{35})$

table continued on next page

Table.4(continued)

n_i	l_i	n_f	l_f	ℓ	$< j_\ell(kr) >_{n_i l_i, n_f l_f} \cdot \exp(+k^2b^2/4)$
1	p	1	f	4	$k^4b^4/(12\sqrt{35})$
1	p	2	p	0	$\sqrt{2/5}\ k^2b^2(10-k^2b^2)/24$
1	p	2	p	2	$\sqrt{2/5}\ k^2b^2(k^2b^2-4)/24$
1	d	1	d	0	$1+k^2b^2(k^2b^2/20 - 1)/3$
1	d	1	d	2	$k^2b^2(7-k^2b^2/2)/30$
1	d	1	d	4	$k^4b^4/60$
1	d	2	s	2	$\sqrt{2/5}\ k^2b^2(k^2b^2-8)/24$
1	d	1	f	1	$\sqrt{7/18}\ kb(1-k^2b^2/5 + k^4b^4/140)$
1	d	1	f	3	$3\sqrt{2/7}\ k^3b^3(1-k^2b^2/18)/20$
1	d	1	f	5	$\sqrt{2/7}\ k^5b^5/120$
1	d	2	p	1	$kb(3k^2b^2/20 - 1/3 - k^4b^4/120)$
1	d	2	p	3	$k^3b^3(k^2b^2/8 - 1)/15$
1	f	1	f	0	$1 - k^2b^2/2 + k^4b^4/20 - k^6b^6/840$
1	f	1	f	2	$k^2b^2(3(1-k^2b^2/7) + k^4b^4/84)/10$
1	f	1	f	4	$k^4b^4(11-k^2b^2/2)/420$
1	f	2	p	2	$\sqrt{2/7}\ k^2b^2(k^2b^2(13-k^2b^2/2)-56)/120$
1	f	2	p	4	$\sqrt{2/7}\ k^4b^4(k^2b^2-12)/240$
2	p	2	p	0	$1 - k^2b^2(1-k^2b^2(11-k^2b^2/2)/60)/2$
2	p	2	p	2	$k^2b^2(9-2k^2b^2 + k^4b^4/8)/30$